FABRICATION AND PHOTOCHEMICAL SURFACE MODIFICATION OF PHOTOREACTIVE THIN-FILM COMPOSITE MEMBRANES AND MODEL DEVELOPMENT FOR THIN FILM FORMATION BY INTERFACIAL POLYMERIZATION

By

JIANG JI, M. ENG.

A Thesis

Submitted to the School of Graduate Studies

in Partial Fulfilment of the Requirements

for the Degree

Doctor of Philosophy

McMaster University

FABRICATION AND PHOTOCHEMICAL SURFACE MODIFICATION OF PHOTOREACTIVE THIN-FILM COMPOSITE MEMBRANES AND MODEL DEVELOPMENT FOR THIN FILM FORMATION BY INTERFACIAL POLYMERIZATION

for Mom and Dad,

and for Chunfeng and the Whole Family

DOCTOR OF PHILOSOPHY (1996) McMaster University
Department of Chemistry Hamilton, Ontario

TITLE: Fabrication and Photochemical Surface Modification of Photoreactive Thin-Film Composite Membranes and Model Development for Thin Film Formation by Interfacial Polymerization

AUTHOR: Jiang Ji, B. Eng. and M. Eng. (Dalian Institute of Technology)

SUPERVISORS: Professors R. F. Childs and J. M. Dickson

NUMBER OF PAGES: xxviii, 287

ABSTRACT

A simple route for the synthesis of a monomer containing a diazoketone functionality and two disulfonyl chloride groups has been developed. Polymerization of this monomer by reaction with a diamine leads to the formation of a polymer in which the photoreactive group is incorporated as a side chain. The polymer can be formed as a thin film in a thin-film composite membrane.

The factors that affect the interfacial polymerization, membrane morphology and performance have been systematically investigated. It was found that monomer concentration, the presence or absence of a surfactant, solvent and polymerization time are important factors in determining membrane morphology and separation/flux performance.

Small molecule model reactions have been studied in order to establish the chemistry of the photochemical surface modification of diazoketones. The range of photochemical transformations of diazoketones has been broadened, potentially leading to the photochemical conversion of the surface barrier layer of the diazoketone containing thin-film composite membranes to carboxylic acid, hydroxyl, ethyl ester and sulfur-containing crown ether.

A method for the preparation of specimens for surface characterization of the thin-film composite membranes by infrared spectroscopy has been developed. Surface

analysis techniques, such as Attenuated Total Reflectance Fourier Transform Infrared (ATR-FT-IR) Spectroscopy and Scanning Electron Microscopy (SEM), proved to be useful in monitoring the photochemical surface modifications of the photolabile thin-film composite membranes.

The performance of the initial diazoketone precursor membrane and photochemically modified membranes has been examined with a series of aqueous solutions of inorganic salts. It was found that photochemical surface modification can significantly alter the separation/flux performance of the membranes.

A theoretical model that considers both diffusion- and reaction-controlled interfacial polymerization, under nonsteady-state conditions, has been developed. The model can describe the formation of both dense and porous thin films. The results predicted by the model are consistent with experimental results. The general model developed in this thesis for thin film formation by interfacial polymerization can include the special model already reported in the literature. The work conducted in this thesis significantly extends existing theories for the formation of thin films by interfacial polymerization and provides an important guide for effective control of the thickness of the surface barrier layer of thin-film composite membranes prepared by interfacial polymerization.

ACKNOWLEDGEMENTS

I would like to extend sincere gratitude to Drs. R. F. Childs and J. M. Dickson, my research supervisors, for their continued guidance and support during my study at McMaster and during the writing of this thesis.

I would like to thank Dr. B. E. McCarry for his help with infrared spectroscopy and continuous advice particularly when Dr. Childs was on sabbatical. I am also very grateful to Dr. H. D. H. Stöver for his valuable advice over these years.

To both Dr. Childs' and Dr. Dickson's groups, thanks so much for your daily help and friendship. I would particularly like to thank my friends: B. Trushinski.

I am very grateful to the member of the NMR facility at McMaster, Dr. D. Hughes and Mr. B. Sayer, and the members of the Electron Microscopy Unit in the Department of Biology, Mr. K. Schultes and D. Flannigan, for their assistance. I would also like to acknowledge Dr. M. G. Liu for his help with computer programming.

I would also like to thank the staff members in the Department of Chemistry for giving me scientific inspiration, friendship and help. I would like to express my special thanks to C. Dada for her generous help and kindness over these years.

I wish to thank the financial support of The Natural Sciences and Engineering Research Council Canada (NSERC), 3M Canada Inc., and The University Research Incentive Fund (URIF).

Finally, I would like to thank my family for their constant support.

TABLE OF CONTENTS

LIST OF TABLES

LIST OF FIGURES

LIST OF SCHEMES

LIST OF ABBREVIATIONS

ATR	Attenuated Total Reflectance
ATR-FT-IR	Attenuated Total Reflectance Fourier Transform Infrared
DK	Diazoketone
EDS	Energy Dispersive Spectroscopy
EI	Electron Ionization
FT-IR	Fourier Transform Infrared
IR	Infrared
MF	Microfiltration
MS	Mass Spectra
NMR	Nuclear Magnetic Resonance
NOE	Nuclear Overhauser Enhancement
PEI	Poly(ethyleneimine)
RO	Reverse Osmosis
SEM	Scanning Electron Microscopy
TFC	Thin-Film Composite
TMS	Tetramethylsilane
UF	Ultrafiltration
UV	Ultraviolet

LIST OF SYMBOLS

A_0	a constant defined in Eq. 5.12, $m^7/(kmol.s^2)$
A_1	a constant defined in Eq. 6.7, $m^7/(kmol.s^2)$
B_0	a constant defined in Eq. 5.13, $m^6/(kmol.s^2)$
B_1	a constant defined in Eq. 6.8, $m^6/(kmol.s^2)$
C_0	a constant defined in Eq. 5.14, $m^4/(kmol.s)$
C_1	a constant defined in Eq. 6.9, $m^4/(kmol.s)$
C_a	concentration of 1,2-ethanediamine in the aqueous phase, $kmol/m^3$
$C(0,0)$	initial concentration of monomer **A** in the newly formed thin film as shown in Fig. 5.1, $kmol/m^3$
$C_f(0,0)$	initial concentration of monomer **A** in the support-membrane phase as shown in Fig. 5.1, $kmol/m^3$
$C(0,t)$	concentration of monomer **A** at the surface of the support membrane at time t as shown in Fig. 5.1, $kmol/m^3$
$C(x,t)$	concentration of monomer **A** in the newly formed thin film as shown in Fig. 5.1, $kmol/m^3$
$C(X,t)$	concentration of monomer **A** in the reaction zone as shown in Fig. 5.1, $kmol/m^3$

C_b	concentration of monomer **B** in the organic phase as shown in Fig. 5.1, kmol/m^3
D	diffusion coefficient of monomer **A** in the thin film formed by interfacial polymerization, (Eq. 5.7), m^2/s
D_0	a constant defined in Eq. 5.15, m^5/(kmol.s)
D_1	a constant defined in Eq. 6.10, m^5/(kmol.s)
D_M	a constant defined in Eqs. 5.8 and 6.5, m^5/(kmol.s)
D_P	diffusion coefficient of monomer **A** in the polymer of a porous thin film formed by interfacial polymerization, (Eq 6.3), m^2/s
D_v	diffusion coefficient of monomer **A** in the voids of a porous thin film formed by interfacial polymerization, (Eq. 6.3), m^2/s
dv_p/dt	the volume growth rate of the thin film formed by interfacial polymerization, m^3/s
dX/dt	the growth rate of the thin-film thickness, m/s
E_0	a constant defined in Eq. 5.16, m^6/(kmol.s)
E_1	a constant defined in Eq. 6.11 m^6/(kmol.s)
f	a constant, $0 < f < 1$, defined in Eqs. 5.21 and 6.21, respectively
J_A	flux of 1,2-ethanediamine across the newly formed membrane (Eq. 6.12), kmol/s

J_{WATER}	flux of water across the newly formed membrane, (Eq. 6.12), kmol/s
K	partition coefficient of monomer **A** between the support-membrane phase and the newly formed thin-film phase
K'	a pseudo-partition coefficient of 1,2-ethanediamine between aqueous phase and the support membrane phase, (Eq. 3.1)
k	the apparent reaction rate constant defined in Eq. 5.4, $m^4/(kmol.s)$
k_1	a constant defined in Eq. 5.5, $m^7/(kmol^2.s)$
k_r	second order reaction rate constant, (Eqs. 5.1 and 6.1), $m^3/(kmol.s)$
L	thickness of the support membrane as shown in Fig. 5.1, m
M_{47}	molecular weight of disulfonyl chloride, **47**, kg/kmol
M_{74}	molecular weight of 1,2-ethanediamine, **74**, kg/kmol
M_A	molecular weight of monomer **A**, kg/kmol
M_B	molecular weight of monomer **B**, kg/kmol
M_P	average molecular weight of the polymer, kg/kmol
M_u	equivalent molecular weight of the repeat unit of the polymer, kg/kmol
M_Z	molecular weight of a small molecule, **Z**, formed from each condensation reaction, kg/kmol
P	the average degree of polymerization
r_{max}	the maximum growth rate of the thin film, m/s
r_{min}	the minimum growth rate of the thin film, m/s

S	membrane area, m^2
t	polymerization time required for the thin-film thickness, X, s
V_{MEMB}	volume of the support polysulfone membrane, (zone I in Fig. 5.1), m^3
v_P	volume of the thin film formed by interfacial polymerization, (zone II in Fig. 5.1), m^3
$w_{a,MEMB}$	1,2-ethanediamine absorbed by the support polysulfone membrane, kmol
x	coordinate x, m
X	thickness of the thin film formed by interfacial polymerization as shown in Fig. 5.1, m
X_{max}	the maximum thickness of the thin film formed by interfacial polymerization as shown in Fig. 5.1, m
y	coordinate y, m
z	coordinate z, m
Z	a small molecule formed from each condensation reaction
ß	a molar ratio of water to monomer A or 1,2-ethanediamine transported together by diffusion, (Eq. 6.13)
δ	thickness of the reaction zone, (Fig. 5.1), m
η	viscosity, kg/(m.s)
π	osmotic pressure, kPa
ρ_P	density of the thin film formed by the interfacial polymerization, kg/m^3

ρ_w	density of water, kg/m^3
ϕ_1	volume fraction of the voids in the thin film formed by interfacial polymerization, (zone II in Fig. 5.1)
ϕ_2	volume fraction of polymer in the thin film formed by interfacial polymerization, (zone II in Fig. 5.1)

Chapter 1

Introduction

Separation is a critical component in many chemical and related processes. Indeed, the separation step is the single most expensive step in many industrial chemical processes. The range of processes in which a separation is required is very broad ranging from the isolation of high value components from complex mixtures in the pharmaceutical industries, the removal of water for concentration of a product in food industry, the purification of water by removing salts in conversion of brine to potable water, the removal of noxious contaminants prior to discharge of industrial and municipal waste streams, to the whole of the oil refining processes.[1]

Given the centrality of separation in modern industrial processes, it is not surprising that a broad range of separation techniques have been developed. The continued goals in this area are to improve selectivity of separation while reducing the cost associated with the separation.

Membrane based separations offer the prospect of high selectivity and low cost. These processes, including reverse osmosis (RO), ultrafiltration (UF), microfiltration (MF), dialysis, pervaporation and gas separation, play very important roles in chemical, pharmaceutical and food industries, as well as in environmental

protection.[2-5] The breakthrough in reverse osmosis that has occurred in the past three decades, continues to play a role in stimulating the development of membrane science and technology.

This thesis is concerned with just one of these processes, namely reverse osmosis.[2]

1.1 Principle of Reverse Osmosis Separation

Reverse osmosis is a membrane separation process, in which pressure is employed to reverse the normal osmotic flow of water across a semipermeable membrane while solutes are rejected by the membrane.[2] The critical component in reverse osmosis is the semipermeable membrane. This membrane should allow the transport of water while strongly rejecting dissolved salts or organic materials. Low water permeability leads to increased operating cost as increased pressure or larger membrane areas are required. Similarly, the leaking of solute through the membrane also leads to increased costs as multiple steps are required to produce a product with satisfactory quality.

The principle of reverse osmosis separation is illustrated in Fig. 1.1. In a container, two aqueous solutions having different solute concentrations are separated by a semipermeable membrane. Before osmotic equilibrium is established, the osmotic pressure difference, $\Delta\pi$, across the membrane is higher than the hydrostatic pressure, ΔP, applied to the concentrated solution ($\Delta P < \Delta\pi$). Under these conditions

water in the dilute solution migrates across the membrane to the concentrated solution. When the osmotic equilibrium is reached ($\Delta P = \Delta \pi$), the osmotic pressure difference, $\Delta \pi$, across the membrane is exactly counterbalanced by the hydrostatic pressure, ΔP, applied to the concentrated solution, hence there is no net flow of water across the membrane. If an external pressure, ΔP_{ex}, higher than the osmotic pressure, i.e. $\Delta P_{ex} > \Delta \pi$, is applied to the concentrated solution side, water flows from the concentrated solution to the dilute solution. This flow is a reverse of normal osmotic flow, and as a result this process is called reverse osmosis.[3] Reverse osmosis has been successfully used in seawater desalination to produce drinkable water as well as many other industrial separation processes.[1-5]

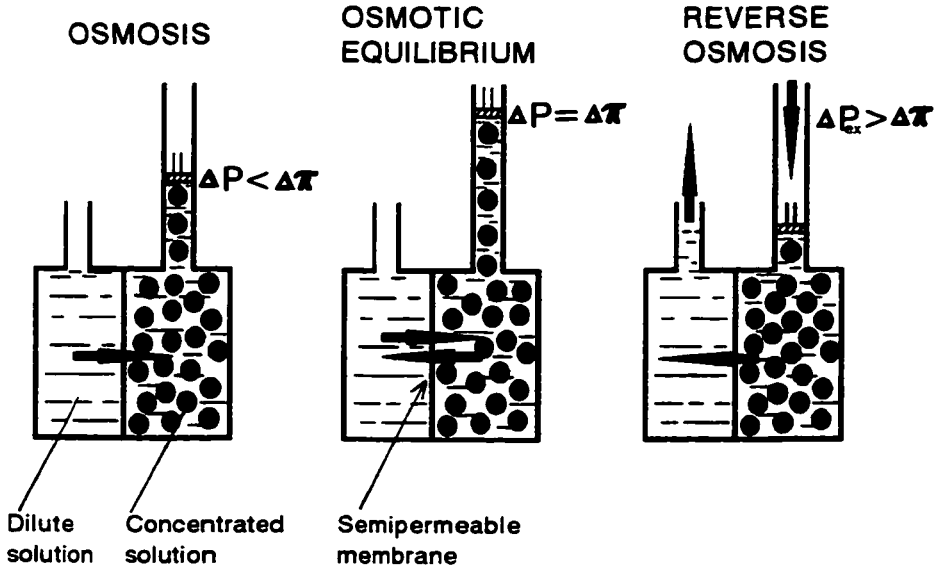

Fig. 1.1 Osmotic phenomena and reverse osmosis.

Flux and separation are two important parameters which characterize the efficiency of reverse osmosis. In the current work, the permeate flux across a membrane is expressed as kilograms of permeate solution per square meter of membrane per second, i.e. kg/m^2s.

$$FLUX=\frac{W}{At}$$

where W is the weight (kg) of collected permeate across the membrane during time t (s) and A is the membrane area (m^2).

Solute separation is defined by,

$$SEPARATION,\% = 100\left(\frac{C_F - C_P}{C_F}\right)$$

where C_F is the concentration (mol/L) of feed solution, C_P is the concentration (mol/L) of permeate solution.

The ideal membrane would exhibit a performance in which the separation is 100%, as the flux approaches infinity. In fact, this is impossible. Normally, a high separation is accompanied with a low flux. It is a challenging task to obtain both high flux and high separation.

1.2 Methods for Preparation of Skinned Membranes

In reverse osmosis separation, both experiment and theory have shown that the

permeate flux across a membrane decreases with an increase in thickness of the barrier layer of a membrane.[6-12] This has led to the formation of skinned membranes, in which a dense thin layer is supported on a more porous base membrane. The advantage of skinned membranes over homogeneous membranes lies in the use of an extremely thin skin layer to achieve high flux without any loss in selectivity.[1-5] The porous sublayer offers good mechanical properties to the membrane.

The phase inversion method developed by Lobe and Sourirajan[13,14] and interfacial polymerization method first used by Cadotte[15-17] are the two most important methods used in the preparation of the integrally-skinned asymmetric and nonintegrally-skinned thin-film composite (TFC) membranes, respectively. These two types of skinned membranes are the most important commercial types of reverse osmosis membranes.

The barrier layers are formed in different ways for these two different types of skinned membranes. In the phase inversion method, a concentrated polymer solution is cast onto a glass plate or onto a porous support. Partial evaporation of the solvent occurs giving rise to a higher local concentration at the surface. This is then followed by gelation in a precipitation bath to yield an asymmetric membrane, in which the skin and porous sublayers are composed of the same polymeric material. Except for high salt separation and flux, the asymmetric membrane approach has the advantage of being a low cost method of manufacturing membranes.[5]

With thin-film composite membranes, the barrier layer is prepared by an

interfacial polymerization on one surface of a porous support membrane. The skin layer is normally thinner than that of the asymmetric membranes. The major advantage of the thin-film composite membrane approach over the phase inversion method is that each layer of a composite membrane can be individually optimized for high separation, good chemical stability and high mechanical strength. In addition, large quantities of monomers are not required to fabricate the thin-film barrier layer. This allows the use of more expensive chemicals to fabricate the skin layer to yield special surface chemical properties.[17]

1.3 Structure of Thin-film Composite Membrane

A typical structure of a thin-film composite reverse osmosis membrane is schematically shown in Fig. 1.2. The top layer represents a thin barrier layer, **A**. This barrier layer, normally prepared by interfacial polymerization, has a thickness of less than 3 μm. This barrier layer is generally supported on a second porous layer, **B**, consisting of an asymmetric membrane prepared by the phase inversion method described above. It has a thickness between 50 and 100 μm and consists of the various zones as indicated in Fig. 1.2. The third layer, **C**, which may or may not be necessary depending on the mechanical strength of the top two layers, is usually an nonwoven cloth with a thickness around 100 μm. The function of this third layer is to provide mechanical strength.

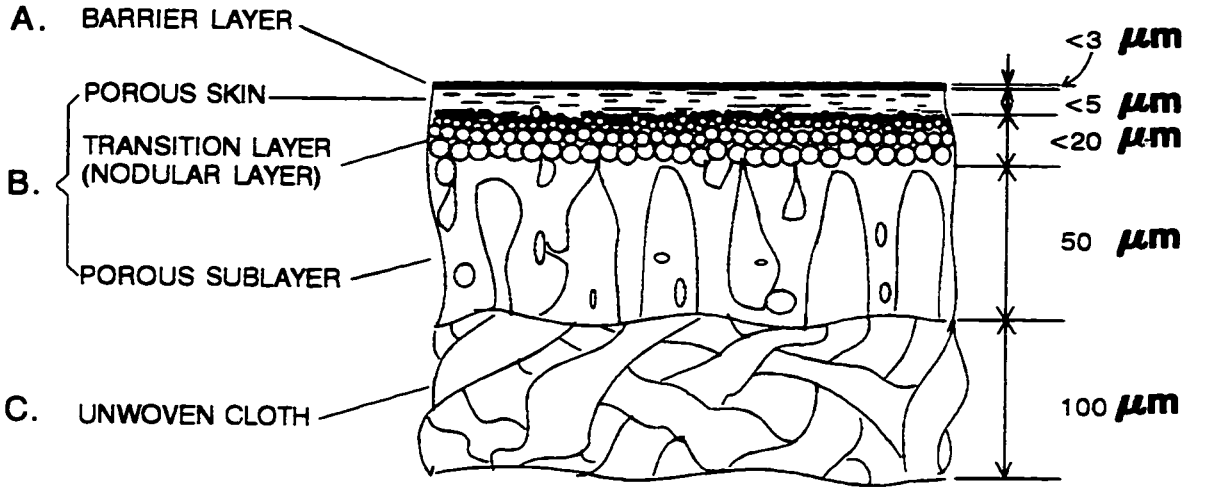

Fig. 1.2 Structure of a thin-film composite membrane.

1.4 Membrane Materials

Synthetic membranes can be made either of organic or inorganic materials. A variety of synthetic polymers have been used to fabricate membranes.

Membrane performance strongly depends on both the chemical nature and physical structure of a membrane, as well as on interactions of the membrane with the solvent and solute(s).[1-5] The chemical nature of a membrane can be controlled either by the initial selection of materials for its manufacture[1-5] or by chemical treatment after it has been formed.[5,18,19] On the other hand, the physical structure is mainly dependent on the fabrication methodology and chemistry.[20] However, in some instances, structure, can be altered by a post manufacturing treatment.[21]

The aromatic polyamide, **3**, is widely used to form the barrier layer of a TFC membrane.[5] Membranes based on **3**, show superior separation properties for seawater

desalination.[5] The polymer **3** is formed by interfacial polymerization of m-phenylene diamine, **1**, with trimesoyl chloride, **2**, Scheme 1.1.

Polysulfone, **4**, has been widely used as a support membrane material, which shows good chemical stability and mechanical properties.[5] The interfacial polymerization is carried out by treating an asymmetric membrane formed from **4** that is impregnated with an aqueous solution of m-phenylene diamine with an organic solution of the trimesoyl chloride.

In order to obtain a membrane with good separation performance as well as good mechanical and chemical stability, the choice of membrane materials must be carried out with due consideration of physicochemical effects, including dispersive

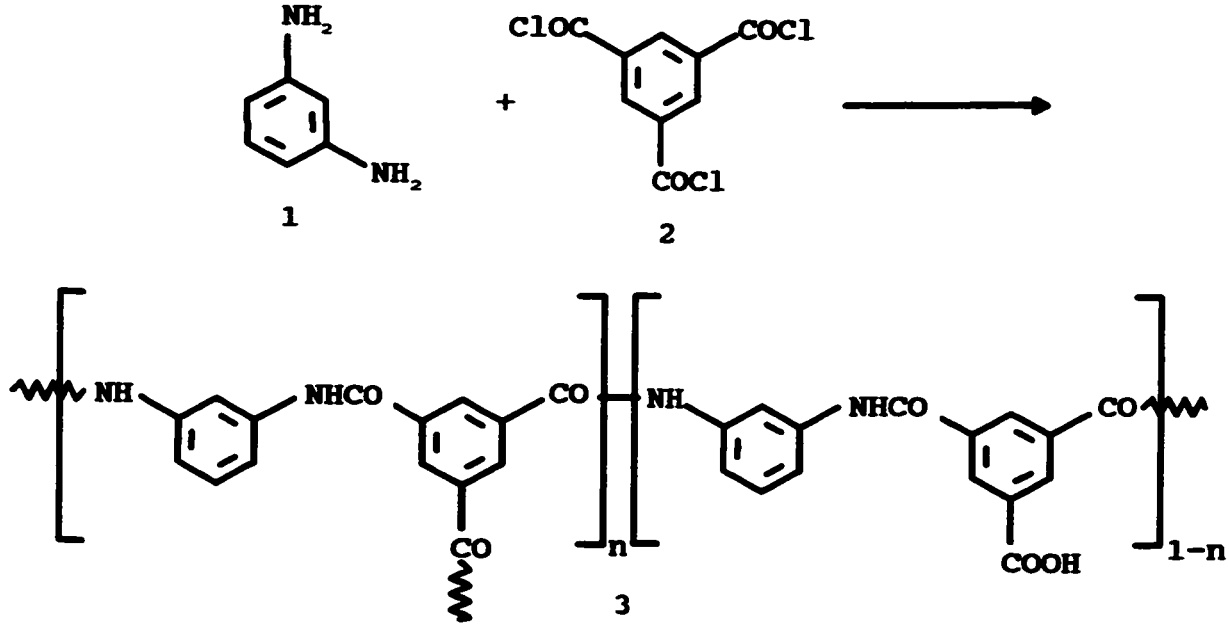

Scheme 1.1 Synthesis of FT-30 thin-film composite membrane.

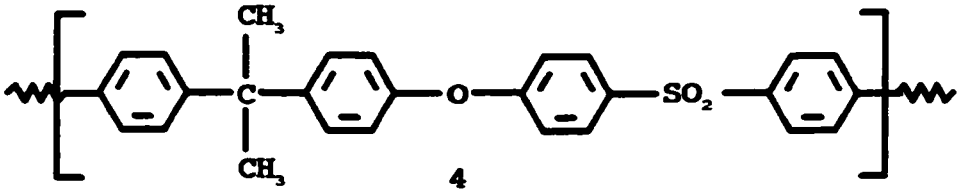

4

forces, polar interactions, hydrogen bonding and steric hindrance.[1-5,22-28]

Sourirajan, Matsuura and co-workers[23-27] have proposed guidelines for the selection of membrane materials based on both experimental and theoretical studies on reverse osmosis. They correlated Hansen's solubility parameters[29] with the results of reverse osmosis and HPLC measurements and found that polymers useful for barrier materials seem to have solubility parameters in the range of δ_h = 4-10 $cal^{1/2}$ $cm^{-3/2}$ and δ_d=7-10 $cal^{1/2}$ $cm^{-3/2}$, where δ_h and δ_d are the hydrogen bonding component and dispersion component of Hansen's solubility parameters. For example, the aromatic polyamide, 11, has δ_h = 9.30 $cal^{1/2}$ $cm^{-3/2}$ and δ_d=9.27 $cal^{1/2}$ $cm^{-3/2}$.[28]

Lloyd and Meluch[22] have explored the use of Hansen's solubility parameter as a basis for the estimation of dispersive forces, polar and hydrogen bonding interactions, and steric parameters Ψ_M (the effective size of the transport corridor within the membrane) and Ψ_i (the effective size of a permeate molecule) for evaluation of the steric effect.

Hoehn[30] has discussed the relationship between membrane structure and separation properties of aromatic polyamide membranes, developed by the Du Pont

company, in terms of four structure levels.

(I) segmental composition of polymeric membrane materials,

(II) steric relationship between the segmental structures,

(III) morphology of asymmetric membranes,

(IV) morphology of thin-film composite membranes.

Five diamine monomers and two diacid chloride monomers, used in the Du Pont polyamides, are shown in Scheme 1.2. The polyamides prepared from these monomers have different hydrophilicity and rigidity; factors which are important in determining the reverse osmosis properties of membranes prepared from these polymers. The polyamide, **11**, in Scheme 1.3 illustrates the importance of level II structure. It was found that the homopolymers of either 1,3-diamino benzene, **1**, or 1,4-diamino benzene, **5**, with either 1,4- or 1,3-benzene dicarboxylic acid chloride crystallized so readily that suitable casting solutions of these polyamides could not be made. This problem could, in principle, be overcome by using the thin-film composite membrane approach. In contrast, the polyamide prepared from mixed monomers of these four meta- and para-diamines and diacid chlorides not only show good casting properties but also excellent reverse osmosis separation properties. A space filling model of a segment of this polymer shows a relatively open character and low symmetry, compared to the homopolymers discussed above. A low level of segmental symmetry yields a more open membrane structure.

Structural characteristics of membranes on a microscopic level, defined by

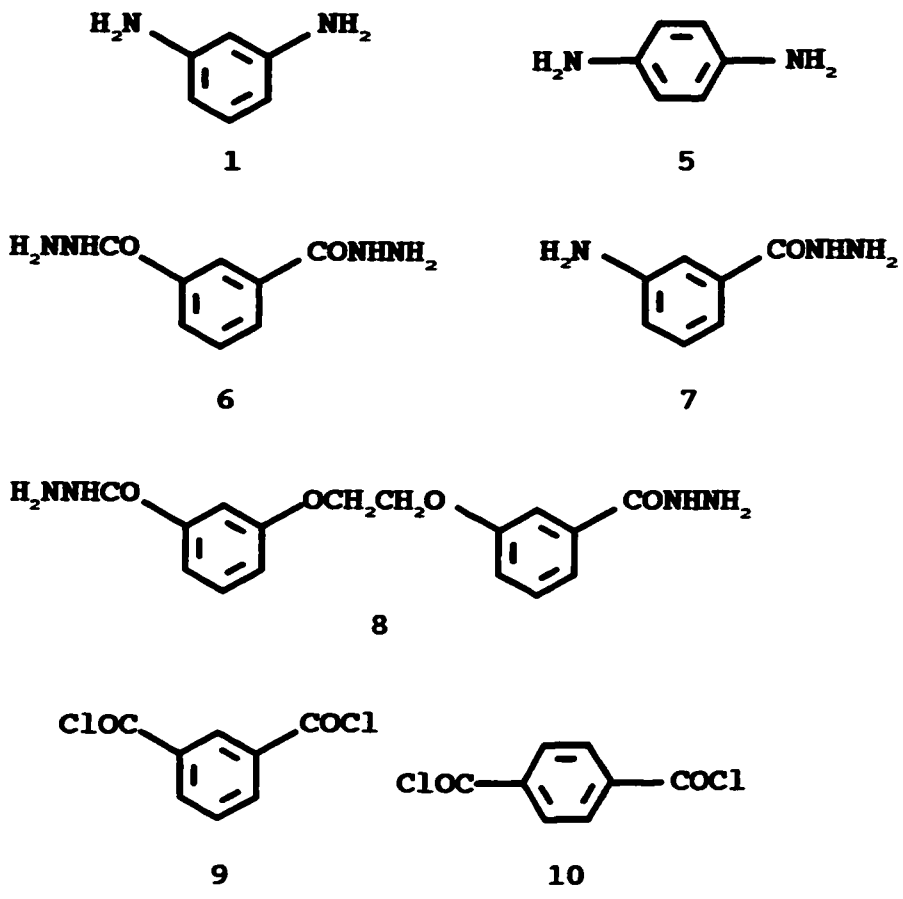

Scheme 1.2 Difunctional monomers used by Hoehn.[30]

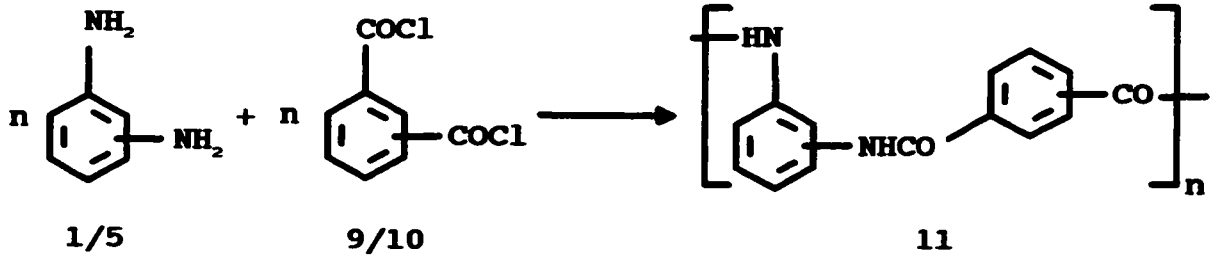

Scheme 1.3 Synthesis of aromatic polyamides.

Hoehn's level III and IV structures, strongly depend upon membrane preparation procedures for integrally- and nonintegrally-skinned membranes, respectively. The first three levels of membrane structure depicted by Hoehn have been well studied,[20,31-47] but the level IV structure and its effect on membrane performance still needs to be further studied.[5]

Lloyd and Meluch[22] used Hoehn's level I structure to establish a material selection index on the basis of hydrogen bonding, polar and dispersive interactions. The size parameter of the transport corridor, identified by Lloyd and Meluch[22] in dense membranes and the skin layers of asymmetric and thin-film composite membranes, can be related to Hoehn's level II-IV structures.[30]

The requirement for an appropriate ratio of hydrophilicity to hydrophobicity in barrier membrane materials has been widely accepted.[2,4,20,28] A variety of cellulosic and polyamide membranes are typical examples.

The incorporation of highly hydrophilic groups, such as -COOH and -SO_3H, into membranes has proven effective in increasing water flux across the membrane.[28] The commercial thin-film composite membranes FT-30 and NS-300 produced by interfacial polymerization are typical examples. The chemical structures of the barrier layer and synthesis of these membranes are shown in Schemes 1.1 and 1.4, respectively. Both membranes have pendent carboxylic acid groups.[5]

Cadotte and co-workers[5] have reported the sulfonation of a polysulfone membrane. Polysulfone, **4**, having both diphenyl sulfone and bisphenol-A-groups in

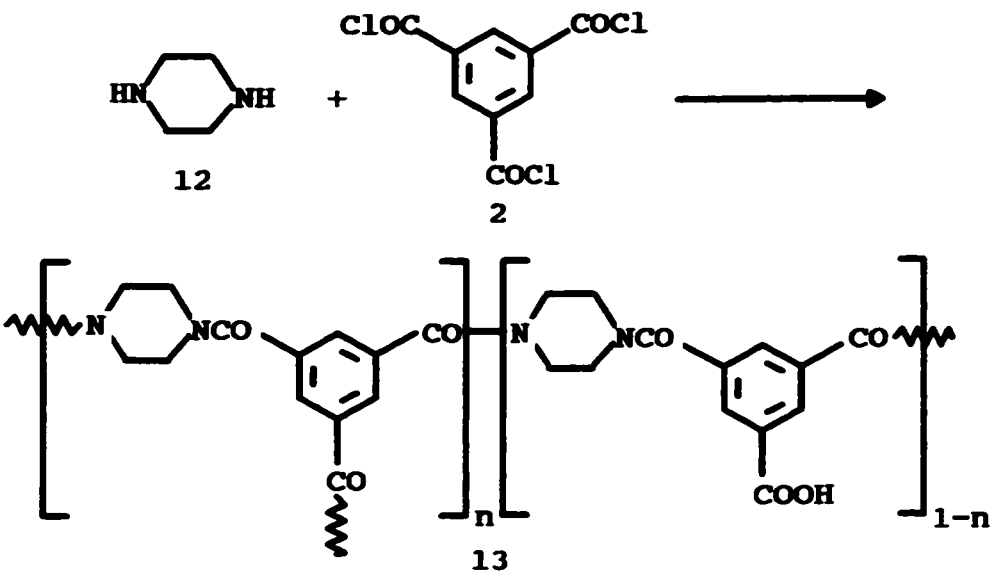

Scheme 1.4 Synthesis of NS-300 membrane.

the polymer backbone, could be selectively sulfonated by using chlorosulfonic acid to yield water soluble sulfonated polysulfone as shown in Scheme 1.5 to introduce hydrophilic groups.

A composite membrane was prepared by coating **14** onto a polysulfone support. The degree of modification of polysulfone rings was reported to be controllable by varying the amount of chlorosulfonic acid used, thereby generating differing degrees of hydrophilicity. Crosslinking was achieved via the addition of polyols or polyphenols and the formation of sulfonic acid ester linkages. Unfortunately, sulfonic acid esters are not particularly stable to hydrolysis, which led to a low chemical stability of this type of membrane.

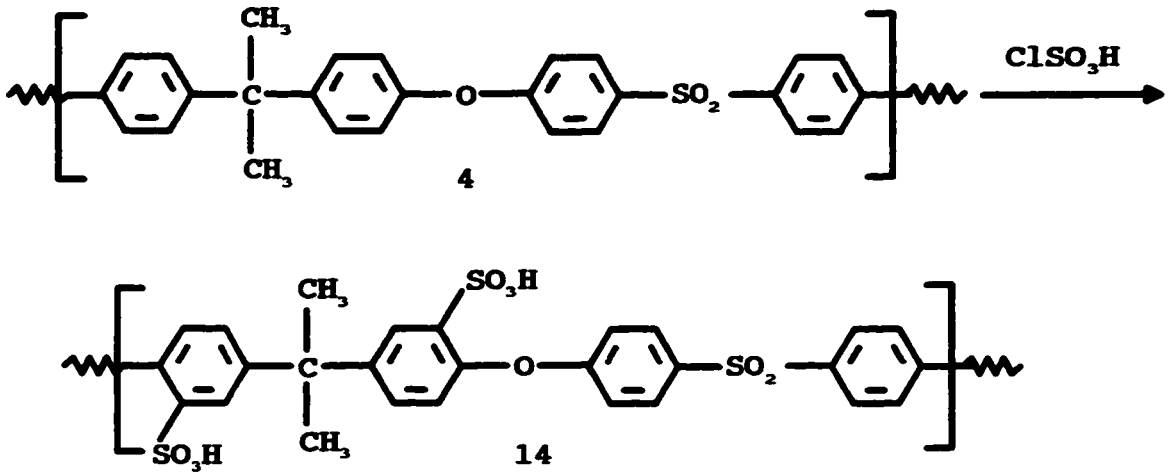

Scheme 1.5 Preparation of sulfonated polysulfone.

More recently, Nolte et al.[48] reported the formation of a partially sulfonated poly(arylene ether sulfone) membrane, **16**, that has versatile proton conducting properties and is used as a solid polymer electrolyte in electrolysers and fuel cells. Preparation of sulfonated poly(arylene ether sulfones), **16**, is shown in Scheme 1.6. Crosslinking was achieved by sulfonamide formation using a diamine. Thus, the sulfonic groups of the polymers were activated by reaction with 1,1'-carbonyl diimidazole, **17**, to yield the more reactive N-sulfonyl-imidazole, **18**. This subsequently reacts with diamines to give a crosslinked sulfonated polysulfone, **21**, with sulfonamide linkage as illustrated in Scheme 1.6. The stability problem of sulfonic acid ester linkages encountered in Cadotte's work[5] can be resolved by the use of the polysulfonamide crosslinking.

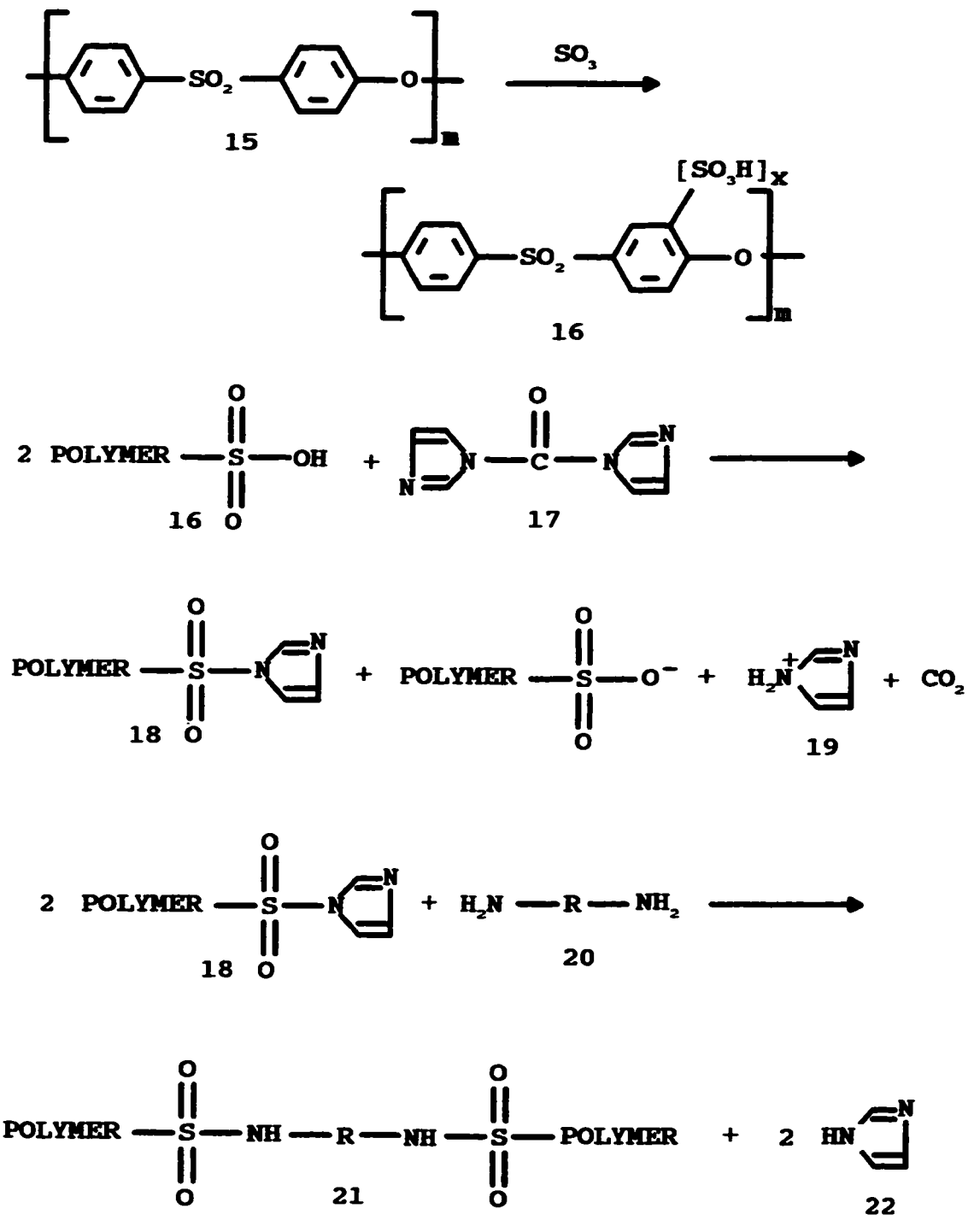

Scheme 1.6 Chemical modification of polysulfone.

Alternatively, an appropriate ratio of hydrophilicity to hydrophobicity in membrane materials has been achieved by incorporating carboxylic acid groups into polysulfones. Guiver and co-workers[49,50] modified Udel P-1700 polymer by lithiation, followed by carbonation to put carboxylic acid groups in the ortho positions to the sulfone linkages yielding polymer **23**, Scheme 1.7. Carboxylated polysulfone having 0.62 acid groups per polymer repeat unit was cast into asymmetric membranes for reverse osmosis.

Himeshima and Kurihara[51,52] have reported the incorporation of carboxylic acid groups into the bisphenol rings of Udel P-1700 by reacting with acetyl chloride, catalyzed by aluminum chloride to place acetyl groups on the phenyl rings. This was followed by a haloform reaction to convert acetyl into a carboxylic group, as displayed in Scheme 1.7. The membrane prepared from the carboxylated polysulfone, **24**, showed an increased water flux as compared to that from the unmodified polysulfone, **4**.

The chemical stability of membrane materials is also important, particularly in terms of industrial applications. In spite of the superior separation properties of polyamide based membranes, these membranes were reported to be susceptible to oxidation and hydrolysis under strongly basic or acidic conditions.[5] In the hope of achieving more chemically stable membranes, poly(amide-sulfone), **26**, and poly(amide-sulfonamide), **30**, based membranes have been developed.[53-57] The synthesis of **26**[53] and **30**[56-60] are shown in Schemes 1.8 and 1.9, respectively. It should

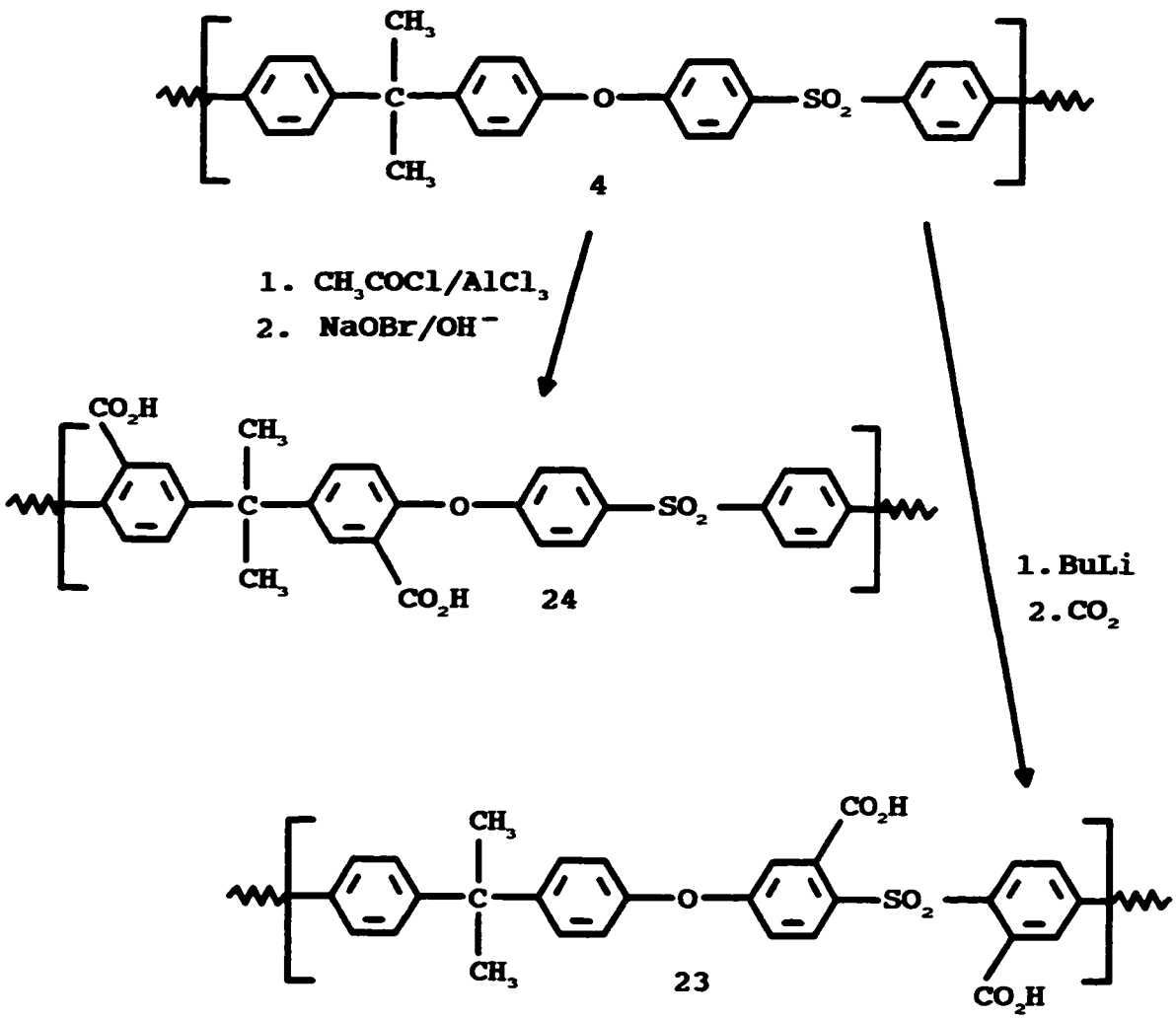

Scheme 1.7 Modification of polysulfone.

be noted in contrast to the authors claim **26** can not be classified as a polysulfonamide.[53]

Although each of the polymers **26** and **30**, have an amide functionality, they appear to be more stable than most polyamide films due to the presence of electron-withdrawing groups in the backbone of the polymers. Wang et al.[54] reported that after an 8 month test using 5-10 g/L CrO_3 solution at 4000 kPa and 25 °C, no significant change in performance was observed for a membrane based on the poly(amide-sulfone), **26**. Infrared spectra showed that after the 8 month separation test with chromium waste water, all of the characteristic absorption bands of the membrane were the same as those of a fresh poly(amide-sulfone) membrane, **26**. No significant change in the IR spectrum of a **26** based membrane was observed after immersion in an aqueous NaOH solution at pH=12 for 14 months. It was suggested that the electron-withdrawing sulfone groups in the polymer backbone were responsible for the increase in chemical stability of the membranes based on **26** as compared to simple polyamides, such as **3** and **11**, towards oxidation and hydrolysis.[53-55] The authors reported that longer exposure (34 months) to aqueous CrO_3 solution caused degradation of the polymer.[54]

Chan et al.[56,57] have reported that poly(amide-sulfonamide), **30**, based membranes showed good reverse osmosis properties and good chemical resistance towards hydrolysis and oxidation compared to simple polyamide based membranes.

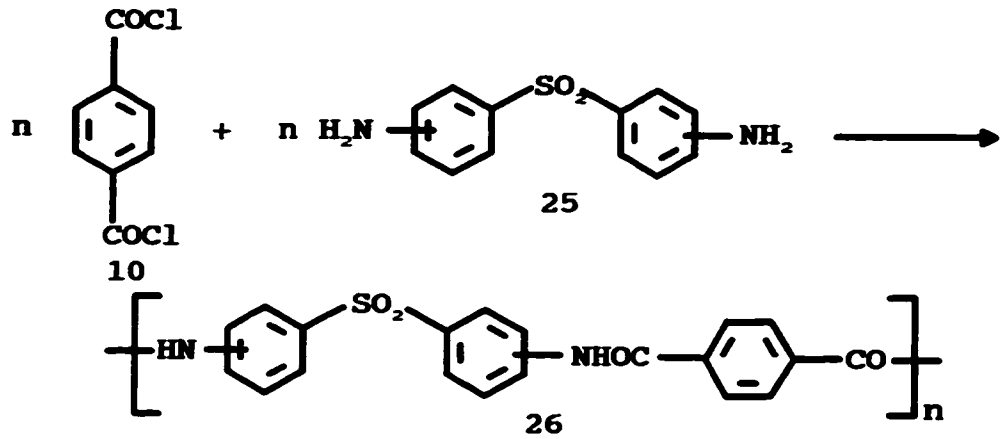

Scheme 1.8 Synthesis of poly(amide-sulfone).

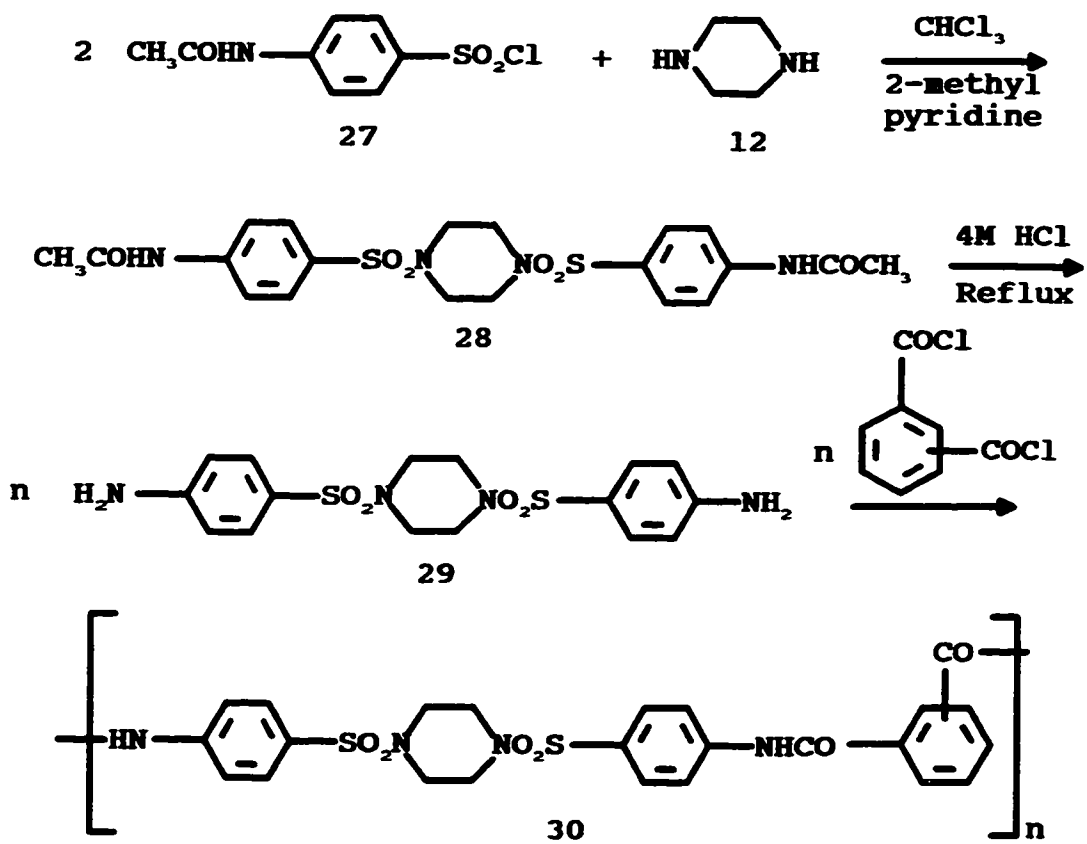

Scheme 1.9 Synthesis of poly(amide-sulfonamide).

1.5 Modification of Preformed Membranes

A variety of polymers have been used to prepare membranes designed to meet the needs of specific separations.[1-5] For example, Lloyd and Meluch[22] listed more than twenty-seven polymers, copolymers and blends used for liquid separation membranes in their 1985 review article. Since then, the number of different polymers used as membrane materials has rapidly increased.[5]

Optimization of the chemical nature and physical structure of a membrane can be a lengthy task. Any change in the polymer selected for either the base membrane or the thin film requires that such an optimization be undertaken. This is not very efficient. Therefore, a variety of methods have been developed to modify preformed membranes. The intent of most of these chemical treatments is to introduce functional groups onto the membrane surface.

Kobayashi et al.[61] reported the modification of commercial polyethylene hollow fiber membranes by electron beam radiation-induced grafting and subsequent chemical modification. Typical reactions are shown in Scheme 1.10. Commercial polyethylene hollow fibers were irradiated with an electron beam. Immediately following the irradiation, the membrane was exposed to a vinyl monomer. It is well known that irradiation of a polyolefin with an electron beam leads to the formation of radicals. The addition of the vinyl monomer allows a radical induced polymerization to occur. For an anion exchange membrane **33**, the polyethylene trunk polymer, **31**, was grafted with vinyl pyridine which was then quaternized with benzyl chloride.

Tsuneda et al.[62,63] used the same electron beam activation approach to modify commercially available porous polyethylene hollow fiber membranes. The chemistry involved is also shown in Scheme 1.10. The base polyethylene membrane was grafted with acrylonitrile and glycidyl methacrylate (GMA), respectively. The acrylonitrile grafted membrane could be reacted with a hydroxylamine to yield a membrane having amidoximine groups as chelating ligands, **34**. The glycidyl methacrylate grafted membrane, **35**, could be reacted with iminodiacetate (IDA) to yield a membrane having iminodiacetate moieties as chelating ligands, **36**, Scheme 1.10. The modified membranes **34** and **36** having chelating ligands were used for the recovery of metal ions.[64-66]

It should be noted that the chemistry summarized in Scheme 1.10 was not demonstrated by chemical characterization of the membranes, but inferred from the expected results of the reaction condition used. This lack of chemical characterization is a common problem often found in membrane literature. Characterization is difficult but necessary for a proper understanding of membrane performance.

A different approach has been developed by the McMaster membrane group.[67] Microporous polypropylene or polyethylene flat sheet membranes were irradiated in the presence of benzoin ethyl ether and vinyl pyridine. The mass gain can be controlled from a few percent up to about 200%. The polyvinyl pyridine grafted membrane behaved like a pH valve with a stepwise change in permeate flux of 3 orders of magnitude with small change in pH of the feed solution.

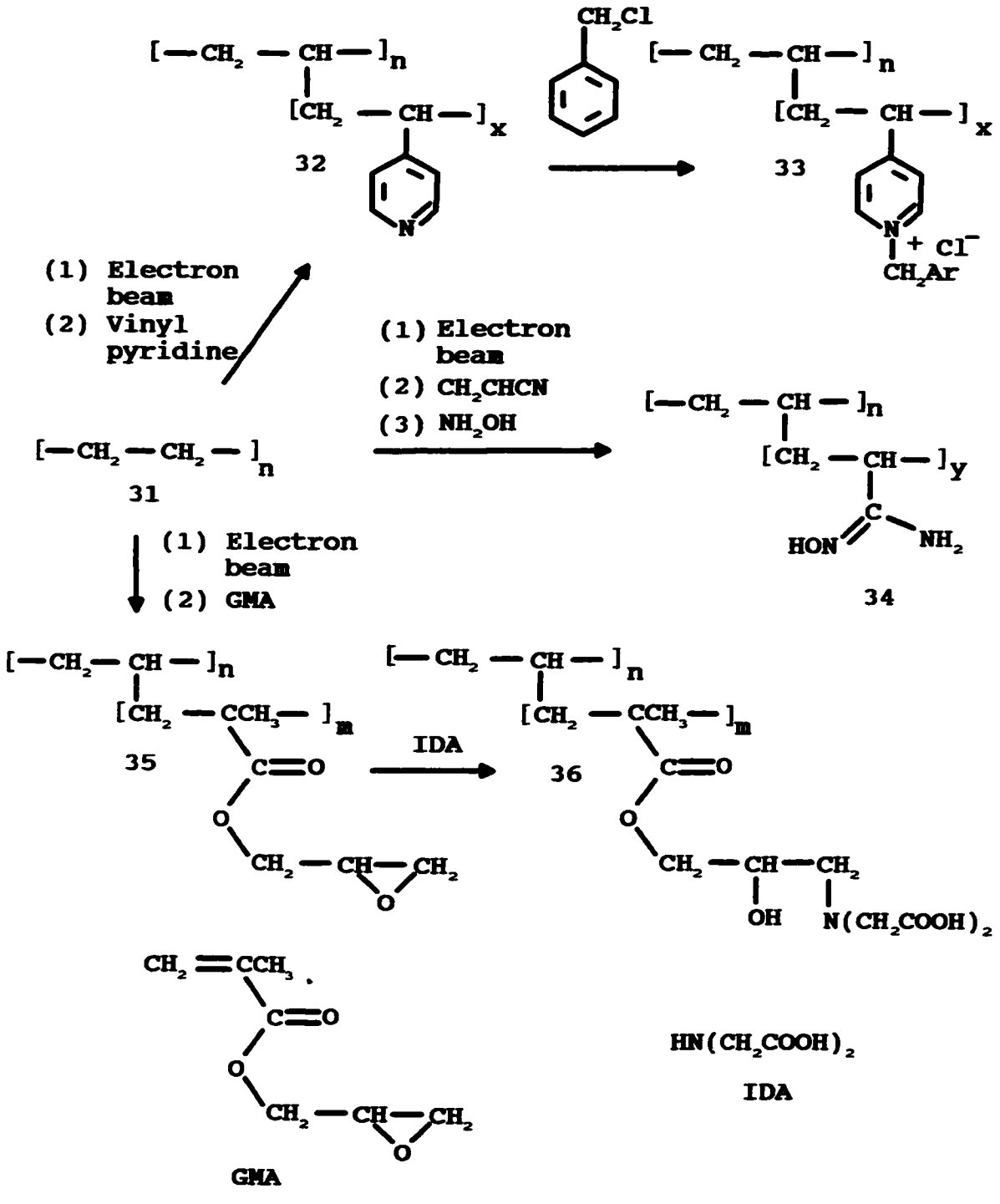

Scheme 1.10 Electron beam radiation-induced grafting and subsequent chemical modifications.

Grafting is an effective approach for the introduction of new functionalities to various forms of existing polymeric membranes.[62] More than 100% mass gain can be easily achieved by grafting, and this leads to a high degree of functionalization.[63,67] In spite of this advantage, special equipment, and severe pretreatment of the solvent and reactant to remove radical scavengers, such as oxygen, are often required in these grafting reactions. Self polymerization of the grafting reagent can compete significantly with graft polymerization reducing the efficiency of the grafting reaction. Although reproducible and controllable results have been reported, the effective control of grafted polymer chain length, and chain length distribution, which affect membrane performance and reproducibility, are still challenging tasks.

An alternative approach that claims to improve the hydrophilicity of membranes is photochemical surface modification. Nyström and Järvinen[68] modified polysulfone ultrafiltration membranes by UV irradiation in the presence of water or ethanol. Nyström and Järvinen[68,69] proposed that irradiation of the polysulfone membrane at 254 nm causes the polysulfone to undergo a variety of possible bond scissions as shown in Scheme 1.11. No characterization on these radicals was made. The subsequent radical reactions were not discussed in detail, however, it was suggested that sulfonic acid groups are formed from the combination of sulfonyl radicals with hydroxyl radicals under those conditions.[69]

The bond scission reactions proposed by Nyström and Järvinen (see Scheme 1.11) cause polymer degradation. Hence, the degree of modification has to be kept

at a low level in order to maintain the integrity of the modified membrane. In spite of this limitation, Nyström and Järvinen were able to demonstrate in the separation of proteins from aqueous solutions that the photochemical surface modification significantly increased flux due to the increase in membrane hydrophilicity. Flux increases of up to a factor of 4 were achieved. The flux was found to vary with pH and the type of modification agents used. The best retention of the proteins was observed when both the protein and the membrane were negatively charged as a result of strong electrostatic repulsions between the proteins and the membranes.

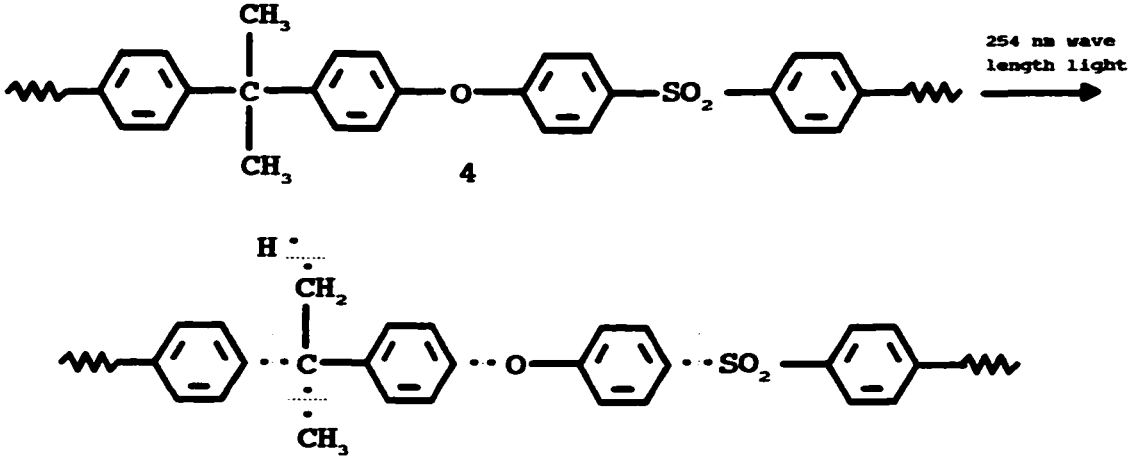

Scheme 1.11 Chain scissions induced by UV irradiation of polysulfone.

The major drawbacks of the photochemical surface modifications presented above lies in the irradiation of membranes with short wavelength (high energy) UV light. This causes both polymer degradation, due to the bond scission of polymer backbone, and poor chemical selectivity in the modification reactions. Poor

reproducibility is often observed in these reactions. For this reason, the degree of modification has to be low, and often lower than that obtained using the other approaches discussed above. As a result the photochemical surface modification by direct irradiation of membranes with high energy UV light is not as popular as the other modification methods discussed above.

1.6 Modification of Photolabile Thin-film Composite Membranes

In order to overcome the fundamental problems discussed above, particularly those encountered by the direct irradiation of membranes with high energy (short wavelength $\leq$254 nm) UV light, the membrane group at McMaster has developed a unique approach for the modification and efficient functionalization of thin-film composite membranes.[21,70-72] The strategy is illustrated in Scheme 1.12. Photolabile groups are introduced into the surface layer of a thin-film composite membrane by interfacial polymerization involving photoreactive monomers. The photoreactive precursor membrane is subsequently irradiated using long wavelength light in different reactive media to give different surface properties.

The photoreactive thin-film composite membrane, **40**, having a photolabile diazoketone group in the backbone was synthesized by interfacial polycondensation of the diazoketone-containing disulfonyl chloride, **37**, and 1,3,6-naphthalene trisulfonyl chloride, **38**, with 1,6-hexanediamine, **39**, on the surface of a commercially available polysulfone ultrafiltration membrane (Scheme 1.13). The use of sulfonamide linkages

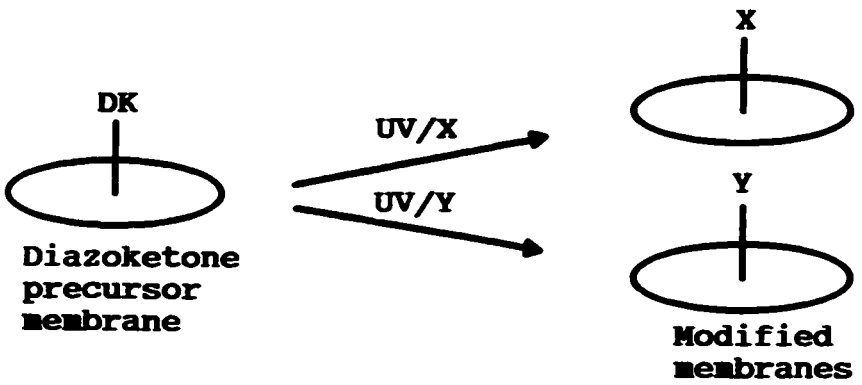

Scheme 1.12 Strategy for photochemical surface modification of a TFC membrane.

in the polymer backbone was expected to increase the chemical stability of the membrane as compared to the more generally used polyamides.

Subsequent photochemical surface modification was accomplished by exposure of the photolabile precursor membrane, **40**, to light (350 nm wavelength), Scheme 1.14. Various functionalized membranes having different surface properties were obtained by photochemical surface modification of the precursor membrane, **40**, in different chemical media. For example, irradiation in water yielded a membrane having indene acid groups. The use of ethanol as a solvent produced a membrane having indene acid ethyl ester groups in the thin-film barrier layer. The degree of functionalization obtained by this method was high as each repeat unit of the polymer contained one or more functional groups. In addition, the reproducibility of photochemical modification reactions can, in principle, be well controlled.

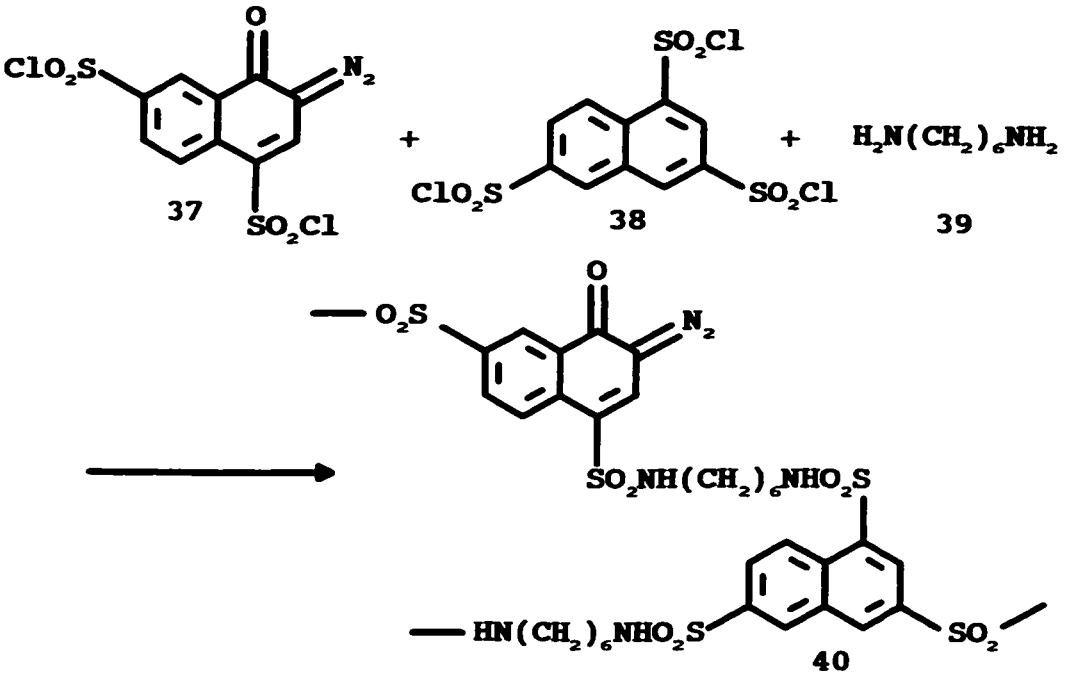

Scheme 1.13 Synthesis of a photoreactive TFC membrane.

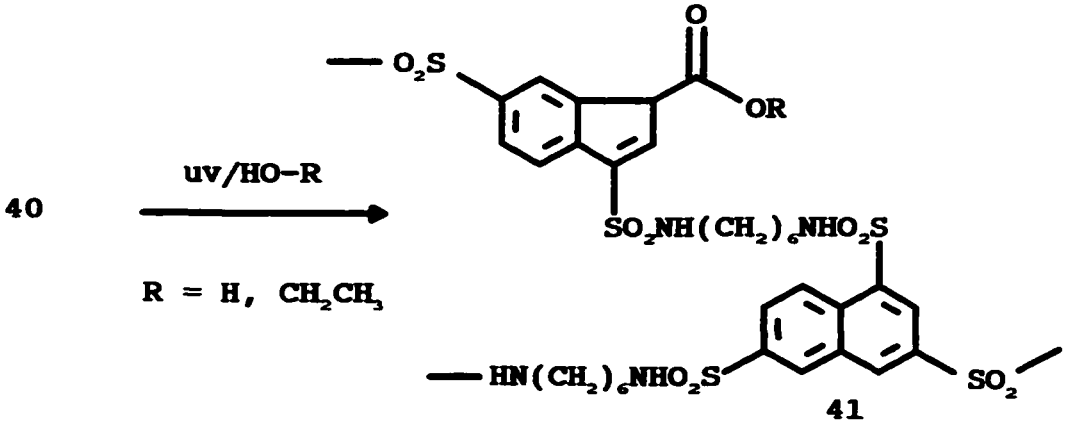

Scheme 1.14 Photochemical surface modification of TFC membrane.

The advantage of the approach developed by the McMaster membrane group over the other photochemical approaches discussed above is that the photolabile diazoketone groups were incorporated into the thin-film composite precursor membrane prior to the photochemical modification, thus allowing the use of low energy 350 nm wavelength light. In contrast to the high energy UV light employed by Nyström and Järvinen,[68] such a low energy UV light significantly reduces degradation of the base polymeric membrane material. High selectivity, reactivity, and yield of surface modification reactions and a high degree of the modification have been successfully achieved. The problems associated with polymer degradation, poor selectivity, poor reproducibility and a low degree of modification encountered in the photochemical modification of membranes by direct irradiation with short wavelength UV light[68] have, to a large extent, been overcome by the previous work of the McMaster membrane group.[21, 70-72]

Despite the obvious potential of the approach developed by the McMaster membrane group to the surface modification of membranes, the existing delivery system needs to be improved or developed in the following aspects.

(1) The monomer used in previous work was prepared in low overall yield by a difficult seven step synthesis. A simpler method is needed.

(2) The diazoketone functional group was incorporated into the backbone of the thin-film polymer. This could lead to a change in conformation of

the polymer as the six-membered ring is converted into a five-membered ring during the photochemical modification (Scheme 1.14).

(3) The factors that influence interfacial polymerization and membrane performance need to be systematically studied.

(4) The types of functional groups introduced by photochemical surface modification of diazoketone precursor membrane need to be further expanded.

The current work described here builds on the past work of the McMaster membrane group and seeks to address some of the outstanding problems alluded to in the previous paragraphs.

1.7 Objectives of the work

The objectives of this work are as follows:

1. to develop a more readily accessible diazoketone-containing monomer that will lead to the photoreactive group being incorporated as a side chain to the backbone of the resulting polymer,
2. to broaden the range of photochemical transformations which can be achieved with the surface modification of the diazoketone membrane,
3. to develop methods to characterize the surface chemistry of these membranes,

4. to investigate methods of studying the impact of photochemical surface modification on membrane performance,
5. to develop a model for thin film formation by interfacial polymerization.

Incorporation of the photolabile diazoketone group into a side chain of the polymer avoids a possible effect of ring shrinkage on membrane structure and performance discussed above. In addition, the functional group in a side chain is more accessible to interact with a solute than in the backbone of the polymer. This might enhance the separation performance. For example, Cussler et al.[73] have reported for facilitated transport that the efficiency of the solute transport and separation depends strongly on the mobility of the chained carriers in the membrane.

In order to synthesize a new monomer that will lead to the photoreactive group being incorporated as a side chain to the backbone of the resulting polymer, a commercially available diazoketone containing sulfonyl chloride is connected to a naphthalene trisulfonyl chloride through a piperazine spacer. A sulfonamide, formed from 1,2-ethanediamine and a naphthalene disulfonyl chloride, is used as a key linkage in the polymer backbone. The combination of the rigid naphthalene moiety with the flexible ethanediamine moiety is expected to give a good thin-film barrier layer, and the sulfonamide linkage is expected to give the membrane good chemical stability.

To broaden the range of the photochemical transformation, model reactions are

used to establish the chemistry required for surface modification of the diazoketone membrane. These photochemical transformations will produce a variety of membranes having different surface chemical properties. This allows a study of the impact of surface chemistry on membrane performance. Two methods are studied to transform photochemically the diazoketone membrane to different ester functionalized membranes in an attempt to optimize the conditions for the transformation.

In order to characterize the photochemically modified membranes, the methods to prepare samples for surface analysis are studied by preparing a thin film as a control using liquid-liquid interfacial polymerization and by pealing the skin layer of a TFC membrane. In combination with attenuated total reflectance FT-IR and transmittance FT-IR, these methods allow the chemical structure of the barrier layer of a TFC membrane to be characterized and the photochemical surface modification of a TFC membrane to be monitored.

In order to investigate the impact of the photochemical surface modification on membrane performance, the modified membranes are evaluated by the separation of inorganic solutes from aqueous solutions and then compared with the parent diazoketone membrane.

Both the experiment and membrane transport theory indicate that the permeate flux across a membrane increases with the decrease in the thickness of the barrier layer.[6-12] Effective control of the thickness of the barrier layer is very important to the control of the flux. However, after an extensive search, no systematic study on the

thickness of the barrier layer of a thin-film composite membrane has been reported. The thickness of the barrier layer of a TFC membrane is, to a large extent, determined by a trial and error method. This is not very efficient. The major difficulty in the study of the formation of the barrier layer by interfacial polymerization is due to the nonsteady-state nature as the monomer concentration and the thickness change with time during the interfacial polymerization. A clear understanding of the factors that influence the thickness of the barrier layer of a TFC membrane is very important to the efficient control of the barrier layer thickness and membrane performance. Thus, a model for thin film formation by interfacial polymerization under nonsteady-state conditions is developed by considering both monomer diffusion and interfacial reaction, to establish the relationships between the thickness of the barrier layer and the kinetics of interfacial polymerization in an attempt to provide a guide for effective control of the thickness of the barrier layer of a TFC membrane.

Monomer synthesis and model reactions to establish the chemistry for modification of the diazoketone precursor membrane are investigated in Chapter 2. Preparation of a thin-film composite diazoketone precursor membrane is discussed in Chapter 3. Photochemical surface modification, characterization of the TFC membranes and the impact of the photochemical surface modification on membrane performance are studied in Chapter 4. A theoretical model for the formation of a dense membrane by interfacial polymerization is developed in Chapter 5. A more

general model for the formation of both dense and porous membranes is described in Chapter 6, in which the theoretical prediction is compared with the experimental results. Finally, the conclusions drawn from the above chapters are summarized in Chapter 7. Chapters 3 to 6 are written in a style to facilitate submission to journals.

The molar concentration, M (mol/l), is often used for a chemical thesis and the SI unit of $kmol/m^3$ is often used for an engineering thesis. These two units are identical in values. Since this thesis studies both chemistry and engineering modelling, these two units are used exchangeably in this thesis.

Chapter 2

Monomer Synthesis and Model Reactions

2.1 Monomer Synthesis

The first step in the entire project is to incorporate photolabile diazoketone functional groups into the side chain of a polymer. This requires the synthesis of a new monomer.

The diazoketone, **42**, was commercially available. The key to forming a covalently bound pendant group in a polymer was to react the diazoketone with other molecules to link to a suitable difunctional monomer for use in an interfacial polymerization. As the previous work of the McMaster membrane group involved the formation of polysulfonamides, polymers which offer the promise of enhanced chemical stability over the more often used polyamides,[21,72] it was decided to prepare a monomer containing two sulfonyl chloride groups. In order to accomplish this, **42** was reacted first with piperazine, **12**, to give **43** (Scheme 2.1), which was subsequently treated with 1,3,6-naphthalenetrisulfonyl chloride, **45**, to give a mixture of disulfonyl chlorides **47**. In each step, a sulfonamide linkage was formed. The reaction mechanism between sulfonyl chlorides and amines in homogeneous solutions have been well studied and the nucleophilic addition-elimination mechanism has been

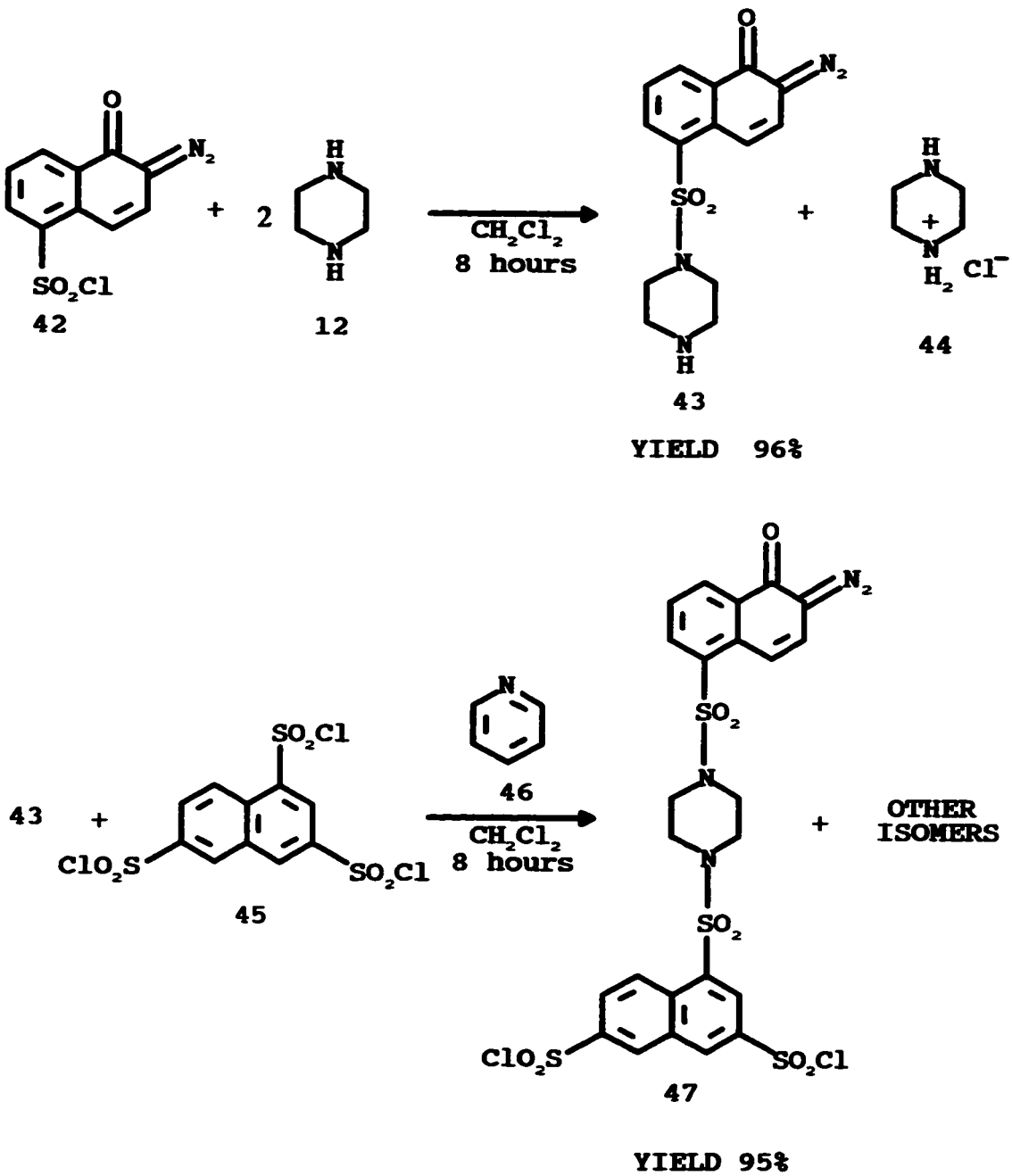

Scheme 2.1 Synthesis of 47.

proposed.[74-78] The sulfonamide formation reaction is catalyzed by pyridine, triethylamine, and other bases.[79-86] Dichloromethane and toluene have proven to be good solvents for the reaction.[84-86] Therefore, pyridine was used as an acid acceptor and either dichloromethane or toluene were used as solvents in the synthesis of compound **47**.

The reaction of **42** with **12** was carefully examined in order to achieve a high yield of compound **43**. It was found that with a 1:2 molar ratio of **42** to **12**, and the selection of a solvent in which the by-product, **44**, was insoluble and could be removed by filtration, high yields of **43** could be obtained. With toluene as a solvent, **43** could be obtained as a crystalline solid in 82% yield. The product **43** was fully characterized and shown to have the indicated structure. In terms of a preparative route to **43** it was found to be more convenient to use CH_2Cl_2 as a solvent, however, while in this case the isolated material was not crystalline, it had identical spectroscopic properties and melting point to that prepared using toluene.

The reaction of **43** with **45** can potentially yield three different products. It was found that this reaction proceeded well in CH_2Cl_2 as a solvent, in the presence of pyridine as a proton acceptor. Pyridinium hydrochloride and any excess pyridine could be removed by washing with water. NMR examination of the product revealed that **47** had been formed as a mixture of isomers. Attempts were made to isolate the different isomers using column chromatography. However, these attempts were not successful and the mixture was used in the subsequent polymerizations. The mixture

of isomers, **47**, was fully characterized using spectroscopic techniques and elemental analysis.

The synthesis of **47** from **43** and **45** is shown in Scheme 2.1. The conditions were optimized so as to obtain a high yield of **47**.

Initially (method 1), **43**, **45** and **46** in a molar ratio of 1:1.05:2 was used. The reaction was carried out in dichloromethane at room temperature for 8 hours. The ^{1}H NMR spectrum of a crude product, obtained after removal of dichloromethane, is shown in Fig. 2.1 (A). The peaks attributed to the protons attached to the naphthalene moieties of compound **47** can be clearly seen, along with three strong peaks marked with a "Py", which are attributed to pyridine. Purification of the mixture using column chromatography with silica gel as a stationary phase was attempted. Four fractions were collected and the ^{1}H NMR spectra are displayed in Fig. 2.1 (B)-(E). The first fraction was unreacted **45**, characterized by spectrum (B) in Fig. 2.1. The remaining fractions appeared to be **47**, characterized by spectra (C)-(E) in Fig. 2.1, which are consistent with the indicated structure of **47** (Scheme 2.1). This result is also consistent with elemental analysis. In addition, the ^{1}H NMR spectrum of each fraction has a broad peak at 3.29 ppm (not shown in Fig. 2.1), which is attributed to the hydrogen atoms of the piperazine moiety of **47**. This is a characteristic of disubstituted piperazine derivatives. Instead of a broad peak at 3.29 ppm, mono-substituted piperazine, such as **43**, shows two peaks at 2.89 and 3.12 ppm, respectively. Spectra (C) and (D) suggest that the composition of three isomers

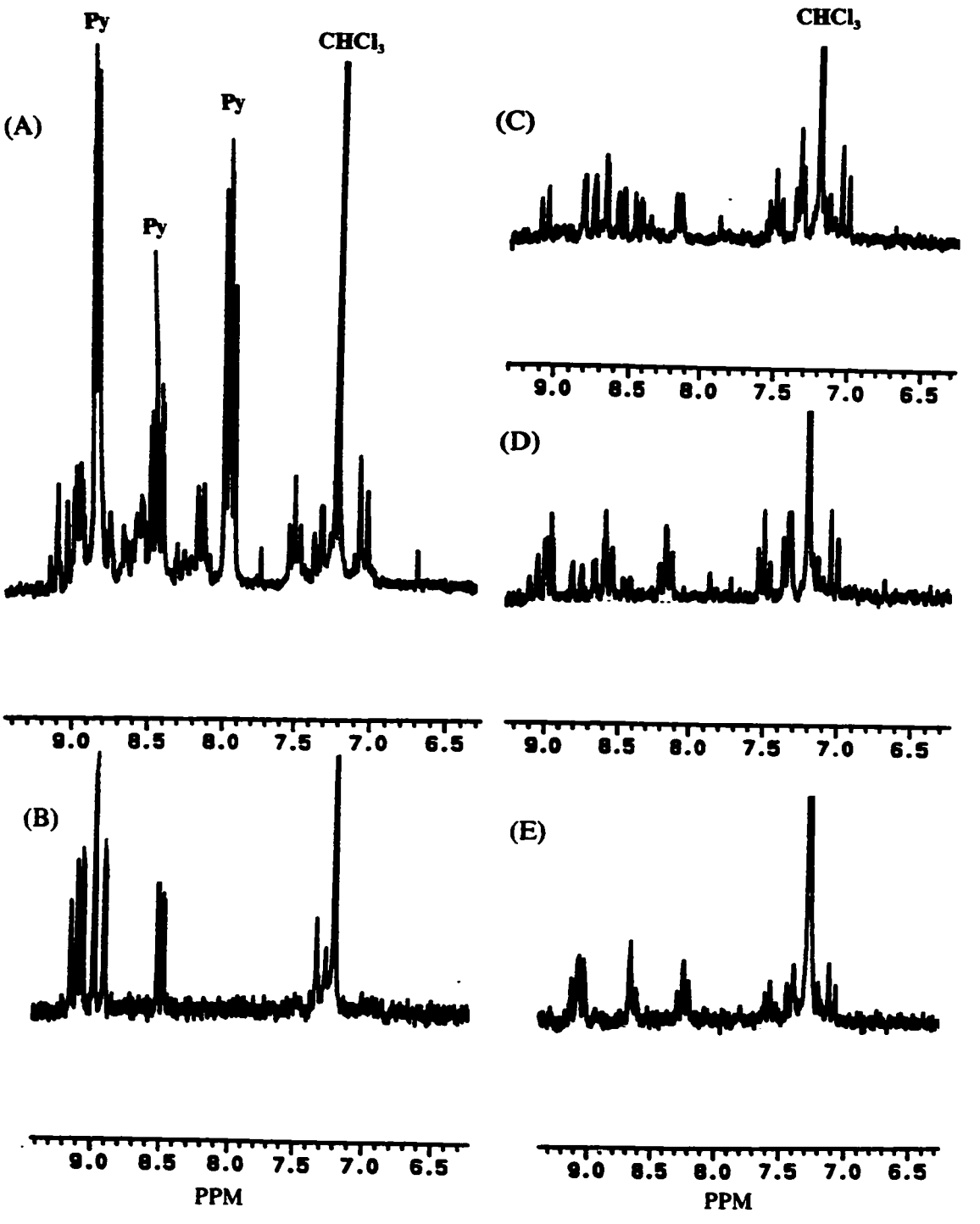

Fig. 2.1 ^{1}H NMR ($CDCl_3$) spectra of crude product **47** prepared by method 1 and fractions obtained from column separation using silica gel as stationary phase.

(A) crude product of **47**, (B) first fraction, (C) second fraction,
(D) third fraction, and (E) fourth fraction.

of **47** was different in each fraction, spectrum (E) seems to be attributed to one of the isomers.

It was observed from the ^{1}H NMR spectra of **47**, that the product usually contained about 1% of the solvent that it was last in contact with. It was not possible to remove this solvent even when the product was dried *in vacuo* at 50 °C for 8-24 hours.

Although method 1 led to the formation of the isomers of **47**, the purification of the product could only be achieved using column chromatography. This is not a practical method of preparing large quantities of **47** for membrane fabrication. Hence, alternative conditions were studied.

Secondly (method 2), in order to reduce the formation of possible di- or tri-substitution of **45**, a reaction in which there was an excess of **45** was examined. A molar ratio of **45**:**43**:**46**=1.2:1:1 was used resulting in a 91% yield of **47**. As 1,3,6-naphthalenetrisulfonyl trichloride, **45**, is soluble in diethyl ether, but **47** is insoluble, the unreacted **45** was easily removed by diethyl ether extraction after the reaction. The NMR spectrum of this product, illustrated in Fig. 2.2 (A), is consistent with the indicated structure of **47**.

It has been reported that sulfonyl chlorides react quantitatively with amines.[75,79,81,82] Mita and co-workers[87] found that after one of the sulfonyl chloride groups of 1,5-naphthalene disulfonyl chloride reacted with primary aliphatic amines, having 4-18 carbons, such as 1-butylamine and 1-octadecylamine, the reaction of the

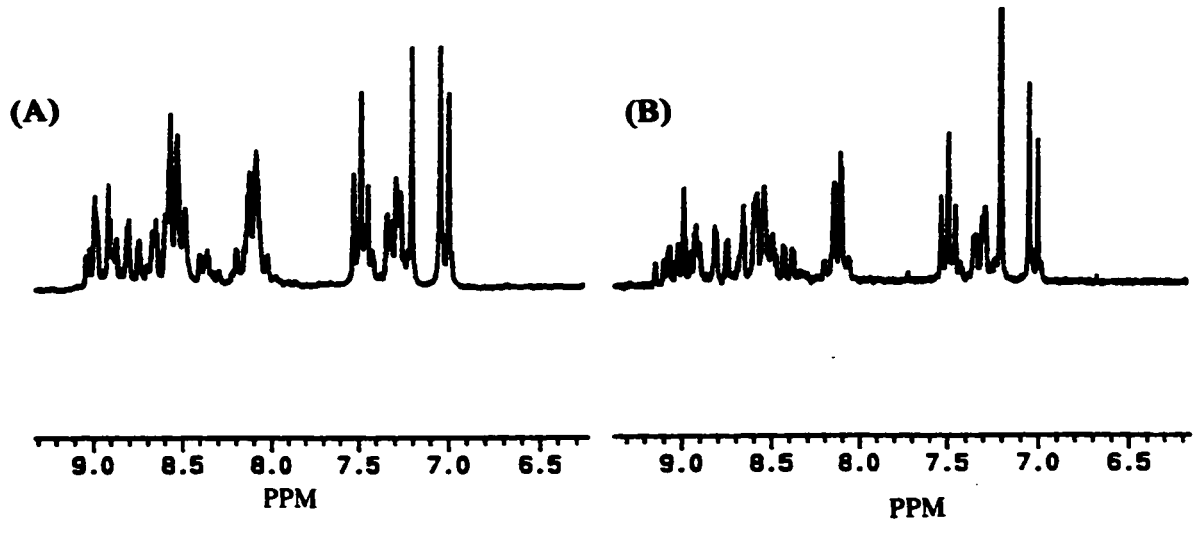

Fig. 2.2 ^{1}H NMR ($CDCl_3$) spectra of **47** prepared by method 2, (A), and by method 3, (B).

second sulfonyl group with the same amine occurs in chloroform at 40 °C about 10 times slower than the first one. These findings suggested that it would be possible to prepare **47** using a molar ratio of **43**:**45** =1:1 in the presence of pyridine. Accordingly, the reaction of **43** with **45** in the presence of **46** (molar ratio of **43**:**45**:**46**=1:1:1, method 3) was attempted. The reaction mixture was filtered to remove any pyridinium hydrochloride formed, then washed with a 1% HCl aqueous solution, followed by water to give an orange coloured solution. After removal of the solvent, **47** was obtained in 95% yield. Further purification of the product using column chromatography was attempted and was unsuccessful, however, no unreacted **45** was found. The ^{1}H NMR spectrum of the product obtained prior to the column

chromatography purification is shown in Fig.2.2 (B), which is quite similar to spectrum (A) in Fig. 2.2 and consistent with the indicated structure of **47**.

Both methods 2 and 3 worked well, which were used to prepare **47** for the fabrication of membranes.

The above results indicate that the problems associated with the low yield of monomer synthesis encountered in the previous work of the McMaster membrane group discussed in the introduction, have been successfully resolved by this work.

2.2 Photochemical Reactions

2.2.1 Reaction Mechanism

2-Diazo-1-napththoquinone derivatives have been used as photoresist materials in the microlithographic industry for many years.[88-90] However, the detailed reaction mechanisms of 2-diazo-1-napthoquinone derivatives have not been reported in the open literature until fairly recently. The proposed reactive intermediates and major products isolated from photolysis of 2-diazo-1-naphthoquinone derivatives are summarized in Scheme 2.2. Ponomareva et al.[91] have reported that photolysis of 2-diazo-1-oxo-1,2-dihydronaphthalene, **48**, yielded 3-indene carboxylic acid ester, **57**, as the major product. 1-Hydroxy-2-alkoxynaphthalene, **52**, and 1-hydroxynaphthalene **55** were found as minor products under different conditions. The product distribution between **52**, **55** and **57** was found to depend on the wavelength of light used, the

structure and particularly chain length of the reacting alcohols, and the presence or absence of oxygen. Ponomareva and co-workers[91] suggested that 1-hydroxy-2-alkoxy-naphthalene, **52**, and 1-hydroxynaphthalene, **55**, are formed by the capture of singlet and triplet carbenes, respectively. The formation of the indene carboxylic acid ester, **57**, is favoured by solvents which are weak hydrogen donors, the presence of oxygen, the addition of radical traps, and the use of long wavelength light. Ponomareva and co-workers[91] suggested that to account for this wavelength effect, the ratio of the singlet carbene, **50**, to triplet carbene, **54**, formed during the direct excitation of **48** depends on the excitation wavelength.

More recently, Vleggaar et al.[92] studied the photoinduced Wolff-rearrangement of 2-diazo-1-naphthoquinones. They also found that the 1-H-indene derivative, **57**, was the major product, with **52** as a minor product. The yield of **52** was found to increase with the increase in alcohol concentration in the reaction media. The maximum yield of **52** was 8.8%. In contrast to the work of Ponomareva and co-workers,[91] no 1-hydroxynapthalene derivative, **55**, was detected by Vleggaar and co-workers.[92] Based on a detailed product analysis and picosecond transient measurement, Vleggaar and co-workers[92] suggested that a carbene intermediate was formed prior to the formation of ketene, **51**, but no specific spin state of this carbene was discussed.

The ketene intermediate, **51**, was for the first time unambiguously identified by means of infrared spectra of a matrix obtained at 77 K by Rosenfeld et al.[93] and

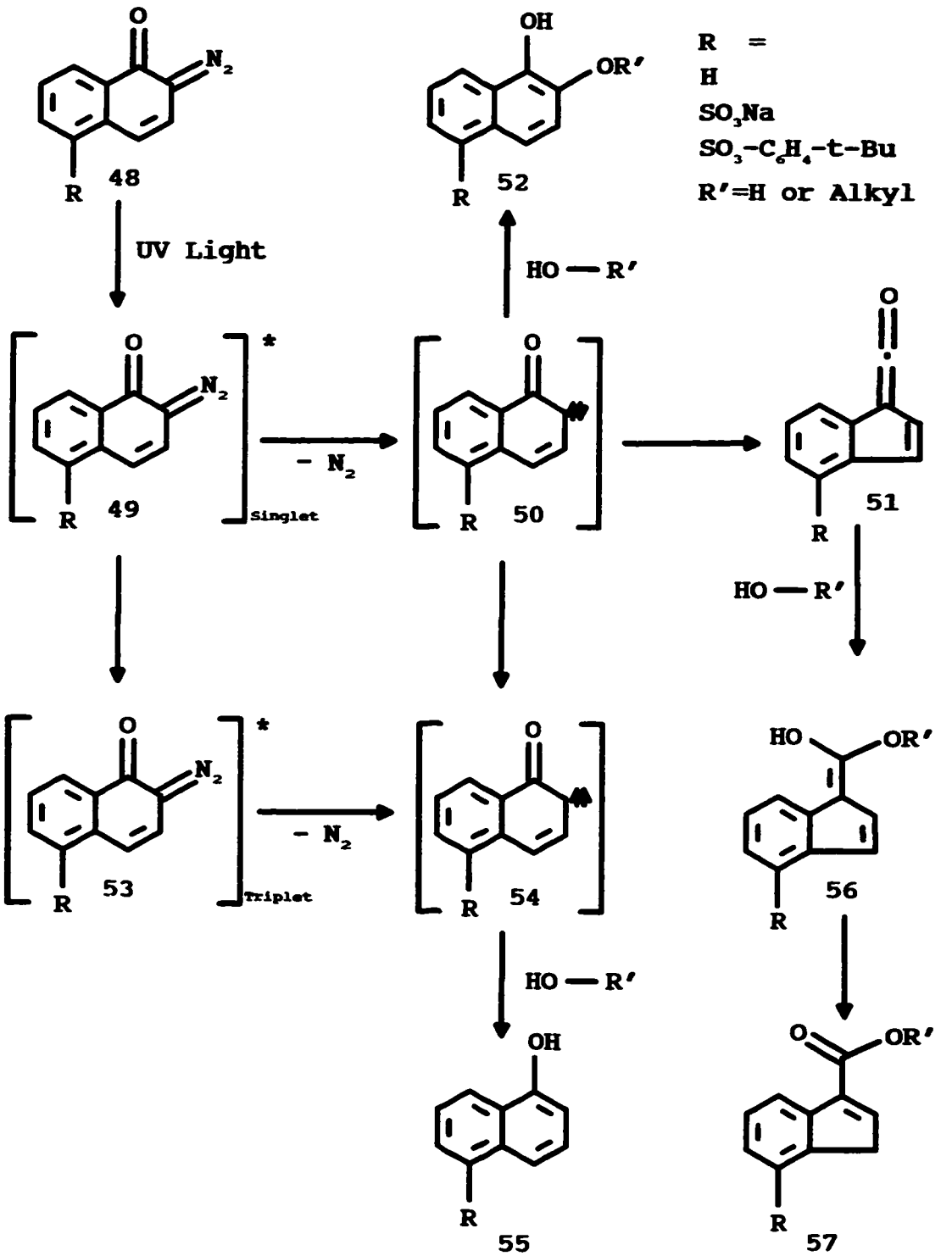

Scheme 2.2 Proposed mechanism of photolysis of 2-diazo-1-naphthoquinone derivatives.

later further confirmed by others.[92,94] On gradually warming, the ketene was converted into a carboxylic enol, **56**.

Andraos et al.[94] have shown that the ketene, **51**, and carboxylic acid enol, **56**, could be observed during flush photolysis of diazonaphthoquinones in aqueous solutions. Decay of the ketene intermediate, **51**, was found to be catalyzed weakly by hydroxide ions but not by dilute perchloric acid nor by acetic acid buffers. However, the conversion of the carboxylic acid enol intermediate, **56**, to the indene carboxylic acid derivative, **57**, was catalyzed by these acids.

Yagihara et al.[95,96] have reported that the dye, **63**, is formed on the photolysis of **58** in methanol. Two reaction path ways were proposed as shown in Scheme 2.3. The ketene, **60**, was suggested to react with **58** to yield **63** (path A). Alternatively, the ketene, **60**, could react with alkoxide to form **62**, which could couple with **58** to yield **63** (path B). This second path way was supported by the reaction reported by Tanigaki and co-workers,[97] in which **64** couples with **65** in tetrahydrofuran in the presence of triethylamine to give **66** (Scheme 2.4). Dye formation is a side reaction in the synthesis of indene carboxylic acid and its derivatives from 2-diazo-1-napththoquinone. This side reaction can be prevented by the addition of acetic acid to the reaction system.[91]

This reported work on the photochemistry is useful in selecting the reaction conditions to prepare model compounds.

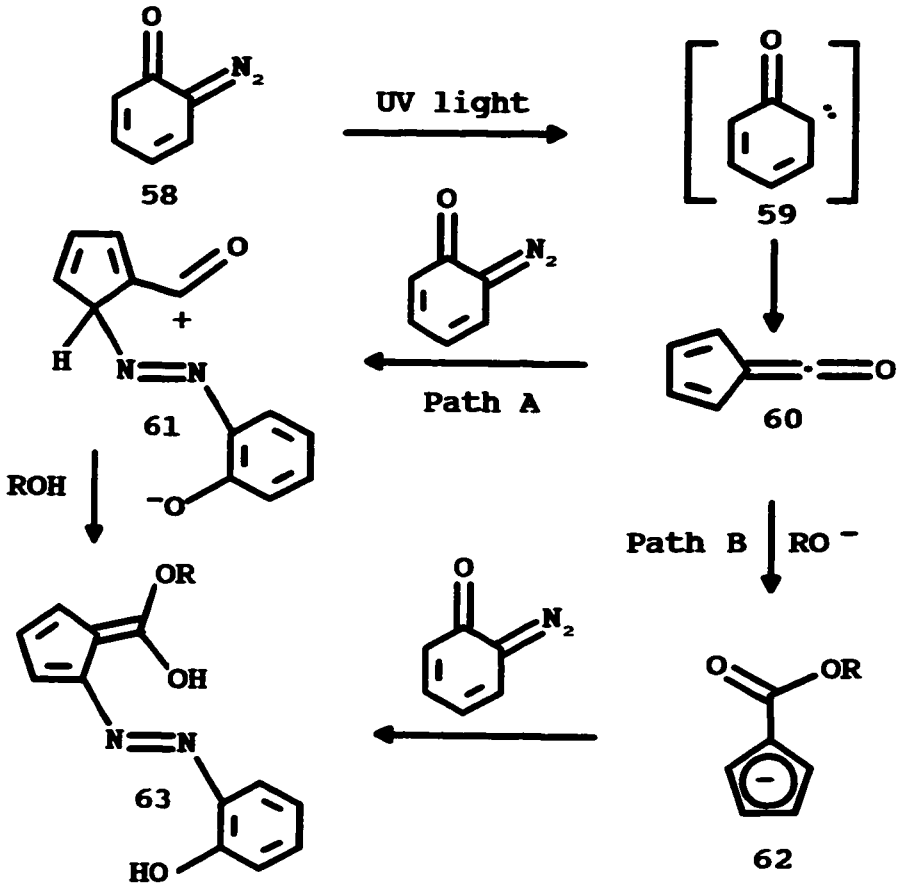

Scheme 2.3 Proposed mechanism of dye formation.

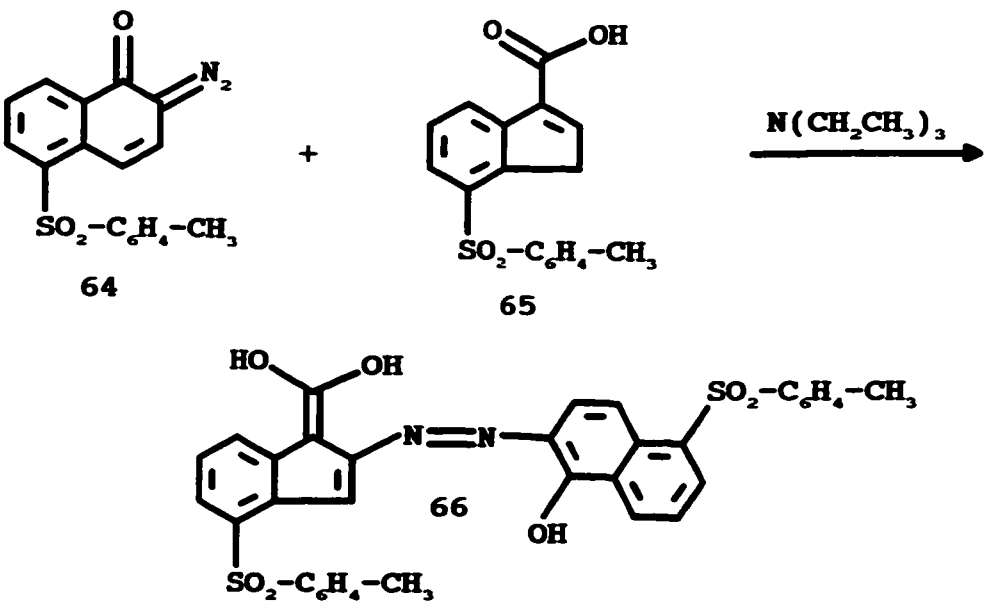

Scheme 2.4 Formation of 66.

In summary, the optimum conditions for the synthesis of indene acid derivatives by photolysis of 2-diazo-1-naphthoquinones are considered as follows:
(1) the use of long wavelength light, such as 350 nm, as an irradiation source,
(2) the presence of a radical scavenger and an acid in the reaction system,
(3) the use of alcohols having large alkyl groups as reactants.

These conditions were used to study the photochemical transformation of model compounds in this work.

2.2.2 Photochemical Transformation of Model Compounds

Model reactions using small molecules were studied in order to establish the appropriate conditions for the photochemical functionalization of diazoketone containing thin-film composite membranes.

The previous work of the McMaster membrane group has shown that indene acid, its ethyl ester and 2-hydroxyl ethyl ester have been successfully incorporated onto the surface of thin-film composite membranes by photochemical surface modification of the diazoketone containing precursor membrane.[21,70,72] The introduction of pendent carboxylic acids onto the membrane surface is important as it provides a method of modifying the surface property by the incorporation of negatively charged groups. However, it has been reported that indene acid undergoes decarboxylation easily in the presence of base at temperatures over 70 °C.[88-90] Such a decarboxylation of an indene acid is undesirable in a membrane. In order to resolve

this problem, the photochemical incorporation of glycolic acid was examined in order to give carboxylic acid **69**, which has a methylene unit between the carboxylic group and indene ring. Compound **69** is expected to be stable and not readily undergo decarboxylation.

The incorporation of hydroxyl and ester groups onto the membrane surface by photochemical modification potentially allows systematic modification of the hydrophilicity of the membrane surface. For this purpose, glycerol and ethanol were selected to react with **67**, respectively.

The introduction of chelating groups onto the membrane surface could provide a membrane with special ion selectivity. A sulfur containing crown ether, **73**, was chosen as a chelating group.

Finally, the incorporation of reactive epoxy or alkene groups onto the membrane surface could allow further functionalization of the membrane by subsequent chemical modification. Glycidol and 2-methyl-2-propene-1-ol were employed to react with **67**.

The photochemical reactions shown in Scheme 2.5 were examined in terms of the optimum conditions for maximum conversion to indene derivatives.

In each case, in order to avoid possible side reactions such as formation of **52** or **55** and **66** shown in Schemes 2.2 and 2.4, respectively, photolysis of **67** was carried out at low concentrations of the alcohol reactants (ROH in Scheme 2.5). Oxygen was not removed from the system and 350 nm wavelength light was used so

as to give the maximum yield of indene acid derivatives.[91] Either diethyl ether or acetic acid was used as a solvent for the photolysis. Based on the work of Ponomareva,[91] Vleggaar and their co-workers,[92] these conditions should minimize the side reactions discussed above and give a high yield of desired 1H-indene-3-carboxylic acid ester.

The yield of the isolated products and the composition of expected products determined by ^{1}H NMR spectra of the primary products of the photolysis are shown in Scheme 2.5.

The products were fully characterized using ^{1}H, ^{13}C NMR, FT-IR, UV and mass spectrometry. The results are given in the experimental section. The proton and carbon chemical shifts were assigned according to the ^{1}H-^{13}C correlation spectra and the NOE difference spectra of **72**. Assignment of the doublet at 7.7 ppm to the aromatic proton at the 6 position is based on the fact that there is a positive enhancement at 7.7 ppm upon irradiation of methylene protons of the ethyl group of **72** at 3.3 ppm. Assignments for carbons at 8 and 9 position could be reversed due to the lack of ^{1}H-^{13}C correlations.

In preparation of **69**, the reaction was carried out in acetic acid, which was freshly distilled from acetic anhydride. No dye formation was observed under the acidic conditions.[91,96]

Irradiation of **67** in an acetic acid solution containing glycerol yielded **72** with relatively high yield and selectivity.

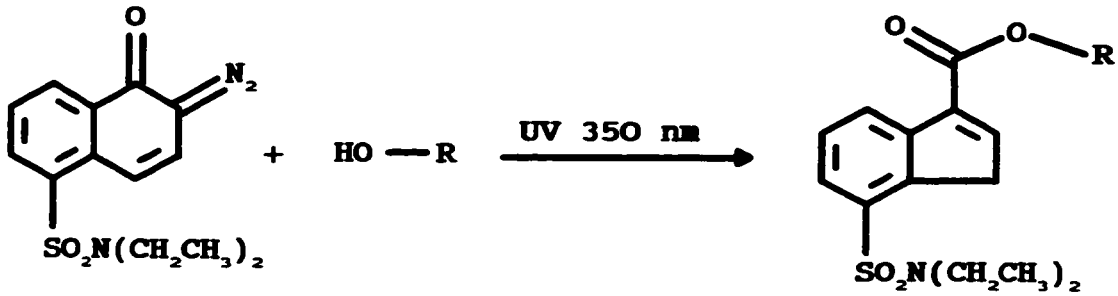

67 68-73

	R	SOLVENT USED	PRODUCT COMPOSITION % ^{1}H NMR	ISOLATED YIELD %
68	H	CH_2Cl_2/H_2O	-	74*
69	CH_2COOH	ACETIC ACID	>90	73
70	$CH_2CH(O)CH_2$	DIETHYL ETHER	>95	71
71	$CH_2(CH_3)C=CH_2$	DIETHYL ETHER	>95	66
72	$CH_2CH(OH)CH_2OH$	ACETIC ACID	>95	75
73	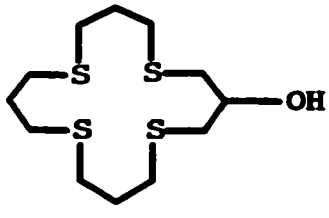	ACETIC ACID	>90	53

*Obtained from reference 70

Scheme 2.5 Model reactions for functionalization of thin-film composite membranes.

Glycidol derivatives are generally not stable in acidic media. As a result, **67** was irradiated in a glycidol diethyl ether solution, instead of an acetic acid solution. The product, **70**, was sufficiently stable to survive purification using water extraction to remove unreacted glycidol.

It was interesting to find that irradiation of **67** in diethyl ether solution containing 2-methyl-2-propene-1-ol yielded **71**, with high yield and selectivity. No cycloaddition of the reactive ketene intermediate with the double bonds of 2-methyl-2-propene-1-ol was observed. It has been reported that the cycloaddition reaction of the ketene with an alkene is the major reaction in the absence of protic nucleophiles.[96] The result implies that the reactive ketene intermediate formed from photolysis of the diazoketone reacts with hydroxyl much faster than with double bonds of 2-methyl-2-propene-1-ol. Although the double bond of the indene moiety could be used for further functionalization, the photochemical modification provides an alternative way to introduce additional alkene functionality onto the membrane surface. This could be useful, particularly for preparation of charge mosaic or amphoteric membranes, in which the functional groups are introduced into specific domains of a membrane using an appropriate mask.

Irradiation of **67** in acetic acid containing 1,5,9,13-tetrathiacyclohexadecane-3,11-diol yielded compound **73**, in a reasonable yield.

In all reactions no formation of side products, such as **52**, **55**, and **66**, in Schemes 2.2 and 2.4 could be observed.

In general, all of the model reactions took place easily with high yield and selectivity under mild conditions.

2.3 Summary

1. A photoreactive monomer has been successfully synthesized from commercially available starting materials by two step reactions in high yield. The problems associated with the low yield of monomer synthesis encountered in the previous work[21,72] of the McMaster membrane group have been successfully resolved by this work.
2. The photolysis of the model compound under mild conditions confirms that a variety of functional groups have been incorporated into the model compound through an ester linkage in high yield. These model reactions provide a good foundation for the photochemical surface modification of thin-film composite diazoketone membranes.

2.4 Experimental

2.4.1 Materials

6-Diazo-5-oxo-5,6-dihydro-naphthalenesulphonyl chloride was obtained from Fluka. 1,2-Ethanediamine, piperazine, glycerol, ethanol, glycolic acid, glycidol, 2-methyl-2-propene-1-ol, 1,5,9,13-tetrathiacyclohexadecane-3,11-diol, diethyl ether,

acetic acid, acetic acid anhydride, phosphorous pentachloride, chloroform, dichloromethane and 1,3,6-naphthalenetrisulfonic acid trisodium salt were purchased from Aldrich Chemicals Inc.

Acetic acid was freshly distilled from acetic anhydride before use. The other chemicals were used as received without further purification unless noted below.

1,3,6-Naphthalene trisulfonyl trichloride was prepared from 1,3,6-naphthalene-trisulfonic acid trisodium salt and phosphorus pentachloride according to published methods.[98] The identity of the product was confirmed by its melting point, NMR and high resolution MS spectra, which were the same as those reported in the literature.[72]

2.4.2 General Equipment

^{1}H and ^{13}C nuclear magnetic resonance (NMR) spectra were recorded on Bruker AM500 and AC200 NMR spectrometers, respectively. The chemical shifts were measured relative to tetramethylsilane (TMS). UV spectra were recorded on a Hewlett Packard 8451A Diode Array spectrophotometer. Infrared spectra were obtained using a Biorad-Digilab FTS-40 spectrometer. Mass spectra were recorded on a VG ZAB-E mass spectrometer. Photolysis were carried out using a Rayonet photoreactor (Southern New England Ultraviolet Company) with sixteen Model PRP 3500 Å lamps (35 watts). The diameter of the reactor is 200 mm. A Pyrex tube of 45 mm in diameter and 450 mm in length was used for preparative work. During the photolysis, the Pyrex tube was put in the center of the reactor and irradiated.

2.4.3 Chemical synthesis

6-Diazo-5-oxo-5,6-dihydro-1-naphthalene piperazinesulfonamide, 43

Method 1:

A solution of 6-diazo-5-oxo-5,6-dihydro-1-naphthalenesulfonyl chloride (2.00 g, 7.4 mmol) in 50 ml of toluene was slowly added to a solution of piperazine (1.28 g, 14.8 mmol) in 100 ml of toluene. The mixture was stirred at room temperature for 8 hours. Piperazine hydrochloride was removed by gravity filtration and the filtrate concentrated by evaporation of the solvent using a rotary evaporator until crystallization started. The solution was kept in the freezer for two days. The product was collected by filtration and washed twice with ice cold toluene. The product was dried *in vacuo* overnight to give 1.93 g (82.3%) of yellow needle-like crystalline product **43**, mp. (decomp.) 124-125 °C. ^{1}H NMR (500MHz, $CDCl_3$) δ 1.56 (s, N-H), 2.89 (t, J=4.9 Hz, 4 H, CH_2), 3.12 (t, J=4.9 Hz, 4 H, CH_2), 7.07 (d, J=10.0 Hz, 1 H, H-8), 7.55 (t, J=7.8 Hz, 1 H, H-3), 7.56 (d, J=10.0 Hz, 1 H, H-7), 8.26(dd, J=7.7Hz, J=1.4 Hz, 1 H, H-2), 8.62 (d, J=7.9 Hz, 1 H, H-4). ^{13}C NMR (125 MHz, $CDCl_3$) δ 45.60, 46.48, 78.40 (C-N_2), 113.70, 118.85, 126.05, 131.04, 131.46, 133.38, 134.93, 135.20, 178.41 (C=O). MS *m/z* (rel. int.): 318 ($M^{\cdot+}$, 3), 290 (22), 142 (10), 113 (37), 85(100). M^+ calc. for $C_{14}H_{14}N_4O_3S$ 318.0787, found 318.0783. UV (CH_2Cl_2) λ_{max}=398 nm, log ϵ = 3.80. IR (NaCl, cm^{-1}): $\nu_{(C=N=N)}$=2162, 2115, $\nu_{(C=O)}$=1621.

Method 2:

A solution of 6-diazo-5-oxo-5,6-dihydro-1-naphthalenesulfonyl chloride (2.00 g, 7.4 mmol) in 50 ml of dichloromethane was added to a solution of piperazine (1.28 g, 14.8 mmol) in 100 ml of dichloromethane. The mixture was stirred at room temperature for 8 h and gravity filtered to remove piperazine hydrochloride. The filtrate was washed with 2x100 ml water and dried with anhydrous sodium sulfate. After removal of the sodium sulfate by filtration, the filtrate was evaporated to obtain 2.29 g (96.6%) of **43** as a yellow powder. The melting point, proton NMR and IR spectra of the product were identical to those obtained by method 1, above.

1-[4-(2-Diazo-1-oxo-1,2-dihydro-5-sulfonyl)naphthalenyl-1-piperazinyl]sulfonyl-3,6-naphthalene disulfonyl chloride, 3-[4-(2-Diazo-1-oxo-1,2-dihydro-5-sulfonyl)naphthalenyl-1-piperazinyl]sulfonyl-1,6-naphthalene disulfonyl chloride, 6-[4-(2-Diazo-1-oxo-1,2-dihydro-5-sulfonyl)naphthalenyl-1-piperazinyl]sulfonyl-1,3-naphthalene disulfonyl chloride, 47

Method 1:

A solution of **43** (0.10 g, 0.31 mmol) in 50 ml of dichloromethane was added slowly to a solution of 1,3,6-naphthalene trisulfonyl chloride **45** (0.14 g, 0.33 mmol) and pyridine **46** (0.05 g, 0.62 mmol) in 100 ml of dichloromethane. The mixture was

stirred at room temperature for 8 h. The dichloromethane was removed by evaporation using a rotatory evaporator to give a yellow solid. The ^{1}H NMR spectrum of this crude product is shown in Fig. 2.1 (A). The crude product was purified using column chromatography with silica gel as a stationary phase and a mixed solvent of toluene:diethyl ether:acetic acid:methanol in a volume ratio of 120:60:18:1 as a mobile phase. After column chromatography, 0.10 g (45.5%) of **47** (yellow powder) was obtained. **47** decomposed at about 164 °C. ^{1}H NMR (200 MHz, $CDCl_3$, Fig. 2.1 (D)): δ 3.29 (s, 8 H, CH_2), 7.09 (d, J=10.0 Hz, 1 H, H-8), 7.38 (d, J=10.0 Hz, 1H, H-7), 7.55 (t, J=7.8 Hz, 1H, H-3), 8.19 (d, J=7.8 Hz, 1 H, H-2), 8.61 (d, J=7.8 Hz, 1 H, H-4), 8.5-9.2 (m, multiple peaks of protons on naphthalene rings of the three isomers). ^{13}C NMR (50 MHz, $CDCl_3$): δ 45.11, 45.56, 78.61 (C-N_2), 112.51, 119.87, 177.87 (C=O), 126.18-144.68 (multiple peaks of the three isomers). UV (CH_2Cl_2) λ_{max}=396 nm, log ϵ = 3.66. IR (NaCl, cm^{-1}): $\nu_{(C=N=N)}$=2161, 2111, $\nu_{(C=O)}$=1619. Anal. calcd for $C_{24}H_{18}N_4O_9S_4Cl_2$: C, 40.85; H, 2.57. Found: C, 40.94; H, 2.72.

Method 2:

A solution of **43** (5.0 g, 15.7 mmol) in 100 ml of dichloromethane was added slowly to a solution of 1,3,6-naphthalene trisulfonyl chloride **45** (8.01 g, 18.9 mmol) and pyridine **46** (1.25 g, 15.8 mmol) in 100 ml of dichloromethane. The mixture was

stirred at room temperature for 14 h, then washed with 2 x 50 ml of 1% HCl aqueous solution, followed by 3 x 100 ml of water. The dichloromethane solution was dried with anhydrous Na_2SO_4, and the dichloromethane was evaporated using a rotatory evaporator until precipitation occurred. This concentrated solution was added slowly into 200 ml of rapidly stirred diethyl ether to give a yellow precipitate, which was collected and washed with 3 x 100 ml of diethyl ether and dried *in vacuo* overnight; 10.11 g (91.2%) of **47** (yellow powder) was obtained. ^1H, ^{13}C NMR, UV and IR spectra of this product showed that it was the same as that obtained by method 1.

Method 3:

A solution of **43** (5.6231 g, 17.66 mmol) in 50 ml of dichloromethane was added slowly to a solution of 1,3,6-naphthalene trisulfonyl chloride **45** (7.4822 g, 17.66 mmol) and pyridine **46** (1.3970 g, 17.66 mmol) in 100 ml of dichloromethane. The mixture was stirred at room temperature for 8 h, then washed with 2 x 50 ml of 1% aqueous HCl, followed by 3 x 50 ml of water. The dichloromethane solution was dried with anhydrous Na_2SO_4 and the dichloromethane was evaporated using a rotatory evaporator. The residue was dried *in vacuo* at 50 °C overnight to give 11.86 g (95.2%) of **47** (yellow powder). ^1H, ^{13}C NMR, UV and IR spectra of this product showed that it was the same as that obtained by method 1.

Model Compounds

6-Diazo-5-oxo-5,6-dihydro-1-naphthalene (N,N-diethyl)sulfonamide, 67

Model Compound **67** was prepared by reaction of 6-diazo-5-oxo-5,6-dihydro-1-naphthalenesulfonyl chloride with diethylamine as published elsewhere.[70]

1H-indene-3-carboxylic acid (2'-carboxylmethylenyl) ester, 7-[(diethylamino) sulfonyl], 69

Glycolic acid (1.00 g, 13.1 mmol) and acetic anhydride (0.613 g, 6.0 mmol) were dissolved in 200 ml of acetic acid freshly distilled from acetic anhydride. The solution was stored overnight before photolysis. **67** (0.1 g, 0.34 mmol) was dissolved in the above solution and irradiated with 350 nm wavelength light for 1 h. The solvent was evaporated *in vacuo* to yield a crude product. The ^{1}H NMR spectrum of this crude product was taken at this point to determine the composition of the desired product in a primary product of the photolysis (column 4 in Scheme 2.5). The crude product was dissolved in 200 ml of chloroform, washed with 2 x 50 ml of water, and the solvent was evaporated using a rotary evaporator to give a viscous liquid. The crude product was purified by column chromatography using silica gel as stationary phase and a mixture solvent of toluene/diethyl ether/acetic acid/methanol (120/60/18/1 vol. ratio) as a mobile phase. After the column separation, 0.088 g (73.2% yield) of **69**, a viscous liquid, was obtained. ^{1}H NMR data are given in Tables 2.1 and 2.2. ^{13}C NMR data are presented in Table 2.3. UV and infrared data are given in Table

2.4. MS data are displayed in Tables 2.5 and 2.6.

1H-indene-3-carboxylic acid glycidyl ester, 7-[(diethylamino)sulfonyl], 70

A solution of 6-diazo-5-oxo-5,6-dihydro-1-naphthalene (N,N-diethyl)sulfonamide **67** (0.3 g, 1.03 mmol) and glycidol (0.8 g, 10.3 mmol) in 200 ml of diethyl ether was irradiated in a Pyrex tube at 350 nm for 1h. The reaction mixture was evaporated using a rotary evaporator to give a viscous liquid. The ^{1}H NMR spectrum of this crude product was taken at this point to determine the composition of the desired product in a primary product of the photolysis (column 4 in Scheme 2.5). This crude product was dissolved in 200 ml of diethyl ether and was washed with 3 x 100 ml of water. After removal of diethyl ether by rotary evaporation, followed by drying *in vacuo* overnight, 0.257 g (yield 71.2%) of **70**, a viscous liquid, was obtained. ^{1}H NMR data are given in Tables 2.1 and 2.2. ^{13}C NMR data are presented in Table 2.3. UV and infrared data are given in Table 2.4. MS data are displayed in Tables 2.5 and 2.6.

1H-indene-3-carboxylic acid (2'-methyl-2'-propenyl) ester, 7-[(diethylamino)sulfonyl], 71

A solution of 6-diazo-5-oxo-5,6-dihydro-1-naphthalene (N,N-diethyl)sulfonamide (0.10 g, 0.34 mmol) and 2-methyl-2-propene-1-ol (0.25 g, 3.4 mmol) in 200 ml of diethyl ether was irradiated in the Pyrex tube at 350 nm for 1 h.

The reaction mixture was evaporated using a rotary evaporator to give a viscous crude product. The ^{1}H NMR spectrum of this crude product was taken to determine the composition of the desired product in a primary product of the photolysis (column 4 in Scheme 2.5). The crude product was dissolved in 200 ml of diethyl ether and washed with 2 x 50 ml of 1% Na_2CO_3 aqueous solution, followed by 3 x 100 ml of water. After evaporation of diethyl ether and drying *in vacuo* overnight, 0.078 g (65.7%) of **71**, a viscous liquid, was obtained. ^{1}H NMR data are given in Tables 2.1 and 2.2. ^{13}C NMR data are presented in Table 2.3. UV and infrared data are given in Table 2.4. MS data are displayed in Tables 2.5 and 2.6.

1H-indene-3-carboxylic acid (2',3'-dihydroxyl-propanyl) ester, 7-[(diethylamino)sulfonyl], 72

A solution of 6-diazo-5-oxo-5,6-dihydro-1-naphthalene (N,N-diethyl)sulfonamide (0.1 g, 0.34 mmol) and glycerol (0.31 g, 3.4 mmol) in 200 ml of acetic acid was irradiated in a Pyrex tube at 350 nm for 1 h. The reaction mixture was evaporated using a rotary evaporator to give a viscous liquid. The ^{1}H NMR spectrum of this crude product was taken to determine the composition of the desired product in a primary product of the photolysis (column 4 in Scheme 2.5). The crude product was dissolved in 200 ml of chloroform and washed with 2 x 50 ml of water. The solvent was removed by evaporation using a rotary evaporator to give a viscous liquid. The crude product was purified by column chromatography using silica gel as

a stationary phase and a mixture solvent of toluene/diethyl ether/acetic acid/methanol (120/60/18/1 vol. ratio) as a mobile phase. After column purification, 0.0945 g (74.6%) of **72**, a viscous liquid, was obtained. ^{1}H NMR data are given in Tables 2.1 and 2.2. ^{13}C NMR data are presented in Table 2.3. UV and infrared data are given in Table 2.4. MS data are displayed in Tables 2.5 and 2.6.

1H-indene-3-carboxylic acid [3'-(11'-hydroxyl-1',5',9',13'-tetrathiacyclohexadecanyl)] ester, 7-[(diethylamino)sulfonyl], 73

A solution of 6-diazo-5-oxo-5,6-dihydro-1-naphthalene (N,N-diethyl)sulfonamide **67** (0.1 g, 0.34 mmol) and 1,5,9,13-tetrathiacyclohexadecane-3,11-diol (0.14 g, 0.43 mmol) in 200 ml of acetic acid was irradiated in a Pyrex tube at 350 nm for 1 h. The reaction mixture was evaporated using a rotary evaporator to give a viscous liquid. The ^{1}H NMR spectrum of this crude product was taken to determine the composition of the desired product in a primary product of the photolysis (column 4 in Scheme 2.5). This crude product was dissolved in 200 ml of chloroform and was washed with 2 x 50 ml of water, followed by evaporation using a rotary evaporator to give a viscous liquid. This crude product was purified by column chromatography. Silica gel 60 (230-400 mesh) was used as a stationary phase and a mixture solvent with volume ratio of toluene:diethyl ether:acetic acid:methanol=120:60:18:1 was used as a mobile phase. After the column purification, 0.11 g (52.5% yield) of **73**, a viscous liquid, was obtained. ^{1}H NMR

data are given in Tables 2.1 and 2.2. ^{13}C NMR data are presented in Table 2.3. UV and infrared data are given in Table 2.4. MS data are displayed in Tables 2.5 and 2.6.

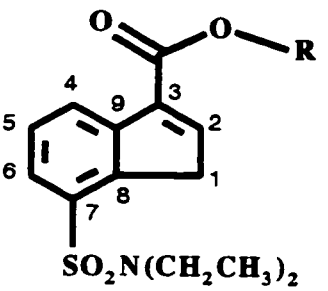

Table 2.1 ^{1}H NMR chemical shifts (ppm) of model compounds in $CDCl_3$

		COMPOUNDS				
No.		69	70	71	72	73
1	(doublet)	3.92	3.81	3.91	3.92	3.84
2	(triplet)	7.67	7.52	7.62	7.61	7.55
4	(doublet)	8.25	8.19	8.27	8.26	8.20
5	(triplet)	7.48	7.40	7.49	7.50	7.43
6	(doublet)	7.68	7.60	7.69	7.69	7.62
CH_2	(quartet)	3.31	3.24	3.33	3.33	3.25
CH_3	(triplet)	1.09	1.02	1.11	1.12	1.04

Table 2.2 ^{1}H NMR coupling constants of model compounds in $CDCl_3$

Coupling constant (Hz)	COMPOUNDS				
	69	**70**	**71**	**72**	**73**
J_{45}	7.7	7.7	7.7	7.7	7.7
J_{56}	7.7	7.7	7.7	7.7	7.7
J_{12}	2.0	2.1	2.0	1.9	2.0
$J_{CH_2CH_3}$	7.1	7.1	7.1	7.1	7.1

Pendent glycolic acid moiety of compound **69**:
^{1}H NMR: δ 4.88 (s, 2 Hs, CH_2),
10.69 (broad, 1 acid proton)

Pendent glycidol moiety of compound **70**:
^{1}H NMR: δ 4.67 (a part of AB spin system, dd, J=12.3 Hz, J=3.0 Hz, 1 H, 1′ -CH_2O-),
4.17 (a part of AB spin system, dd, J=12.3 Hz, J=6.3 Hz, 1 H, 1′-CH_2O-),
3.35 (quintet, J=6.3 Hz, J=4.8 Hz, J=4.5 Hz, J=3.0 Hz, 1 H, 2′ -CHO-),
2.91 (a part of AB spin system, triplet, 4.5 Hz, 1 H, 3′ -CH_2O-),
2.74 (a part of AB spin system, dd, J=4.8 Hz, J=2.5 Hz, 1 H, 3′ -CH_2O-).

Pendent 2-methyl propene moiety of compound **71**:
^{1}H NMR: δ 4.95 (doublet, J=15.9 Hz, 2 Hs, 3′ =CH_2),
4.66 (singlet, 2 Hs, 1′-CH_2O-),
1.75 (singlet, 3 Hs, 4′ -CH_3).

Pendent glycerol moiety of compound **72**:
^{1}H NMR: δ 4.45 (a part of AB spin system, dd, J=11.4 Hz, J=4.6 Hz, 1 H, 1′ -CH_2OH),
4.43 (a part of AB spin system, dd, J=11.4 Hz, J=6.1 Hz, 1 H, 1′ -CH_2OH),
4.09 (quintet, J=4.6 Hz, J=6.1 Hz, J=4.0 Hz, J=5.7 Hz, 1 H, 2′ CHOH),
3.80 (a part of AB spin system, dd, J=11.6 Hz, J=4.0 Hz, 1 H, 3′ CH_2OH),
3.71 (a part of AB spin system, dd, J=11.6 Hz, J=5.7 Hz, 1 H, 3′ CH_2OH).

Pendent sulfur containing crown ether moiety of compound 73:
^{1}H NMR: δ 5.23 (quintet, J=6.0 Hz, 1 H, 3′ -CHO-),
3.84 (quintet, J=6.0 Hz, 1 H, 11′-CHOH),
2.90 (broad, 8 Hs),
2.68 (broad, 8 Hs),
1.92 (quintet, J=6.8 Hz, 4 Hs),

Table 2.3 ^{13}C NMR chemical shifts (ppm) of model compounds in $CDCl_3$

No.	COMPOUNDS				
	69	70	71	72	73
1	40.4	39.6	39.4	39.6	40.3
2	148.1	146.1	146.3	146.6	147.2
3	134.5	135.0	135.1	134.5	135.4
4	125.8	126.6	126.4	126.5	127.2
5	128.4	127.8	127.7	127.8	128.4
6	127.1	125.1	125.0	125.0	125.8
7	136.7	136.2	136.7	136.2	136.9
8	143.2	143.1	143.5	142.7	143.5
9	141.8	141.5	141.9	141.3	142.1
C=O	163.1	163.0	163.8	163.7	163.6
CH_2	42.0	41.5	41.5	41.4	42.1
CH_3	14.6	14.0	14.0	13.9	14.6

Pendent glycolic acid moiety of compound 69:
^{13}C NMR: δ 60.9 (CH_2), 174.0 (C=O).

Pendent glycidol moiety of compound 70:
^{13}C NMR: δ 65.0 (1′, -CH_2O-), 49.7 (2′, -CHO-), 44.6 (3′, -CH_2O-).

Pendent 2-methyl propene moiety of compound 71:
^{13}C NMR: δ 68.0 (1′, -CH_2O-), 139.9 (2′, -C(CH_3)=), 113.4 (3′,=CH_2), 19.7 (4′, -CH_3).

Pendent glycerol moiety of compound 72:
^{13}C NMR: δ 70.2 (1′, CH_2OH), 63.4 (2′, CHOH), 62.3 (3′, -CH_2OH).

Pendent sulfur containing crown ether moiety of compound 73: ^{13}C NMR: δ 73.5 (3', -O-CH-), 69.8 (11', -CHOH), 38.8, 35.7, 32.3, 31.7, 30.4.

Table 2.4 UV and IR absorbance of model compounds

Model Compound	UV		IR(NaCl)	
	λ_{max} (nm)	logε	C=O (cm^{-1})	C=O (cm^{-1})
69	242	4.00	1728	1768
70	232	4.16	1722	-
71	242	3.92	1721	-
72	242	4.82	1721	-
73	242	4.02	1715	-

$CHCl_3$ was used as a solvent and reference.

Table 2.5 Composition and formula weight of model compounds

No.	Formula	Formula Weight	
		Calculated	Found
69	$C_{16}H_{19}NO_6S$	353.0933	353.0921
70	$C_{17}H_{21}NO_5S$	351.1140	351.1125
71	$C_{18}H_{23}NO_4S$	349.1348	349.1365
72	$C_{17}H_{23}NO_6S$	369.1246	369.1229
73	$C_{26}H_{39}NO_5S_5$	605.1432	605.1436

Table 2.6 Mass spectra of model compounds

Peak number	COMPOUNDS									
	69		**70**		**71**		**72**		**73**	
	m/e	%	m/e	%	m/e	%	m/e	%	m/e	%
molecular ion ($M^{+\cdot}$)	353	13	351	42	349	53	369	22	605	55
1	338	12	336	29	334	27	354	14	587	5
2	217	40	309	13	277	6	278	15	328	100
3	141	13	278	12	251	7	233	20	310	55
4	114	18	215	49	236	8	205	5	295	8
5	72	100	173	28	213	53	142	20	271	50
6			141	38	179	9	115	23	51	52
7			114	84	141	5	72	100	236	68
8			72	100	115	23			197	62
9					84	58			179	98
10					72	100			163	100

Chapter 3

Fabrication of Thin-Film Composite Membranes with Pendant, Photoreactive Diazoketone Functionality

The second step of the entire project is the incorporation of photolabile diazoketone functional groups into the thin-film barrier layer of the membrane. This can be achieved by interfacial polymerization.

In interfacial polycondensation, two reactants are normally dissolved in a pair of immiscible liquids, respectively. Polymer formation takes place at or near the liquid-liquid interface when the two solutions are brought in contact with each other.[99,100] Formation of polyamides has been proven to take place in the organic phase near the interface.[99-101] For instance, in the synthesis of nylon 6-10, 1,6-hexanediamine in the aqueous phase diffuses across the interface to react with 1,8-octanedicarbonyl chloride in the organic phase.

$$n\ H_2N(CH_2)_6NH_2 + n\ ClOC(CH_2)_8COCl \longrightarrow [-HN(CH_2)_6NHOC(CH_2)_8CO-]_n$$

For polymer film thickness to build up, the diamine continually crosses the water/organic interface, diffuses through the polyamide layer already formed, then reacts with the diacid chloride in the organic solution side of the polyamide layer.

Thus the polyamide film grows towards the organic phase perpendicular to the interface. This has been visually demonstrated by depositing coloured powder on the surface of the film facing the organic phase as shown in Fig. 3.1. The coloured powder becomes embedded inside the film as interfacial polymerization continues. However, the powder does not become embedded in the film if it is deposited on the film facing the aqueous phase side.

In liquid-liquid interfacial polymerization, many variables affect the reaction. These factors include the partition coefficients of monomers between the two phases, the molar ratio of one monomer to the other, the presence of phase transfer agents and catalysts, the choice of solvent and co-solvent, reaction time, polymer solubility, etc.[99,100]

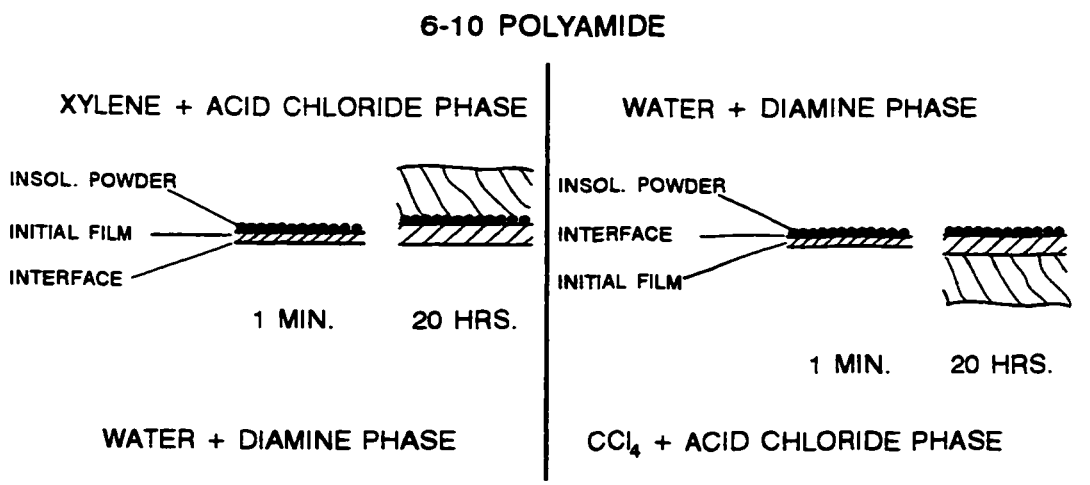

Fig. 3.1 Diagrams of polymer film growth at liquid interfaces.

Water is normally used as one phase to dissolve diamine monomers or other water soluble monomers. Dichloromethane, chloroform, carbon tetrachloride, hexane etc. are typical solvents for the water-immiscible phase. Diacid chlorides or other water insoluble monomers are dissolved in this organic phase.[99,100] In addition, completely or partially water-miscible solvents have been added to organic phase for the preparation of polyamide,[99,100,102] polyester,[100,102] polyurethane,[100,102] and polysulfonamide polymers.[100] Acetone, tetrahydrofuran and isopropyl alcohol are typical examples of completely water-miscible solvents.[100] Cyclohexanone and methyl ethyl ketone are examples of partially water-miscible solvents studied.[100] The water-miscible solvents facilitate the partition of diamine monomer into the organic phase, accelerate polymerization rate, enhance polymer swelling, and facilitate product recovery.[100] The water-solvent ratio is an important factor that influences interfacial polymerization.[100,102]

In liquid-liquid interfacial polymerization, phase-transfer agents are often used in water-immiscible solvent systems to promote interfacial polymerization by enhancing the transfer of the aqueous intermediate across the interface boundary into the presence of the complementary intermediate. The use of phase-transfer agents increases the rate of polymerization and can result in high molecular weight and yield. A variety of surfactants and crown ethers have been used as phase-transfer agents.[99,100]

Sundet et al.[103] studied interfacial polycondensation of a series of aliphatic diamines with aromatic disulfonyl chlorides to form polysulfonamides.

Dichloromethane and a mixture of chloroform and carbon tetrachloride were found in general to be good solvents for disulfonyl chloride and were used as the organic phase. The optimal monomer concentration was about 0.1 kmol/m^3, and the optimal molar ratio of the disulfonyl chloride to diamine was close to 1:1. Base is often added to react with the condensation product (typically HCl). The weaker base Na_2CO_3 was found to give a polysulfonamide with higher molecular weight than the stronger base NaOH, due to reduced hydrolysis of sulfonyl chloride. In addition, the use of surfactants was helpful in producing polymers with higher yield and higher molecular weight.

In principle, the factors that influence liquid-liquid interfacial polymerization also influence the membrane supported interfacial polymerization used in the fabrication of thin-film composite membranes.[5] Cadotte and co-workers[104] investigated some of these factors on the formation of thin-film composite membranes. Recently, Petersen reviewed the advance in thin-film composite membranes.[5] However, very little has been published with respect to the effect of the factors, that influence interfacial polymerization, on the formation of thin-film composite membranes.

This chapter studies some of the above issues including the effects of monomer concentration, reaction time, surfactant and solvents on interfacial polymerization, membrane structure, and performance.

3.1 Solubility of monomer 47

The interfacial polymerization step in the formation of a TFC membrane is typically carried out with solutions of the diacid chloride in an organic solvent in contact with an aqueous diamine solution contained within the pores of a support membrane. Leaving aside environmental considerations, the requirements for the organic solvent are stringent. The diacid chloride should be reasonably soluble in, and not react with the organic solvent. The organic solvent must not adversely affect the supporting base membrane. In addition, water should be poorly soluble in the organic solvent.[5,104] There should also be a suitable partitioning of the diamine between the organic and the aqueous phases.

In this work, a commercial polysulfone ultrafiltration membrane reinforced by a nonwoven cloth was used as a support membrane. This resulted in a restriction on selection of organic solvents for interfacial polymerization, as the polysulfone membrane dissolves in many common organic solvents.[5,70] The disulfonyl chloride monomer, **47**, and 1,2-ethanediamine, **74**, were used as monomers to prepare the thin-film composite diazoketone membrane by interfacial polymerization as shown in Scheme 3.1. The disulfonyl chlorides, **47**, are large molecules and, as might be expected, they have a relatively low solubility in many organic solvents. It was found that **47** was essentially insoluble in CCl_4, a typical solvent used in interfacial polymerizations.[100,102] The addition of $CHCl_3$ or acetone to the CCl_4 improved the solubility. However, it is known that the supporting polysulfone ultrafiltration

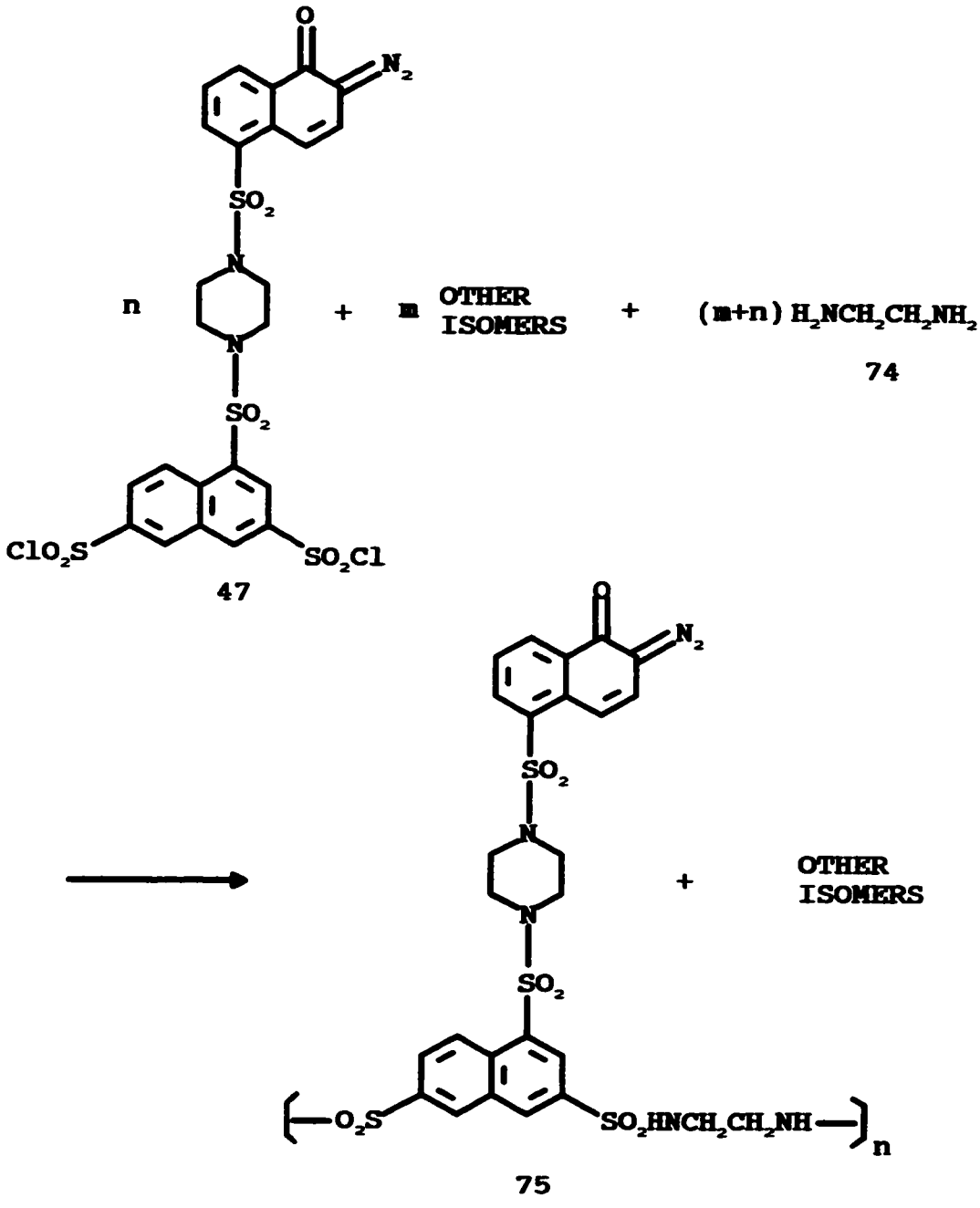

Scheme 3.1 Interfacial polymerization.

membrane used in this work is adversely affected by both $CHCl_3$ and acetone.[5,70] In this work a mixture of $CCl_4/CHCl_3$ (80:20) or CCl_4/acetone (90:10) were used. These mixtures permitted a reasonable solubility of 47, 0.486 and 2.26 kg/m^3, respectively at 25 °C, but did not damage the supporting polysulfone base membrane.

3.2 Absorption of diamine monomer by the supporting polysulfone membrane

In liquid-liquid interfacial polymerization, the diamine monomer concentration in an aqueous phase, C_a, can be easily controlled by adding a precise amount of diamine in the solution. However, in membrane fabrication it is not the diamine monomer concentration in the aqueous phase, C_a, but the concentration of diamine in the support membrane phase that directly influences the interfacial polymerization.

Therefore, the partitioning of 1,2-ethanediamine into the supporting polysulfone membrane was examined. It was found that the uptake of the diamine by the membrane was linearly related to the concentration in solution as shown in Fig. 3.2. Assuming that the polysulfone occupies no space, a pseudo-partition coefficient, K', was determined.

In a control experiment, no surfactant was added to the aqueous solution. The amount of 1,2-ethanediamine absorbed by the supporting polysulfone membrane, $w_{a,MEMB}$ (kmol.), was determined by titration with 0.1 N HCl aqueous solution. The concentration of 1,2-ethanediamine in the support membrane phase, $C_f(0,0)$,

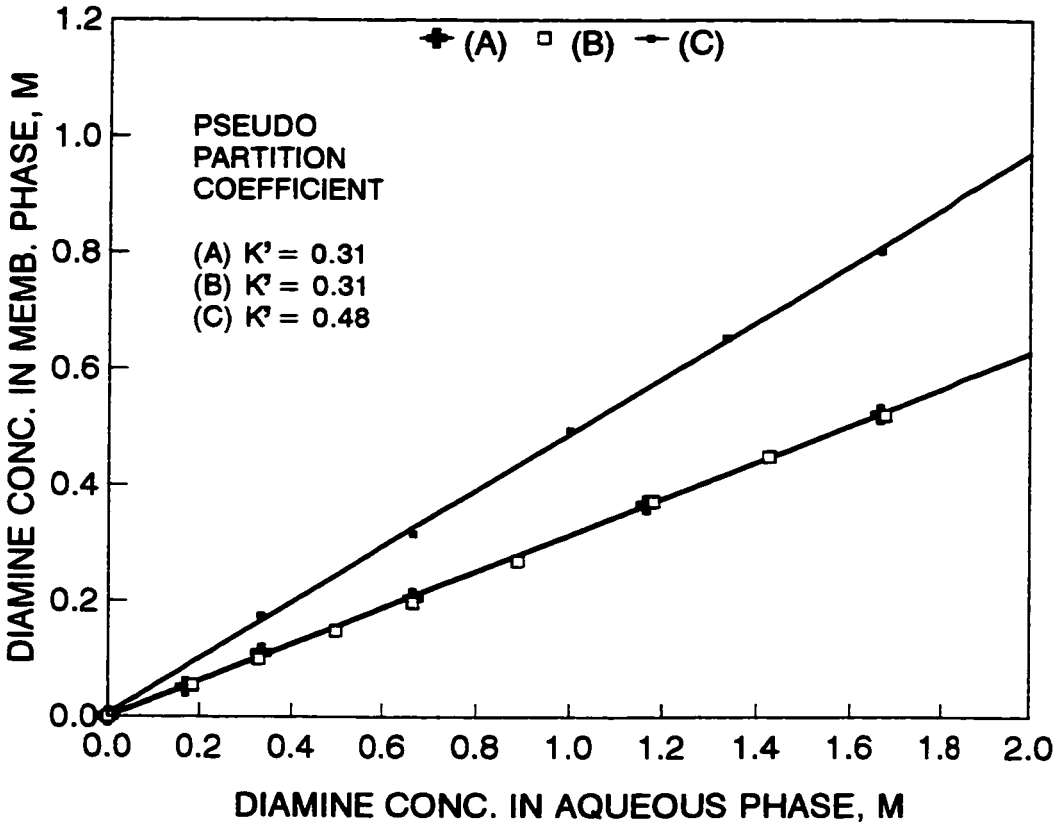

Fig. 3.2 Relationship between 1,2-ethanediamine concentrations in aqueous phase and in the support membrane phase.

(A) no surfactant in the aqueous solution,

(B) 0.1 g/L of poly(ethyleneimine) in the aqueous solution,

(C) 5.89×10^{-4} M of Triton X-114 surfactant in the aqueous solution.

(see Fig. 5.1) was defined as,

$$C_f(0,0) = w_{a,MEMB} / V_{MEMB.} \qquad 3.1$$

where $V_{MEMB.}$ (m^3) is the entire volume occupied by the support membrane including the void volume in the membrane.

A pseudo-partition coefficient, K', of 1,2-ethanediamine between the aqueous phase and the support polysulfone phase was defined by,

$$K' = C_f(0,0)/C_a \qquad 3.2$$

where C_a ($kmol/m^3$) is the concentration of 1,2-ethanediamine in the aqueous solution. The pseudo-partition coefficient, K', of 1,2-ethanediamine between the aqueous phase and the support polysulfone phase was given by the slope of the straight line in Fig. 3.2. For aqueous 1,2-ethanediamine solution without any surfactant, K', was found to be 0.31. It was interesting that the addition of Triton X-114 surfactant to the aqueous solution resulted in an increase in K' to 0.48. In other words, there is about 50% increase in the amount of 1,2-ethanediamine absorbed in the membrane when Triton X-114 is present. Poly(ethyleneimine) did not act in the same manner as Triton X-114, hence no increase in K' was observed when it was added to the aqueous solution.

3.3 Interfacial polymerization and formation of TFC membranes

The interfacial polymerization of **47** with 1,2-ethanediamine, **74**, shown in Scheme 3.1, was examined with the intent of determining the best conditions for producing a TFC membrane in terms of permeability and morphology. It should be noted that sulfonyl chlorides are substantially less reactive towards amines than carbonyl chlorides.[99-107] As a result the reaction times for thin film polymerization are much longer than those normally encountered with polyamides. Despite this drawback, polysulfonamides have been prepared by interfacial polymerization routes.[72,103,108] The conditions used to prepare membranes described in this work are summarized in Table 3.1.

3.3.1 Use of a $CCl_4/CHCl_3$-H_2O system

The interfacial polymerization of **47** in $CCl_4/CHCl_3$ with **74** in water was examined. Triton X-114 was used as a surfactant and the polymerizations were allowed to proceed for different lengths of time. SEM examination of the resulting membranes (I-DK-T-01 to 08) indicated that in each case, the polysulfonamide films were formed on the surface of the supporting polysulfone. However, as can be seen in Fig. 3.3, it was apparent that the films, particularly those produced with longer reaction times, had a relatively open or porous morphology. This is readily apparent in the cross section of membrane I-DK-T-05 shown in Fig. 3.3 (D). The thickness of these porous films was determined using SEM. It was found that after a 3 h

TABLE 3.1 Fabrication of thin-film composite diazoketone membranes by interfacial polymerization of **47** with **74**

Membranes	Surfactant in aqueous phase		1,2-Ethane-diamine in aqueous phase	Aqueous Phase volume ratio Ethanol /Water	Disulfonyl chloride in organic phase	Organic phase*	Poly-meri-zation time	Membrane Performance**	
	Triton X-114 x 10^4 kmol/m^3	PEI kg/m^3	kmol/m^3		x 10^4 kmol/m^3		h	FLUX x 10^3 kg/m^{2}s	SEP %
Effect of polymerization time on membrane structure and performance									
I-DK-T-01	5.89	-	0.667	0/100	6.89	I	0.25	20.8	23.9
I-DK-T-02	5.89	-	0.667	0/100	6.89	I	0.50	16.6	26.0
I-DK-T-03	5.89	-	0.667	0/100	6.89	I	1.0	13.6	24.0
I-DK-T-04	5.89	-	0.667	0/100	6.89	I	2.0	11.6	26.8
I-DK-T-05	5.89	-	0.667	0/100	6.89	I	3.0	11.8	23.9
I-DK-T-06	5.89	-	0.667	0/100	6.89	I	5.0	12.9	25.1
I-DK-T-07	5.89	-	0.667	0/100	6.89	I	10	14.1	22.1
I-DK-T-08	5.89	-	0.667	0/100	6.89	I	15	13.7	22.2
II-DK-T-01	5.89	-	0.667	0/100	14.2	II	0.25	9.72	29.8
II-DK-T-02	5.89	-	0.667	0/100	14.2	II	0.50	8.60	31.4

II-DK-T-03	5.89	-	0.667	0/100	14.2	II	1.0	7.51	31.4
II-DK-T-04	5.89	-	0.667	0/100	14.2	II	2.0	7.18	32.4
II-DK-T-05	5.89	-	0.667	0/100	14.2	II	5.0	6.83	33.9
II-DK-T-06	5.89	-	0.667	0/100	14.2	II	24	5.86	38.6
Effect of Triton X-114 surfacant concentration on membrane structure and performance									
II-DK-0-00	0	-	0.667	0/100	14.2	II	2.0	21.9	17.8
II-DK-T-07	0.886	-	0.667	0/100	14.2	II	2.0	8.26	41.4
II-DK-T-08	5.89	-	0.667	0/100	14.2	II	2.0	10.9	37.2
II-DK-T-09	17.7	-	0.667	0/100	14.2	II	2.0	10.2	28.9
Effect of 1,2-ethanediamine concentration on membrane structure and performance									
II-DK-PEI-01	-	0.1	0.166	0/100	14.2	II	2.0	46.9	22.2
II-DK-PEI-02	-	0.1	0.333	0/100	14.2	II	2.0	45.5	36.1
II-DK-PEI-03	-	0.1	0.499	0/100	14.2	II	2.0	44.2	47.1
II-DK-PEI-04	-	0.1	0.667	0/100	14.2	II	2.0	42.5	59.0
II-DK-PEI-05	-	0.1	0.900	0/100	14.2	II	2.0	39.7	55.5

II-DK-PEI-06	-	0.1	1.16	0/100	14.2	II	2.0	31.1	53.2
II-DK-PEI-07	-	0.1	1.41	0/100	14.2	II	2.0	23.7	55.5
II-DK-PEI-08	-	0.1	1.66	0/100	14.2	II	2.0	25.7	55.5
Effect of poly(ethyleneimine) concentration on membrane structure and performance									
II-DK-0-00	-	0	0.667	0/100	14.2	II	2.0	21.9	17.8
II-DK-PEI-09	-	$3.0x10^{-2}$	0.667	0/100	14.2	II	2.0	32.6	53.6
II-DK-PEI-04	-	0.10	0.667	0/100	14.2	II	2.0	35.2	55.1
II-DK-PEI-10	-	7.0	-	0/100	14.2	II	2.0	16.6	56.6
Effect of ethanol volume fraction in aqueous phase on membrane structure and performance									
II-DK-T-E-00	5.89	-	0.667	0/100	14.2	II	2.0	14.3	20.0
II-DK-T-E-01	5.89	-	0.667	25/75	14.2	II	2.0	-	-
II-DK-T-E-02	5.89	-	0.667	50/50	14.2	II	2.0	-	-
II-DK-T-E-03	5.89	-	0.667	75/25	14.2	II	2.0	27.9	30.7
II-DK-T-E-04	5.89	-	0.667	100/0	14.2	II	2.0	50.8	13.9

*Organic phase: I. volume ratio: $CCl_4/CHCl_3$ (80:20), II. volume ratio: CCl_4/CH_3COCH_3 (90:10)
**Test conditions: feed solution: 0.17 M NaCl in water, 1.0 L/min., T: 25±2 °C, P: 6000 kPa

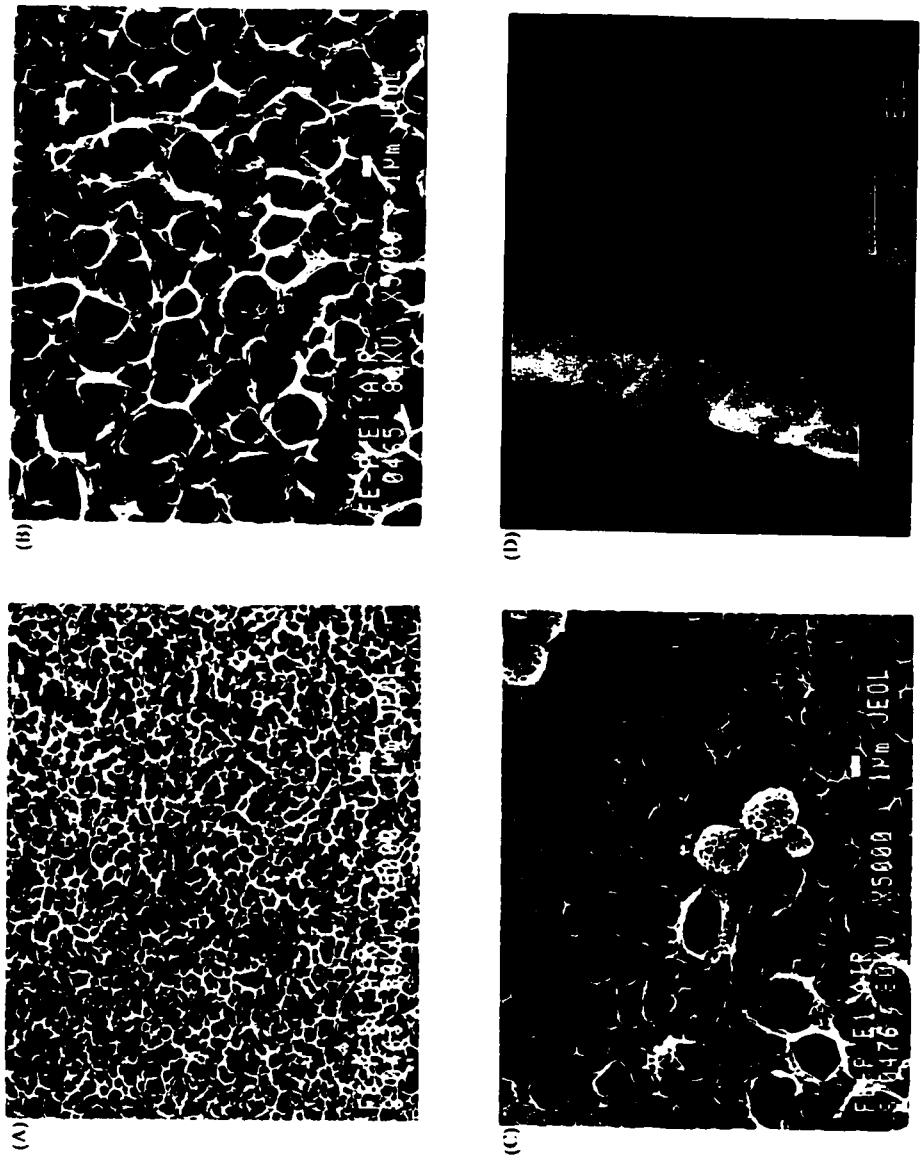

Fig. 3.3 SEM microphotographs of the thin-film composite diazoketone membranes prepared using a $CHCl_3$ /CCl_4 system. Polymerization time and membrane No.: (A) 0.50 h, I-DK-T-02, (B) 1.0 h, I-DK-T-03, (C) and (D) 3.0 h, I-DK-T-05. (A), (B) and (C) top views, (D) cross section view.

polymerization time, a limiting thickness of approximately 2 μm was reached and after this point no further growth in film thickness occurred (Fig. 3.4).

The permeability of these membranes was examined using aqueous NaCl solutions (Table 3.1). As can be seen from the data summarized in Fig. 3.5, all of the membranes exhibited a similar, relatively low separation of NaCl (24%). There was virtually no change in separation as the film increased in thickness. This behaviour would tend to indicate that separation is determined by an initially formed dense layer, further polymerization produces the thick porous layer. The increase in thickness of the film does have an effect on permeate flux (Fig. 3.5). There is a rapid drop in flux over the first hour of the polymerization and subsequently a levelling out at a flux some 65% of the initial value observed. The break point in flux occurs after 1 h polymerization time (Fig. 3.5), whereas the maximum film thickness is reached only after 3 h (Fig. 3.4).

It was clear from these preliminary results, using $CCl_4/CHCl_3$ as the organic solvent, that the TFC membranes produced are far from optimal in terms of their properties. For this reason the use of other solvent systems was examined.

3.3.2 Use of CCl_4/acetone - H_2O system

As was noted above the solubility of **47** is improved in a CCl_4/acetone solvent system. There are previous reports of the use of acetone and related water soluble solvents in the organic phase of an interfacial polymerization.[100] Water miscible

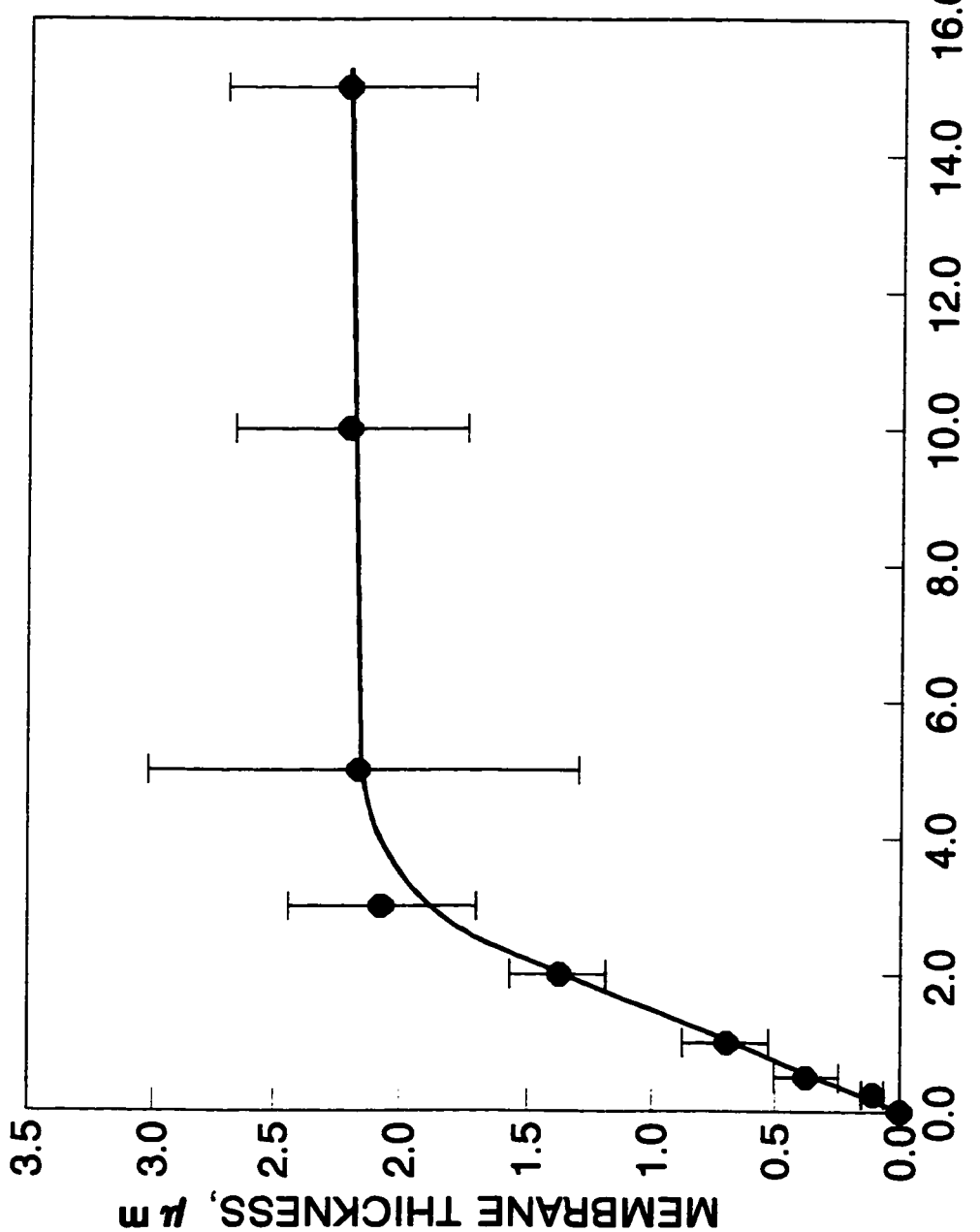

Fig. 3.4 Effect of polymerization time on thickness of the thin-film composite diazoketone membranes with $CHCl_3/CCl_4$ solvent system, Table 3.1: I-DK-T-01 to I-DK-T-08.

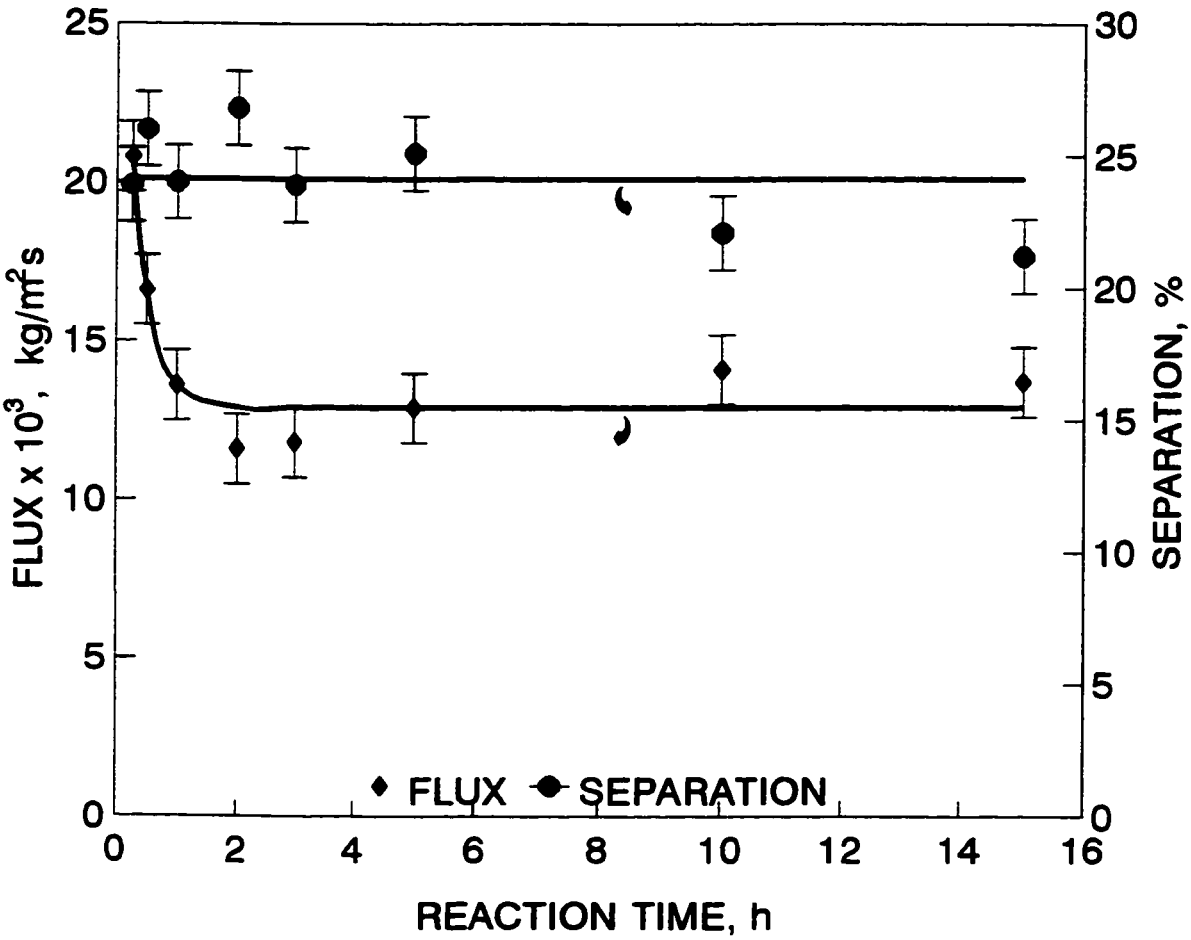

Fig. 3.5 Effect of polymerization time on the performance of thin-film composite diazoketone membranes with $CHCl_3/CCl_4$ solvent system. Table 3.1: I-DK-T-01 to I-DK-T-08.

Test conditions:

Pressure: 6000 kPa,
Temperature: 25 °C,
Feed: 0.17 M NaCl, 1 L/min.

organic phase co-solvents appear to facilitate partitioning of the diamine into the organic phase, thus, accelerating the rate of polymerization.

Interfacial polymerization using a CCl_4/acetone solution of **47** with **74** in water with Triton X-114 as a surfactant once more led to the formation of polysulfonamide films. SEM examination of membrane II-DK-T-01 to 04 showed that at longer polymerization times, the film once more had a textured morphology (Fig. 3.6). However, in the case of this solvent system the pores appeared to have opened or burst to form an open texture. As with $CCl_4/CHCl_3$ at shorter reaction times, the films were smoother (Fig 3.6).

Examination of the permeation properties of the membranes, produced using CCl_4/acetone as organic solvent, showed that the separation of NaCl had slightly improved while the flux had decreased by about 50%, compared to those formed with $CCl_4/CHCl_3$. The effect of variation in the polymerization time on flux and separation are shown in Fig. 3.7. A similar drop in flux and a slight increase in separation was observed, as seen with the previous solvent system (Fig. 3.5).

It was found that the concentration of surfactant (Triton X-114) used in the interfacial polymerization affected both the nature and the permeability of the membrane. The open-pore type morphology was largely eliminated when the polymerization was carried out in the absence of any surfactant (Fig. 3.8). However, membranes formed without any surfactant demonstrated a much reduced NaCl separation and an increased permeate flux (Table 3.1, II-DK-0-00).

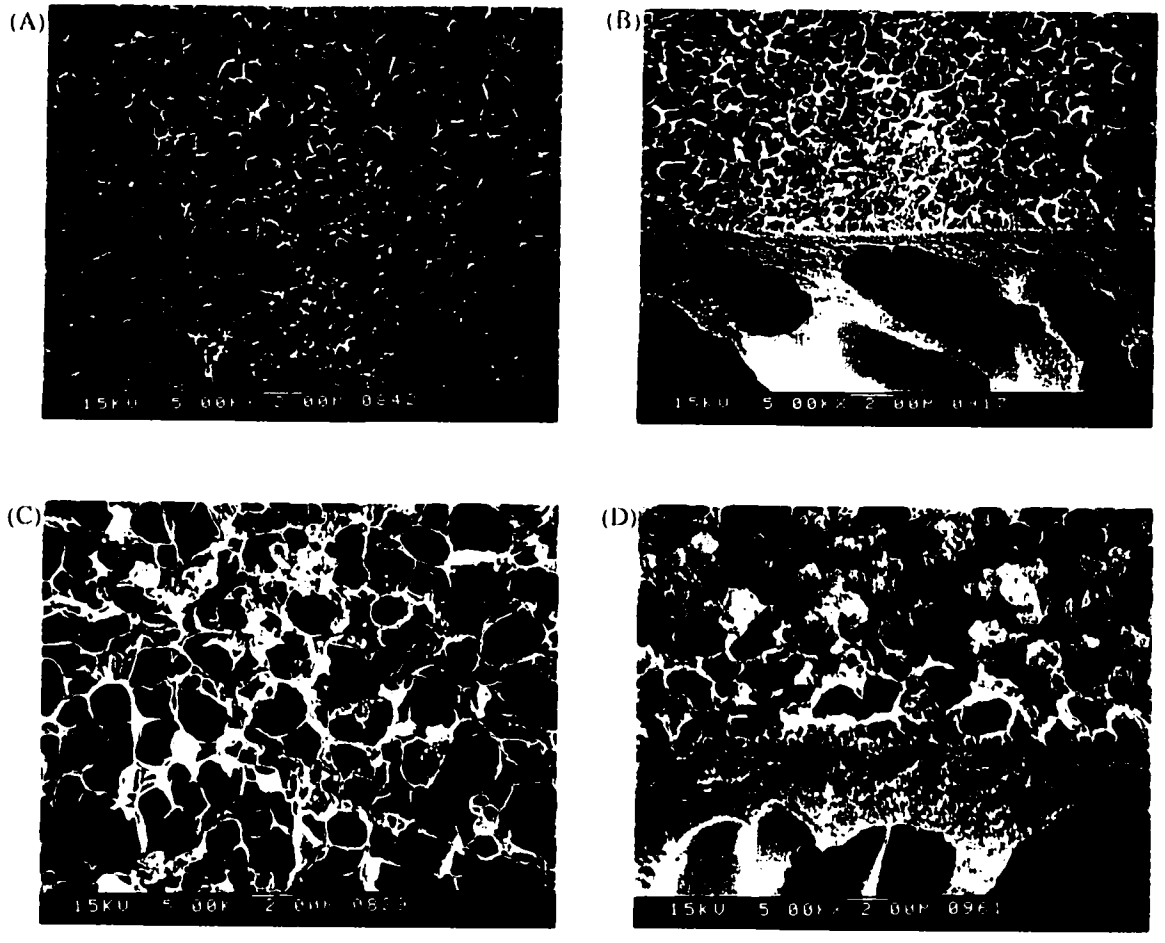

Fig. 3.6 Effect of polymerization time on morphologies of the thin-film composite diazoketone membranes prepared using a CH_3COCH_3/CCl_4 system. Polymerization time and membrane No.: (A) and (B) 0.5 h, II-DK-T-02, (C) and (D) 2.0 h, II-DK-T-04. (A) and (C) top views, (B) and (D) edge-on cross section views.

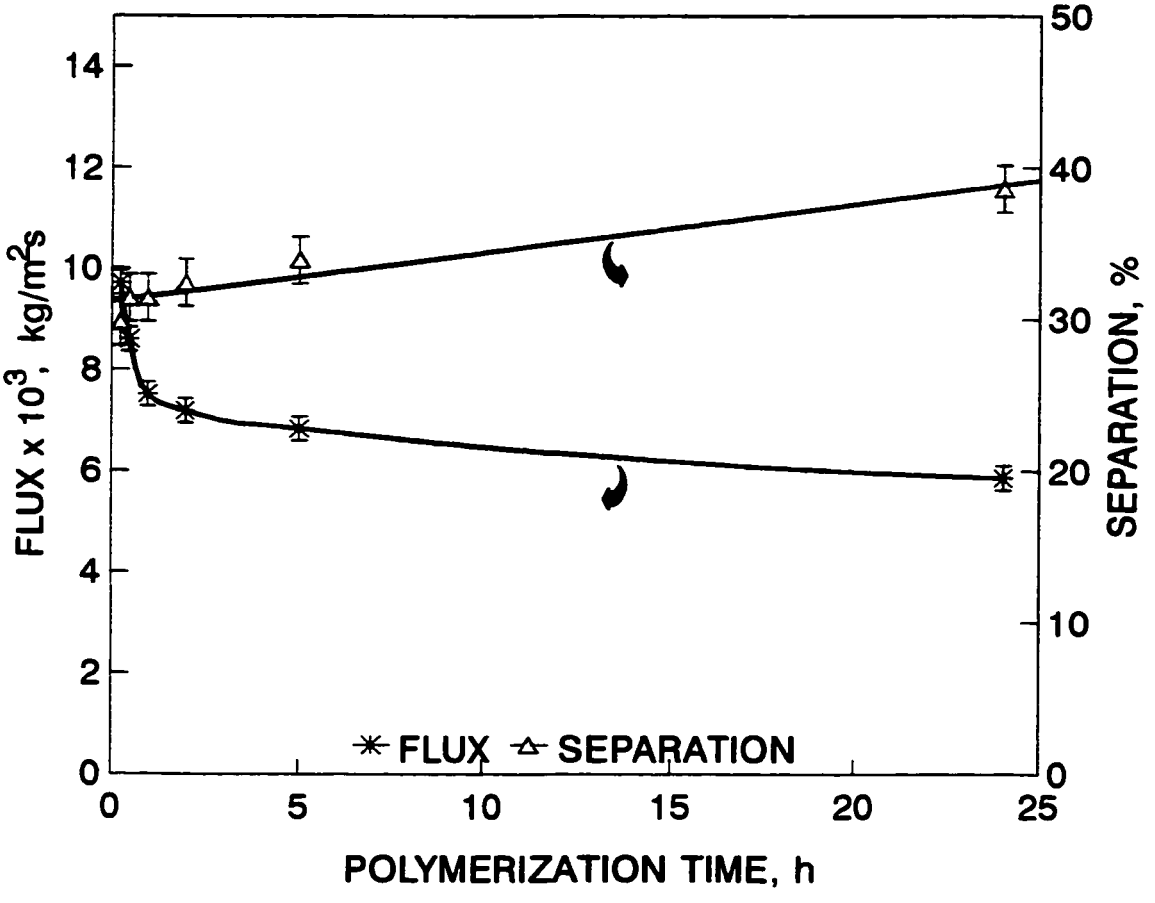

Fig. 3.7 Effect of polymerization time on the performance of thin-film composite diazoketone membranes with acetone/CCl_4 solvent system, Table 3.1: II-DK-T-01 to II-DK-T-06.

Test conditions:

Pressure: 6000 kPa,
Temperature: 25°C,
Feed: 0.17 M NaCl, 1 L/min.

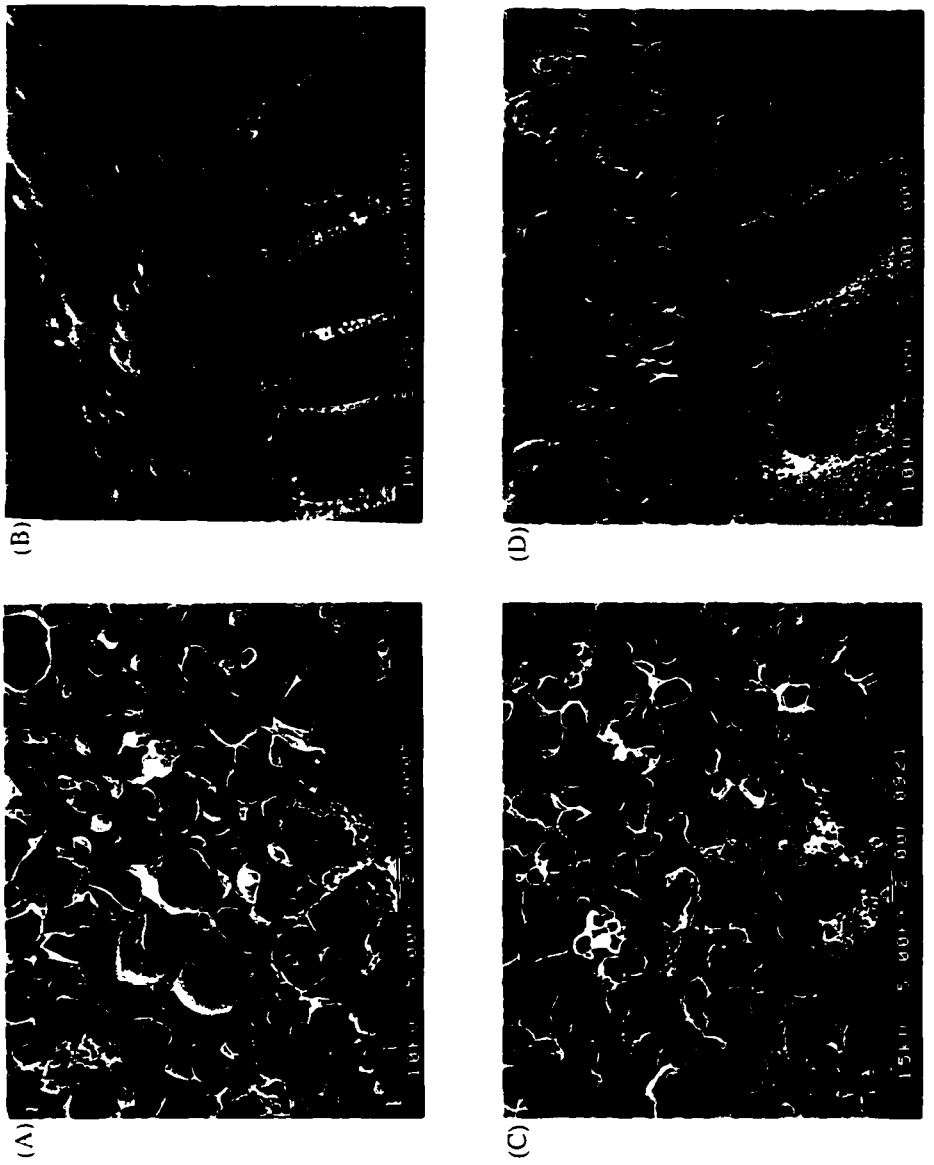
(A)
(B)
(C)
(D)

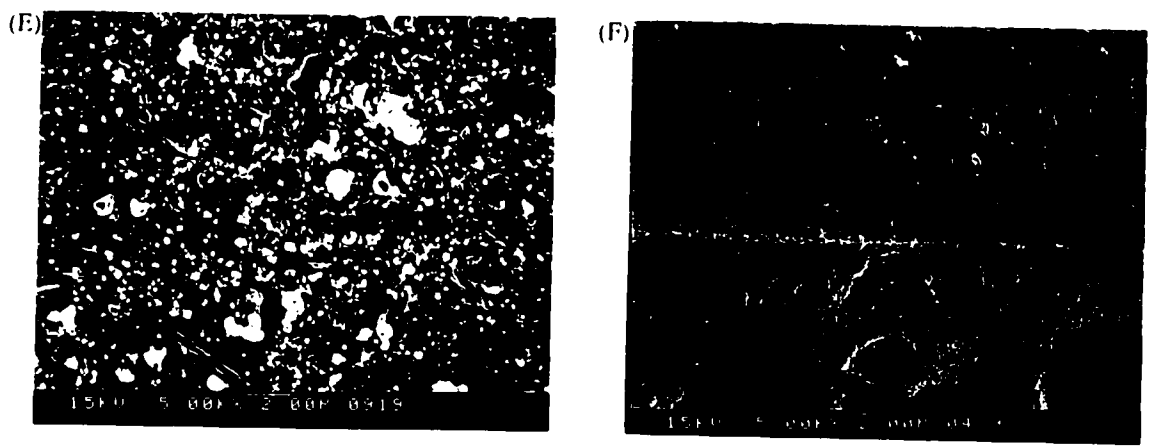

Fig. 3.8 **Effect of Triton X-114 surfactant in aqueous solution on morphologies of the thin-film composite diazoketone membranes. Concentration of Triton X-114 surfactant and membrane No.: (A) and (B) 17.7 x 10^{-4} M,II-DK-T-09, (C) and (D) 5.89 x 10^{-4} M, II-DK-T-08, (E) and (F) 0 M, II-DK-0-00. (A), (C) and (E) top views, (B), (D) and (F) edge-on cross section views.**

As variation in Triton X-114 concentration altered the nature of the thin films produced with the CCl_4/acetone system the use of poly(ethyleneimine) (PEI) as a surfactant was also examined. It should be noted, however, that PEI can function as both a surfactant and a reactant in the interfacial polymerization. Indeed Cadotte et al.[104] have reported the formation of TFC's based on polyamide formation using PEI as the water soluble base component.

The effect of variation in PEI concentration on film morphology and permeability was examined using a standard polymerization time of 2 h. At the highest PEI concentration no 1,2-ethanediamine, **74**, was present in the aqueous phase. TFC membranes were produced under conditions presented in Table 3.1. The SEM's reproduced in Fig. 3.9, illustrate that even with these long polymerization times relatively dense films were produced that seemed to lack the large pore type structures formed with Triton X-114 as the surfactant. The formation of this smooth dense coating layer was perhaps due to a change in interfacial energy with the presence of PEI in the system. The membranes produced with PEI as a surfactant/reactant displayed enhanced separations of NaCl (Table 3.1). There was a large increase in flux of the membranes formed from **74** and PEI, as compared to those prepared without PEI. The importance of the ratio of **74** to PEI was explored by systematically varying the concentration of **74** while keeping that of PEI constant. The results of this study are shown in Fig. 3.10. As can be seen from Fig. 3.10, the maximum separation of NaCl was reached with a concentration of **74** of 0.667 mol/l.

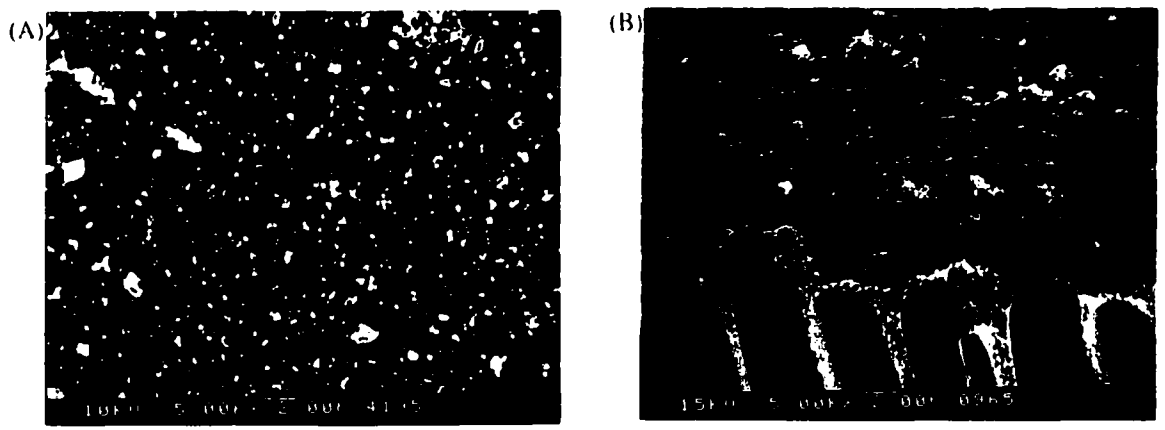

Fig. 3.9 **Effect of poly(ethyleneimine) on membrane morphology. Membrane No.: II-DK-PEI-04, (A) top view, and (B) edge-on cross section view.**

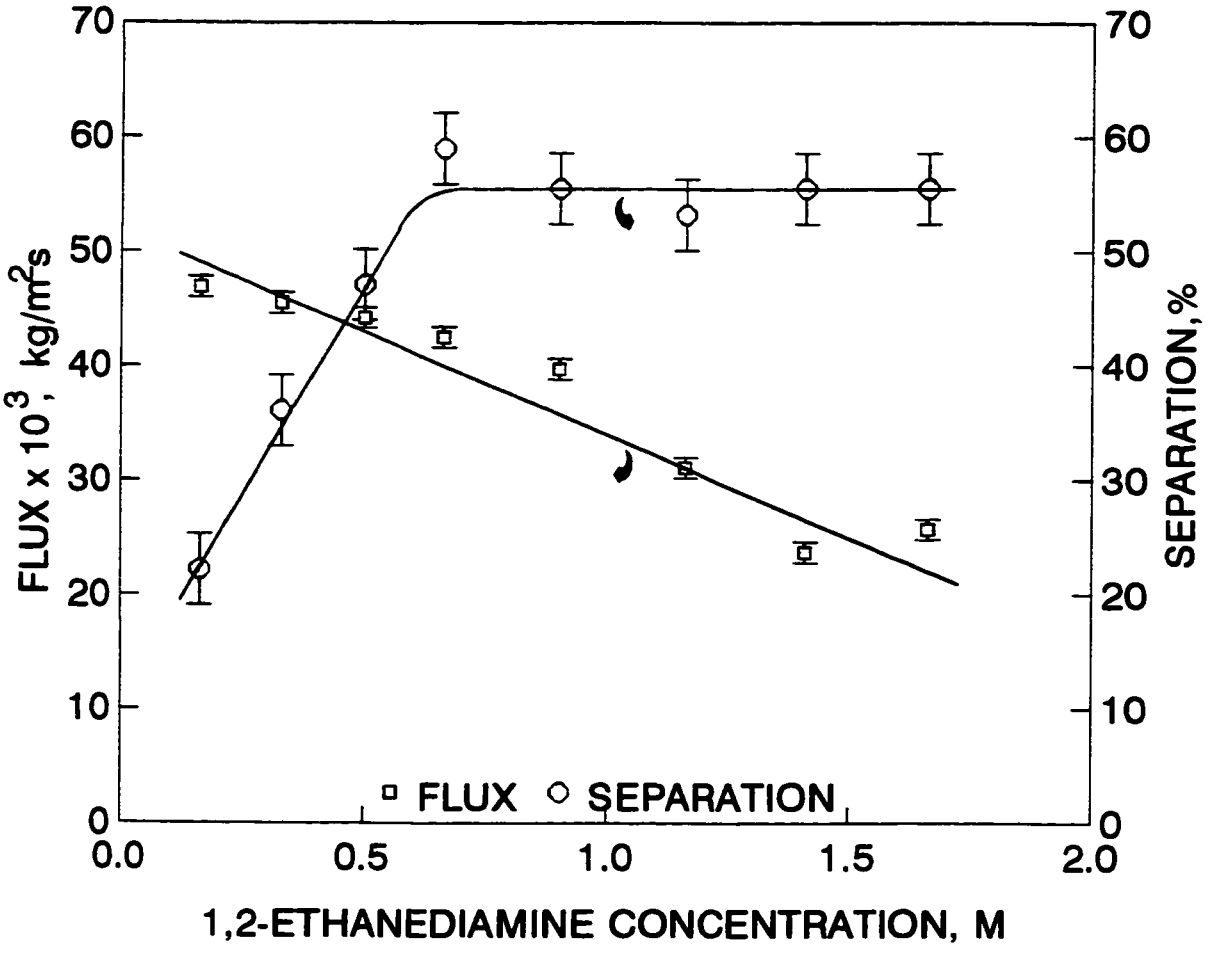

Fig. 3.10 Effect of 1,2-ethanediamine monomer concentration in aqueous phase on the performance of thin-film composite diazoketone membranes with acetone/CCl_4 solvent system, Table 3.1: II-DK-PEI-01 to II-DK-PEI-08.

Test conditions:

Pressure: 6000 kPa,
Temperature: 25°C,
Feed: 0.17 M NaCl aqueous solution.

Flux decreased steadily as the concentration of **74** increased.

In summary, the use of CCl_4/acetone as the organic solvent gave membranes with improved separations but decreased fluxes compared to those formed with $CCl_4/CHCl_3$. The morphology of the membranes produced with CCl_4/acetone was also different, with a more open but still heavily textured surface with Triton X-114 as a surfactant. The membranes produced with PEI as a surfactant look promising in terms of flux and separation. However, for the photochemical transformations intended with these membranes, the unreacted amine functionality present as a result of the use of PEI could present a limitation.

The improvement in the properties of the TFC membranes with the addition of a water soluble co-solvent to the organic phase suggested that it would be instructive to add an organic co-solvent to the aqueous phase. The use of water soluble co-solvents such as ethanol in interfacial polymerizations has previously been reported.[100]

3.3.3 Use of a CCl_4/acetone - H_2O/ethanol system

Interfacial polymerizations were carried out using a standard 2 h reaction time with Triton X-114 (5.89×10^{-4} M) and **74** (0.667 M). The volume ratio of ethanol to water was varied from 0/100 to 100/0. The results of this study are summarized in Fig. 3.11 and Table 3.1.

Examination of the morphology of the TFC membranes produced using these solvent systems indicated that when ethanol was used as the solvent with no water

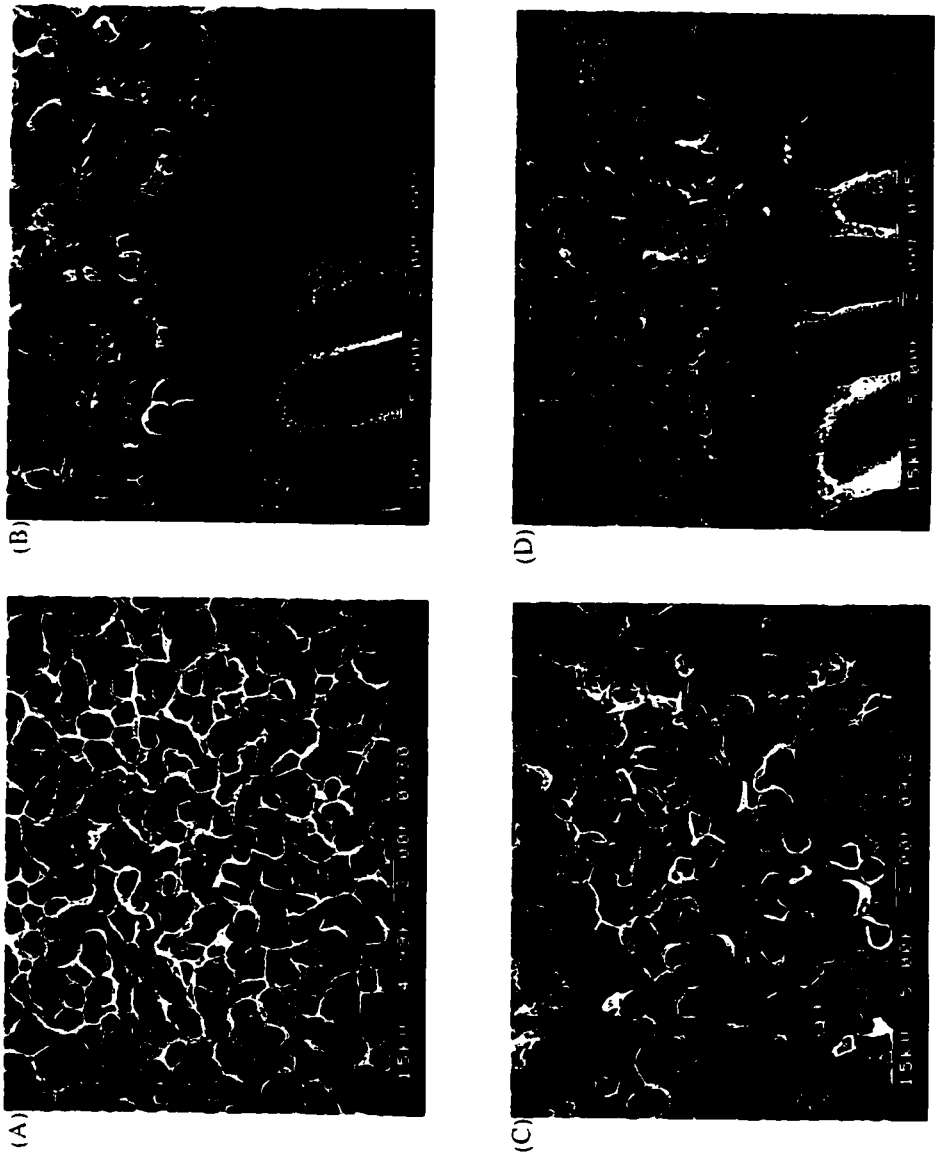
(A)
(B)
(C)
(D)

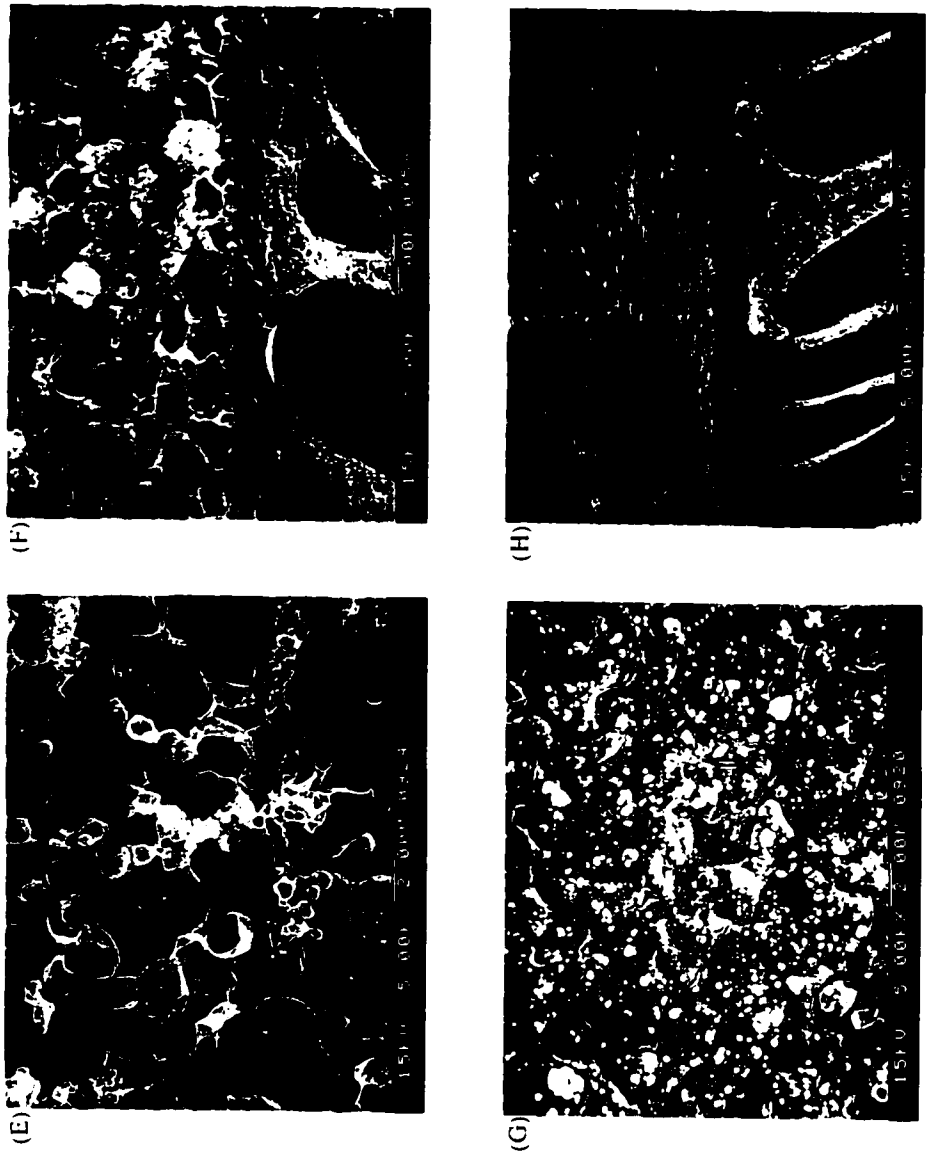
(E)
(F)
(G)
(H)

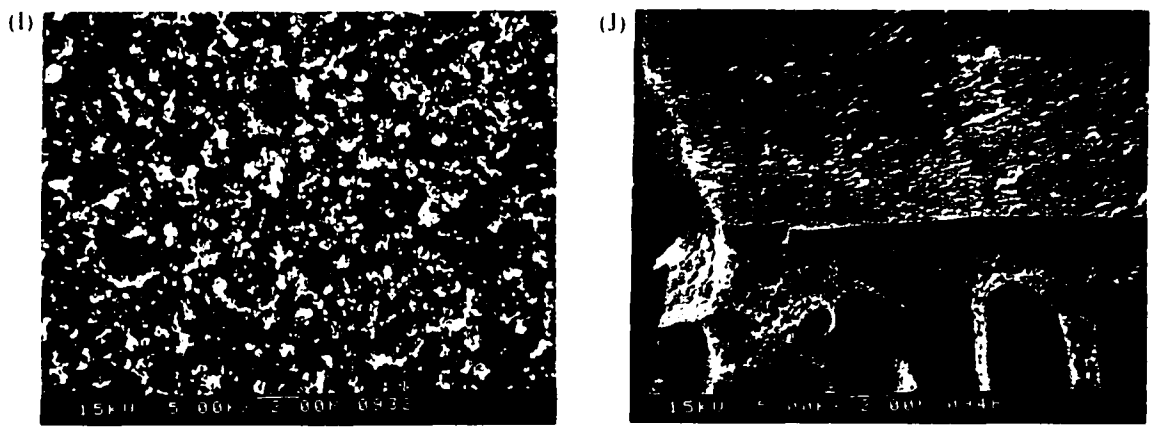

Fig. 3.11 Effect of ethanol volume fraction in aqueous phase on morphologies of the thin-film composite diazoketone membranes. Volume ratio of ethanol to water and membrane No.: (A) and (B): 0/100, II-DK-T-E-00, (C) and (D): 25/75, II-DK-T-E-01, (E) and (F): 50/50, II-DK-T-E-02, (G) and (H): 75/25, II-DK-T-E-03, (I) and (J): 100/0, II-DK-T-E-04. (A), (C), (E), (G) and (I): top views, (B), (D), (F), (H) and (J): edge-on cross section views.

present or with a ethanol/water ratio of 75:25 that a relatively dense, non-textured thin film was formed (Fig. 3.11 (G)-(J)). When the ratio of ethanol to water was 50:50 or less, there were variations in the nature of the open-textured surface, once more rough surfaces were produced. Control experiments in which a membrane formed without ethanol being present was soaked in ethanol for 24 h showed that, once formed, the thin films were not significantly modified by the presence of ethanol. This means that ethanol in the 'aqueous' phase, affects the polymerization process and the formation of the thin film.

The separation/flux of these membranes was examined using aqueous NaCl solutions. As can be seen from the data in Table 3.1 the separation and flux increased by about 50% and 100%, respectively when an ethanol/water ratio of 75:25 was used in the interfacial polymerization as compared to the control membrane having no ethanol present. However, there were major increases in flux and a small drop in separation with membranes produced using just ethanol as a solvent for **74**. The use of ethanol may alter the interfacial energy and, as a result, may cause a disappearance of the textured structure from the coating layer of the thin-film composite membranes so as to give the above observed results (Fig. 3.11 and Table 3.1).

3.4 Characterization of TFC membranes by infrared spectroscopy

The nature of the membranes produced from the interfacial polymerization of **47** and **74** was examined. The surface functionality was probed using ATR FT-IR.

The ATR FT-IR spectra of the base polysulfone and a TFC membrane are shown in Fig. 3.12. The key additional feature in the TFC membrane is the presence of two strong absorptions just above 2000 cm^{-1} that are characteristic of the diazo functionality. It is clear that the interfacial polymerization has led to the incorporation of the desired photochemically active diazoketone grouping, thus allowing the study of the subsequent photochemical surface modification of the thin-film composite membranes.

3.5 Summary

The work described above clearly demonstrates that it is possible to prepare TFC composite membranes based on the formation of a polysulfonamide. Dense and relatively flat films appear to be formed at short polymerization times, however, more open thick films are produced with longer reaction times when using Triton X-114 as a surfactant.

The thin-film composite membranes having smooth and dense coating layers have been prepared in the presence of either PEI or ethanol with a volume fraction $\geq$ 75% in aqueous solution.

The use of Triton X-114 surfactant can significantly increase the uptake of 1,2-ethanediamine monomer by the supporting polysulfone membrane, and the use of water soluble organic solvents in either the aqueous or immiscible organic phase of the interfacial polymerization would seem to improve the properties of the thin film.

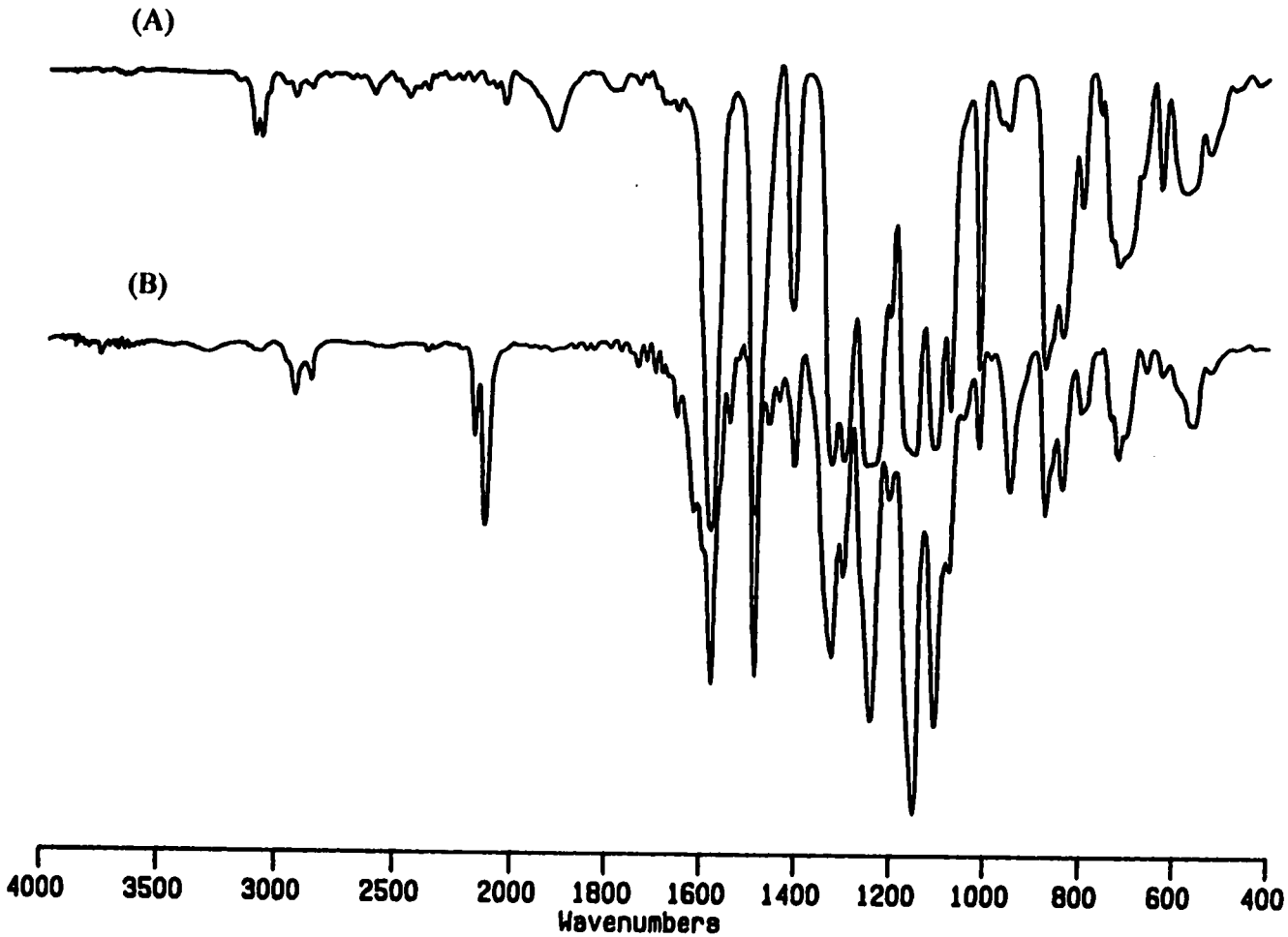

Fig. 3.12 Attenuated total reflectance FT-IR spectra of (A) the supporting polysulfone membrane and (B) the thin-film composite diazoketone membrane

It is also clear from this work, that the rejections (NaCl) of these membranes are not high, but the thin films do contain diazoketone functionality. As such, these membranes should be suitable vehicles to probe the impact of photochemical surface modification on the properties of the membranes.

3.6 Experimental

3.6.1 Materials

All of the chemicals used in this chapter were purchased from Aldrich Chemical Inc. No further purification was applied before use. The water used was deionised using reverse osmosis followed by carbon absorption and ion exchange resin.

The room temperature was controlled at approximately 25 ± 2 °C.

3.6.2 Solubility of monomer 47 in a mixed solvent of 10%(vol.) acetone and 90%(vol.) carbon tetrachloride

Monomer 47 (1.0 g) was dissolved in 25 ml of acetone in a 250 ml volumetric flask, to which carbon tetrachloride was added while stirring to make a total volume of 250 ml. A yellow precipitate appeared after about 100 ml of carbon tetrachloride was added to form a suspension. This suspension was stirred for 3 h, then gravity filtered, producing 100 ml of an orange coloured solution in a 100 ml volumetric flask. This saturated solution was transferred to a preweighed 250 ml flask. The

solvents were removed by evaporation using a rotary evaporator under reduced pressure at about 70 °C to give a yellow solid, which was further dried *in vacuo* for 3 h. The flask with the yellow solid was weighed again. Duplicate experiments were carried out to give a solubility of **47** in 10%(vol.) acetone and 90%(vol.) carbon tetrachloride as 2.26 kg/m^3. The possible volume change due to mixing was not considered.

A similar procedure was used to determine the solubility of **47** in 20%(vol.) chloroform and 80%(vol.) carbon tetrachloride to give a solubility 0.486 kg/m^3.

3.6.3 Measurement of the uptake of 1,2-ethanediamine, 74, by the support polysulfone membrane

The support polysulfone membrane was pretreated by soaking in a mixed solvent of 10%(vol.) chloroform and 90%(vol.) carbon tetrachloride overnight, then rinsed with ethanol and water, sequently. This treated membrane was immersed in 100 ml of aqueous solution containing 5.89x10^{-4} M of Triton X-114 surfactant and varying amounts of 1,2-ethanediamine for 2.5 h, then removed from the aqueous diamine solution and rolled with a plastic roller to remove the aqueous solution on the membrane surface. At this point, some of the membranes were used to measure the membrane thickness. At each diamine concentration, 20 pieces of membrane samples were divided into two groups and titrated with 0.1 N HCl aqueous solution. A solution of methyl red and cresol was used as an indicator.[109] The titration results were

averaged to give the uptake of 1,2-ethanediamine by the support polysulfone membrane. The concentration of 1,2-ethanediamine in the support membrane was calculated based on the total volume occupied by the membrane.

The uptake of 1,2-ethanediamine by the support polysulfone membrane, from the aqueous solutions containing either no surfactant or 0.1 g/L of poly(ethyleneimine) and varying amounts of 1,2-ethanediamine, was measured in a similar way described above.

3.6.4 Membrane fabrication

The thin film composite membranes were prepared by the interfacial polymerization of **47** with **74**. The support polysulfone UF membrane (area=3.2 x 10^{-3} m^2) was soaked in water overnight, then immersed in 100 ml of an aqueous 1,2-ethanediamine solution containing either Triton X-114 or poly(ethyleneimine) as a surfactant for 2.5 h. The concentration of **74** in the aqueous solutions was changed from 0.2 to 1.5 M, Triton X-114 from zero to 1.77×10^{-3} M, and poly(ethyleneimine) from zero to 7 g/L. Then, the membrane was taken out of the above solution, rolled with a plastic roller to remove the extra solution on the membrane surface. The membrane was immersed into 200 ml of a solution of 1.42×10^{-3} M of **47** in a mixture solvent of 10%(vol.) acetone and 90%(vol.) carbon tetrachloride for a certain time period to polymerize into a thin film composite membrane. The interfacial polymerization occurred on both sides of the support membrane.

The thin-film composite membranes were prepared in the same way described above when using other solvent systems.

3.6.5 Measurement of the membrane morphologies and thickness

Morphology and thickness of the thin-film layers were measured by scanning electron microscopy (SEM). The thin-film composite membrane was fractured in liquid nitrogen. For each membrane, 3-5 specimens were mounted on a copper holder, and coated with gold before observation. The cross sections were observed at 80 kV and 20000 magnification using a JEOL 1200 EX II SEM. The thin-film thickness are tabulated in Appendix A and B.

The area occupied by the pores in the cross section of the thin-film layer, formed by interfacial polymerization, was measured using a Sigma Scan System.[110] The porosity of the thin film formed by interfacial polymerization was calculated using a ratio of the area occupied by the pores to the total area of the cross section of the surface layer of the thin-film composite membrane. The measured porous area, total area and porosity of the thin film are given in Appendix C.

3.6.6 Infrared Spectroscopy

The membranes were cut into two identical 1 cm x 5 cm pieces and mounted on both sides of a ZnSe single crystal. The ATR-FT-IR spectra were obtained using a twin parallel mirror reflection attachment. The sample chamber was swept by

nitrogen for 10 min. before recording the spectra and 256 scans were collected using a Biorad Digilab FTS-40 spectrometer.

3.6.7 Reverse osmosis experiments

The flat thin-film composite membranes were tested in a reverse osmosis radial flow test system, which consisted of a pump, six RO cells, a pressure gage and a pressure regulator. The effective membrane area was 1.5×10^{-3} m^2, the feed flow rate was 1.0 L/min. A feed solution was pressurized and circulated over the surface of the membranes. The membranes were stabilized by circulating the feed solution at 6000 kPa for at least four days before any measurements were taken.

The reverse osmosis experiments were carried out at 6000 kPa and 25 ± 2 °C. Samples of the permeate were collected in certain time intervals to determine the permeate flux through the membrane (in kg/m^2s). The flux measured at a slightly different temperature from 25 °C was corrected to 25 °C using the following equation,[12]

$$FLUX_{25^oC} = FLUX_T \left(\frac{\eta_T \, \rho_{25}}{\eta_{25} \, \rho_T} \right) \qquad 3.3$$

where η_{25} and η_T are the viscosity of water at 25 and T °C, respectively, ρ_{25} and ρ_T are the density of water at 25 and T °C, respectively.

The conductivity of the permeate and feed solution were measured (YSI Model

31) and compared with calibration curves to give solute concentration in the permeate and feed solution, respectively. The separation of solute was defined by:

$$\text{Separation}, \% = (C_F - C_P)/C_F \times 100\%$$

where C_F is the solute concentration in the feed solution, C_P is the solute concentration in the permeate. Duplicate membranes were tested under the same conditions and the results were averaged.

Chapter 4

Photochemical Surface Modification of Thin-Film Composite Membranes

The results of the photochemical surface modification of the thin-film composite membranes are reported in this chapter. In order to monitor the photochemical surface modification, methods for characterization of the membrane surface have been developed. The impact of photochemical surface modification on membrane performance has been systematically examined so as to evaluate the effectiveness of this photochemical modification method.

This chapter consists of three major sections. The first section outlines the strategy. The second section studies surface modification, characterization and the impact of photochemical surface modification on membrane performance. Experimental details are given in the third section.

4.1 Strategy

A strategy for photochemical surface modification is illustrated in Scheme 4.1 for membranes bearing a diazoketone functionality.

The use of long wavelength (350 nm) light should allow the activation of the diazoketone group without any significant absorption of light by molecules in the polymer

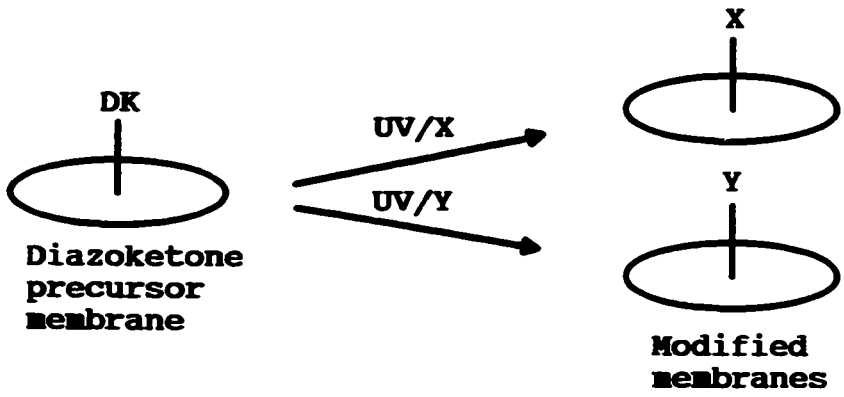

Scheme 4.1 Strategy for photochemical surface modification of a TFC membrane.

backbone.[21,69-72] The base membrane should not be affected by the photoreactions and, as a result, the membranes should possess the same morphology as the starting diazoketone-containing membrane and differ only in the chemical composition of the surface. As was shown in Chapter 2, the chemical modification of the diazoketone groups depends on the solvent/reagents present during the photoreaction. This should allow a systematic investigation of the effect of surface functionality on the membrane performance.[70-72]

The membranes were characterized in this work by both transmittance and attenuated total reflectance FT-IR. A key problem encountered was how to prepare samples for measurement of transmittance spectra. A peeling method was developed to prepare suitable samples for infrared analysis. For comparison purposes, the thin films were also prepared by liquid-liquid interfacial polymerization.

4.2 Photochemical Surface Modification

As was shown in the previous chapter, shorter polymerization times, such as 15 min., gave membranes with thinner and denser surface layers (Fig. 3.6). With longer polymerization times, such as 2 h, the membranes exhibited textured structures in the surface layer (Fig. 3.6). These different physical structures in the surface layer affected membrane performance. As a result, in this work, the photochemical surface modification of the DK membranes was examined for membranes prepared using different polymerization times.

Two methods for photochemical surface modification were examined. These two methods differ in the drying of the diazoketone precursor membrane prior to the irradiation and the conditions used in the photoreactions. The membranes prepared by these two methods are listed in Table 4.1.

4.2.1 Method 1

In method 1, the initial DK membrane was air dried prior to the photochemical surface modification. It was then irradiated in air with 350 nm wavelength light in the presence of a reactant.

4.2.1.1 Polymerization for 2 Hours

Previous work of the McMaster membrane group has shown that the photochemical surface modification of the DK membrane not only altered the surface

Table 4.1 **Photochemical surface modification of the thin-film composite DK membranes**

* Conditions * * * Membranes *	Polymers shown in Scheme 4.2	Poly-meri-zation time h	Drying condi-tion	hν Solvent	hν Atmos-phere	Characterization		
						IR	SEM	SEP.
Method 1								
II-DK-T-01-hν-INDENE ACID	**76**	0.25	in air	1%AcOH/H_2O	air	+	-	+
II-DK-T-01-hν-GLYCEROL	**77**	0.25	in air	AcOH	air	+	-	+
II-DK-T-01-hν-ETHYL ESTER	**78**	0.25	in air	CH_3CH_2OH	air	+	-	+
II-DK-T-01-hν-S. CROWN ETHER	**79**	0.25	in air	AcOH	air	+	-	+
II-DK-T-01-CROSS LINKED-hν-GLYCEROL	**77**	0.25	in air	AcOH	air	+	-	+
II-DK-T-04-hν-INDENE ACID	**76**	2.0	in air	1%AcOH/H_2O	air	+	+	+
Method 2								
II-DK-T-04-D-hν-INDENE ACID	**76**	2.0	*in vacuo*	1%AcOH/H_2O	nitrogen	+	+	+
II-DK-T-04-D-hν-GLYCEROL	**77**	2.0	*in vacuo*	$HOCH_2CH(OH)CH_2OH$	nitrogen	+	+	+
II-DK-T-04-D-hν-ETHYL ESTER	**78**	2.0	*in vacuo*	CH_3CH_2OH	nitrogen	+	+	+
II-DK-T-04-D-hν-S. CROWN ETHER	**79**	2.0	*in vacuo*	AcOH	nitrogen	+	+	+

chemistry but also changed the physical structure of the surface layer.[21] As was shown in the previous chapter of this thesis, with polymerization times of 2 h, thin-film composite membranes having honey comb-like structures in the thin-film coating layer were produced.

Photochemical surface modification reactions are shown in Scheme 4.2. The indene acid functionalized membrane was prepared by irradiation of the DK membrane in water containing 1% acetic acid. The performance of the initial DK membrane and indene acid functionalized membranes are shown in Fig. 4.1. All of the data presented in Fig. 4.1 were obtained from duplicate specimens of the membranes, except for the data for II-DK-T-04 with NaCl, which was taken from a single sample of the membrane. In this instance, one of the duplicate samples was broken when taking this data. The upper and lower ends of an error bar represent the measured values of the duplicate samples with the center of the error bar being the average of the two data. The lines joining the data points in Fig. 4.1 and other similar figures in this chapter are not meant to imply a continuum of expected values; they are merely an aid in viewing the changes in the data with solute.

The pH of the feed solution was about 6. At this pH indene acid is expected to be mainly in the ionized or carboxylate form.[111,112] The effect of conversion of the diazoketone functionality to the indene acid in the surface layer of the thin-film composite membrane on membrane performance can be clearly seen in Fig. 4.1. In reverse osmosis tests on the indene acid membrane, low rejections were seen for salts with monovalent

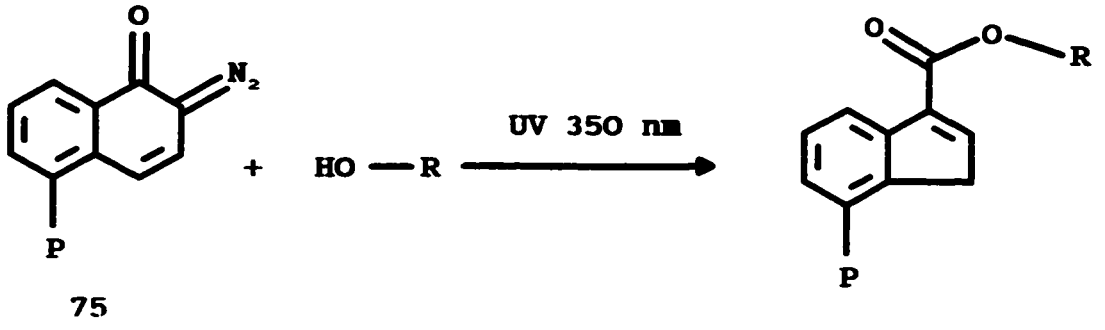

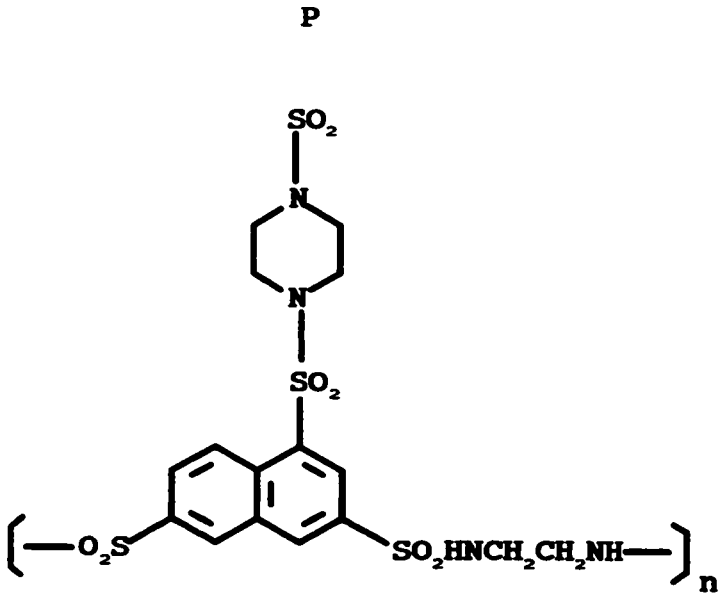

and other isomers

R

76 H

77 $CH_2CH(OH)CH_2OH$

78 CH_2CH_3

79

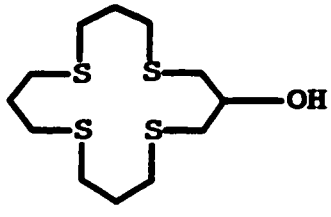

Scheme 4.2 Functionalization of TFC membranes.

anions (chloride), but high rejections for salts with divalent anions (sulfate). No significant selectivity differences were noted between monovalent (sodium) and divalent (magnesium) cations. This result strongly suggests an anionically charged surface barrier layer. The negatively charged carboxylic group rejects solute by Donnan exclusion.[72,113,114] This effect enhances the separation of all solutes with the acid membrane as compared to the DK membranes. This result is consistent with that previously reported by the McMaster membrane group.[72] The result is also consistent with the negatively charged piperazine-trimesoyl chloride membrane, in which the hydrolysis of the unreacted carbonyl chloride formed carboxylic acid.[5]

It can also be seen from Fig. 4.1 that a similar trend is observed with the parent DK membrane, suggesting that this membrane was also negatively charged. The origin of this negatively charge is probably due to the hydrolysis of the sulfonyl chloride end groups of the polymer. However, the impact of this negatively charged surface on separation was less pronounced than that of the indene acid functionalized membrane. Overall, the enhanced separation observed with the irradiated membrane demonstrates that photochemical surface modification is occurring.

The acid membrane is expected to be more hydrophilic than the initial DK membrane. However, the former exhibits lower flux than the latter (Fig. 4.1). This result is unexpected and can not be explained by the suggested change in surface chemical properties. Factors other than chemical properties of the membrane surface might operate in this case. For example, the physical structure of the membrane might change

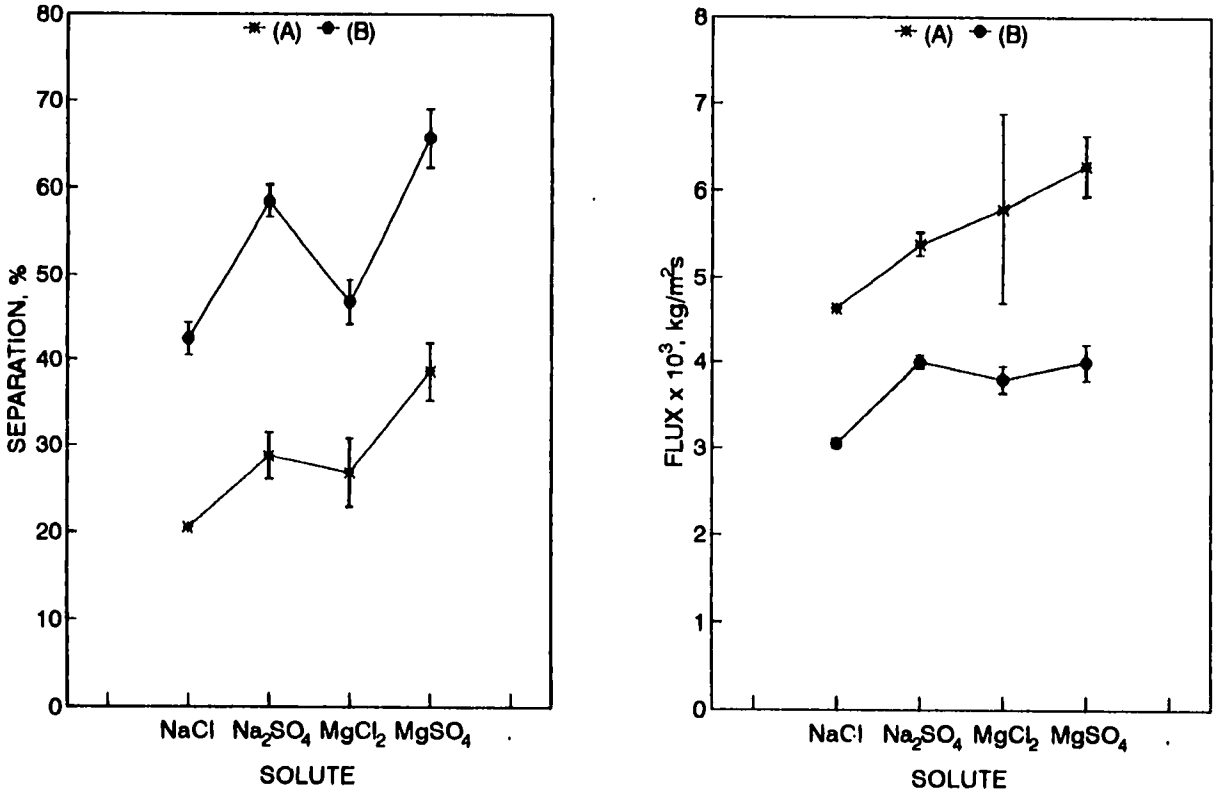

Fig. 4.1 Effect of photochemical surface modification on membrane performance.

The membranes were prepared by method 1 under the conditions given in Tables 3.1 and 4.1, respectively.

(A) II-DK-T-04, (B) II-DK-04-hv-INDENE ACID.

Test conditions: Feed: 0.17 M solute, 1.0 L/min., P: 6000 kPa, T: 25°C, pH=6.

to some extent upon irradiation, resulting in a decrease in flux. In order to evaluate this possibility, the morphologies of these membranes were studied.

The morphologies of the initial DK membrane and the indene acid functionalized membranes are shown in Fig. 4.2. The initial DK membrane had the honey comb-like or cellular structures in the surface layer (Fig. 4.2 (A) and (B)). The average thickness of the surface layer was of the order of 1 micrometer. Upon the photochemical conversion of the diazoketone to the indene acid, these open textured structures partially collapsed (Fig. 4.2 (C) and (D)). It is suggested that this change results in the substructure becoming more dense leading to a reduction in flux.[21]

ATR-FTIR spectra of the parent DK membrane and the indene acid membrane are shown in Fig. 4.3. Strong peaks at about 2150 cm^{-1} attributed to the diazo groups were observed (Fig. 4.3 (A)), indicating that the polysulfone support membrane was successfully coated with a thin film of 75. These bands attributed to the diazo groups disappeared upon irradiation, and a new peak at 1721 cm^{-1} was observed (Fig. 4.3 (B)), suggesting that the indene acid was formed in the surface layer of the thin-film composite membrane. This result is consistent with the membrane performance and morphologies discussed above.

The above results suggest that the photochemistry is affecting not only the surface of the thin-film layer, but also the working level where the separation characteristics are determined. The results also suggest that the photochemical derivatization process studied for altering the surface functionality of a thin-film composite membrane can, with certain

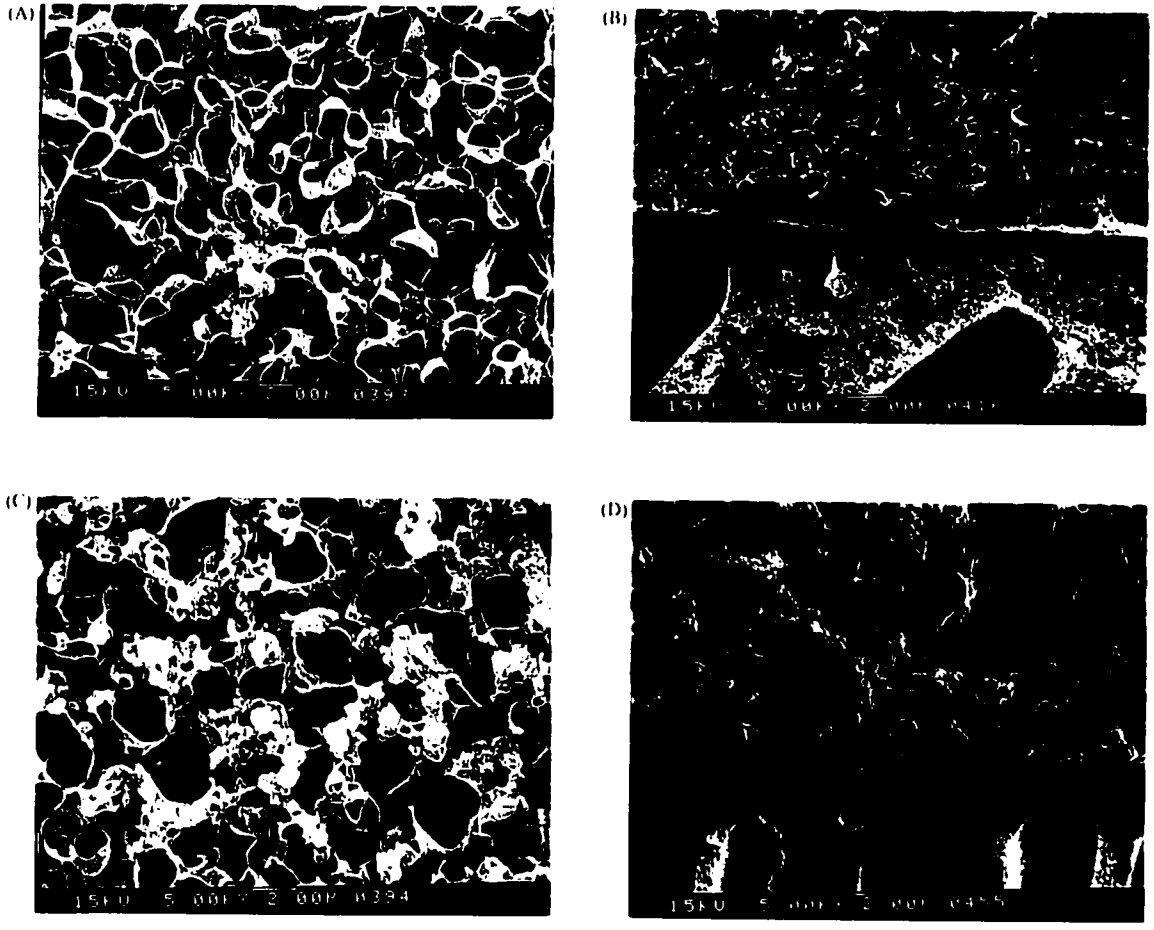

Fig. 4.2 **Effect of photochemical surface modification on membrane morphologies**

The membranes were prepared by method 1 under the conditions given in Tables 3.1 and 4.1, respectively.
(A) and (B) II-DK-T-04, (C) and (D) II-DK-T-04-hv-INDENE ACID.
(A) and (C) top views, (B) and (D) cross section views.

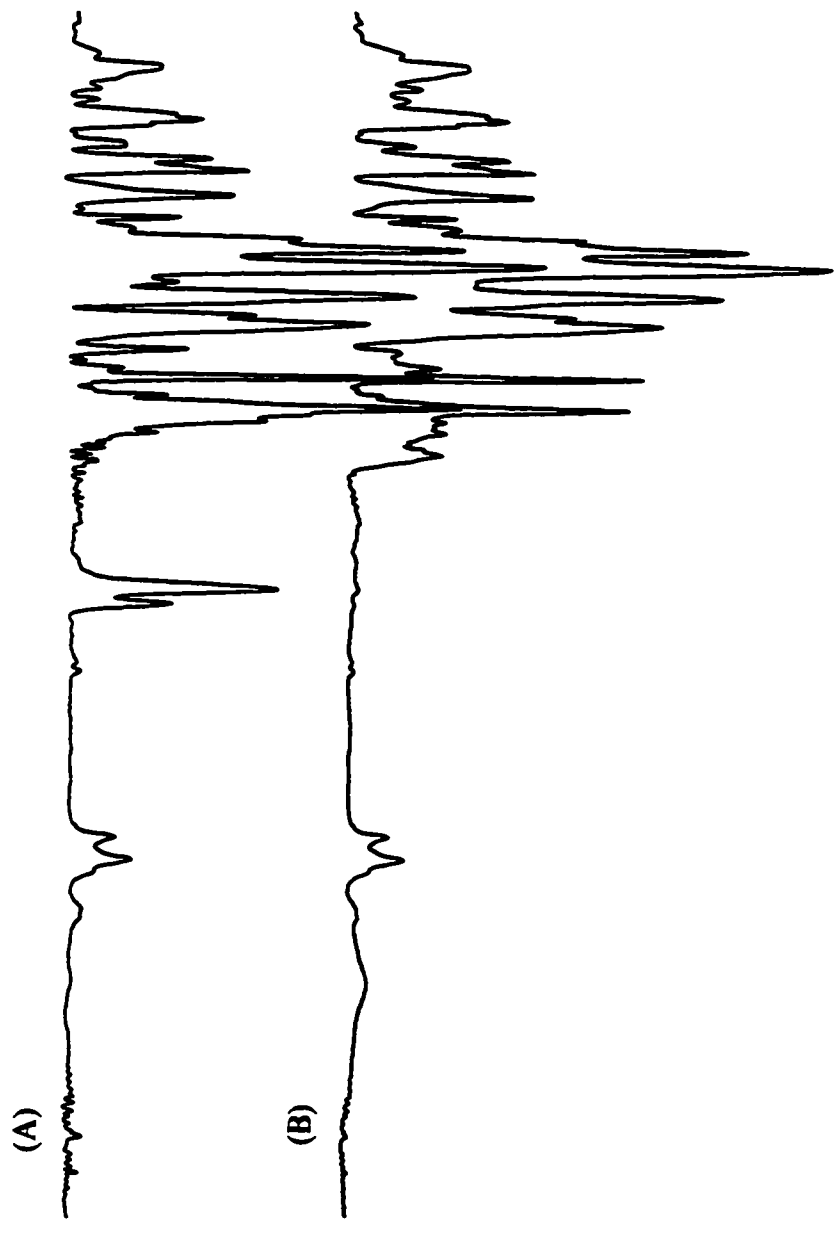

Fig. 4.3 ATR-FTIR spectra of an initial diazoketone membrane and a photochemically modified membrane.

(A) II-DK-T-04, Table 3.1,
(B) II-DK-T-04-hv-INDENE ACID, Table 4.1.

reagents, lead to an alteration in the physical structure of the thin film.

4.2.1.2 Polymerization for 15 Minutes

In order to avoid the interference of the morphology change upon irradiation, thin-film composite DK membranes were prepared by the interfacial polymerization of disulfonyl chloride, **47**, with 1,2-ethanediamine, **74**, (Scheme 3.1) for 15 min. This membrane has a thin and relatively smooth surface layer (Fig. 3.6 (A) and (B)).

Four photochemical reactions shown in Scheme 4.2 were studied. These potentially produce functionalized membranes having pendent carboxylic acid, hydroxyl, ethyl ester and sulfur-containing crown ether groups. The basis for these transformations has been discussed in Chapter 2 of this thesis.

The indene acid membrane was prepared by irradiation of the DK membrane in water containing 1 % acetic acid. The presence of the acetic acid can eliminate formation of coloured (dye) by-products.[91,96] The ethyl ester membrane was obtained by the irradiation of the DK membrane in ethanol. The glycerol and sulfur-containing crown ether functionalized membranes were prepared by the irradiation of the DK membranes in acetic acid solutions containing glycerol and 1,5,9,13-tetrathiacyclohexadecane-3,11-diol, respectively.

Examination of the surface of the parent DK membrane and the photochemically modified membranes by ATR-FTIR showed that detectable quantities of the diazoketone were being incorporated into the thin film. The infrared spectrum of the DK membrane,

II-DK-T-01, exhibited the characteristic diazo bands at about 2150 cm^{-1} (Fig. 4.4 (A)). Irradiation of the DK membrane with 350 nm wavelength light in the presence of ethanol resulted in the replacement of the 2150 cm^{-1} bands (Fig. 4.4 (A)), with strong bands at about 1717 cm^{-1}, which are apparently attributed to carbonyl stretching vibrations (Fig. 4.4 (D)). In a control experiment, a DK membrane was soaked in ethanol in the absence of light for the same time period (30 min.) as that used in the photoreaction. This control membrane (Fig. 4.4 (B)), showed essentially the same infrared spectrum as the untreated DK membrane. Irradiation of the DK membrane in 1% aqueous acetic acid solution also resulted in the replacement of the 2150 cm^{-1} bands (Fig. 4.4 (A)) with strong bands at about 1717 cm^{-1} (Fig. 4.4 (C)). Clearly, the results show that a photochemical modification is occurring with these membranes. However, it is hard to distinguish between spectra (C) and (D) (Fig. 4.4), and this raises questions as to what photoreactions are taking place.

In order to characterize further these membranes, the RO performances of the thin-film composite DK membrane and the photochemically modified membranes were studied. The results are shown in Fig. 4.5. The data reported for the DK membrane and ethyl ester functionalized membranes were obtained by averaging the results of tests on four pieces of membrane from two different experiments. The data reported for other membranes were an average of two pieces of membrane sample from a single batch.

In reverse osmosis tests on these photochemically modified membranes, low rejections were observed for salts with monovalent anions (chloride), but high rejections

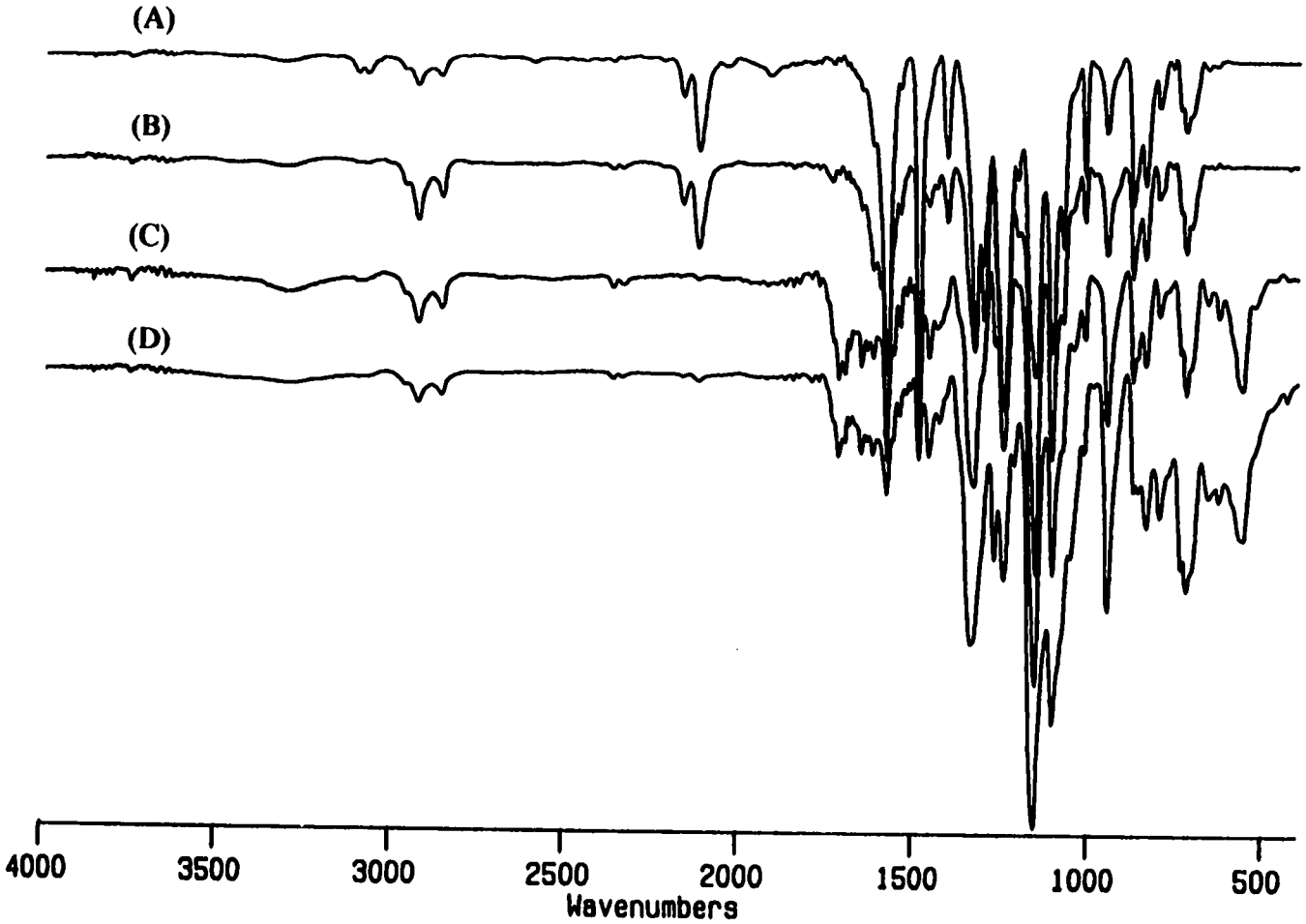

Fig. 4.4 ATR-FTIR spectra of the initial diazoketone and photochemically modified membranes.

(A) II-DK-T-01, Table 3.1,
(B) II-DK-T-01-ETHANOL TREATED,
(C) II-DK-T-01-hν-INDENE ACID, Table 4.1,
(D) II-DK-T-01-hν-ETHYL ESTER, Table 4.1.

for salts with divalent anions (sulfate) (Fig. 4.5). Less pronounced selectivity differences were noted between monovalent (sodium) and divalent (magnesium) cations (Fig. 4.5). These results suggest that the barrier layers of all these membranes, including the starting DK membrane, are negatively charged.

As shown in Scheme 4.2, a negatively charged barrier layer was only expected for the indene acid functionalized membrane. The pH of the feed solution was about 6 ($pH=6\pm0.5$), and at this pH the indene acid exists mainly in the ionized form.[111,112] However, the separation behaviour of the DK membrane and the ethyl ester functionalized membrane shown in Fig. 4.5 suggests that the negative charge in the barrier layer is attributed to the presence of $-SO_3H$ formed by hydrolysis of the end group $-SO_2Cl$ of the polymer. This effect appears to overwhelm the impact of photochemical surface modification.

Despite small differences in relative separations observed between the indene acid and ethyl ester functionalized membranes, these two modified membranes showed significantly higher separations towards the four inorganic solutes studied than the control DK membranes.

As expected the indene acid functionalized membrane is more hydrophilic than the parent DK membrane and as a result shows a higher flux than the latter (Fig. 4.5). The more hydrophobic ester membrane should show lower flux than both the DK and indene acid membranes. However, an opposite result was observed (Fig. 4.5).

In order to understand this unexpected result, a control experiment of soaking the

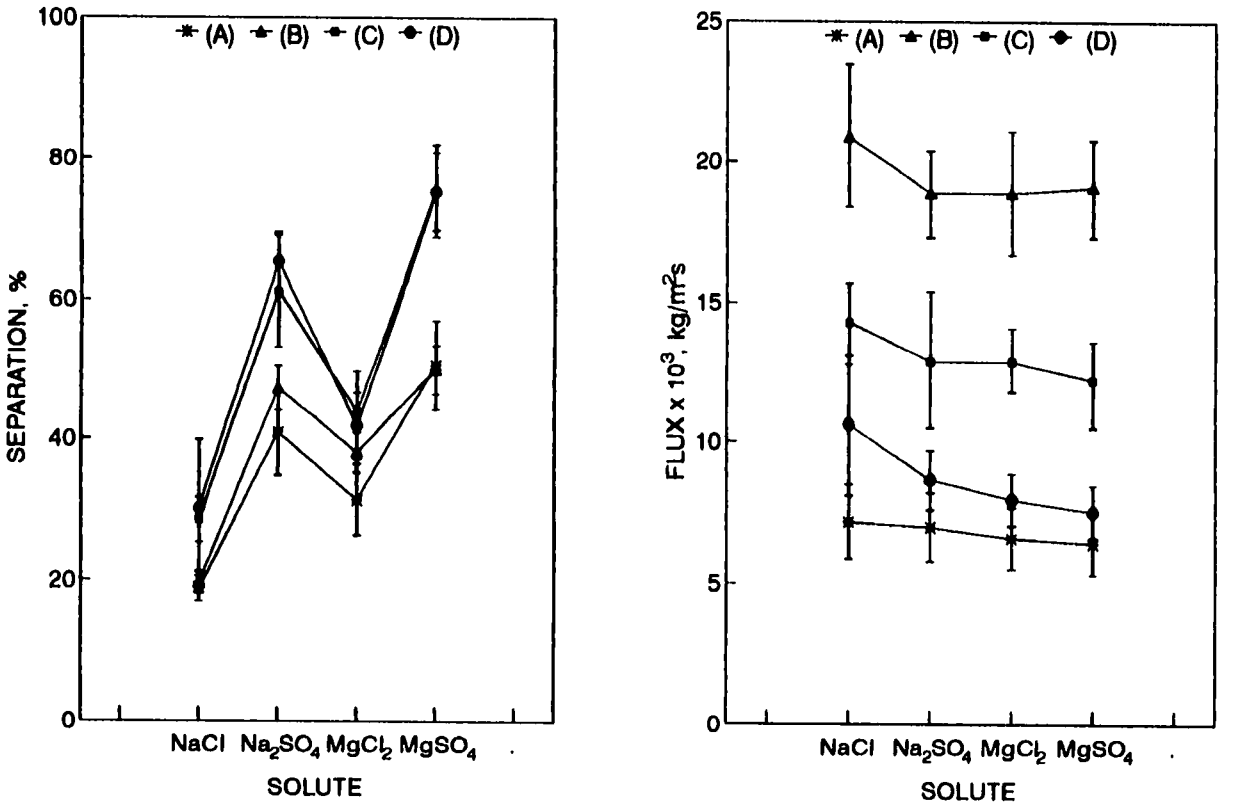

Fig.4.5 Effect of photochemical surface modification on membrane performance. The membranes were prepared by method 1 under the conditions given in Tables 3.1 and 4.1, respectively.

(A) II-DK-T-01,
(B) II-DK-T-01-ETHANOL TREATED,
(C) II-DK-T-01-hv-ETHYL ESTER,
(D) II-DK-T-01-hv-INDENE ACID.

Test conditions: Feed: 0.17 M solute, 1.0 L/min., P: 6000 kPa, T: 25 °C, pH=6.

DK membrane in ethanol in the absence of light for the same time period (30 min.) as that used in the photoreaction was conducted. The ethanol treatment showed a substantial effect on the membrane, increasing the flux by about 200% without significantly changing the separation. This result is consistent with that reported for a related diazoketone-containing membrane,[72] and also consistent with that recently reported for a commercial thin-film composite membrane.[115] This irreversible change to the membrane that is observed for the control experiment is large and is presumably also present in the membrane irradiated in ethanol. The result of the control experiment makes interpretation of the results obtained with irradiated membrane very difficult.

In order to demonstrate further the concept outlined in Scheme 4.1, the DK membrane was photochemically converted into the glycerol and sulfur-containing crown ether functionalized membranes. ATR-FTIR spectra of the parent DK membrane and the photochemically modified membranes are shown in Fig. 4.6. Again, irradiation of the DK membrane with 350 nm wavelength light in acetic acid in the presence of either glycerol or 1,5,9,13-tetrathiacyclohexadecane-3,11-diol resulted in the replacement of the diazo bands at about 2150 cm^{-1} (Fig. 4.6 (A)) with strong bands at about 1717 cm^{-1}, which are apparently attributed to carbonyl stretching vibrations (Fig. 4.6 (C) and (D)). In a control experiment, the DK membrane soaked in acetic acid in the absence of light for the same time period (30 min.) as that used in the photoreaction showed essentially the same infrared spectrum as the untreated DK membrane (Fig. 4.6 (B)). These results again suggest that the photochemical modification is occurring with these membranes.

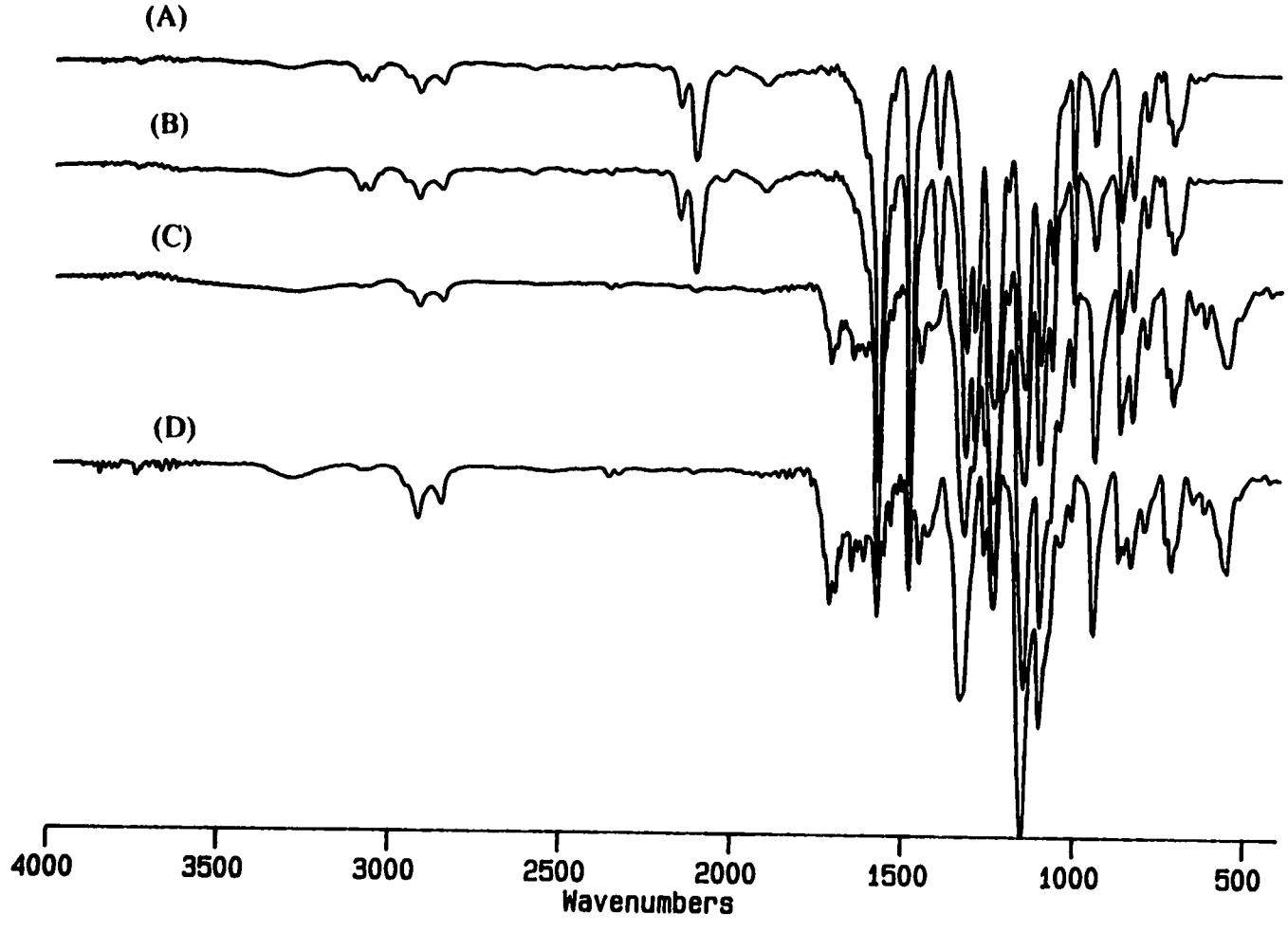

Fig. 4.6 ATR-FTIR spectra of the initial diazoketone and photochemically modified membranes.

(A) II-DK-T-01, Table 3.1,
(B) II-DK-T-01-ACETIC ACID TREATED, Table 4.1,
(C) II-DK-T-01-hν-GLYCEROL, Table 4.1,
(D) II-DK-T-01-hν-S. CROWN ETHER, Table 4.1.

These photochemically modified membranes and the parent DK membrane were further characterized by reverse osmosis tests. The results are presented in Fig. 4.7. The data reported for the DK membrane as a control are the same as those presented in Fig. 4.5. The data reported for the glycerol functionalized membrane were obtained by averaging the results of tests on three pieces of membrane from two different experiments. The data reported for the DK membrane soaked in acetic acid in the absence of light for the same time period (30 min.) as that used in the photoreaction was from a single membrane sample, as the duplicate membrane sample was broken. Again, low rejections were observed for salts with monovalent anions (chloride), but high rejections for salts with divalent anions (sulfate) (Fig. 4.7). Less pronounced selectivity differences were noted between monovalent (sodium) and divalent (magnesium) cations (Fig. 4.7). These results suggest that the barrier layers of all these membranes, including the starting DK membrane, are negatively charged.

Despite small differences in separations observed between the glycerol and sulfur-containing crown ether functionalized membranes, these two membranes showed significantly higher separations towards the four inorganic solutes studied than the control DK membranes.

The glycerol and sulfur-containing crown ether functionalized membranes are expected to be more hydrophilic than the parent DK membrane, so as to show a higher flux than the latter (Fig. 4.7). However, in a control experiment, the DK membrane soaked in acetic acid in the absence of light for the same time period as that used in the

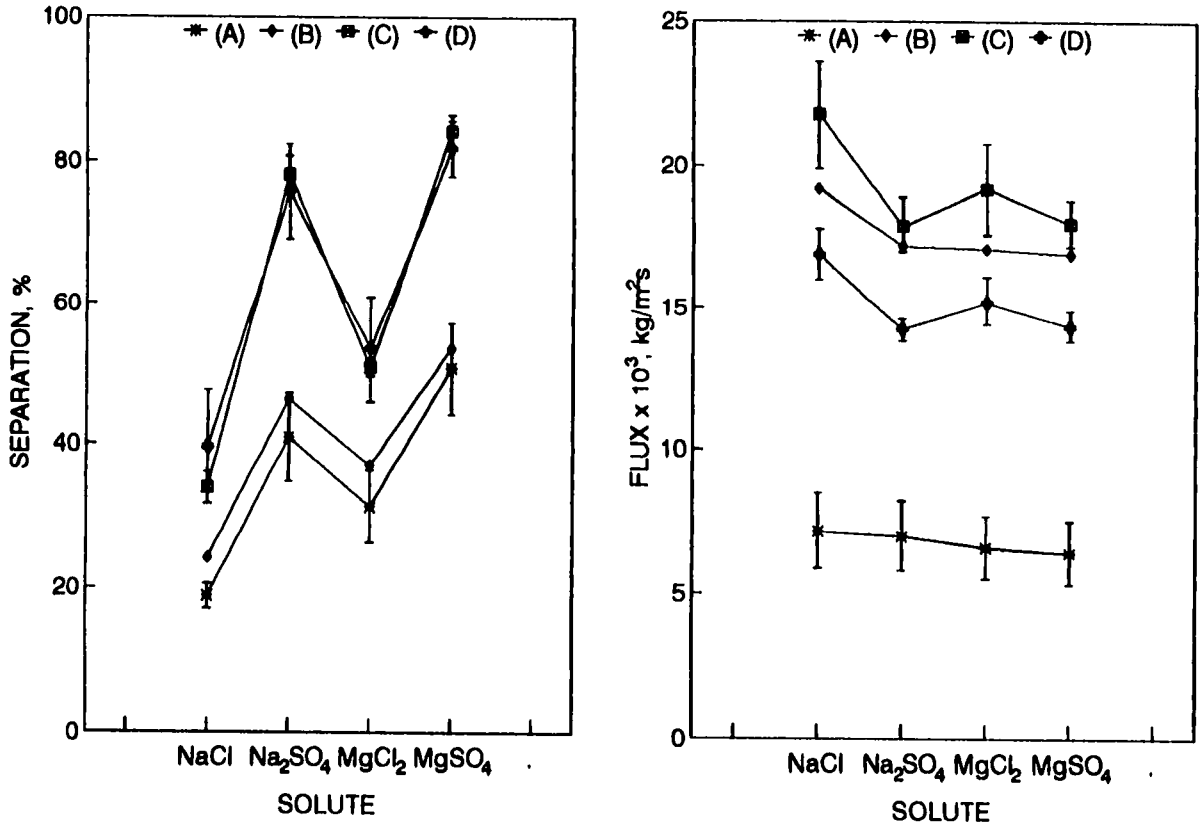

Fig.4.7 Effect of photochemical surface modification on membrane performance. The membranes were prepared by method 1 under the conditions given in Tables 3.1 and 4.1, respectively.

(A) II-DK-T-01,
(B) II-DK-T-01-ACETIC ACID TREATED,
(C) II-DK-T-01-hv-GLYCEROL,
(D) II-DK-T-01-hv-S. CROWN ETHER.

Test conditions: Feed: 0.17 M solute, 1.0 L/min., P: 6000 kPa, T: 25°C, pH=6.

photoreaction showed a similar flux to those of the glycerol and sulfur-containing crown ether functionalized membranes, but almost the same separation as that of the untreated DK membrane (Fig. 4.7).

The presence of a diazoketone-containing material was detected by UV spectroscopy in the acetic solution in which the DK membrane was soaked in the control experiment. This result suggests that low molecular weight polymers formed by interfacial polymerization of **47** with **74** are removed by acetic acid from the coating layer of the thin-film composite DK membrane. In addition, the acetic acid treatment appeared to cause the membrane to swell. These results suggest that the increased flux observed for the glycerol and sulfur-containing crown ether functionalized membranes as compared to the untreated DK membrane is attributed to the changes in not only the surface chemical properties but also the physical structures.

It is important to point out, despite the interference caused by using acetic acid as a solvent with the photochemical surface modification, the glycerol functionalized membrane showed a higher flux than the sulfur-containing crown ether functionalized membrane, as would be expected that the former is more hydrophilic than the latter. This difference can be attributed to differences in the surface chemical properties between the two membranes in as much as both the glycerol and sulfur-containing crown ether functionalized membranes were prepared by irradiation of the DK membrane in acetic acid solutions.

In principle, the problem associated with the membrane swelling and the loss of

low molecular weight polymer from the coating layer by acetic acid treatment discussed above can be overcome to some extent by crosslinking the thin-film polymer used in the membranes.[72] Therefore, a crosslinked thin-film composite DK membrane was prepared by interfacial polymerization of **47** with **74** in the presence of 1,3,6-naphthalene trisulfonyl chloride, **45**, as a crosslinking reagent. The percentage of **45** was 16.7% of the total sulfonyl chlorides (**45** and **47**). Subsequently, this membrane was irradiated in acetic acid in the presence of glycerol.

ATR-FTIR spectra of the DK membranes and glycerol functionalized membrane are shown in Fig. 4.8. As can be seen from the strong bands at about 2150 cm^{-1} attributed to diazo functionality (Fig. 4.8 (A)), detectable quantities of the diazoketone were successfully incorporated into the thin-film layer. Soaking this diazoketone-containing membrane in acetic acid for the same time period (30 min.) as that used for the photochemical surface modification of the membrane did not cause a disappearance of the diazoketone from the membrane (Fig. 4.8 (B)). However, irradiation of the DK membrane resulted in a replacement of the diazo bands at about 2150 cm^{-1} (Fig. 4.8 (A) and (B)) with a strong carbonyl band at about 1720 cm^{-1} as would be expected for a glycerol functionalized membrane. A broad band above 3000 cm^{-1} observed is consistent with the presence of the hydroxyl groups on the surface of the glycerol functionalized membrane.

The RO performance of the crosslinked DK and glycerol functionalized membranes is shown in Fig. 4.9. The reported data for the membranes in Fig. 4.9 were

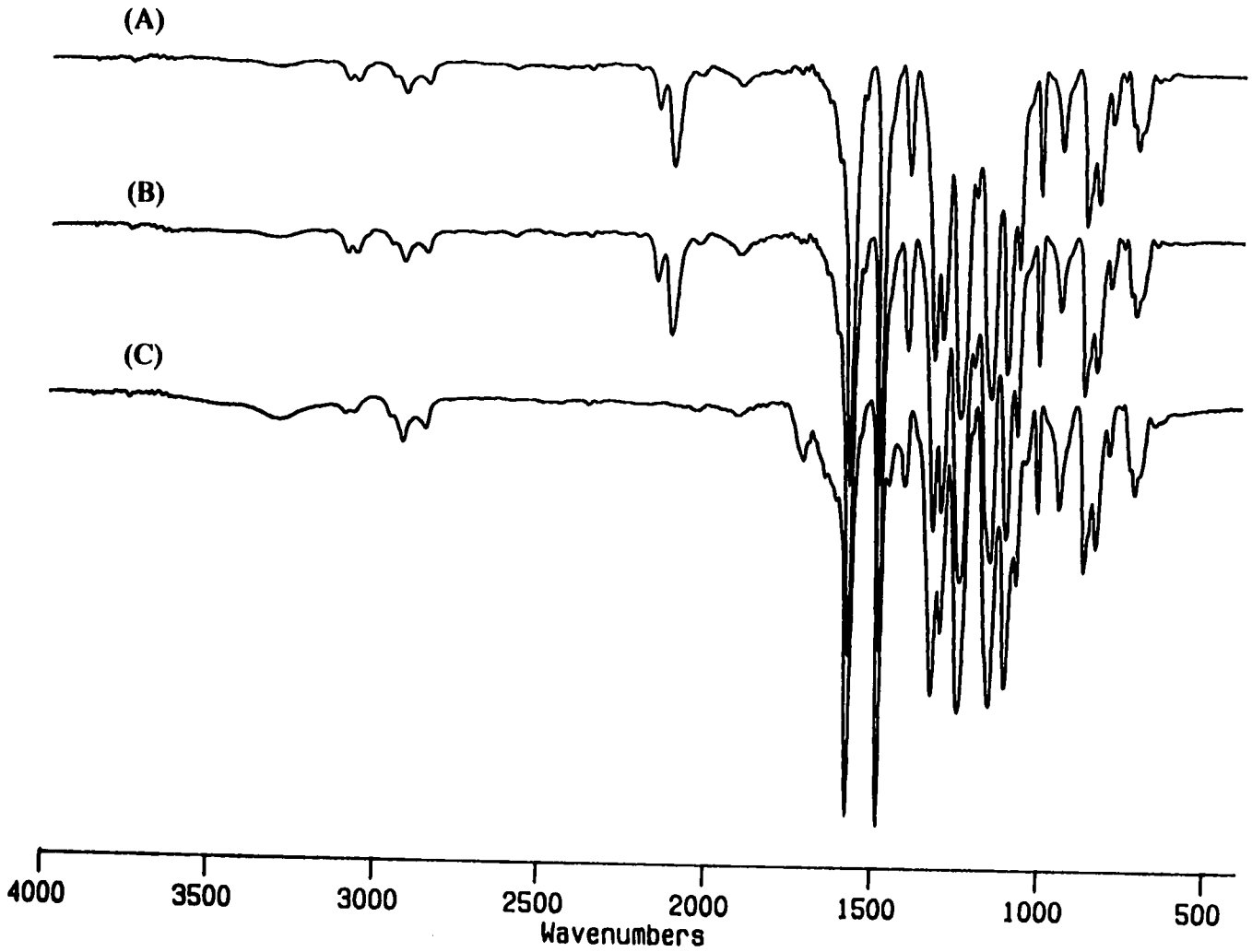

Fig. 4.8 ATR-FTIR spectra of the initial diazoketone and photochemically modified membranes.

(A) II-DK-T-01-CROSS LINKED, Table 3.1,
(B) (A) TREATED WITH ACETIC ACID,
(C) II-DK-T-01-CROSS LINKED-hv-GLYCEROL, Table 4.1.

an average of two pieces of membrane sample from a single batch. As can be seen, the acetic acid treatment showed no effect on the separation of crosslinked DK membrane towards four inorganic solutes, but a significant increase in flux as compared to the untreated DK membrane. In contrast to the results for the non crosslinked membranes shown in Fig. 4.7, the crosslinked glycerol functionalized membrane showed significantly higher separation and flux than the acetic acid treated DK membrane, and a much higher flux than the untreated DK membrane as shown in Fig. 4.9. These results are consistent with that of the infrared studies shown in Fig. 4.8, indicating that the photochemical surface modification is occurring. These results also suggest that the crosslinking of the thin-film composite membrane can indeed reduce the interference of the solvent, acetic acid in this case, with the photochemical surface modification of the membrane.

In order to further probe the impact of photochemical surface modification on membrane performance, the dependence of membrane performance on the pH of the feed solution was studied by measuring the separation of NaCl from the aqueous solution. Three different membranes were investigated. The pH of the test solutions was cycled back and forth from acidic to basic conditions several times using HCl and NaOH, respectively. The reported flux and separation of the indene acid functionalized membrane were the average of four membrane samples from two different batches, while all other data in Fig. 4.10 were the average of two membrane samples from a single batch.

As can be seen from Fig. 4.10, the separation and flux of the indene acid

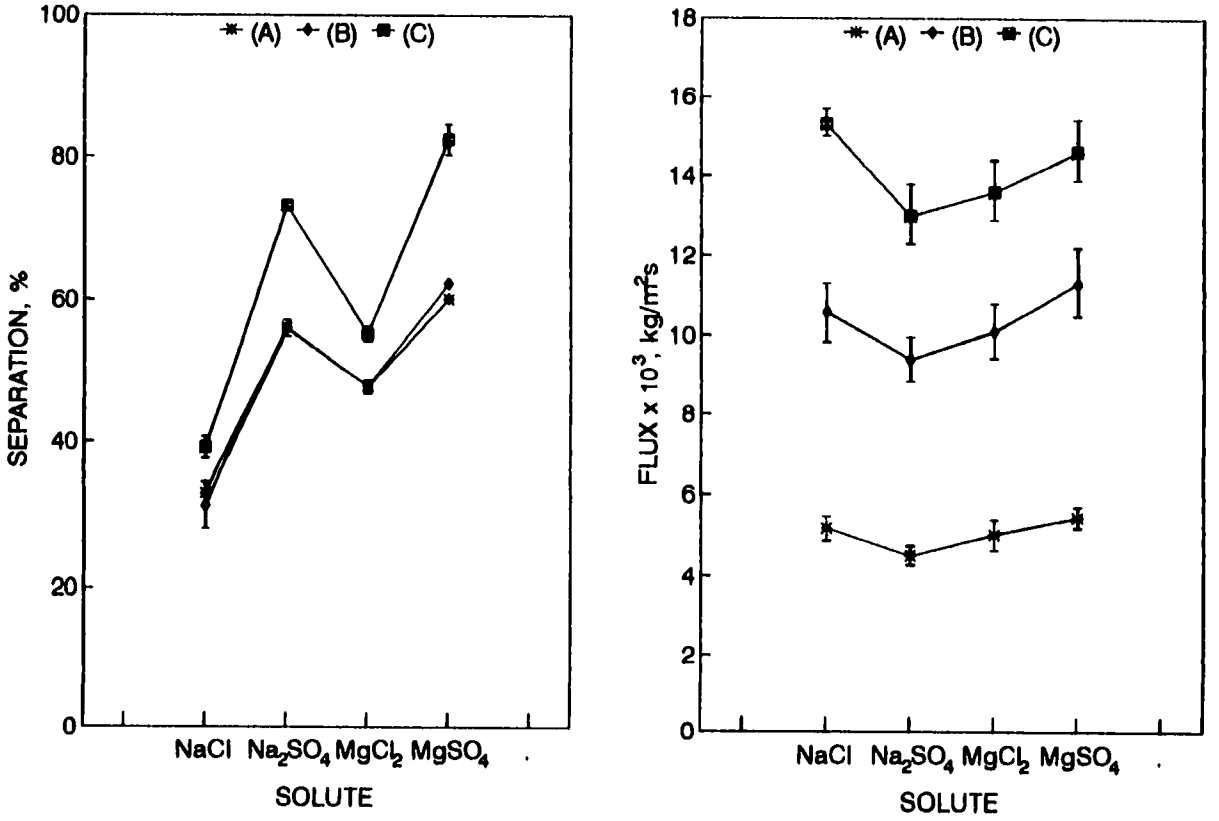

Fig.4.9 Effect of photochemical surface modification on membrane performance. The membranes were prepared by method 1 under the conditions given in Tables 3.1 and 4.1, respectively.

(A) II-DK-T-01-CROSS LINKED, (B) (A) TREATED WITH ACETIC ACID,
(C) II-DK-T-01-CROSS LINKED-hv-GLYCEROL,

Test conditions: Feed: 0.17 M solute, 1.0 L/min., P: 6000 kPa, pH=6, Flux corrected to 25°C.

functionalized membranes was significantly higher than that of the initial DK membrane over a wide range of pH from 2 to 11. As expected, the separations and fluxes of the initial DK membrane and ethyl ester functionalized membrane were independent of the pH of the test solution.

While the separation of NaCl by the indene acid functionalized membrane would appear to be independent of the pH under acidic conditions, it significantly increased with an increase in the pH under basic conditions (Fig. 4.10). On the other hand, the flux of the indene acid membrane slightly increased with the pH.

Kono et al.[116] reported a strong pH-dependence of the degree of neutralization of poly(acrylic acid).

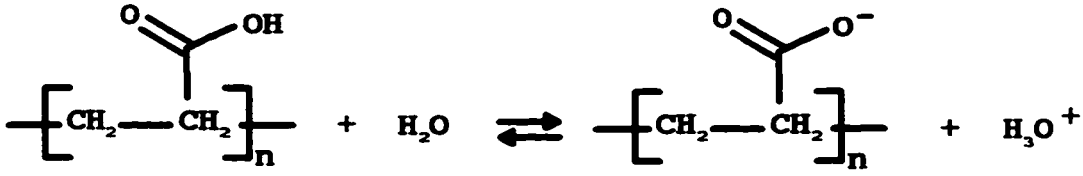

A relative scale from zero to one was used to characterize the degree of neutralization of poly(acrylic acid). When poly(acrylic acid) is in acid form, the degree of neutralization is defined as one. When poly(acrylic acid) is completely ionized, the degree of neutralization is defined as zero. The degree of the neutralization of poly(acrylic acid) was determined by electric potential titration. It was found that the degree of neutralization of poly(acrylic acid) linearly increased with the decrease in the pH of the aqueous poly(acrylic acid) solution. The zero degree of the neutralization of

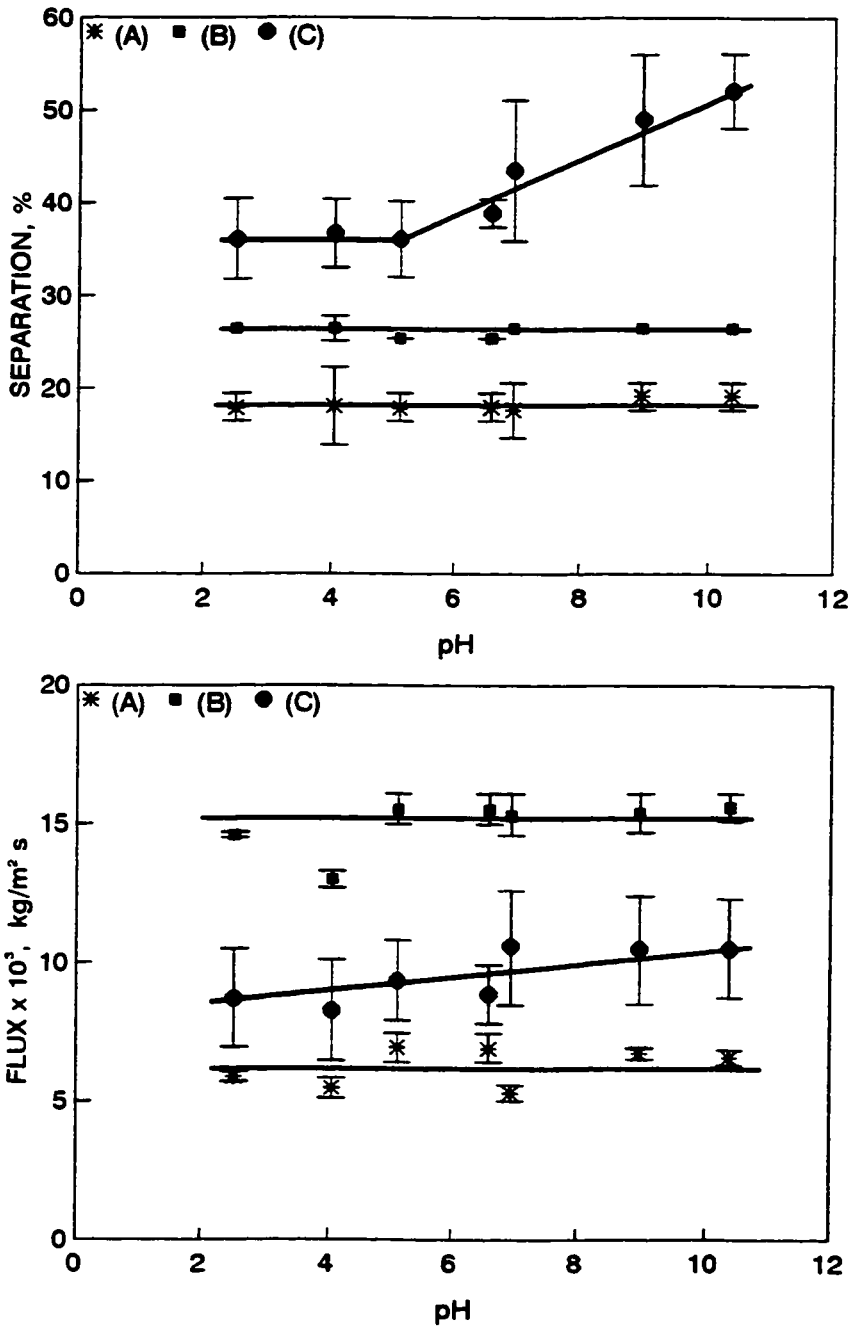

Fig.4.10 Reverse osmosis separation and solution flux of NaCl vs. pH for the initial diazoketone, ethyl ester and indene acid functionalized membranes.

The membranes were prepared by method 1 under the conditions given in Table 3.1 and 4.1, respectively.

(A) II-DK-T-01, (B) II-DK-T-01-hv-ETHYL ESTER,

(C) II-DK-T-01-hv-INDENE ACID.

Test conditions: 0.17 NaCl, 1.0 L/min., P: 6000 kPa, T: 25 °C.

poly(acrylic acid) was reported at pH=10.5 and one was reported at pH=4.5.

The pK_a of an indene acid is 4.5,[111,112] which is similar to that of acrylic acid.[117]

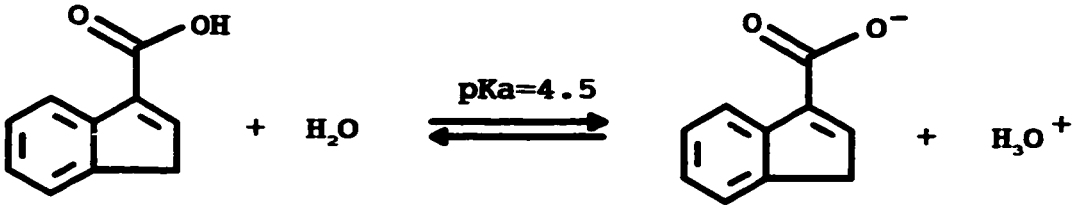

Comparing an indene acid functionalized membrane with poly(acrylic acid), the degree of the dissociation of the indene acid moieties in the surface layer of the thin-film composite membranes is expected to increase with pH, from pH=4.5 to 10.5, in a similar manner as poly(acrylic acid) does.[116]

The results in Fig. 4.5 suggest that the surface layer of the membranes are negatively charged due to the presence of $-SO_3^-$ groups. The surface concentration of $-SO_3^-$ groups is not expected to change with pH in a range from 4.5 to 10.5.[118] Additional negative charges formed by ionization of the indene acid functionalized membrane under basic conditions are superimposed with negatively charged $-SO_3^-$ groups in the surface layer of the thin-film composite membrane. The increase in ionization degree of the indene acid functionalized membrane with the increase in the pH of the system seems to account for the observed increase in separation (Fig. 4.10). Donnan exclusion[72,113,114] as a result of the presence of the negatively charged $-COO^-$ groups in the surface layer of the indene acid functionalized membrane appears to enhance solute-water separations to the level above those of the parent DK membrane and neutral ester membrane (Fig.

4.10). The above results suggest that photochemical surface modifications are occurring.

4.2.2 Method 2

The irradiation of the diazoketone functionality as either the model compound or a thin film in the presence of water, leads to the formation of an indene acid. This reaction is a potential side reaction when attempting to convert photochemically the diazoketone to the other functionalities if water is present in the system; trace amounts of water may be left in the support membrane from the earlier aqueous diamine solution. Indeed, as was pointed out earlier, the infrared spectra of the carboxylic acid and ester containing membranes (Fig. 4.4), are very similar. Thus, the question is raised as to the relative conversions of the diazoketone functionality to an ester as compared to the conversion to a carboxylic acid.

In order to minimize the presence of water in the thin-film composite DK membranes, attempts were made to remove water by drying the membranes *in vacuo* overnight. The photoreactions were subsequently carried out under an atmosphere of nitrogen.

4.2.2.1 Formation of Sulfur-Containing Crown Ether Functionalized Membrane

In order to demonstrate that a complex molecule can be photochemically incorporated into the surface layer of a thin-film composite membrane, a diazoketone-

containing membrane, **75**, was irradiated in the presence of 1,5,9,13-tetrathiacyclohexadecane-3,11-diol in acetic acid as a solvent. After the irradiation the original yellow colour of the DK membrane disappeared.

The morphologies of the irradiated membranes are shown in Fig. 4.11 (G). As can be seen by comparing (G) with (A) in Fig. 4.11, the textured structure of the parent DK membrane is maintained after the irradiation.

The photochemically modified thin films were characterized by infrared spectroscopy. Attenuated total reflectance FT-IR is a useful technique for surface characterization of thin films.[119] The sample preparation for an ATR-FTIR spectrum is easier than that for a transmittance FT-IR spectrum. However, the ATR-FTIR has some drawbacks as compared to transmission infrared spectroscopy, such as low sensitivity and spectral distortion.[119] Therefore, in this work both attenuated total reflection and transmission techniques were used to characterize the surface of the thin-film composite membranes.

ATR-FTIR spectra of the irradiated membrane, the parent DK membrane and transmittance FT-IR spectra of the related model compound and thin films are shown in Fig. 4.12. Although the transmittance spectra were collected using 64 scans, and the ATR spectra were collected using 256 scans, the former (Fig. 4.12 (E)), still shows higher intensity and sharper bands than the latter (Fig. 4.12 (D)). Clearly, the quality of the transmittance spectra is better than that of the ATR spectra.

For this reason, attempts were made to characterize the surface of the irradiated

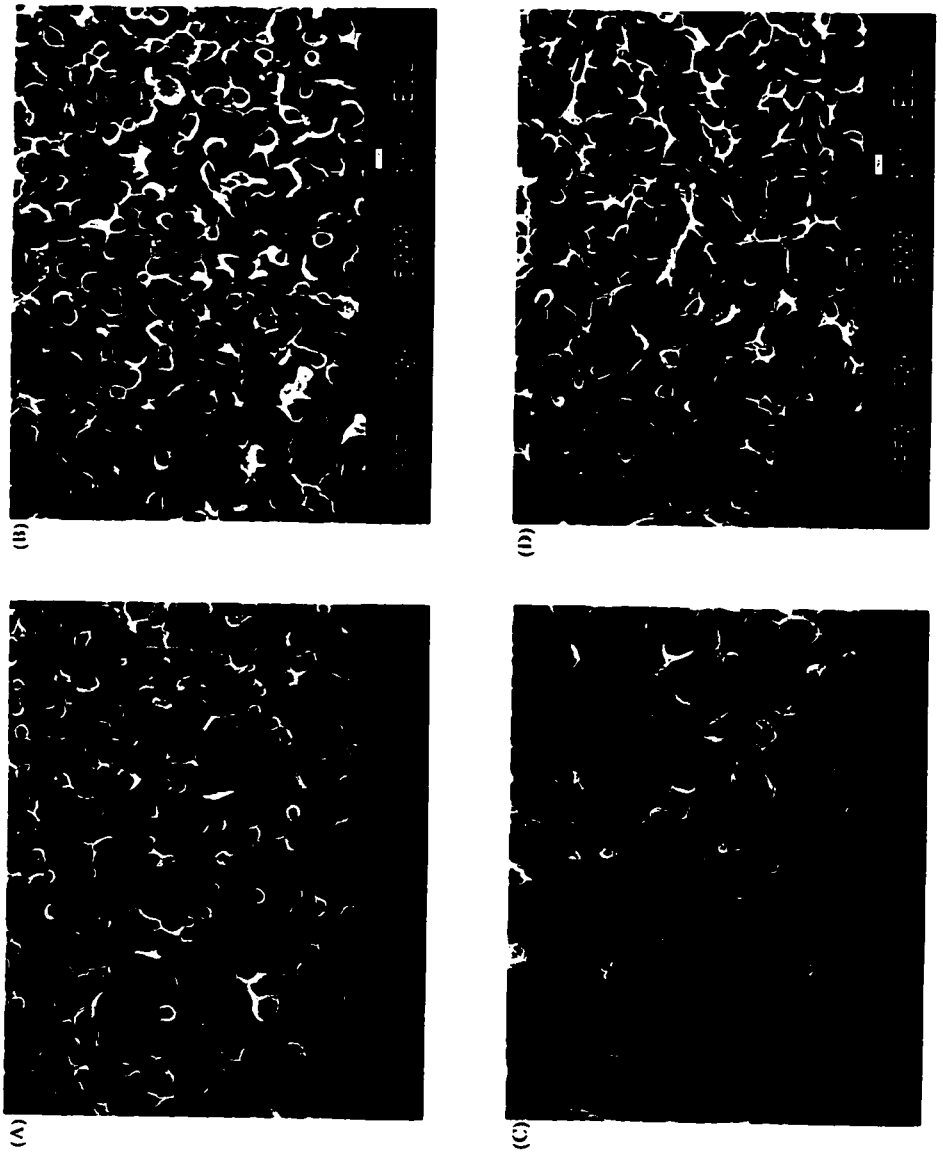
(B)
(D)
(A)
(C)

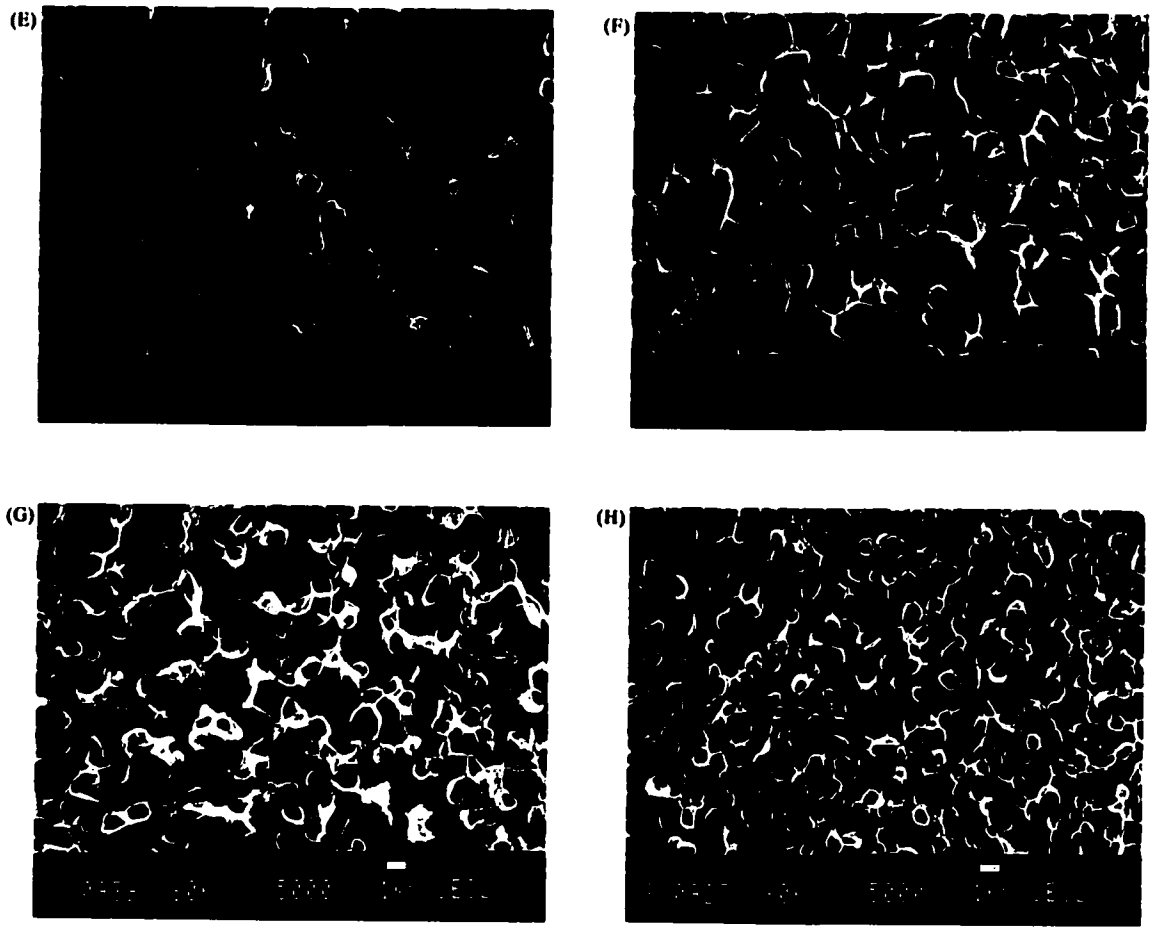

Fig. 4.11 Effect of photochemical surface modification on membrane morphologies

The membranes were prepared by method 2 under the conditions given in Tables 3.1 and 4.1, respectively.
(A) II-DK-T-04-D,
(B) (A) after separation test at 6000 kPa for a month,
(C) II-DK-T-04-D-hv-INDENE ACID,
(D) (C) after separation test at 6000 kPa for a month,
(E) II-DK-T-04-D-hv-ETHYL ESTER,
(F) II-DK-T-04-D-hv-GLYCEROL,
(G) II-DK-T-04-D-hv-S. CROWN ETHER,
(H) II-DK-T-04-D-ACETIC ACID TREATED.

membrane using transmission infrared spectroscopy. The major difficulty encountered was how to prepare a suitable sample for surface characterization of a thin-film composite membrane using transmission infrared spectroscopy, because the entire thin-film composite membrane is not transparent. The surface layer formed by interfacial polymerization on the support polysulfone membrane is tightly bonded to the support. As a result, it is difficult to peel the surface layer from the support.

Before examination of the spectra in Fig. 4.12 in detail, it would be better to discuss how the membrane samples for ATR and transmittance spectra were prepared. Preparation of the membrane samples for ATR-FTIR analysis was straight forward. The thin-film composite membrane was simply cut into pieces of 1 cm x 5 cm.

In order to prepare samples for characterization of the surface layer of the thin-film composite membrane using transmission IR spectroscopy, isolation of the surface layer from the support was attempted by removal of the polysulfone support using a variety of organic solvents. These solvents include acetone and chloroform, which are known to dissolve the polysulfone.[5,70] Unfortunately, these attempts were unsuccessful. However, it proved possible to peel the surface layer and the polysulfone support layer together from the polyester nonwoven cloth layer. The peeled thin film was compressed into a transparent film. This allowed characterization of the surface layer using transmission infrared spectroscopy. The transmittance spectrum of the peeled polysulfone layer of the support polysulfone membrane reinforced by a polyester nonwoven cloth is shown in Fig. 4.13 (A). The spectrum of the surface layer of the DK membrane

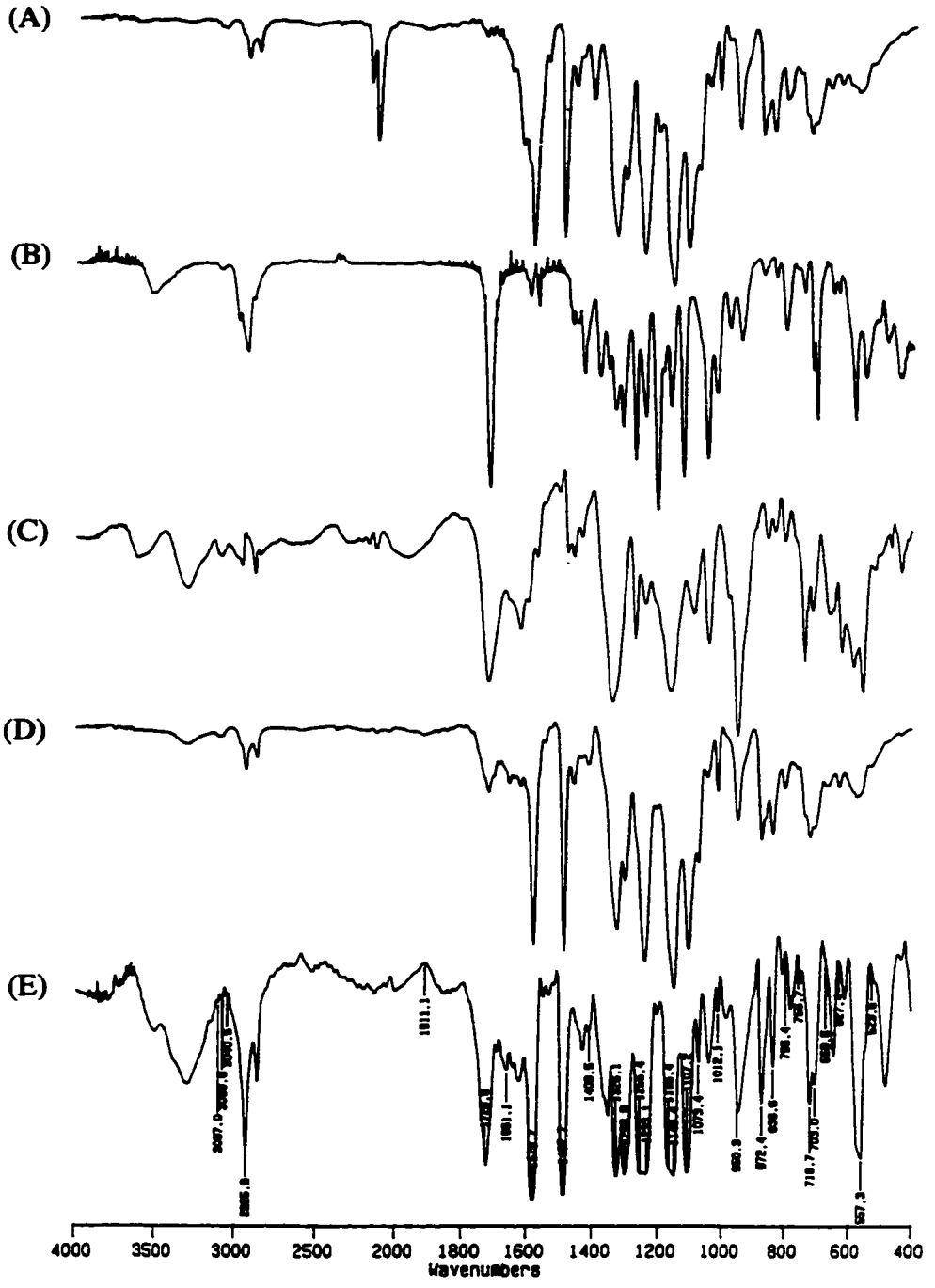

Fig. 4.12 FT-IR spectra of the initial DK membrane, sulfur-containing crown ether functionalized membrane, related model compound and thin film.
(A) ATR-FT-IR spectrum of the initial DK membrane, II-DK-T-04-D, Table 3.1,
(B) transmittance FT-IR spectrum of model compound, **73**, Scheme 2.5,
(C) subtraction spectrum, spectrum (C) in Fig. 4.15,
(D) ATR-FT-IR spectrum of sulfur-containing crown ether functionalized membrane, II-DK-T-04-D-hν-S. CROWN ETHER, Table 4.1,
(E) subtraction spectrum, spectrum (C) in Fig. 4.13.

irradiated in the presence of 1,5,9,13-tetrathiacyclohexadecane-3,11-diol in acetic acid as a solvent is shown in Fig. 4.13 (B). Subtraction of spectrum (A) from spectrum (B) gave a subtraction spectrum, (C) (Fig. 4.13). The subtraction spectrum shows a strong carbonyl peak at 1729 cm^{-1} and broad hydroxyl peaks above 3100 cm^{-1}, as would be expected for a sulfur-containing crown ether functionalized membrane. In addition, the residual peaks attributed to the polysulfone membrane are clearly visible below 1600 cm^{-1}. The presence of these residual peaks made it difficult to analyze the spectrum.

In order to overcome the difficulties in analysis of the spectrum caused by the presence of polysulfone residuals, a diazoketone-containing thin film was prepared by the liquid-liquid interfacial polymerization of disulfonyl chloride, **47**, with 1,2-ethanediamine, **74**, according to the reaction shown in Scheme 3.1. Water and ethyl acetate were used as solvents, respectively. The thin film was picked up from the water-ethyl acetate interface on a microporous polyethylene film. Unlike the diazoketone-containing monomer, **47**, the yellow coloured thin film formed by the liquid-liquid interfacial polymerization did not dissolve in acetone, suggesting that a polymer was indeed formed.

The transmission infrared spectrum of the thin film prepared by liquid-liquid interfacial polymerization is shown in Fig. 4.14 (B). Subtraction of the spectrum of polyethylene thin film, (A), from spectrum (B) yielded a subtraction spectrum, (C), (Fig. 4.14). The strong diazo bands at 2161.2 and 2115.8 cm^{-1} are observed, suggesting that the diazoketone functionality was successfully incorporated into the thin film.

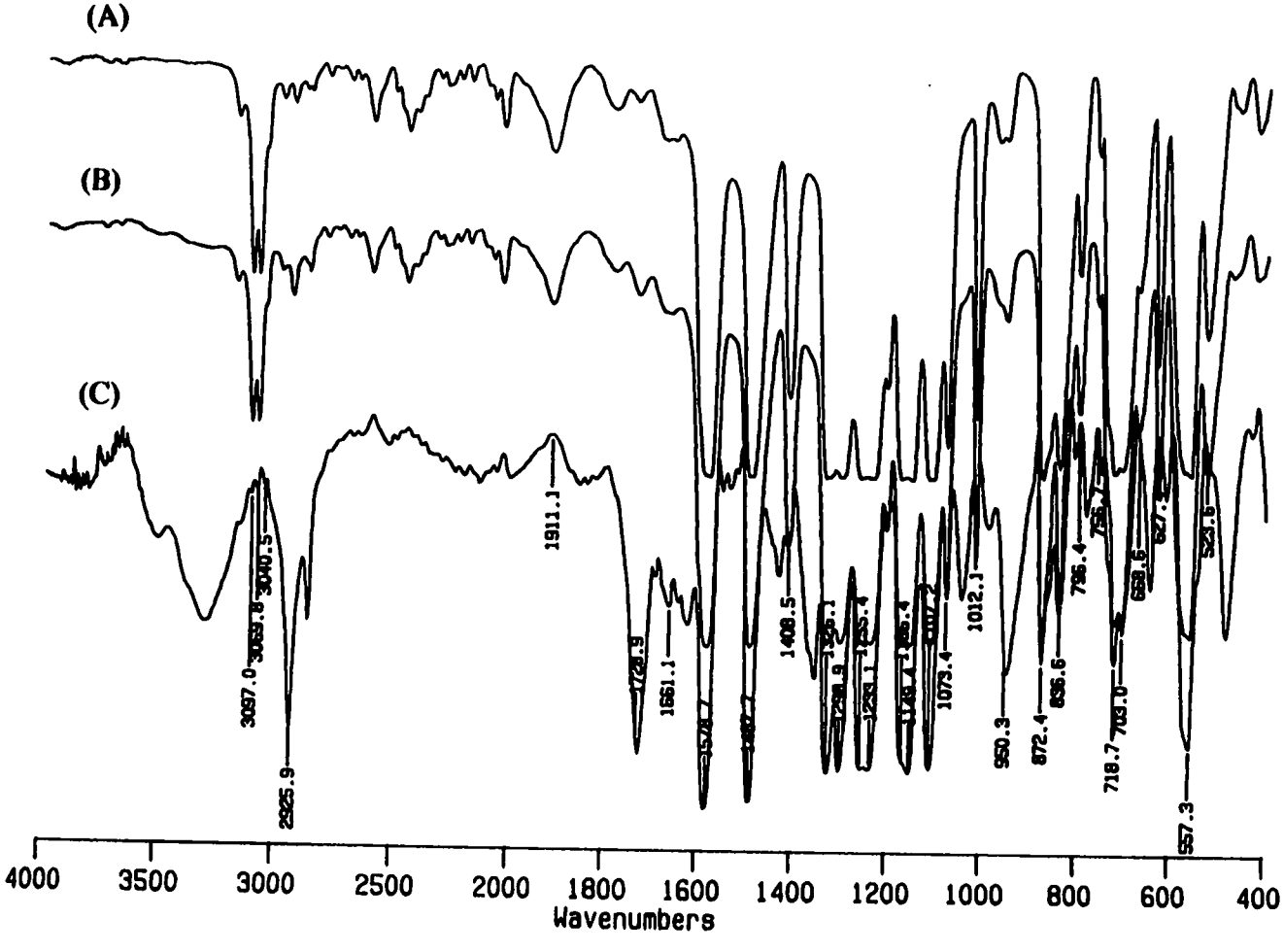

Fig. 4.13 Infrared spectra of the supporting polysulfone membrane and sulphur-containing crown ether functionalized membrane.

(A) supporting polysulfone membrane,
(B) sulphur-containing crown ether functionalized membrane, II-DK-T-04-D-hv-S. CROWN ETHER, Table 4.1,
(C) subtraction spectrum of (A) from (B).

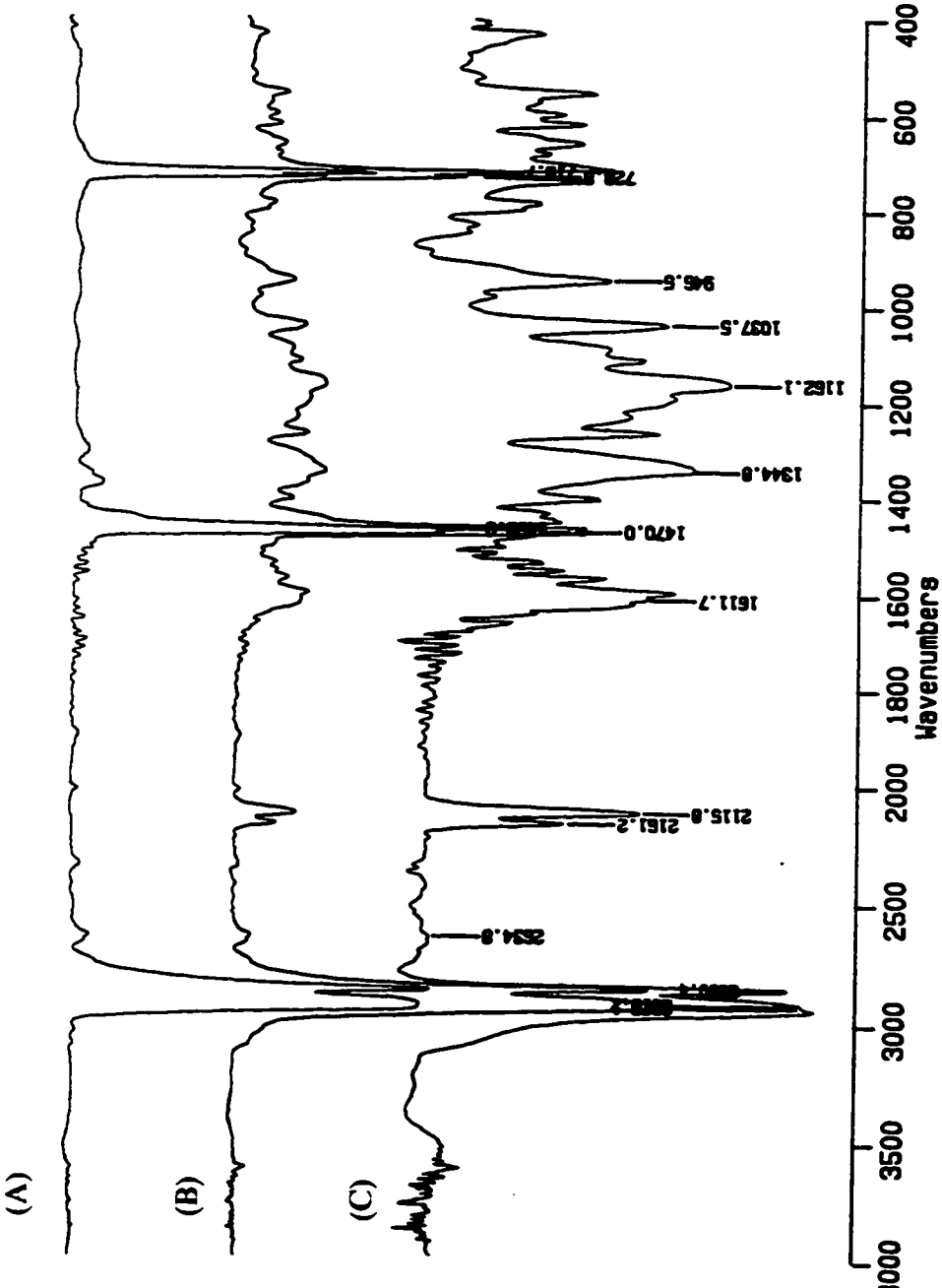

Fig. 4.14 Infrared spectra of a polyethylene film and a diazoketone-containing thin film prepared by liquid-liquid interfacial polymerization

(A) polyethylene thin film,
(B) diazoketone-containing thin film,
(C) subtraction spectrum of (A) from (B).

Irradiation of the above diazoketone-containing thin film in the presence of 1,5,9,13-tetrathiacyclohexanedecane-3,11-diol in acetic acid as a solvent resulted in decolorization of the originally yellow coloured film. The transmission IR spectrum of the irradiated film supported on a polyethylene film is shown in Fig. 4.15 (B). Subtraction of the IR spectrum of the polyethylene film from spectrum (B) produced a subtraction spectrum of the photochemically modified thin film, (C), (Fig. 4.15). The IR spectrum of polyethylene is very simple, which makes the subtraction spectrum more simple than the corresponding one using a polysulfone film as a reference (Fig. 4.13 (C)). No strong diazo bands at about 2161 and 2116 cm^{-1} are observed (Fig. 4.15 (C)). Instead, a strong carbonyl band at 1717.8 cm^{-1} and broad bands above 3100 cm^{-1} are observed (Fig. 4.15 (C)), as would be expected for sulfur-containing crown ether functionalized thin film.

For comparison purposes, the transmission IR spectrum of model compound, **73**, in Scheme 2.5, is shown in Fig. 4.12 (B). The ATR-FTIR spectra of the initial DK membrane and the irradiated membrane along with the two subtraction spectra discussed above are shown in Fig. 4.12. After the photochemical modification, strong bands around 2150 cm^{-1} attributed to diazo group disappeared. Carefully examining spectra (D) and (E) in Fig. 4.12, these spectra of the irradiated membrane show a strong carbonyl band at about 1728 cm^{-1} and the absence of the diazo bands around 2150 cm^{-1}. The position of the carbonyl band is similar to that of the model compound (Fig. 4.12 (B)), and also similar to that of the thin film prepared by liquid-liquid interfacial

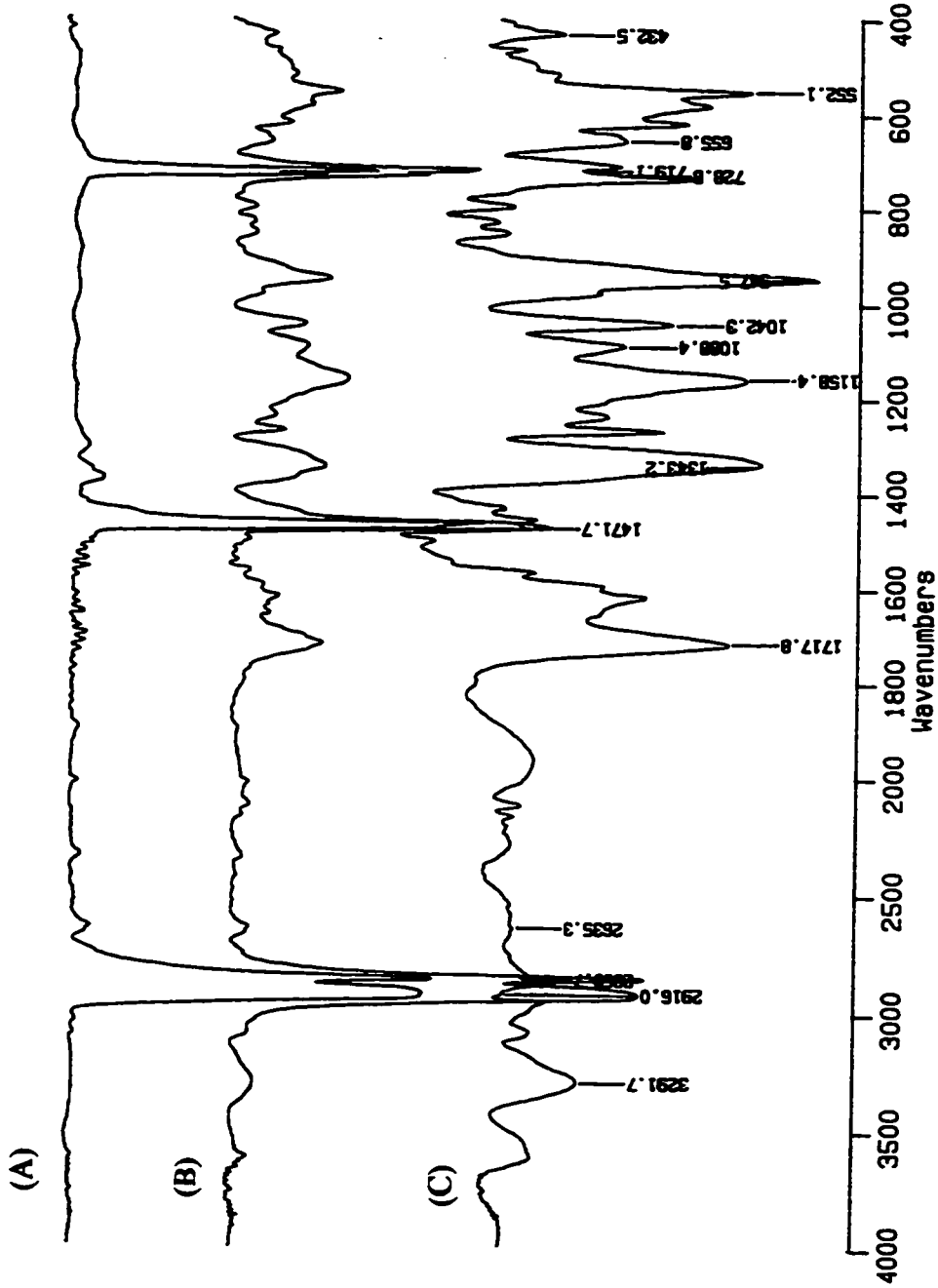

Fig. 4.15 Infrared spectra of a polyethylene film and a sulphur-containing crown ether functionalized thin film prepared by liquid-liquid interfacial polymerization and subsequent photochemical modification.

(A) polyethylene thin film,
(B) sulphur-containing crown ether functionalized thin film,
(C) subtraction spectrum of (A) from (B).

polymerization followed by the photochemical modification (Fig. 4.12 (C)). These results suggest that sulfur-containing crown ether functionalized membrane, **79**, (Scheme 4.2) is formed.

The sulfur-containing crown ether functionalized membrane was examined in terms of its separation performance. The results are illustrated in Fig. 4.16.

As can be seen from the data in Fig. 4.16, the sulfur-containing crown ether functionalized membrane showed a significantly lower separation and higher flux than the starting DK membrane. This observation raised concerns that the acetic acid used as a solvent in the photoreaction might be damaging the membranes.

As a control experiment, the DK membrane was soaked in acetic acid in the dark for the same time period (30 min.) as that used in the photochemical surface modification. As can be seen from the data in Fig. 4.16, the flux of this acetic acid treated membrane, II-DK-T-04-D-ACETIC ACID TREATED, is about four times as high as the untreated one. This acetic acid treated membrane also showed a significant decrease in separation as compared to the untreated DK membrane. No significant change in morphology was observed for the acetic acid treated DK membrane (Fig. 4.11 (H)), as compared to the untreated one (Fig. 4.11 (A)).

Overall, it is clear that acetic acid is damaging the membrane based on separation/flux performance observed. However, the degree of the damage caused by acetic acid appeared to be reduced by the photochemical conversion of the diazoketone to the sulfur-containing crown ether ester of the indene acid, **79** in Scheme 4.2. Thus,

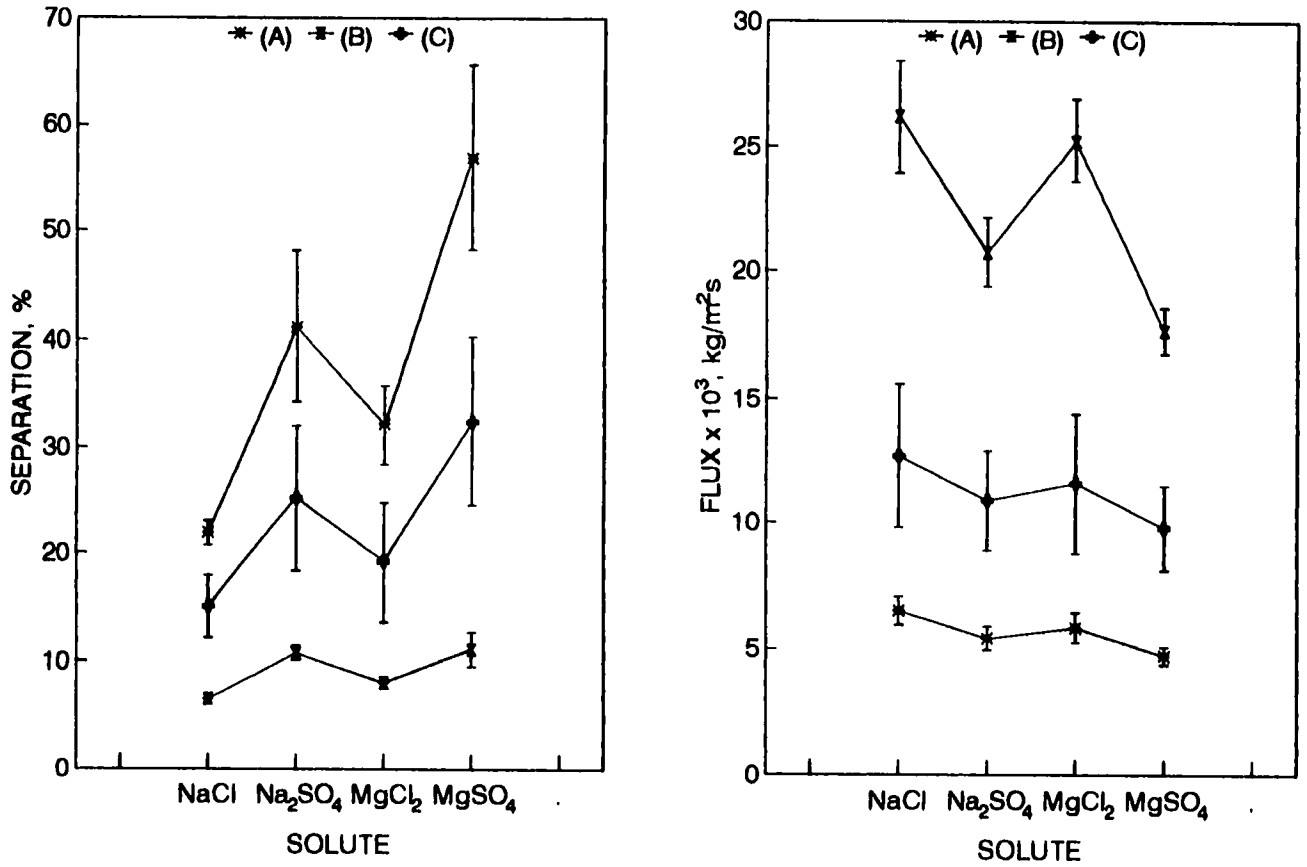

Fig.4.16 Effect of photochemical surface modification on membrane performance. The membranes were prepared by method 2 under the conditions given in Tables 3.1 and 4.1, respectively.

(A) II-DK-T-04-D, (B) II-DK-T-04-D-ACETIC ACID TREATED,

(C) II-DK-T-04-D-hv-S. CROWN ETHER.

Test conditions: Feed: 0.17 M solute, 1.0 L/min., P: 6000 kPa, T: 25 °C, pH=6.

the photochemically modified membrane, II-DK-T-04-D-S. CROWN ETHER, showed a higher separation and a lower flux than the acetic acid treated DK membrane, II-DK-T-04-D-ACETIC ACID TREATED (Fig. 4.16). The impact of the acetic acid treatment was hardly observed in terms of the membrane morphology (Fig. 4.11 (H)), and IR spectra (Fig. 4.12 (D) and (E)).

4.2.2.2 Formation of Ethyl Ester Functionalized Membrane

Ethyl ester functionalized membrane, **78**, in Scheme 4.2 was prepared by the irradiation of the DK membrane in ethanol.

The morphology of the resulting ester membrane is shown in Fig. 4.11 (E). As can be seen by comparing the SEM's shown in Fig. 4.11 (A) and (E), a textured structure was still observed in the surface layer after irradiation in the presence of ethanol. In fact, no significant difference in morphology could be observed in the ester membrane as compared to that of the parent DK membrane (Fig. 4.11 (A)).

Attempts were made to characterize the surface of the irradiated membrane by infrared spectroscopy. The ATR-FTIR spectrum and the subtraction spectrum of the ethyl ester functionalized membrane are shown in Fig. 4.17 (B) and (C). For a comparison purpose, the ATR-FTIR spectrum of the initial DK membrane is also shown in Fig. 4.17 (A). The subtraction spectrum ((C) in Fig. 4.17), was obtained by subtraction of a transmittance infrared spectrum of the support polysulfone membrane from the spectrum of the DK membrane irradiated in ethanol in the same way discussed

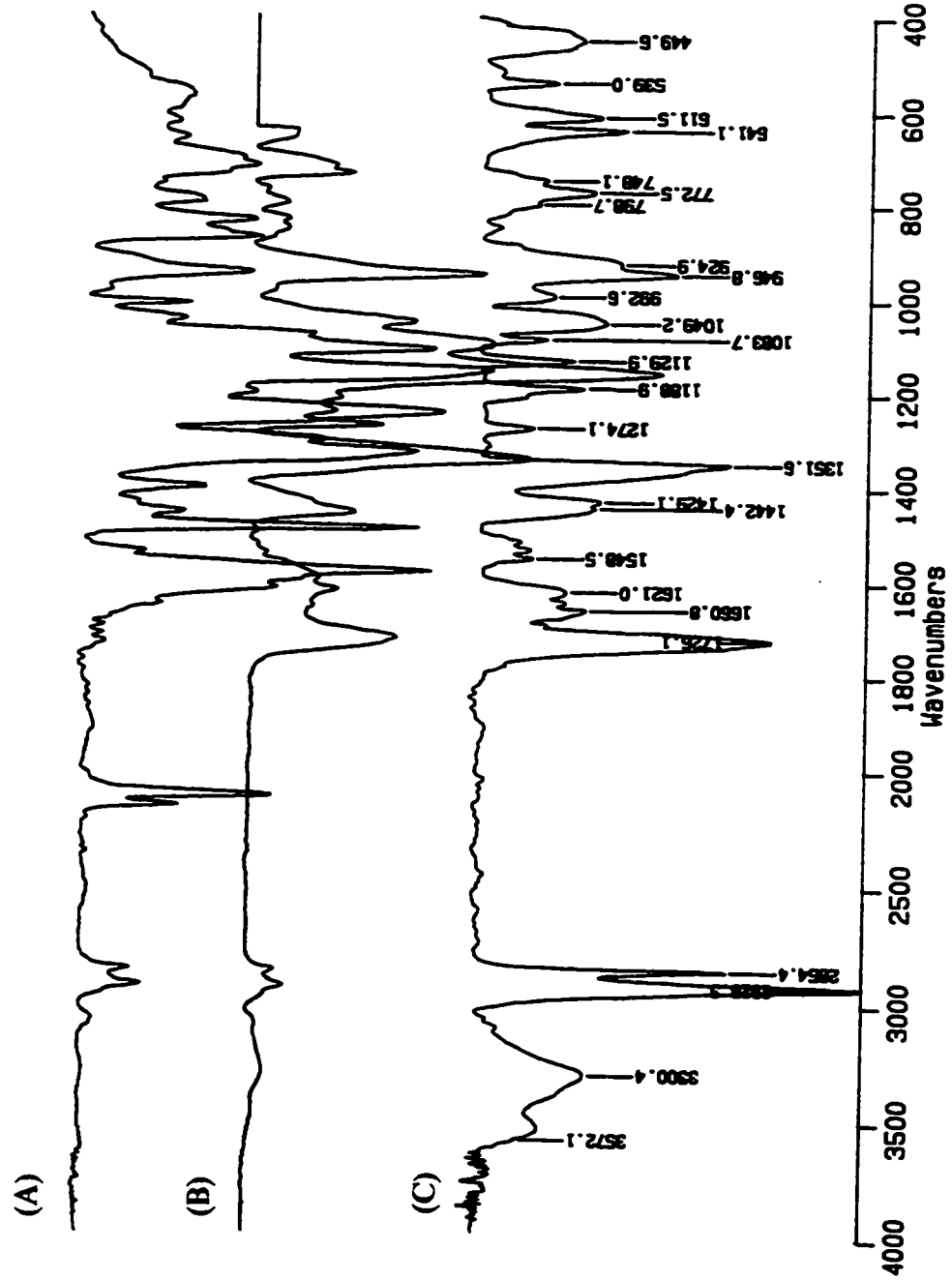

Fig. 4.17 Infrared spectra of the initial diazoketone membrane and photochemically modified membranes.

(A) ATR-FTIR spectrum of initial diazoketone membrane, II-DK-T-04-D, Table 3.1,
(B) ATR-FTIR spectrum of ethyl ester functionalized membrane, II-DK-T-04-D-hv-ETHYL ESTER, Table 4.1,
(C) subtraction spectrum of the supporting polysulfone membrane from ethyl ester functionalized membrane, II-DK-T-04-D-hv-ETHYL ESTER.

earlier. The diazo bands around 2150 cm^{-1} in spectrum (A) of the initial DK membrane disappeared upon irradiation. No band around 2150 cm^{-1} was observed from the spectra of the irradiated membrane ((B) and (C) in Fig. 4.17). Instead, a strong band at 1726 cm^{-1} in spectra (B) and (C) was observed, respectively. These results are consistent with the formation of an ethyl ester functionality in the thin film and also in accord with the previous results reported by the McMaster membrane group.[72] It should be noted that broad peaks between 3600-3100 cm^{-1} were observed in Fig. 4.17. These peaks could be due to the absorbtion of moisture from the air or possible formation of carboxylic acid by traces of water still being present in the photoreaction.

Reverse osmosis tests on the ethyl ester functionalized membrane and the parent DK membrane showed no significant difference in separation between these two membranes (Fig. 4.18). However, the flux of the ester membrane is much higher than that of the initial DK membrane, indicating that a photoreaction is occurring. This is consistent with the infrared spectra discussed above. The reason for the unexpected increase in flux could be similar to that discussed earlier (see Fig. 4.5 in **Section 4.2.1.2**). This result is consistent with that of a related ester membrane reported by the McMaster membrane group.[72] This result is also in accord with that obtained using method 1 (Fig. 4.5).

Both the infrared spectra and the separation/flux performance discussed above suggest the photoreaction is occurring.

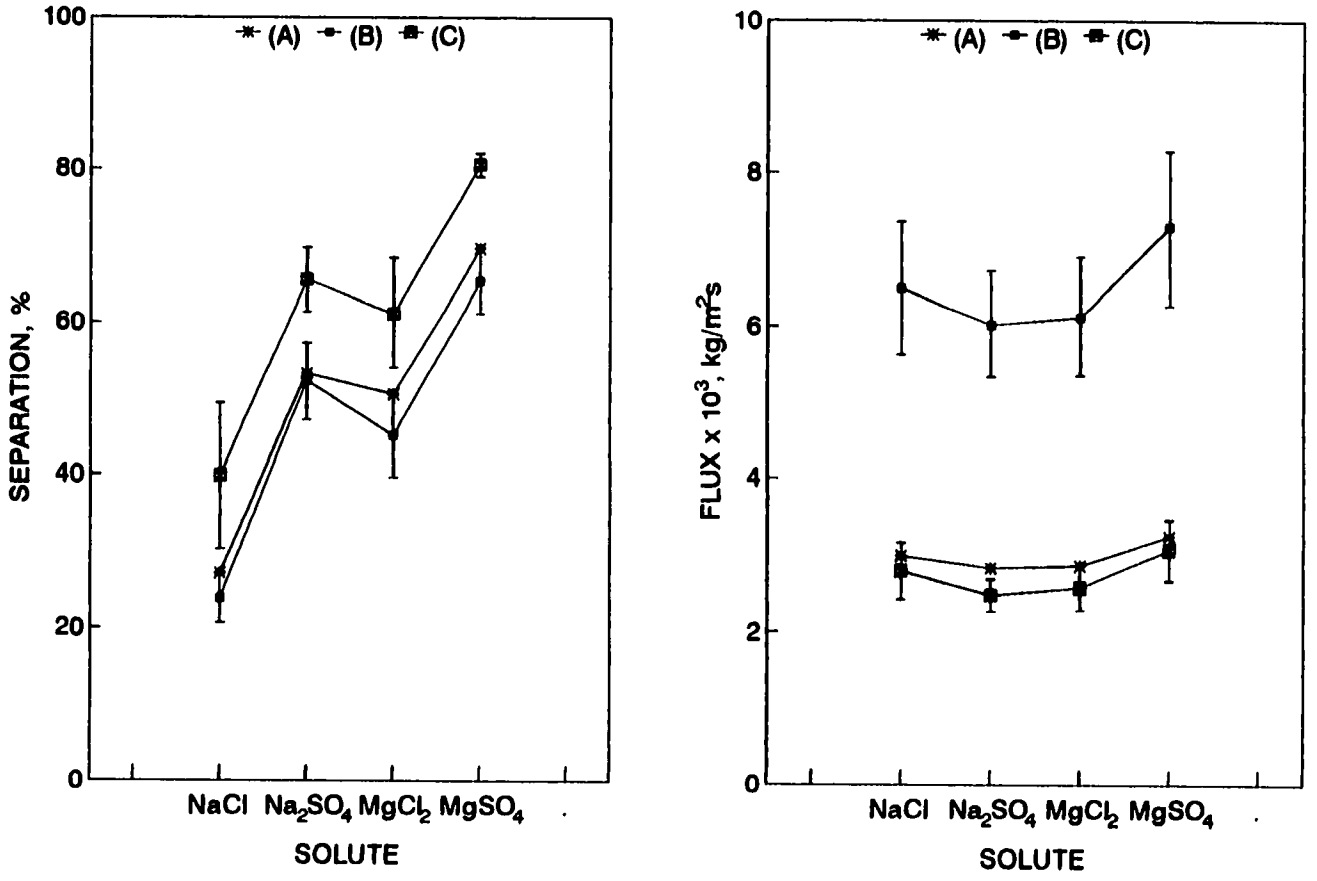

Fig. 4.18 Effect of photochemical surface modification on membrane performance. The membranes were prepared by method 2 under the conditions given in Tables 3.1 and 4.1, respectively.

(A) II-DK-T-04-D, (B) II-DK-T-04-D-hv-ETHYL ESTER, (C) II-DK-T-04-D-hv-GLYCEROL.
Test conditions: Feed: 0.17 M solute, 1.0 L/min., P: 6000 kPa, T: 25°C, pH=6.

4.2.2.3 Formation of Glycerol Functionalized Membrane

Attempts were made to prepare a glycerol functionalized membrane, **77** (Scheme 4.2). The glycerol functionalized membrane is expected to give a hydrophilic surface property.

In method 1, the DK membrane was irradiated in acetic acid containing glycerol as a reactant. As discussed in **Section 4.2.2.1**, the treatment of the dried DK membrane with acetic acid showed a damaging effect on membrane performance. In order to minimize the acetic acid effect, the DK membrane was irradiated in freshly distilled glycerol in method 2.

The morphology of this irradiated membrane is shown in Fig. 4.11 (F). The textured structure was observed on the surface layer and no significant change in morphology was observed after the irradiation as compared to the initial DK membrane (Fig. 4.11 (A)).

The irradiated membrane was characterized by infrared spectroscopy. Both ATR and transmittance infrared spectra of the glycerol functionalized membrane, **77**, are shown in Fig. 4.19, (B) and (D). For comparison purposes, the ATR spectrum of the initial DK membrane and the transmission spectrum of a related model compound, **72**, in Scheme 2.5, are also shown in Fig. 4.19. As can be seen, irradiation of the DK membrane, 4.19 (A), again resulted in a disappearance of the diazo bands around 2150 cm^{-1} and appearance of a strong band at 1728 cm^{-1}, 4.19 (B) and (D). Comparing the spectrum (C) of model compound, **72** (Scheme 2.5), with (B) and (D), in each case a

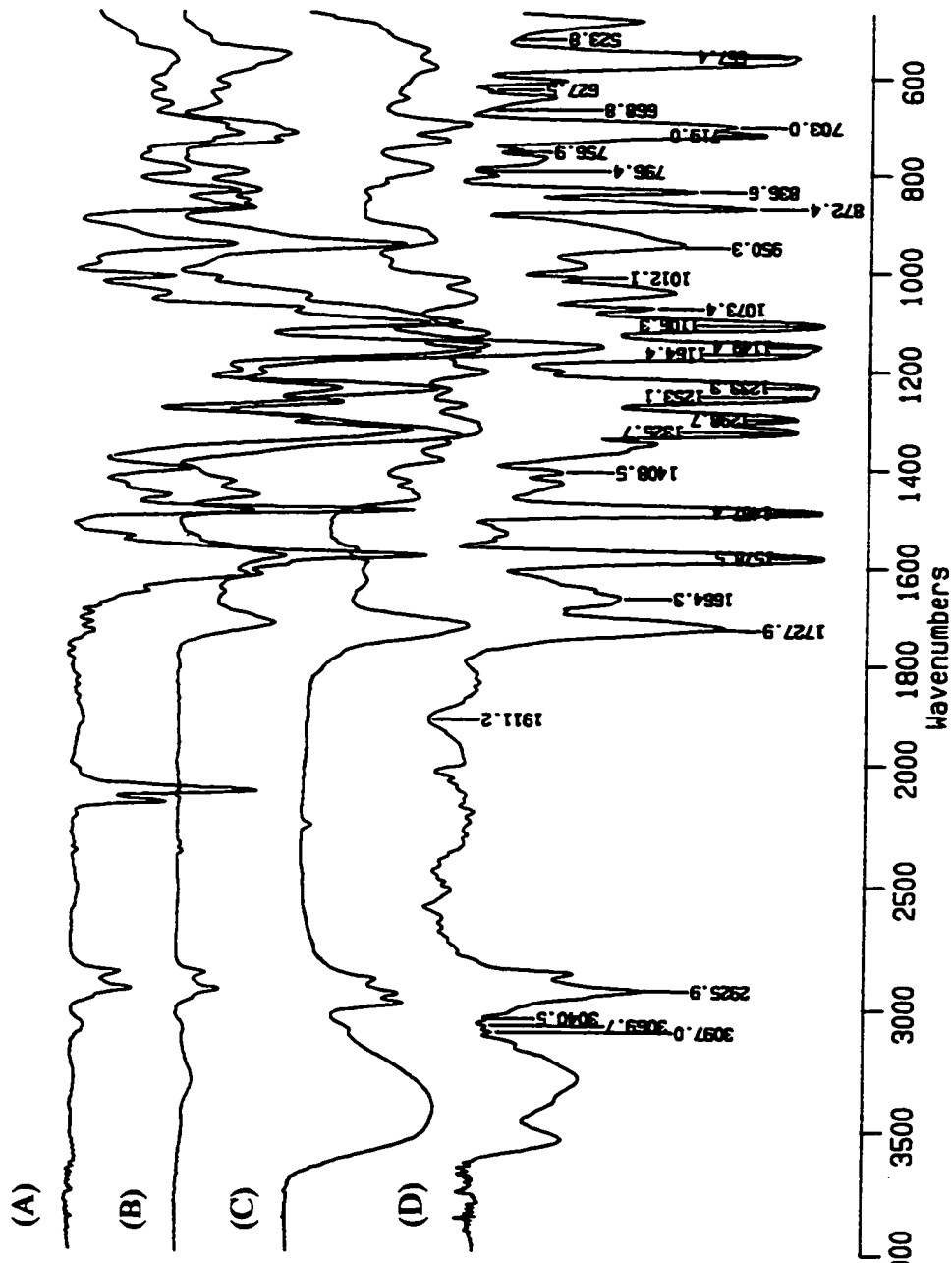

Fig. 4.19 Infrared spectra of the initial diazoketone membrane, glycerol functionalized membrane and related model compound.

(A) ATR-FTIR spectrum of initial diazoketone membrane, II-DK-T-04-D, Table 3.1,
(B) ATR-FTIR spectrum of glycerol functionalized membrane, II-DK-T-04-D-hv-GLYCEROL, Table 4.1,
(C) transmittance spectrum of model compound, **72**, Scheme 2.5,
(D) subtraction spectrum of the support polysulfone membrane from glycerol functionalized membrane, II-DK-T-04-D-hv-GLYCEROL, Table 4.1.

strong band at about 1728 cm^{-1} is observed, which can be attributed to carbonyl stretching vibration of the glycerol ester of the indene acid. Broad peaks between 3600-3100 cm^{-1} indicate the presence of an -OH group as would be expected for the incorporation of glycerol. These spectra are consistent with the formation of the glycerol functionalized membrane, **77** (Scheme 4.2). However, this result can not exclude a possibility of the presence of water absorbed by the membrane as infrared absorbtion in this region is observed.

Comparison of the infrared spectrum obtained using the vacuum dried membrane sample (Fig. 4.19 (B)), with that discussed earlier with an air dried sample (Fig. 4.6 (C)), reveals a difference between the two carbonyl peaks. In the latter case, the spectrum, 4.19 (B), shows a single sharp carbonyl peak. While in the former spectrum (Fig. 4.6 (C)), there is a strong peak at about 1717 cm^{-1} with two shoulders, suggesting the presence of multiple carbonyl species. This could be due to the formation of the indene acid from a side reaction with water as the parent DK membrane was only dried in the air for a very short time period (5 min.) and irradiated in the air without exclusion of moisture. Clearly, the different drying processes prior to the irradiation account, at least in part, for this difference observed from the infrared spectra.

The glycerol functionalized membrane was characterized in terms of the separation of the four inorganic solutes. The results are illustrated in Fig. 4.18.

The glycerol functionalized membrane, II-DK-T-04-D-hν-GLYCEROL, showed slightly higher separation than the parent DK membrane, II-DK-T-04-D, and ethyl ester

membrane, II-DK-T-04-D-hv-ETHYL ESTER. However, no significant difference in flux was observed between the glycerol functionalized membrane and the parent DK membrane.

Comparing the ethyl ester with the glycerol ester functionalized membranes shows that the former membrane has a higher flux than the latter. However, the glycerol functionalized membrane should be more hydrophilic than the ethyl ester membrane and would be expected to show a higher flux than the hydrophobic ethyl ester membrane. This unexpected result is not currently understood.

Although the DK membrane was dried *in vacuo* overnight prior to the irradiation, the same pattern in the separation of the inorganic salts to those found with the air dried membranes (Figs. 4.1, 4.5, 4.7 and 4.9), was observed, namely low rejections towards salts with monovalent anions (chloride), but high rejections towards salts with divalent anions (sulfate). These results again suggest that the parent DK membranes prepared in both methods (method 1 and 2) are negatively charged, probably due to the presence of $-SO_3H$ groups in the barrier layer formed by the hydrolysis of the polymer end groups, $-SO_2Cl$. This effect appears to overwhelm the photochemical surface modification.

4.2.2.4 Conversion of the DK membrane to Indene Acid Functionalized Membrane

The DK membrane was converted to the indene acid membrane by irradiation in a 1% aqueous acetic acid solution. As expected no side reaction of dye formation was

observed under this condition.[91,96]

The membrane was examined by SEM after the irradiation. As can be seen from Fig. 4.11 (C), a textured structure remained after the irradiation. No significant difference in morphology was observed as compared to the parent DK membrane (Fig. 4.11 (A)).

The irradiated membrane was characterized by infrared spectroscopy. The ATR-FTIR spectrum and the subtraction spectrum of the irradiated membrane are shown in Fig. 4.20 (B) and (C). For comparison purposes, the transmission FT-IR spectrum of a model compound, **68** (Scheme 2.5), and the ATR-FTIR spectrum of the initial diazoketone membrane are also shown in Fig. 4.20. After the photochemical surface modification of the DK membrane, the diazo bands around 2150 cm^{-1} disappeared and were replaced by a strong band at 1721 cm^{-1}, spectra (B) and (C) in Fig. 4.20. As can be seen from a comparison of spectra (B) and (C) with (D) in Fig. 4.20, the carbonyl peak of model compound, **68** (1687 cm^{-1}) occurs at a different position to the new (carbonyl) peak (1721 cm^{-1}) in the spectra of the photochemically modified film, (B) and (C).

Examination of the photomodified membrane (Fig. 4.20 (B) and (C)), showed that there were a series of broad bands in the 3600-3100 cm^{-1} range, indicating the presence of hydroxyl groups. The model compound showed a typical OH stretching pattern for a carboxylic acid (Fig. 4.20 (D)).[120] The broad bands encountered in the OH region of the spectrum are likely attributed to the formation of dimeric species.[120,121,122] This result

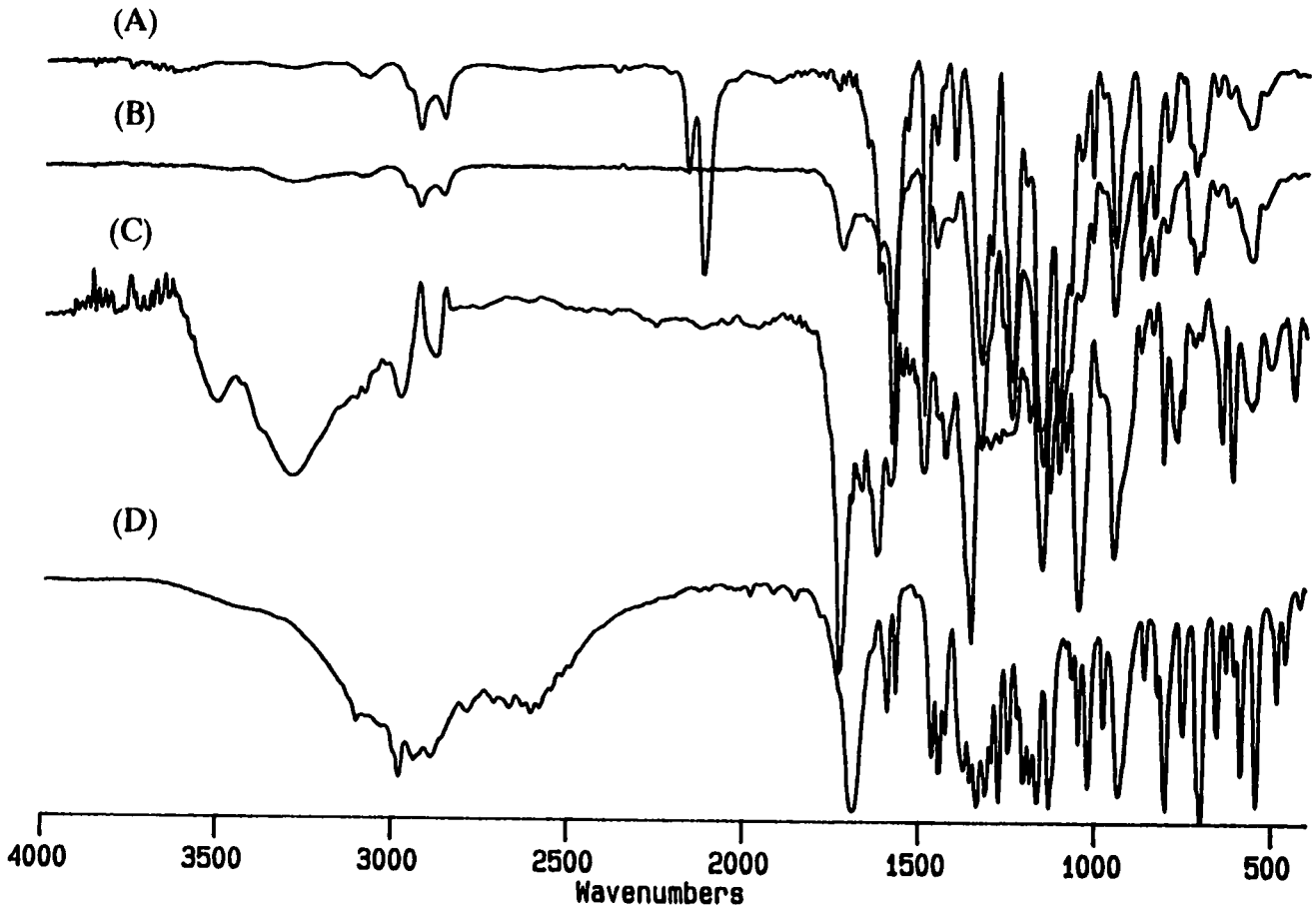

Fig. 4.20 Infrared spectra of the initial DK membrane, an indene acid functionalized membrane and a related model compound.
(A) ATR-FTIR spectrum of initial DK membrane, II-DK-T-04-D, Table 3.1,
(B) ATR-FTIR spectrum of indene acid functionalized membrane, II-DK-T-04-D-hv-INDENE ACID, Table 4.1,
(B) subtraction spectrum of the support polysulfone membrane from indene acid functionalized membrane, II-DK-T-04-D-hv-INDENE ACID, Table 4.1,
(C) transmittance spectrum of model compound, **68**, Scheme 2.5, (KBr pellet).

is consistent with the observed carbonyl band at 1687 cm^{-1}.[120,121,122] These broad bands are particularly evident in spectra obtained from solid samples.[120] The membrane environment used here is different from a typical environment of carboxylic acid used in infrared spectroscopy, in that strong molecular association between carboxylic acid groups is likely limited by the presence of the polymer backbone. As a result, it suggests that the spectra of the photomodified membrane (Fig. 4.20 (B) and (C)), with a band at 1721 cm^{-1} attributed to a carbonyl and the sharper OH stretching region are consistent with the formation of largely isolated carboxylic acid groups in the membrane. The observed carbonyl frequency for the carboxylic acid groups in the irradiated membranes is consistent with that reported for monomeric carboxylic acids.[123] All of the infrared spectra of the irradiated membranes discussed above look similar. In order to distinguish between the indene acid functionalized membrane and several different ester functionalized membranes, attempts were made by treating these membranes with either NaOH or $Ca(OH)_2$ to generate carboxylate salts. In general, when the ionization of a carboxylic acid occurs, giving the COO^- group, the characteristic carbonyl absorbtion vanishes and is replaced by two bands, one between 1610 cm^{-1} and 1550 cm^{-1} and the other between 1400 cm^{-1} and 1300 cm^{-1}, which correspond to the anti-symmetric and symmetric vibration of the COO^- structure.[120,124,125] However, the infrared spectra of the base treated indene acid membranes did not show the expected shift for the carbonyl groups. The reason is not presently understood. It should be noted that the indene acid functionalized membrane showed a small dependence of separation on the pH of feed

solution and no such dependence was observed for the ethyl ester functionalized membrane (Fig. 4.10).

In a further experiment, the support polysulfone membrane and the indene acid functionalized membrane were treated with $Ca(OH)_2$. The presence of calcium on the surface of these $Ca(OH)_2$ treated membranes was examined with energy dispersion spectroscopy (EDS). Typical results are shown in Fig. 4.21. After soaking in a saturated $Ca(OH)_2$ aqueous solution, both the support polysulfone membrane as a control, and the indene acid membrane showed strong calcium signals (Fig. 4.21 (A) and (C)), indicating the presence of the calcium on the surface of these membranes. After rinsing with water, no calcium was detected on the surface of the support polysulfone membrane (Fig. 4.21 (B)), indicating that the physically adsorbed calcium on the surface of the control polysulfone membrane was completely removed. However, the calcium on the surface of the indene acid membrane was still detectable. This result is consistent with the presence of the indene acid functionality on the surface of the membrane.

The photomodified membrane was characterized in terms of its separation/flux performance. The results are presented in Fig. 4.22. Duplicate membrane specimens were tested and the results were averaged and the errors shown by the error bars. The indene acid functionalized membrane, namely II-DK-04-D-hν-INDENE ACID, shows slightly lower separation but much higher flux than the initial DK membrane, II-DK-04-D.

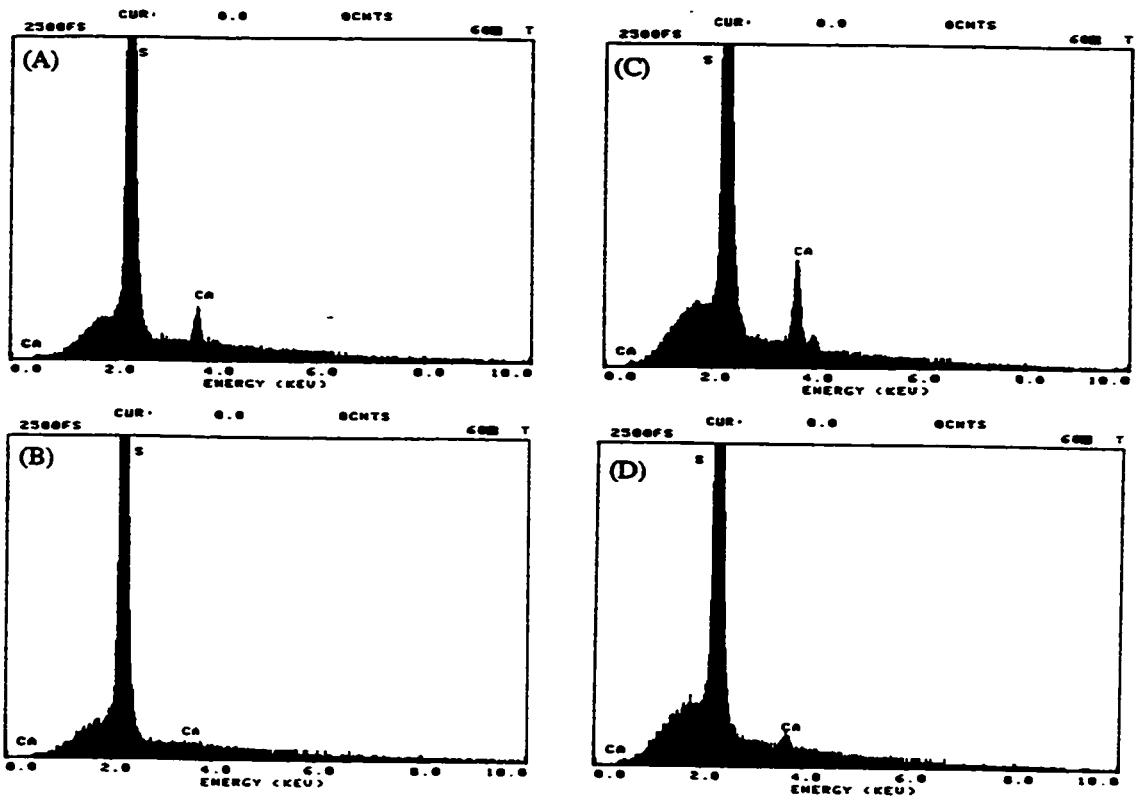

Fig. 4.21 EDS spectra of the polysulfone membrane and the indene acid functionalized membrane.

(A) the polysulfone membrane soaked in $Ca(OH)_2$ saturated aqueous solution for 2 days,
(B) (A) washed with water for 10 hours,
(C) the indene acid functionalized membrane soaked in $Ca(OH)_2$ saturated aqueous solution for 2 days,
(D) (C) washed with water for 10 hours.

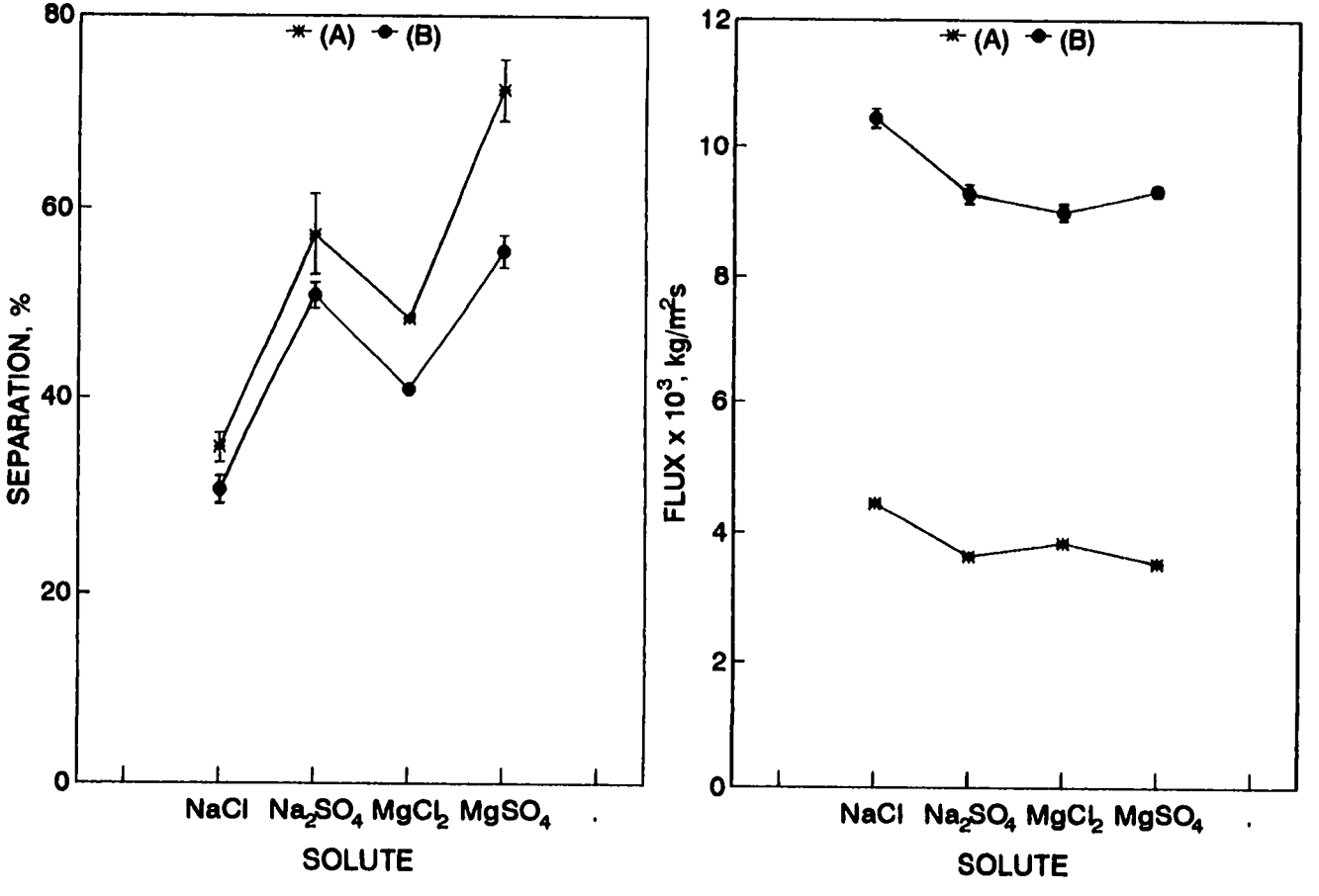

Fig.4.22 Effect of photochemical surface modification on membrane performance. The membranes were prepared by method 2 under the conditions given in Tables 3.1 and 4.1, respectively.

(A) II-DK-T-04-D, (B) II-DK-T-04-D-hv-INDENE ACID.

Test conditions: Feed: 0.17 M solute, 1.0 L/min., P: 6000 kPa, T: 25 °C, pH=6.

The results of both the infrared characterization and permeability test suggest that the photoreaction is occurring. However, the separation performance is not what would be expected for an indene acid functionalized membrane. This result is different from those presented earlier in Figs. 4.1 and 4.5 and that reported previously by the McMaster membrane group.[72] Drying the membrane *in vacuo* overnight might cause damage to the membrane to give the observed result (Fig. 4.22).

4.3 Overall Discussion

In this section, the two methods used for photochemical surface modification of the TFC membranes are compared with each other.

4.3.1. Reproducibility

In order to evaluate the methods used here, reproducibility of the membrane performance as a function of membrane fabrication was examined. A typical result is shown in Tables 4.2.

Table 4.2 Comparison of RO performance between different batches of DK membrane (II-DK-T-01) prepared using method 1

PERFORMANCE	SEPARATION, %		FLUX x 10^3, kg/m^{2}s	
SPECIMEN	A	B	A	B
BATCH 1	19.5	16.5	6.10	7.40
BATCH 2	21.3	18.2	6.02	9.23

Feed: 0.17 M NaCl aqueous solution, pressure: 6000 kPa, temperature: 25±2 °C.

In method 1, two different batches of DK membrane were prepared under identical conditions using a 15 min. polymerization. The same polysulfone base membrane was used in each batch. The DK membranes obtained were air dried in a dark place for 5 min., then stored in water in a dark place before the reverse osmosis test. Duplicate membrane specimens were tested for each batch. As can be seen from Table 4.2, the flux difference between the duplicate membrane samples from batch 2 is larger than that between the two batches, indicating a good reproducibility in flux between the different batches. The variation in separation between the duplicate membrane samples within each batch is similar to that between the two different batches. The differences in both separation and flux within a batch and between the different batches observed from the data in Table 4.2 are comparable with those reported in the literature.[72]

In method 2, three different batches of DK membrane were prepared under identical conditions using a 2 h polymerization. The same polysulfone base membrane

Table 4.3 Comparison of RO performance between different batches of DK membrane (II-DK-T-04-D) prepared using method 2

PERFORMANCE	SEPARATION, %		FLUX x 10^3, kg/m^{2}s	
SPECIMEN	A	B	A	B
BATCH 1	27.1	20.7	2.99	3.22
BATCH 2	32.1	34.4	4.04	3.96
BATCH 3	21.9	23.6	6.37	5.29

Feed: 0.17 M NaCl aqueous solution, pressure: 6000 kPa, temperature: 25±2 °C.

was used in each batch. The DK membranes obtained were dried *in vacuo* overnight, then stored in water in a dark place before the reverse osmosis test. Duplicate membrane specimens were tested for each batch.

As can be seen from Table 4.3, the variations in both separation and flux within a batch are less than that between the batches. The magnitude of the variation in both flux and separation is comparable with that of a related system previously reported by the McMaster membrane group.[72] However, the variation in flux between the different batches is significant (Table 4.3). The possible reasons could be as follows.

(1) The support polysulfone membrane is not uniform.

(2) The concentration of 1,2-ethanediamine, **74**, in the polysulfone support membrane is different from one specimen to another. The membrane was manually rolled with a plastic roller to remove the excess diamine solution on the surface prior to immersion in the organic solution containing disulfonyl chloride, **47**. This may cause a variation in the ratio of 1,2-ethanediamine, **74**, to disulfonyl chloride, **47**, from one specimen to another so as to affect the interfacial polymerization and to give different separation and flux. The ratio of a diamine to a disulfonyl chloride has been shown to be an important factor influencing interfacial polymerization and polymer properties.[103]

(3) The formation of the polysulfonamide (Scheme 3.1), is slow. The morphology study has shown that an asymmetric textured structure is

formed. This asymmetric structure may unevenly affect monomer diffusion.

(4) The preparation of the thin-film composite membrane by hand is a multiple step process, in which technique is a critical factor. An accumulation of human error in each step could be a factor that accounts for the observed variation in separation and flux.

Comparing Table 4.2 with Table 4.3, the DK membranes prepared using method 1 show a better reproducibility in RO performance than the DK membranes prepared using method 2, suggesting that the drying condition used is also an important factor influencing the reproducibility of the membrane performance. In method 2, drying the membrane *in vacuo* overnight may cause a damage to the membrane, such as shrinking and cracking, so as to give a poor reproducibility in RO performance.

4.3.2. Photoreactions

Two different methods were studied in order to optimize the conditions for photochemical surface modification of thin-film composite membranes. These two methods produced significantly different results.

In method 1, the DK membranes were only dried in air for 5 min. before the photoreaction and then irradiated in an atmosphere of air. All of the photochemically modified membranes prepared by method 1 showed increased separations towards the four

inorganic salts as compared to the parent DK membrane.

In method 2, the DK membrane was dried *in vacuo* overnight prior to the photoreaction and irradiated under an atmosphere of nitrogen. Of the photochemically modified membranes prepared by method 2, only the glycerol functionalized membrane showed slightly increased separation as compared to the parent DK membrane.

The ethyl ester functionalized membrane prepared by method 1 showed increased separation and flux as compared to the initial DK membrane (Fig. 4.5). The ethyl ester functionalized membrane produced by method 2, showed essentially no change in separation, but an increased flux, as compared to the parent DK membrane (Fig. 4.18). Comparing Fig. 4.7 with Fig. 4.18, the glycerol functionalized membrane prepared by method 2 showed a less pronounced enhancement in separation than that produced by method 1, and no enhancement in flux. The glycerol functionalized membrane prepared by method 1 showed a significantly higher flux than the initial DK membrane.

The sulfur-containing crown ether functionalized membrane prepared by method 1 also showed increased separation as compared to the parent DK membrane. In contrast, the sulfur containing crown ether functionalized membrane prepared by method 2, showed lower separation than the parent DK membrane.

However, the membranes prepared by method 2 showed better infrared spectra than those prepared by method 1. As discussed earlier, all of the photochemically modified membranes prepared by method 1 showed a strong band at about 1720 cm^{-1} with shoulders, suggesting the presence of the multiple carbonyl species in the surface layer

of the thin-film composite membranes (Figs. 4.4 and 4.6). The shoulders observed could be due to the formation of the indene acid by a side reaction of the diazoketone with trace amounts of water in the systems. In method 2, the membranes were dried *in vacuo* overnight prior to the photoreaction. The effect of water on photoreactions appears to be less pronounced in method 2 than in method 1 based on the infrared spectra of the modified membranes. All of the photochemically modified membranes prepared by method 2 showed a sharper carbonyl band than those prepared by method 1.

The indene acid functionalized membrane produced by method 1 showed increased separation and decreased flux as compared to the parent DK membrane (Fig. 4.1). In contrast, the indene acid functionalized membrane produced by method 2 showed decreased separation and increased flux as compared to the parent DK membrane (Fig. 4.22).

In addition, no significant change in morphology of the membranes produced by method 2 was observed on irradiation, or even after reverse osmosis tests at 6000 kPa for over a month (Fig. 4.11 (B) and (D)). However, the textured structure of the corresponding membrane prepared by method 1, partially collapsed on irradiation (Fig. 4.2). These results suggest that the textured structure of the membranes prepared by method 2 is much more stable than that of the membranes produced by method 1. This extra stability obtained by method 2 could be attributed to the post reaction of 1,2-ethanediamine, **74**, with disulfonyl chloride, **47**, during the drying *in vacuo*. In method 2, the monomers absorbed in the support polysulfone membrane were not removed from

the membrane, after the membrane was taken out of the organic solution containing **47**. The post reaction might increase the average degree of the polymerization and make the membrane stronger than that obtained by method 1. This post reaction was essentially eliminated in method 1, because the 1,2-ethanediamine monomer was immediately removed from the membrane after polymerization by rising with water or other solvents.

In method 2, drying the membranes *in vacuo* overnight could cause damage to the membranes, such as shrinking, cracking and partial detachment of the surface coating layer from the supporting polysulfone membrane. These damages can not be detected by infrared spectroscopy, but could be related to the observed separation/flux performance. As a result, the modified membrane showed unexpected separation/flux performance. In method 2, the treatment of the membranes with acetic acid or the use of acetic acid as a solvent for the photoreaction might deteriorate the damage initiated by drying *in vacuo* overnight to give decreased separation and increased flux as compared to the untreated parent DK membrane (Fig. 4.16).

In method 1, no such harsh drying conditions were used and damage associated with the drying is unlikely to occur. Thus, the use of acetic acid as a solvent for the photoreactions did not damage the membranes. Both the glycerol and the sulfur-containing crown ether functionalized membranes, prepared using acetic acid as a solvent during photoreactions, showed enhanced separation and flux as compared to the parent DK membrane (Figs. 4.7 and 4.9). Although these membrane showed similar increases in separations, the glycerol functionalized membrane showed significantly higher flux

than the sulfur-containing crown ether functionalized membrane, suggesting that the different photoreactions are occurring to give different membrane performances.

Overall, method 1 is better than method 2 in terms of the membrane performance observed.

Reproducibility of the photoreaction between the different batches can be seen from Fig. 4.10. The data for the indene acid functionalized membrane shown in Fig. 4.10 were the average performance of four membrane samples from two different batches. The errors in these data are slightly larger than that of the duplicate membrane samples from a single batch.

4.4 Summary

1. This chapter has presented a photochemical method for the modification of the chemical properties of a thin-film composite membrane. The diazoketone functionality of the initial thin-film composite membrane has been photochemically converted into other functionalities. Two different methods for this conversion have been studied. Method 1 is better than method 2 in terms of the separation/flux performance of the modified membranes.

2. The study has demonstrated, by the separation of four inorganic solutes from aqueous solutions, that photochemical surface modification of a single precursor DK

membrane can significantly alter membrane performance as compared to the initial DK membrane. The photochemical method developed for altering surface functionality of a thin-film composite membrane can, with certain reagents, lead to an alteration in the physical structure of the thin film.

3. A method for preparation of membrane specimens for surface characterization of a thin-film composite membrane by infrared spectroscopy has been developed. In this method, the surface layer together with the support polysulfone layer was peeled from the nonwoven polyester support. In addition, a model thin film was prepared by liquid-liquid interfacial polymerization. Characterization of this model thin film provides useful information for characterization of the surface layer of a thin-film composite membrane.

4. Despite the positive results obtained by the approach of the photochemical surface modification, the current system has some drawbacks. For example, the sulfonic acid groups formed from the hydrolysis of the sulfonyl chloride of the polymer end groups appeared to overwhelm the effect of photochemical surface modification. Water used in the polymerization step is difficult to completely remove from the system and appeared to interfere with the subsequent photoreactions.

5. In general, the photochemical method investigated in this chapter is a useful approach to alter the surface chemical properties and separation performance of a thin-film composite membrane.

4.5 Experimental

In this section, the experimental details are discussed.

4.5.1 Materials

Glycerol, ethanol, 1,5,9,13-tetrathiacyclohexadecane-3,11-diol, acetic acid, acetic acid anhydride, chloroform, dichloromethane, acetone and molecular sieves, 0.4 nm, were all purchased from Aldrich Chemicals Inc..

Acetic acid was freshly distilled from acetic anhydride before use. Molecular sieves, 0.4 nm , was dried at 800 ° C for 6 h. Glycerol was treated with dried molecular sieves, 0.4 nm, for over a week and freshly distilled under reduced pressure before use. The other chemicals were used as received without further purification.

4.5.2 General Equipment

Photoreactor

The photoreactor used for photochemical surface modification of the DK membranes consists of four PRP 350 nm lamps (35 watts) fixed horizontally 3 cm apart and 14 cm from the membranes.

Infrared Spectrometer

Both transmission and attenuated total reflection Fourier Transform Infrared (ATR-FTIR) spectra of the membranes were obtained on a Biorad-Digilab FTS-40

spectrometer.

Scanning Electron Microscope

ISI-DS130 Scanning Electron Microscope and JEOL 1200 EX II Electron Microscope were used to observe membrane morphology.

4.5.3 Photochemical Surface Modification of the DK Membranes

Photochemical surface modification of the DK membranes was studied in this section.

4.5.3.1 Method 1

General Procedure

The DK membranes were prepared by polymerization for 15 min. and 2 h, respectively, as described in Chapter 3. Immediately following the interfacial polymerization, the DK membrane was air dried in a dark cupboard for 5 min. and then rinsed with 3 x 100 mL of the solvent that was to be used for the photochemical surface modification of the membrane. This rinsing process lasted for 5 min.. After this treatment, the DK membrane was immersed in 50 mL of a solution consisting of a reactant and the above solvent contained in a Petri dish, covered by a Pyrex glass cover. The membrane was irradiated with 350 nm wavelength light under an atmosphere of air for 20 min. on the top side and 10 min. on the bottom side. The membranes were rinsed

with water three times after irradiation and stored in water until used. Three membranes were prepared in each batch, two were used for permeability studies and one for surface characterization.

Ethyl Ester Functionalized Membrane

The DK membrane, II-DK-T-01 (see Table 3.1), was irradiated in 50 ml of ethanol using the above general procedure to give an ethyl ester functionalized membrane, namely II-DK-T-01-hν-ETHYL ESTER.

Ethanol Treated DK Membrane

The DK membrane, II-DK-T-01, was immersed in 50 mL of ethanol in a dark place for the same time period (30 min.) as that used for preparation of the ethyl ester functionalized membranes, II-DK-T-01-hν-ETHYL ESTER, then stored in water in a dark place for further testing.

Indene Acid Functionalized Membrane

The DK membranes, II-DK-T-01 and II-DK-T-04, (see Table 3.1) were irradiated in 50 mL of a 1% acetic acid aqueous solution using the above general procedure to give indene acid functionalized membranes, namely II-DK-T-01-hν-INDENE ACID and II-DK-T-04-hν-INDENE ACID, respectively.

Glycerol Functionalized Membrane

The DK membrane, II-DK-T-01, was rinsed with 3 x 100 mL acetic acid, then irradiated in a solution of 0.17 M of glycerol in acetic acid using the general procedure descrived above to give a glycerol functionalized membrane, namely II-DK-T-01-hν-GLYCEROL.

Sulfur-Containing Crown Ether Functionalized Membrane

Immediately following interfacial polymerization, the DK membrane, II-DK-T-01, was dried in a dark cupboard under an air atmosphere for 5 min., then rinsed with 3 x 100 mL of freshly distilled acetic acid. After these treatments, the DK membrane was immersed in a solution of 2.13 x 10^{-3} M of 1,5,9,13-tetrathiacyclohexadecane-3,11-diol in acetic acid, then irradiated to give a sulfur-containing crown ether functionalized membrane, namely II-DK-T-01-hν-S. CROWN ETHER.

Acetic Acid Treated DK Membrane

The DK membrane, II-DK-T-01, was immersed in 50 mL of acetic acid in a dark place for the same time period (30 min.) as that used for preparation of the photochemically modified membranes, II-DK-T-01-D-hν-S. CROWN ETHER and II-DK-T-01-hν-GLYCEROL, then stored in water in a dark place for further testing.

Crosslinked DK and Glycerol Functionalized Membranes

The crosslinked DK membrane, II-DK-T-01-CROSS LINKED, was prepared using 1,3,6-naphthalene trisulfonyl chloride, **45**, as a crosslinking reagent. The concentration of **45** was 2.83 x 10^{-4} M in an organic solution of 10% acetone and 90% carbon tetrachloride. The molar ratio of **47** to **45** was 5 in the organic solution. The other conditions used were the same as those used to prepare the DK membrane, II-DK-T-01, described in Chapter 3.

The crosslinked DK membrane, II-DK-T-01-CROSS LINKED, was irradiated in a solution of 0.17 M of glycerol in acetic acid using the general procedure descrived above to give a crosslinked glycerol functionalized membrane, II-DK-T-01-CROSS LINKED-hν-GLYCEROL.

For an acetic acid treated membrane as a control, the crosslinked DK membrane was immersed in 50 mL of acetic acid in a dark place for the same time period (30 min.) as that used for preparation of the photochemically modified membrane, II-DK-T-01-CROSS LINKED-hν-GLYCEROL, then rinsed with water and stored in a dark place for further testing.

4.5.3.2 **Method 2**

General Procedure

The DK membrane was prepared by polymerization for 2 h as described in Chapter 3. Immediately following interfacial polymerization, the DK membrane (II-DK-

T-04) was air dried in a dark cupboard for 1 h, then covered with an aluminium foil, put into a desiccator and dried *in vacuo* overnight. This vacuum dried membrane, namely II-DK-T-04-D, was transferred into a dry bag filled with dry nitrogen gas, then rinsed with 3 x 100 mL of the solvent, that was used for the photochemical surface modification of the membrane. This rinsing process lasted for 5 min. The DK membrane was immersed in 50 mL of solution consisting of a reactant and the above solvent in a Petri dish, covered by a Pyrex glass cover, and irradiated with 350 nm wavelength light under a nitrogen atmosphere for 20 min. on the top side and 10 min. on the bottom side. The solutions used in the photochemical reactions were not degassed. Three pieces of the membranes were irradiated at the same time under identical conditions, then rinsed with water three times. The irradiated membranes were stored in water until used.

Ethyl Ester Functionalized Membrane

The DK membrane, II-DK-T-04-D, was irradiated in ethanol using the above general procedure to give an ethyl ester functionalized membrane, namely II-DK-T-04-D-hν-Ethyl ESTER.

Indene Acid Functionalized Membrane

The DK membrane, I-DK-T-05-D, was irradiated in a 1% acetic acid aqueous solution to give an indene acid functionalized membrane, namely II-DK-T-04-D-hν-INDENE ACID.

Glycerol Functionalized Membrane

The DK membrane, II-DK-T-04-D, was irradiated in 50 ml of freshly distilled glycerol using the above general procedure to give a glycerol functionalized membrane, namely II-DK-T-04-D-hν-GLYCEROL.

Sulfur-Containing Crown Ether Functionalized Membrane

The above dried DK membrane, II-DK-T-04-D, was rinsed with 3 x 100 mL of freshly distilled acetic acid, then immersed in 50 mL of a solution of 2.13×10^{-3} M of 1,5,9,13-tetrathiacyclohexadecane-3,11-diol in acetic acid, then irradiated to give a sulfur-containing crown ether functionalized membrane, namely II-DK-T-04-D-hν-S. CROWN ETHER.

Acetic Acid Treated DK membrane

The above dried DK membrane, II-DK-T-04-D, was immersed in 50 mL of acetic acid in a dark place for the same time period (30 min.) as that used for preparation of the photochemically modified membrane, II-DK-T-04-D-hν-S. CROWN ETHER, then rinsed with water and stored in a dark place for further testing.

4.5.4 Preparation of a Diazoketone-containing Thin Film by Liquid-Liquid Interfacial Polymerization

Disulfonyl chloride monomer, **47** (1.0 g), was dissolved in 1.0 L of ethyl acetate

in a 1 L volumetric flask.

Triton X-114 surfactant (0.35 g) was added into a 1 L volumetric flask containing 500 mL water and stirred for 10 min.. Then, 40 g of 1,2-ethanediamine and water were added to make the total volume 1 L. After stirring for 30 min., 100 mL of this solution was transferred into a 1 L volumetric flask and diluted to 1 L with water. This diluted solution was stirred for 30 min..

The solution of the disulfonyl chloride in ethyl acetate (100 mL) prepared above was pored into a jar containing 100 mL of the aqueous diamine solution prepared above. The interfacial polymerization was allowed to proceed for three days in a dark cupboard. The originally yellow coloured solution became almost colourless after three days and a yellow coloured thin film formed at the interface between aqueous and organic solutions. This fragile thin film was picked up from the interface on a microporous polyethylene film, and rinsed with ethanol three times followed by water three times. The thin film was air dried in a dark cupboard for 1 h, then covered with an aluminium foil and dried *in vacuo* overnight.

The photochemical surface modification of this thin film was carried out under the same conditions as those described in **Section 4.5.3.2.**

4.5.5 Measurement of Infrared Spectra

Characterization of the DK and modified membranes by infrared spectroscopy is discussed in this section.

4.5.5.1 Attenuated Total Reflectance Spectra

The thin-film composite membrane was cut into two identical 1 cm x 5 cm pieces and mounted on both sides of a ZnSe single crystal. The ATR-FTIR spectra were obtained using a twin parallel mirror reflection attachment. The sample chamber was swept with nitrogen for 10 min. before recording the spectra and 256 scans were collected.

4.5.5.2 Transmittance Spectra

The surface layer together with the polysulfone layer of a thin-film composite membrane was peeled from the polyester nonwoven support layer with a surgical knife and compressed into a transparent film under 2000 kPa. For the support polysulfone membrane, the polysulfone layer was peeled from the nonwoven polyester support and compressed into a transparent film. The transmittance spectra of the above peeled films were recorded. The sample chamber was swept with nitrogen for 10 min. before recording the spectra and 64 scans were collected. The subtraction spectra were obtained by subtracting the polysulfone background from the spectrum of a composite membrane.

The thin film prepared by liquid-liquid interfacial polymerization was supported by a polyethylene film and compressed into a transparent film. The transmittance spectra of this combined film and polyethylene film were recorded, respectively. The subtraction spectra were obtained by subtracting the polyethylene spectrum from that of the combined film.

4.5.6 Morphology Study

The morphologies of the initial diazoketone and modified membranes were observed by SEM as described in Chapter 3.

4.5.7 Energy Dispersion Spectroscopy (EDS)

Duplicate specimens of the polysulfone membrane and the indene acid functionalized membrane were soaked in $Ca(OH)_2$ saturated aqueous solution for 2 days and air dried. One of the duplicate specimens was washed with water for 10 h and air dried. These specimens were carbon coated. The EDS spectra of these membranes were measured using a ISI-DS130 Scanning Electron Microscope.

4.5.8 Reverse Osmosis Experiments

Flat thin-film composite membranes were tested in a reverse osmosis radial flow test system, which consists of a pump, six test cells, a heat exchanger, a pressure gauge and pressure regulator. A feed solution was pressurized and circulated over the surface of the membranes. The membranes were stabilized by circulating the feed solution at 6000 kPa for at least 4 days before collecting the data. Samples of the feed and permeate were collected, weighed, and analyzed in the same way as described in **Section 3.6.7** to determine flux and separation. The membrane area was 1.5×10^{-3} m^2, the feed flow rate was 1.0 L/min., and the pressure was 6000 kPa. The duplicate membranes were tested under the same conditions and the results were averaged.

For the pH tests, after testing at natural pH (around 6 for the McMaster system), the pH of the feed solution was adjusted back and forth using NaOH and HCl, respectively, to cover a wide range of pH from about 2 to 11.

The majority of the membranes were tested at 25 °C. For those tested at slightly different temperature, the flux through the membrane was corrected to 25 °C using Eq. 3.3.

Chapter 5

Model Development for the Formation of Thin-Film Composite Membranes by Interfacial Polymerization

Since Cadotte[15] first prepared thin-film composite membranes by interfacial polymerization, this route has been widely used for membrane fabrication.[5,16,17] The importance of this type of membrane has led to a considerable amount of work reported in the literature on the key interfacial polymerization step. However, most of the studies focus on improving membrane performance by optimizing parameters that influence membrane performance. Little attention has been paid to the kinetics of the membrane-supported interfacial polymerization process, despite the importance of understanding the system in order to improve membrane performance.

One of the major difficulties in a kinetic examination of membrane-supported interfacial polymerization is the nonsteady-state characteristics of the process. The monomer concentration in the support membrane phase, which decreases with polymerization time, is not easy to monitor experimentally.

In contrast to membrane-supported interfacial polymerization, liquid-liquid interfacial polymerization has been well studied. Morgan and co-workers[99-102] have reported a systematic study on the polycondensation of diacid chlorides with diamines.

This study has shown that the reaction, which takes place in the organic phase close to the interface between aqueous and organic phases, involves an S_N2 (bimolecular nucleophilic substitution) mechanism.[99-102,126] Kinetic studies on other systems, such as polyester formation, have been recently reported.[127,128,129]

A model that is based on constant monomer concentrations in the bulk solutions, independent of polymerization time, has been developed by Enkelmann and Wegner[130,131] for the liquid-liquid interfacial polymerization of hexanediamine and 1,8-octanedicarbonyl chloride. This model describes the relationship between film thickness and reaction rate. Since the interfacial polymerization reaction is fast, and diffusion controlled, only diffusion and the competing hydrolysis were considered in the model.[130,131]

Pearson and Williams[132] studied the interfacial polymerization of an isocyanate with a diol. Isocyanate droplets were dispersed in a continuous diol phase. The diol monomer in the continuous phase was assumed to diffuse across the film formed by interfacial polymerization, and the concentration of the diol in the continuous phase was assumed to remain constant. Both steady-state and nonsteady-state models which considered diffusion and reaction rate were developed and solved numerically.[132]

Recently, Mikos and Kiparissides[133] have developed a model describing skin formation in suspension polymerization of methyl methacrylate in water, assuming a liquid-liquid interfacial polymerization. The Flory-Huggins theory,[134] developed for a polymer solution in equilibrium, was used to describe the composition of the newly formed polymeric film. Because of the fast rate of interfacial polymerization, the system

remained far from the equilibrium. Application of the Flory-Huggins theory to this non-equilibrium system is questionable because the basic assumptions of the Flory-Huggins theory are not satisfied. In addition, the use of the Flory-Huggins theory made the model too complicated to be solved analytically.

Janssen and te Nijenhuis[135,136] have studied the kinetics of encapsulation by the polycondensation of terephthaloyl dichloride with diethylenetriamine at the interface of an oil-in-water emulsion. The rate of reaction was much faster than that of diffusion, so the process was diffusion controlled. The model developed was in agreement with experimental results for short polymerization times, with membrane thickness increasing with the square root of polymerization time. However, this model incorrectly predicted the membrane thickness when the polymerization time approached infinity.[135,136]

An extensive literature search indicated that no systematic study had been reported dealing with the relationship between the thin-film thickness and the reaction kinetics of membrane-supported interfacial polymerizations under nonsteady-state boundary conditions. In this chapter, a general model which considers both diffusion- and reaction-controlled interfacial polymerization under nonsteady-state boundary conditions is developed. Subsequently, several special models are derived by simplifying the general model as follows;

(1) under nonsteady-state boundary conditions,

(a) reaction-controlled interfacial polymerization,

(b) diffusion-controlled interfacial polymerization,

(2) under the conditions of constant monomer concentration in the support membrane phase,

(a) both diffusion- and reaction-controlled interfacial polymerization,

(b) reaction-controlled interfacial polymerization,

(c) diffusion-controlled interfacial polymerization.

In this chapter, the discussion is restricted to the formation of a dense film.

5.1 The general model: Both reaction- and diffusion-controlled interfacial polymerization under nonsteady-state boundary conditions

A general model which considers both diffusion- and reaction-controlled interfacial polymerization under nonsteady-state boundary conditions is theoretically developed in this section.

5.1.1 Model Assumptions

The actual process of membrane-supported interfacial polymerization is complex. In order to facilitate model development and solution, the following simplifying assumptions were made:

1. The system considered is the interfacial polycondensation of monomer **A** in an aqueous phase with monomer **B** in an organic phase. **A** small molecule is produced as each condensation reaction occurs. This small molecule reacts with monomer **A**, for instance, **A** acts as an acid acceptor for HCl produced. The net result is that the incorporation of a molecule of monomer **A** into the polymer actually consumes two molecules of monomer **A**.
2. The newly formed polymer does not dissolve in either organic or aqueous phases. The density of the thin film is uniform during the reaction.[130,131,135,136]
3. Reaction takes place in a reaction zone of constant thickness, δ, in the organic phase adjacent to the interface.[99,101,102,106,126]
4. The polymerization reaction has second order kinetics, with the reaction rate being proportional to the concentrations of both monomers, **A** and **B**.[74-78,87,99,101,102,106,126]
5. The concentration of water soluble monomer in the support-membrane phase is uniform throughout the support membrane.
6. The organic soluble monomer concentration is uniform in the organic bulk solution up to the reaction zone and remains constant during the polymerization.[130-132]
7. The temperature of the system is uniform.[132,137]

8. Only monomer A diffusion is important from the support-membrane phase to the reaction zone,[130,131] the diffusion coefficient of monomer A in the newly formed polymer film is constant.[130,131,135,136]

9. All of monomer A arriving at the reaction zone reacts either with monomer B to form polymer or as an acceptor for the condensation product.[135] The average degree of polymerization is used to calculate the mass balance.[133]

10. The concentration profile of monomer A is linear across the newly formed thin film.[130,131,135-137]

11. Only a fraction, *f*, of monomer A diffuses towards the dense surface to form a barrier layer; the remaining monomer diffuses out through the back of the porous support.

In the 1920's, Evans[137] studied the kinetics of tarnishing and corrosion of metals, such as iron and zinc; a theoretical model considering both diffusion and interfacial reaction was developed to describe the formation of an oxidized layer on the surface of the metals. It was assumed that reactant concentrations in both gaseous and solid phases did not change with reaction time, despite the continuous growth of the oxidized layer.

Due to the similarity in some aspects of the physicochemical natures of the interfacial polymerization in the current study with the metal oxidization studied by Evans,[137] some of the assumptions employed by Evans were adopted directly; such as

assumptions 2 and 10. Assumption 7 was used by Pearson and Williams[132] for interfacial polymerization of an isocyanate and a diol. Some of the assumptions made above are mathematically equivalent to Evans', such as assumptions 6 and 8, despite significant differences between the two systems.

Some of the assumptions, used by Enkelmann and Wegner,[130,131] and by Janssen and te Nijenhuis,[135,136] can be traced back to Evans' work. In addition, the average degree of polymerization, constant density of polymer film and a linear monomer concentration profile across the film have been employed by Enkelmann and Wegner,[130,131] and by Janssen and te Nijenhuis.[135,136] These assumptions might not be valid in actual cases. However, the use of these assumptions has significantly simplified the mathematical treatment when solving the models. Some of these assumptions were not explicitly stated by Enkelmann and Wegner,[130,131] Janssen and te Nijenhuis.[135,136] They used only the final simplified diffusion equations. Many details about how to derive those equations were omitted.[130,131,135,136] By doing so, discussion on some of the parameters that are difficult to measure, such as the thickness of the reaction zone δ, could be avoided. In contrast, development of the general model is described in detail in this work, and the parameters that are difficult to measure experimentally are discussed.

5.1.2 Model Development

In the fabrication of thin-film composite membranes, the support membrane is first impregnated with an aqueous solution containing monomer **A**, such as a diamine, then

immersed in an organic solvent containing monomer **B**, such as a diacid or disulfonyl chloride.[72,104] The support membrane is usually an asymmetric polymeric membrane having a skin layer on the surface where the thin film is to be formed.[5,72,104] Monomer **A** absorbed by the support membrane diffuses towards either side of the support membrane during the polymerization. In this chapter, interfacial polycondensation reaction of monomer **A** with monomer **B** is considered. Some of the key terms and a schematic picture of the model are presented in Fig. 5.1. A full list of symbols is given at the beginning of the thesis. The x coordinate, normal to the support membrane, is fixed at $x=0$ at the surface of the support membrane. As the polymerization proceeds and the thin film grows, the reaction zone which is initially located at $x=0$, is found at $x=X(t)$ at time t. Monomer **A** first partitions into the newly formed polymer and then diffuses to the reaction zone. The concentration profile of monomer **A** from the support to the reaction site decreases as the polymerization continues; a typical concentration profile at time t, is illustrated in Fig. 5.1. Since X varies with time, as $X(t)$, this becomes a moving boundary problem.

Given the above assumptions, the following equations can be formulated. At time t, the formation of polymeric thin film due to the second order reaction is given by,

$$\frac{P\rho_p}{M_P}\frac{dv_P}{dt}=k_r C(X,t)C_b\delta S \qquad 5.1$$

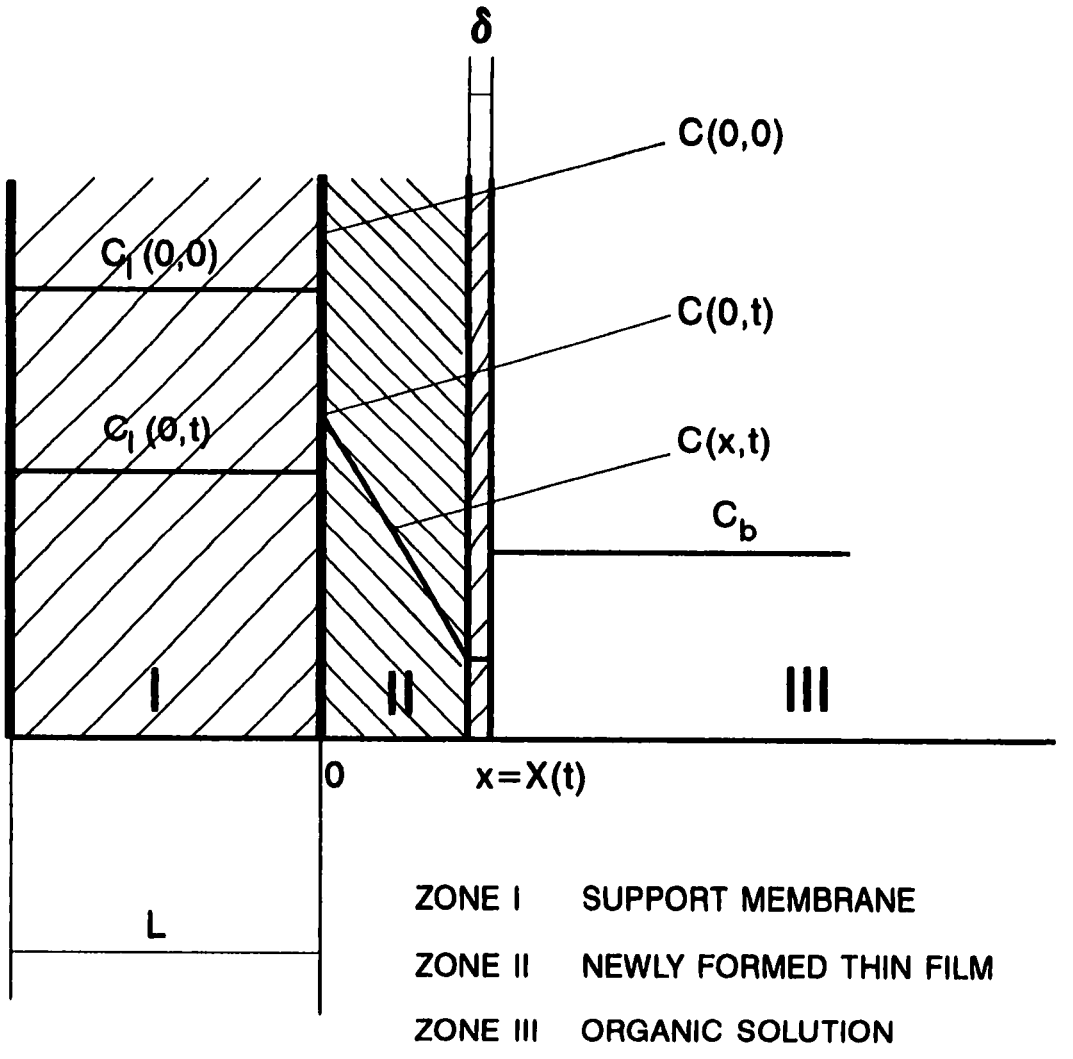

Fig. 5.1 A schematic representation of the model at time t.

where P is the average degree of polymerization, ρ_p is the density of the newly formed polymer film, M_P is the average molecular weight of polymer, dv_p/dt is the volume growth rate of the thin film, k_r is the second order reaction rate constant, $C(X,t)$ is the concentration of monomer **A** in the reaction zone at time t, C_b is the concentration of monomer **B** that reacts with monomer **A** in the organic phase, δ is the reaction zone thickness, S is the area, and $dv_p = SdX$.

The average molecular weight, M_P, is defined by,

$$M_P = PM_U \tag{5.2}$$

where M_U is the equivalent molecular weight of the repeat unit and is given by,

$$M_U = M_A + M_B - 2M_Z \tag{5.3}$$

where M_A is the formula weight of monomer **A**, M_B is the formula weight of monomer **B**, and M_Z is the formula weight of the small molecule that is produced by each condensation reaction.

Defining,

$$k = k_r \delta \tag{5.4}$$

$$k_I = \frac{kM_U}{\rho_P} \tag{5.5}$$

and after rearrangement gives,

$$\frac{dX}{dt} = k_1 C(X,t) C_b \qquad 5.6$$

where dX/dt is the growth rate of the thin film formed by interfacial polymerization.

Based on assumptions 8 and 9, the growth rate of the thin-film thickness must equal the rate of monomer diffusion to the reaction zone. For monomer **A**, one has,

$$\frac{P\rho_P}{M_P}\frac{dv_P}{dt} = -\frac{DS[C(X,t) - C(0,t)]}{X} \qquad 5.7$$

where D is the diffusion coefficient of monomer **A** in the newly formed thin film, $C(0,t)$ and $C(X,t)$ are the concentration of monomer **A** at the surface of the support membrane and in the reaction zone, respectively, at time t.

Defining,

$$D_M = DM_U/\rho_P \qquad 5.8$$

and after rearrangement, the growth rate of the thin film can be written as

$$\frac{dX}{dt} = \frac{D_M[C(0,t) - C(X,t)]}{X} \qquad 5.9$$

A material balance gives,

$$\frac{C(0,t)fLS}{K}+\int_0^x C(x,t)Sdx+\frac{2XS\rho_P P}{M_P}=\frac{C(0,0)fLS}{K} \qquad 5.10$$

where $C(0,0)$ is the initial concentration of monomer A at the surface of the support membrane, f is the fraction of monomer A in the support membrane which diffuses towards the dense surface to form a barrier layer, K is the partition coefficient of monomer A between the support membrane phase and the newly formed thin film. Under nonsteady-state conditions, Eq. 5.10 determines $C(0,t)$, the concentration of monomer A at $(0,t)$. The first term on the left hand side of Eq. 5.10 is the amount of monomer A (kmol) left in the support membrane phase at time t, the second term is the amount of monomer A (kmol) dissolved in the newly formed film, and the third term is the amount of monomer A (kmol) converted into the polymer. A small molecule is produced as each condensation reaction occurs, which in turn reacts with monomer A. The net result is that the incorporation of a molecule of monomer A into the polymer actually consumes two molecules of monomer A. Thus the third terms on the left hand side of Eq. 5.10 is multiplied by 2. The right hand side of Eq. 5.10 is the amount of monomer A (kmol) absorbed in the support membrane phase at time $t=0$.

Based on assumption 10, the linear concentration profile can be solved for the amount of monomer A in the thin film as,

$$\int_0^X C(x,t)Sdx = \frac{1}{2}XS[C(0,t)+C(X,t)] \qquad 5.11$$

It is useful in solving the above equations to define the following constants:

$$A_o = 2D_M k_I C_b C(0,0) fL \qquad 5.12$$

$$B_o = \frac{4KD_M k_I C_b \rho_P}{M_U} \qquad 5.13$$

$$C_o = Kk_I C_b \qquad 5.14$$

$$D_o = 2k_I C_b fL + 2KD_M \qquad 5.15$$

$$E_o = 2D_M fL \qquad 5.16$$

Substitution of Eq. 5.6, 5.10 and 5.11 into Eq. 5.9 and after rearrangement gives,

$$\frac{dX}{dt} = \frac{A_o - B_o X}{C_o X^2 + D_o X + E_o} \qquad 5.17$$

Substitution of Eq. 5.17 into Eq. 5.6 followed by a rearrangement gives,

$$C(X,t) = \frac{1}{k_I C_b} \frac{A_o - B_o X}{C_o X^2 + D_o X + E_o} \qquad 5.18$$

Ssubstitution of Eq. 5.11 and 5.18 into Eq. 5.10 and after rearrangement gives,

$$C(0,t) = \frac{1}{\frac{fL}{K} + \frac{X}{2}} \left[\frac{C(0,0)fL}{K} - \frac{2X\rho_P}{M_U} - \frac{C(X,t)}{2} X \right] \qquad 5.19$$

Integration of Eq. 5.17 gives a relation between the reaction time, t, and the thin-film thickness, X, as,

$$t = -\left(\frac{E_o}{B_o} + \frac{A_o D_o}{B_o^2} + \frac{C_o A_o^2}{B_o^3} \right) \ln\left(1 - \frac{X}{X_{max}} \right) - \frac{C_o}{2B_o} X^2 - \left(\frac{D_o}{B_o} + \frac{C_o A_o}{B_o^2} \right) X \qquad 5.20$$

The parameter f can be obtained from Eq. 5.10, by setting $t = \infty$. When the reaction time, t, approaches infinity, the thin-film thickness, X, approaches a maximum value, X_{max}, and both $C(0,\infty)$ and $C(X,\infty)$ approach zero. Hence Eq. 5.10 can be rearranged to give,

$$f = \frac{2X_{max}\rho_P K}{M_U C(0,0) L} \qquad 5.21$$

In the same manner, the maximum thickness of the thin film has been obtained from Eq. 5.10 as,

$$X_{max} = \frac{f M_U C(0,0) L}{2\rho_P K} \qquad 5.22$$

Alternatively, the maximum thickness can be obtained by dividing Eq. 5.12 with Eq. 5.13.

$$X_{max} = \frac{A_0}{B_0} \qquad 5.23$$

Since X_{max} can be obtained experimentally, Eq. 5.23 is very important because it correlates X_{max} with A_0 and B_0.

5.1.3 Qualitative analysis of the model

The validity of the model can be qualitatively assessed in terms of the physical meaning of the model at certain limits.

For example, at polymerization time $t=0$, the thickness of thin film formed by interfacial polymerization is zero, shown in Eq. 5.20. Also at $t=0$, based on Eq. 5.17, the maximum growth rate, r_{max}, of the thin-film layer is proportional to the initial monomer concentration,

$$r_{max} = \left.\frac{dX}{dt}\right|_{t=0} = \frac{A_0}{E_0} = k_f C(0,0) C_b \qquad 5.24$$

At $t=0$ and $X=0$, both Eq. 5.18 and Eq. 5.19 correctively reduce to the initial concentration of monomer **A**, $C(0,0)$.

When polymerization time, t, approaches infinity, X approaches X_{max} and the right hand side of Eq. 20 indeed approaches infinity. At $t=\infty$, not only does X approach X_{max},

but also the growth rate should approach zero. Indeed, Eq. 5.17 gives the minimum growth rate of zero at $t=\infty$.

$$r_{min}=\left.\frac{dX}{dt}\right|_{t=\infty}=\frac{A_o-B_oX_{max}}{C_oX_{max}^2+D_oX_{max}+E_o}=0 \qquad 5.25$$

In addition, when $t=\infty$ and $X=X_{max}$, Eqs. 5.19 and 5.18 give $C(0,\infty)=0$ and $C(X,\infty)=0$, respectively.

The above analysis indicates clearly that the results derived from this model are physically and mathematically reasonable.

In summary, a physically reasonable model has been proposed and analytical solution derived that can be used to describe the formation of thin film composite membranes.

5.2 Special Models

Several special models can be derived by simplifying the general model.

5.2.1 Interfacial polymerization under nonsteady-state boundary conditions

Under nonsteady-state boundary conditions, the following special models can be obtained.

5.2.1.1 Reaction-controlled interfacial polymerization

If the reaction rate of interfacial polymerization is much slower than that of monomer diffusion ($k_I \ll D_M$), the growth rate of the thin film is controlled by the interfacial reaction.

In this situation, $C(0,t)=C(X,t)$; therefore, Eq. 5.11 reduces to,

$$\int_0^X C(x,t)Sdx=\frac{1}{2}XS[C(0,t)+C(X,t)]=XSC(X,t) \qquad 5.26$$

Eq. 5.17 reduces to,

$$\frac{dX}{dt}=\frac{k_f C_b C(0,0)fL}{K}\frac{1}{\frac{fL}{K}+X}-\frac{k_f C_b}{\frac{fL}{K}+X}\frac{2X\rho_P}{M_U} \qquad 5.27$$

and Eq. 5.20 reduces to,

$$t=-\left(\frac{X_{\max}}{k_f C_b C(0,0)}+\frac{X_{\max}M_U}{2\rho_P k_f C_b}\right)\ln\left(1-\frac{X}{X_{\max}}\right)-\frac{M_U}{2\rho_P k_f C_b}X \qquad 5.28$$

The concentration of monomer **A** at $(0,t)$ and (X,t) is given by,

$$C(X,t)=C(0,t)=\frac{1}{\frac{fL}{K}+X}\left[\frac{C(0,0)fL}{K}-\frac{2X\rho_P}{M_U}\right] \qquad 5.29$$

Eqs. 5.27 to 5.29 can also be obtained directly by simultaneously solving Eqs. 5.6, 5.10 and 5.26 based on the general assumptions discussed previously with the assumption about the rate determining step specified in this section.

The validity of the model can be qualitatively assessed based on the physical meaning of the model at certain limits.

For example, at polymerization time $t=0$, the thickness of the thin film formed by interfacial polymerization should be zero, this is the case in Eq. 5.28. When polymerization time t approaches infinity, X approaches X_{max}, and the right hand side of Eq. 5.28 also approaches infinity, as expected.

A further conclusion, which can be drawn from Eq. 5.27, is that the maximum growth rate, r_{max}, of a thin-film layer is proportional to the initial monomer concentrations as given by Eq. 5.24. When t approaches infinity, Eq. 5.27 yields the minimum growth rate of $r_{min}=0$. In addition, when $t=0$ and $X=0$, Eq. 5.29 gives $C(0,t) = C(X,t) = C(0,0)$. When $t=\infty$ and $X = X_{max}$, Eq. 5.29 yields $C(0,t) = C(X,t) = 0$.

The above analysis demonstrates that the model approaches the correct limits.

5.2.1.2 Diffusion-controlled interfacial polymerization

If the interfacial reaction is much faster than monomer diffusion ($D_M < k_l$), the diffusion becomes the rate determining step. Under this condition, $C(X,t)=0$, and Eq. 5.11 reduces to,

$$\int_0^X C(x,t)Sdx = \frac{1}{2}XSC(0,t) \qquad 5.30$$

The growth rate of the thin-film layer, Eq. 5.17 reduces to,

$$\frac{dX}{dt} = \frac{D_M}{X}\frac{1}{\frac{fL}{K}+\frac{X}{2}}\left[\frac{C(0,0)fL}{K} - \frac{2X\rho_P}{M_U}\right] \qquad 5.31$$

and Eq. 5.20 reduces to,

$$t = -\left(\frac{X_{max}}{4D}+\frac{fL}{2KD}\right)X - \frac{X^2}{8D} - \left(\frac{fLX_{max}}{2KD}+\frac{X_{max}^2}{4D}\right)\ln\left(1-\frac{X}{X_{max}}\right) \qquad 5.32$$

The concentration of monomer **A** at the support, *C(0,t)*, is given by Eq. 5.29, although $C(0,t) \neq C(X,t)$.

Alternatively, Eqs. 5.29, 5.31 and 5.32 can be obtained independently by simultaneously solving Eqs. 5.9, 5.10 and 5.30 based on the general assumptions discussed previously with the assumption about the rate controlling step specified in this section.

The validity of the model can be qualitatively assessed based on the physical meaning of the model in a manner analogous to **Section 5.2.1.1**. For example, at polymerization time $t=0$, the thickness of thin film formed by interfacial polymerization

is zero, as shown in Eq. 5.32. When polymerization time t approaches infinity, X approaches X_{max}, and the right hand side of Eq. 5.32 also approaches infinity.

5.2.2 Interfacial polymerization under the condition of constant concentration of monomer A in the support membrane phase

If the amount of monomer A converted to polymer and the amount of monomer A dissolved in the newly formed film are much less than what is left in the support membrane phase, then the concentration of monomer A in the support membrane is essentially constant, the second and the third terms on the left hand side of Eq. 5.10 are negligible compared to the first term, thus $C(0,t) \approx C(0,0)$. This condition is approximately satisfied in the early stage of the polymerization, even under nonsteady-state boundary conditions.

Despite the thickness of a thin film formed by an interfacial reaction changes with time, the model for this scenario is often referred to as a steady-state model in the literature.[137]

5.2.2.1 Reaction- and diffusion-controlled interfacial polymerization

Assuming that both reaction rate and monomer diffusion are rate controlling steps, Eq. 5.6 still holds and Eq. 5.9 is replaced by Eq. 5.33,

$$\frac{dX}{dt} = k_I C(X,t) C_b \qquad 5.6$$

$$\frac{dX}{dt} = \frac{D_M[C(0,0) - C(X,t)]}{X} \qquad 5.33$$

Substitution of Eq. 5.6 into Eq 5.33, and after a rearrangement gives the thin film growth rate as,

$$\frac{dX}{dt} = \frac{D_M k_I C(0,0) C_b}{k_I C_b X + D_M} \qquad 5.34$$

Integration of Eq. 5.34 gives,

$$t = \frac{X^2}{2D_M C(0,0)} + \frac{X}{k_I C_b C(0,0)} \qquad 5.35$$

and the concentration of monomer **A** at *(X,t)* is obtained as,

$$C(X,t) = \frac{D_M C(0,0)}{k_I C_b X + D_M} \qquad 5.36$$

Evans[137] derived equations similar to Eqs. 5.6 and 5.33 based on a consideration of both diffusion and interfacial reaction, but he did not solve these equations simultaneously, i.e., no equation similar to Eq. 5.35 was obtained. Instead, the equations

were solved for two special cases: (1) the diffusion was a rate controlling step, (2) the reaction was a rate controlling step.[137]

5.2.2.2 Reaction-controlled interfacial polymerization

If the rate of diffusion is much larger than that of reaction, i.e., $D_M \gg k_1$, then the first term on the right hand side of Eq. 5.35 is negligible compared to the second, thus Eq 5.35 reduces to,

$$X = k_f C(0,0) C_b t \qquad 5.37$$

Eq. 5.34 reduces to Eq. 5.24 and Eq. 5.36 gives $C(X,t) = C(0,0)$, as expected.

Mathematically, this result is the same as that obtained by Evans[137] and was verified by the tarnishing of zinc. However, in this work , Eq. 5.37 is obtained as a special case of a more general model derived above.

5.2.2.3 Diffusion-controlled interfacial polymerization

If the reaction rate constant is much larger than that of diffusion, i.e., $k_f \gg D_M$, then the second term on the right hand side of Eq. 5.35 is negligible compared to the first, thus Eq. 5.35 reduces to,

$$X=\sqrt{2D_M C(0,0)t} \qquad 5.38$$

Eq. 5.34 reduces to,

$$\frac{dX}{dt}=\frac{D_M C(0,0)}{X} \qquad 5.39$$

and Eq. 5.36 gives $C(X,t) \approx 0$, as expected.

Mathematically, Eq. 5.38 is the same as obtained by Evans,[137] which was verified experimentally with respect to oxidation of copper. Eq 5.38 is essentially the same as reported by Janssen and te Nijenhuis[135,136] for the polycondensation of terephthaloyl dichloride with diethylenetriamine at the interface of an oil-water emulsion.

5.3 Quantitative analysis of the general model

In this section, a variety of factors that influence interfacial polymerization are systematically studied.

The general model for reaction- and diffusion-controlled interfacial polymerization under nonsteady-state boundary conditions is used to illustrate quantitatively how the reaction rate constant, diffusion coefficient, and monomer concentration influence the kinetic behaviour of interfacial polymerization and thin film formation.

In order to quantitatively evaluate the model, the diffusion coefficient of monomer A and the rate constant of the polymerization are needed. Parameters employed to generate the curves are given in Table 5.1. The details about the selection of these parameters are discussed in Chapter 6.

5.3.1 Effect of the reaction rate constant on interfacial polymerization

The reaction rate constant is an important parameter with respect to the kinetics of thin film formation by interfacial polymerization.[130-136] In this section, the effect of the reaction rate constant, k, defined in Eq. 5.4, on thin film formation is discussed.

The effect of the reaction rate constant and polymerization time on $C(X,t)$ and $C(0,t)$, given by Eqs. 5.18 and 5.19, are displayed in Fig. 5.2. $C(0,t)$ is the concentration of monomer A at the surface of the support membrane, while $C(X,t)$ is the concentration of monomer A in the reaction zone shown in Fig. 5.1. In general, the relationship between $C(0,t)$, $C(X,t)$ and the polymerization time can be used to distinguish the type of interfacial polymerization in terms of the rate controlling step.

For the case when reaction is the rate controlling step, curves A and B, which are generated, completely overlap. This means that the driving force for monomer A diffusion is zero. This is a typical reaction-controlled interfacial polymerization characterized by a small reaction rate constant of 3.69×10^{-8} m^4/(kmol.s) and the diffusion of monomer A has no effect on thin film formation.

Table 5.1 Parameters used to produce curves in Figs. 5.2-5.15

Parameters	Unit
$C(0,0)=0.316$	kmol/m^3
$C_b=6.89\text{x}10^{-4}$	kmol/m^3
$D=5.27 \text{ x } 10^{-15}$	m^2/s
$f=0.0833$	Dimensionless
$k=3.69 \text{ x } 10^{-6}$	m^4/(kmol.s)
$K=1.0$	Dimensionless
$L=2.05 \text{ x } 10^{-4}$	m
$X_{max}=2.21 \text{ x } 10^{-6}$	m
$M_A=60.1$	kg/kmol
$M_Z=36.45$	kg/kmol
$M_B=705.6$	kg/kmol
$\rho_p=1300$	kg/m^3

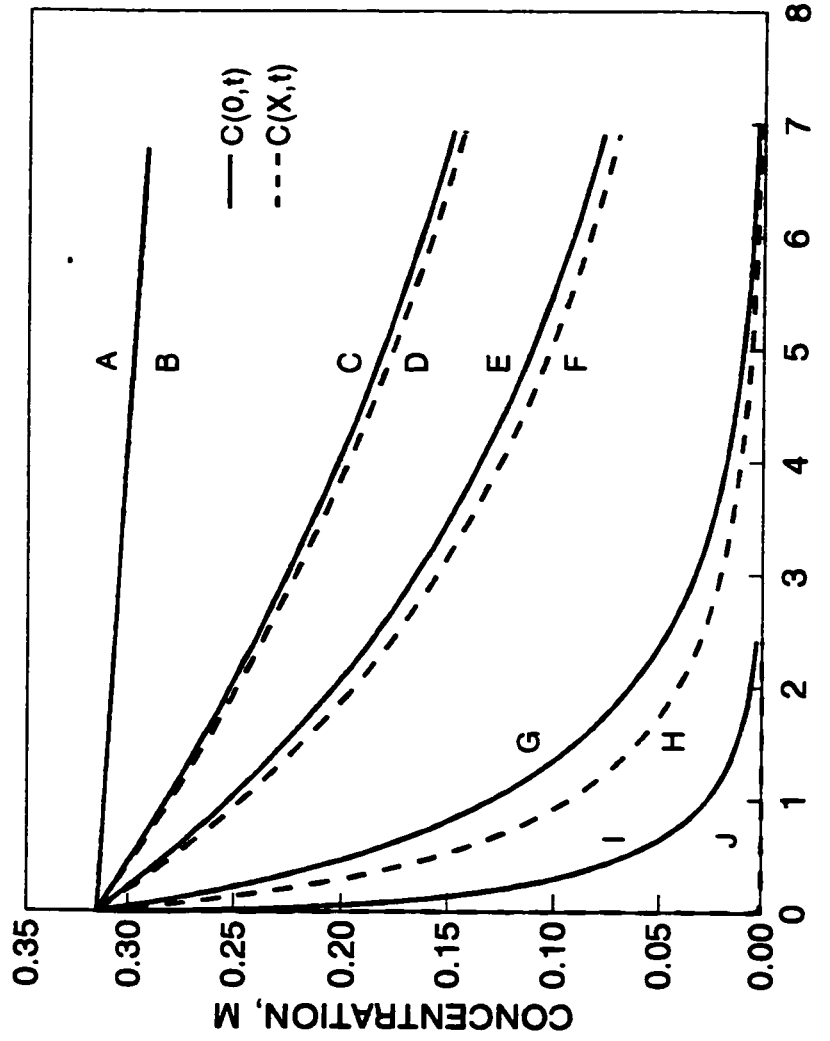

Fig. 5.2 Effect of reaction rate constant and polymerization time on C(0,t) and C(X,t).
A, B: $k=3.69\times10^{-8}$, C, D: $k=3.69\times10^{-7}$, E, F: $k=7.38\times10^{-7}$,
G, H: $k=3.69\times10^{-6}$, I, J: $k=3.69\times10^{-3}$ $m^4/(kmol.s)$.
The remaining parameters used to draw the curves are given in Table 5.1.

For the case when diffusion is the rate controlling step, curves I and J are generated. As soon as the reaction starts, the concentration *C(X,t)* (curve J) falls to zero and *C(0,t)* (curve I) rapidly decreases to zero within a short time, in this case about 2.5 h. This is a fast reaction characterized by a large rate constant, 3.69×10^{-3} $m^4/(kmol.s)$. This is a typical diffusion-controlled interfacial polymerization. In general, the interfacial polymerization of a diamine with a diacid chloride to form polyamide belongs to this type.[130,131,135,136]

For the case when both reaction and diffusion are important, curves C to H are generated. *C(0,t)* differs from *C(X,t)*, but both decrease as the polymerization time increases. These reactions have medium reaction rate constants compared to the two previous cases.

A reduced thin-film thickness is defined as X/X_{max}. This reduced thickness, X/X_{max}, is also the conversion based on monomer **A**. The relationship between the reduced thickness, X/X_{max}, the reaction time and the reaction rate constant is described by Eq. 5.20 and illustrated in Fig. 5.3.

Curve A of Fig. 5.3, with the largest apparent reaction rate constant of 3.69×10^{-3} $m^4/(kmol.s)$ (corresponding to curves I and J in Fig. 5.2) demonstrates that the reduced thickness increases very rapidly with time and reaches the maximum value within 2.5 h. This is for a fast reaction.

Curve B in Fig. 5.3, characterized by a reaction rate constant of 3.69×10^{-6} $m^4/(kmol.s)$ (corresponding to curve G and H in Fig. 5.2), is three orders of magnitude

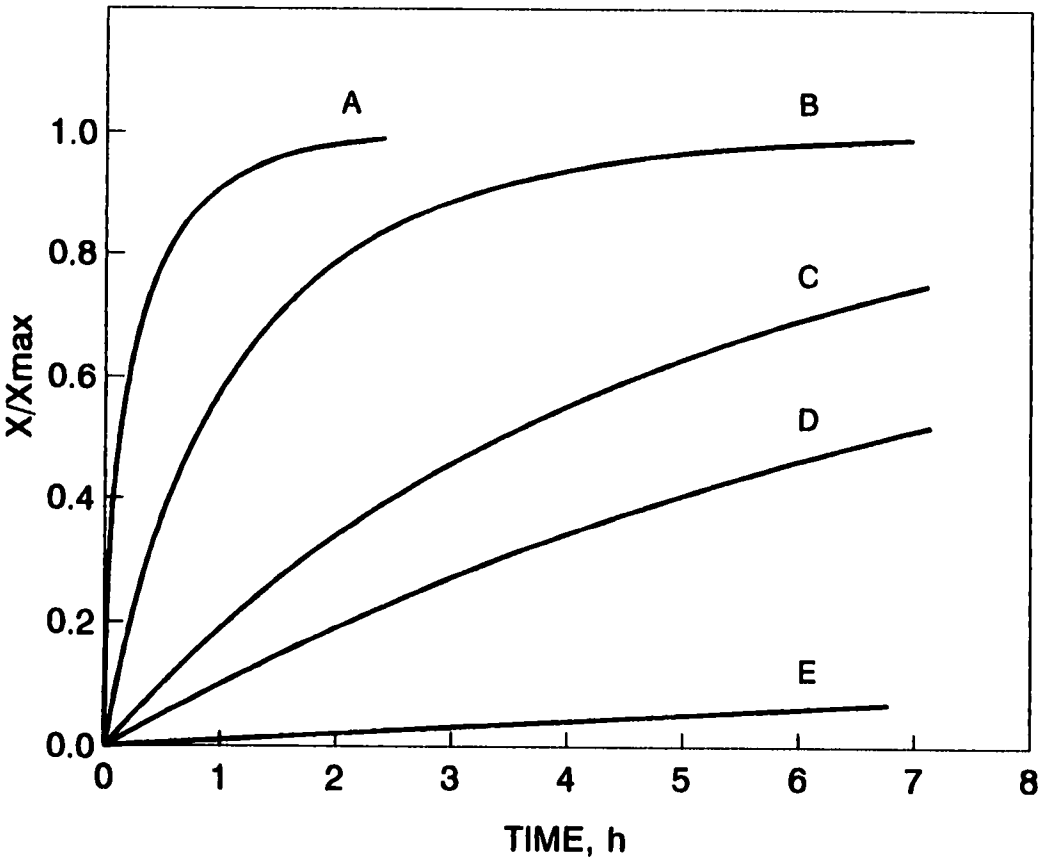

Fig. 5.3 Effect of reaction rate constant and polymerization time on the reduced thickness of the thin film.

A: $k=3.69\times10^{-3}$, B: $k=3.69\times10^{-6}$, C: $k=7.38\times10^{-7}$,
D: $k=3.69\times10^{-7}$, E: $k=3.69\times10^{-8}$ $m^4/(kmol.s)$.

The remaining parameters used to draw the curves are given in Table 5.1.

smaller than curve A. The reduced thickness rapidly increases with time and reaches 80% of the maximum thickness after a polymerization time of 2.3 h, then gradually approaches the maximum thickness after 7 h. Curves C and D in Fig. 5.3, with smaller reaction rate constants of 7.38×10^{-7} and 3.69×10^{-7} $m^4/(kmol.s)$, respectively. The reduced thickness gradually increases with polymerization time, and only 72% and 50% of the maximum thickness are obtained, respectively, after a polymerization of about 7 h. Curve D in Fig. 5.3 corresponds to curves C and D in Fig. 5.2 and curve C in Fig. 5.3 corresponds to curves E and F in Fig. 5.2.

Further decrease of the rate constant to 3.69×10^{-8} $m^4/(kmol.s)$ (corresponding to curves A and B in Fig. 5.2), results in a very small (less than 5%) conversion of monomer A after 7 h. The reduced thin-film thickness increases almost linearly with polymerization time as shown by curve E in Fig. 5.3, This curve is well described by Eq. 5.37 for the special case of reaction-controlled interfacial polymerization, as expected.

The above discussion indicates that the smaller the reaction rate constant is, the longer the polymerization time is needed to reach a certain reduced thickness of the thin film or conversion of monomer A.

The relationship between the thin film thickness and the reaction time with various reaction rate constants, given by Eq. 5.20, is illustrated in Fig. 5.4. The curves in Fig. 5.4 are similar to those in Fig. 5.3 and can be understood in the same manner, since the thickness, X, is proportional to the reduced thickness, X/X_{max}.

The relationships between the polymerization time, the reduced thickness and the growth rate of thin film are presented in Fig. 5.5. The reduced thickness, X/X_{max}, is given by Eq. 5.20, and the growth rate is given by Eq. 5.17. The two curves in Fig. 5.5 appears to be mirror images. As expected, the reduced thickness, X/X_{max}, rapidly increases with time within the first two hours of polymerization, then levels off with time. In contrast, the growth rate of the thin film changes in an opposite direction, rapidly decreasing with time, then levelling off with time.

The relationships between $C(0,t)$, $C(X,t)$, the reduced thickness and the reaction time are illustrated in Fig. 5.6. $C(0,t)$ and $C(X,t)$ are given by Eqs. 5.19 and 5.18, respectively. The difference between $C(0,t)$ and $C(X,t)$ is the driving force for diffusion of monomer **A**. At $t=0$, the thin-film thickness is zero, the reaction is a rate controlling step and the diffusion of monomer **A** has no effect on thin-film growth, thus $C(0,t) = C(X,t)$. As the thin film grows, $X>0$, the difference between $C(0,t)$ and $C(X,t)$ increases, and the diffusion of monomer **A** becomes an important factor controlling the growth rate. When most of monomer **A** is consumed, the difference of $C(0,t)$ and $C(X,t)$ becomes smaller again. The case presented in Fig. 5.6 is very complex in terms of a rate

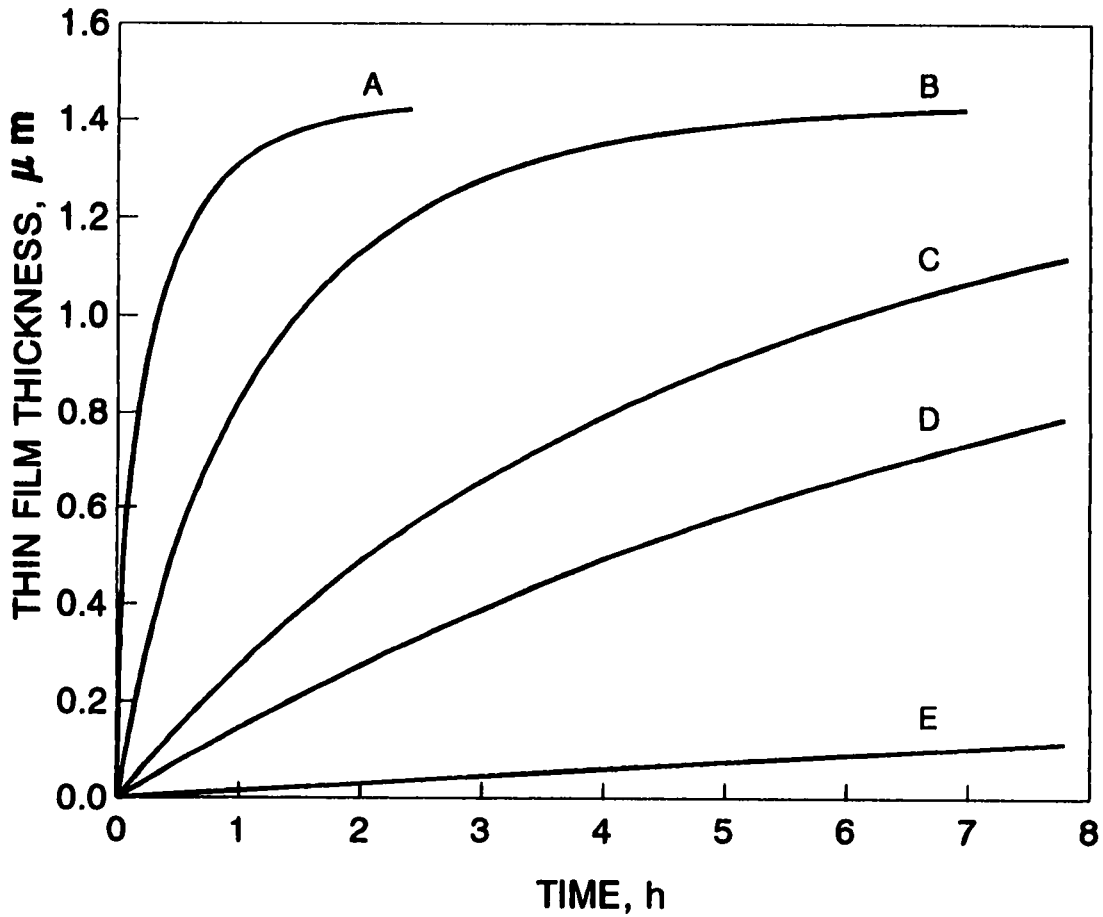

Fig. 5.4 Effect of reaction rate constant and polymerization time on thin film thickness.

A: $k=3.69\times10^{-3}$, B: $k=3.69\times10^{-6}$, C: $k=7.38\times10^{-7}$,
D: $k=3.69\times10^{-7}$, E: $k=3.69\times10^{-8}$ $m^4/(kmol.s)$.
The remaining parameters used to draw the curves are given in Table 5.1.

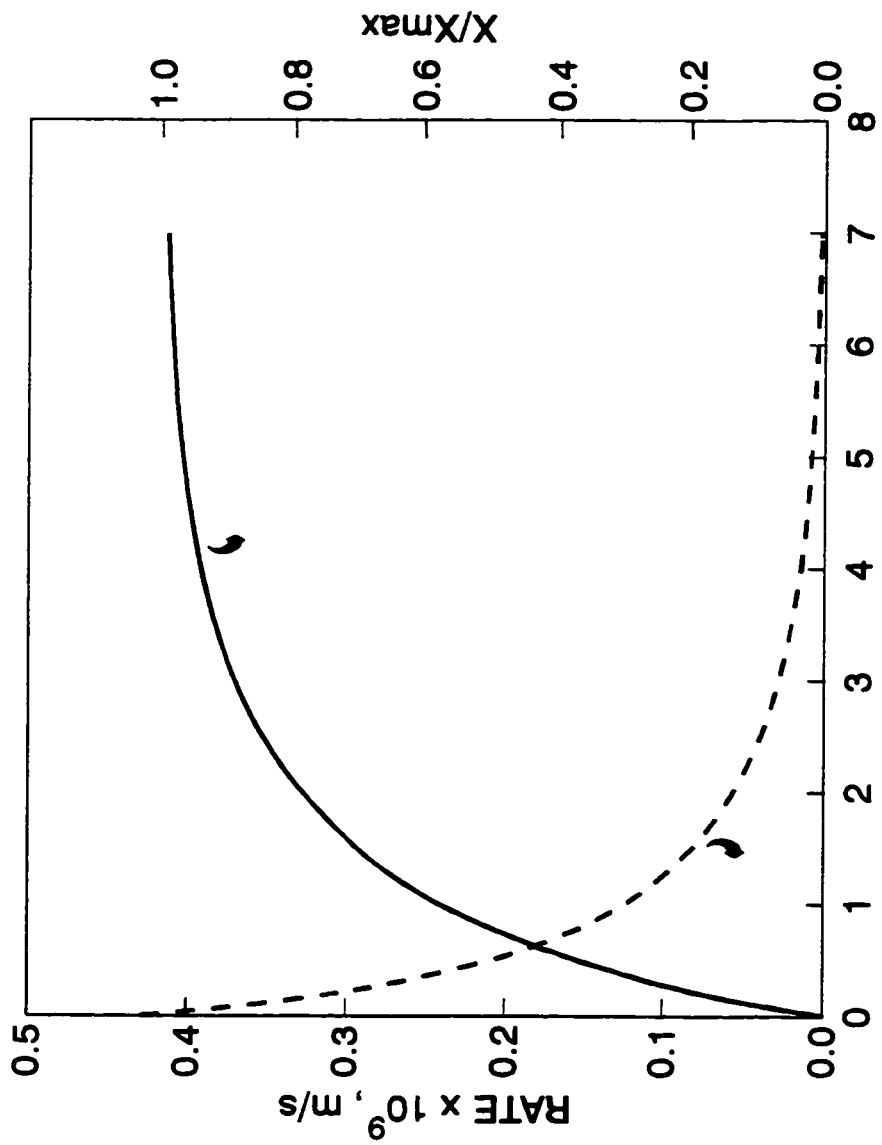

Fig. 5.5 Relationship between the growth rate, the reduced thickness of the thin film and polymerization time.

The parameters used to generate the curves are given in Table 5.1.

controlling step, starting with a reaction-controlled process, then changing to both reaction- and diffusion-controlled and eventually becoming reaction-controlled again.

In Fig. 5.6, the reduced thickness, X/X_{max}, increases rapidly with time in the early stage of polymerization, then levels off with time. In contrast, *C(0,t)* and *C(X,t)* change with time in an opposite direction. This explains the results observed in Fig. 5.5. The increase in the reduced thickness and the decrease in the growth rate of the thin film are due to the consumption of monomer **A**. Both the reduced thickness and the growth rate at low *C(0,t)* and *C(X,t)* change slowly with time. Therefore, a maximum thickness and zero growth rate are approached at long polymerization time.

These results indicate that it is not necessary to lengthen the polymerization time in an attempt to increase the thickness of the thin film layer under the above given conditions. For this particular case, 3 h is sufficient. This result is very important to membrane fabrication, because it provides a guideline for an effective control of the thin film thickness.

5.3.2 Effect of diffusion coefficient on interfacial polymerization

The diffusion coefficient of monomer **A**, *D*, defined in Eq. 5.7, can be used to characterize the effect of monomer diffusion on interfacial polymerization.

The effects of the diffusion coefficient and polymerization time on the concentration profiles of *C(0,t)* and *C(X,t)* are displayed in Fig. 5.7. From these profiles, three types of interfacial polymerization reactions can be distinguished.

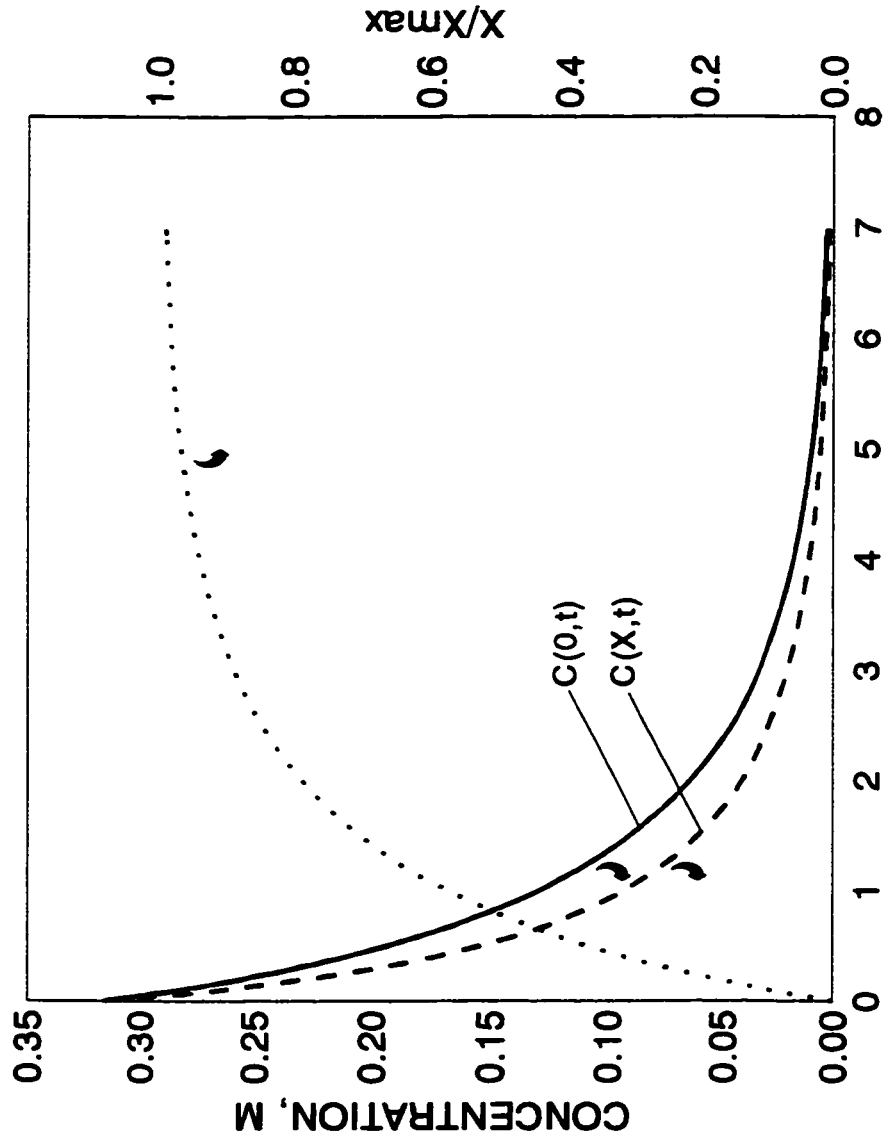

Fig. 5.6 Relationship between polymerization time, the concentrations of monomer A and the reduced thickness of the thin film.

The parameters used to generate the curves are given in Table 5.1.

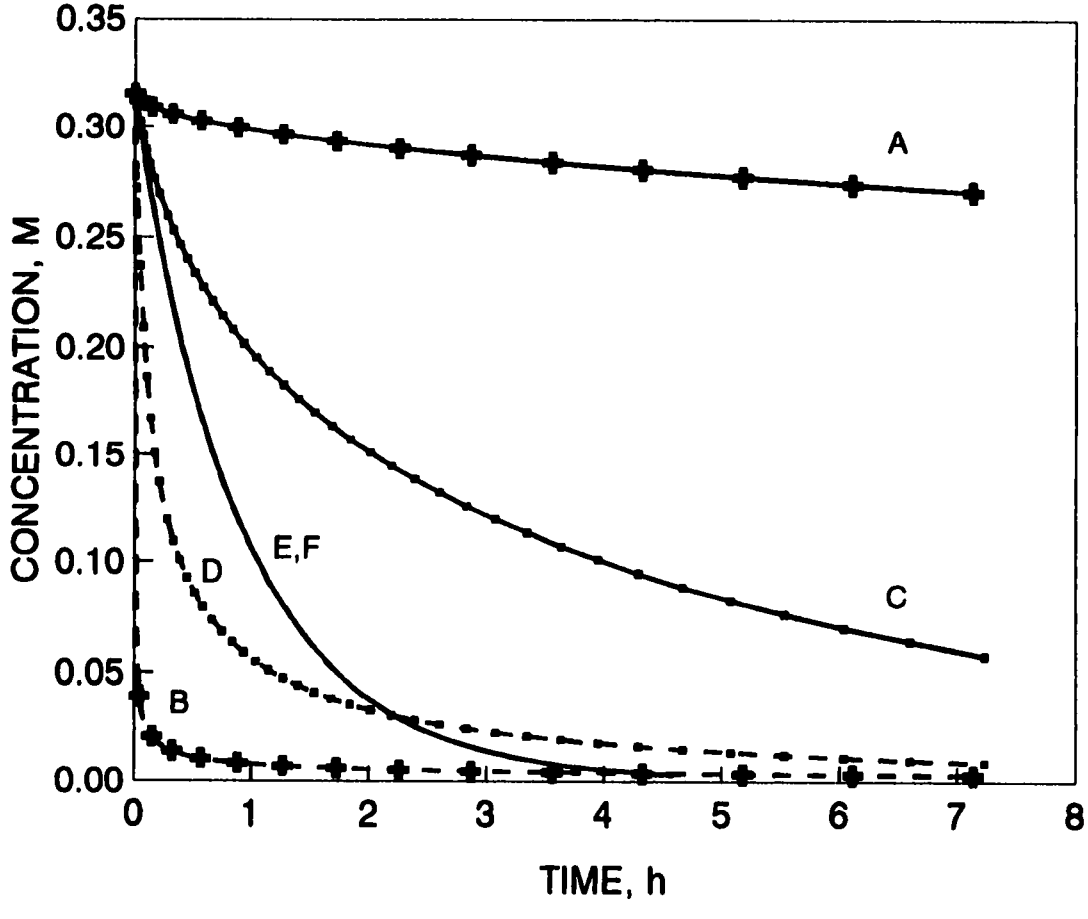

Fig. 5.7 Effect of diffusion coefficient and polymerization time on concentrations C(0,t) and C(X,t).
A, B: $D=5.27\times10^{-18}$, C, D: $D=5.27\times10^{-16}$, E, F: $D=5.27\times10^{-13}$ m^2/s.
A, C, and E: C(0,t), B, D and F: C(X,t).
The remaining parameters used are given in Table 5.1.

The first case, curves E and F, has a large diffusion coefficient of 5.27 x 10^{-13} m^2/s. These curves are actually superimposed on each other. The difference between *C(0,t)* and *C(X,t)*, the driving force for diffusion of monomer A, is zero. Thus, diffusion has no effect on the interfacial polymerization. This is a typical reaction-controlled interfacial polymerization.

The second case, curves A and B, has a small diffusion coefficient of 5.27 x 10^{-18} m^2/s. *C(0,t)* remains almost the same as the initial concentration, *C(0,0)*, after 7 h, but *C(X,t)* decreases almost to zero as soon as the polymerization starts. Analogous to curves I and J in Fig. 5.2 (fast reaction), this behaviour is due to a slow diffusion of monomer A from the support membrane phase to the reaction zone. This is a typical diffusion-controlled interfacial polymerization.

The third case, curves C and D, has an intermediate diffusion coefficient of 5.27 x 10^{-16} m^2/s. Both *C(0,t)* and *C(X,t)* rapidly decrease with time in the early stage of polymerization, then gradually level out, and remain significantly larger than zero. This is a typical reaction- and diffusion-controlled interfacial polymerization.

The effects of the diffusion coefficient and polymerization time on the reduced thickness, X/X_{max}, are shown in Fig. 5.8. Again, three types of reaction can be distinguished from these curves.

The first case, curves A and B, corresponds to large diffusion coefficients of 5.27 x 10^{-13} and 5.27 x 10^{-14} m^2/s, respectively. These two curves essentially overlap. These

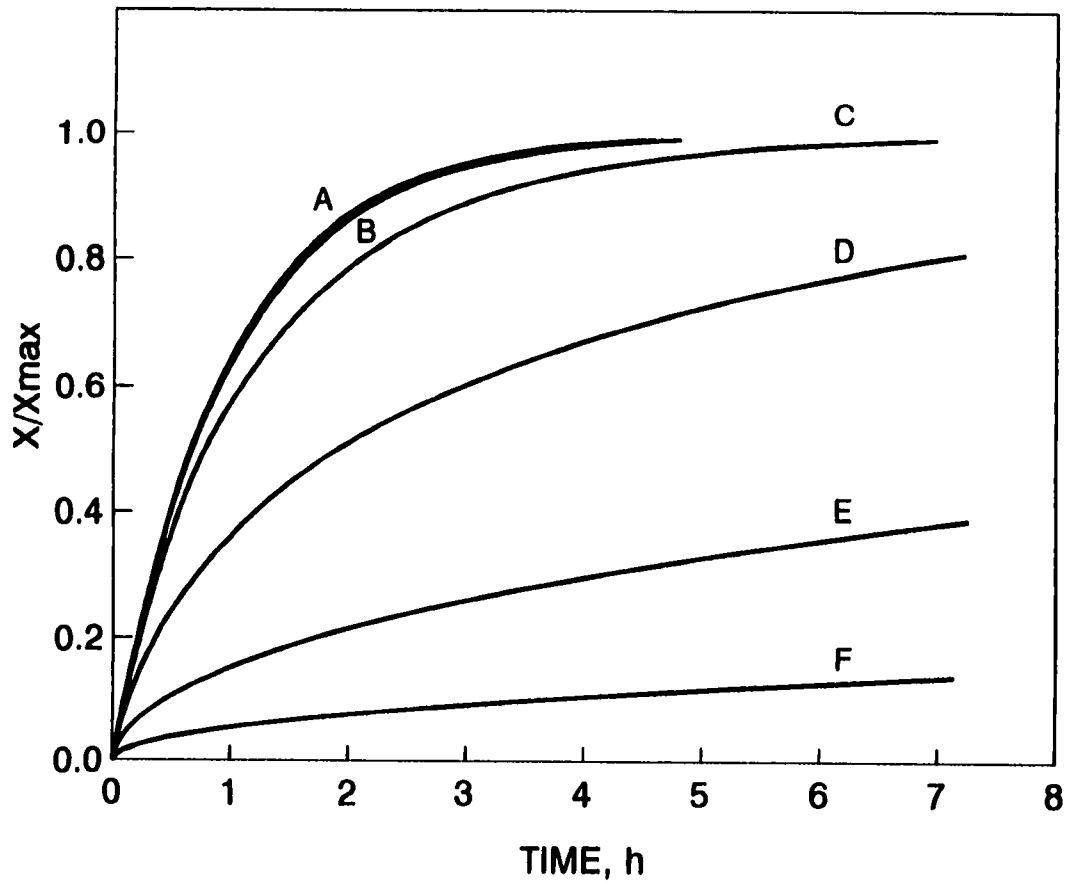

Fig. 5.8 Effect of diffusion coefficient and polymerization time on the reduced thickness of thin films.

A: $D=5.27\times10^{-13}$, B: $D=5.27\times10^{-14}$, C: $D=5.27\times10^{-15}$,
D: $D=5.27\times10^{-16}$, E: $D=5.27\times10^{-17}$, F: $D=5.27\times10^{-18}$ m^2/s.
The remaining parameters used to draw the curves are given in Table 5.1.

are typical reaction-controlled processes, where the diffusion of monomer A has almost no effect on interfacial polymerization.

The second case, curves C and D, corresponds to intermediate diffusion coefficients. The reduced thickness of the thin film rapidly increases with time up to two hours of polymerization, then levels off. This case is typical of both reaction- and diffusion-controlled interfacial polymerization. This result clearly indicates that for these systems, only a short polymerization time period contributes significantly to the formation of thin-film membranes.

The third case, curves E and F, corresponds to small diffusion coefficients. The reduced thickness of the thin film gradually increases with time but less than 40% of the maximum value is reached after a polymerization time of 7 h. This case is typical of a diffusion-controlled process.

The above results indicate that the smaller the diffusion coefficient is, the longer polymerization time is needed to reach a certain reduced thickness.

The relationships between the thin film thickness, reaction time and diffusion coefficient are given by Eq. 5.20 and are illustrated in Fig. 5.9. The curves in Fig. 5.9 look like those in Fig. 5.8 because the thickness, X, only differs from the reduced thin film thickness, X/X_{max}, by a constant, $1/X_{max}$. The thin-film thickness given in Fig. 5.8 is on a relative scale, but on an absolute scale in Fig. 5.9.

In order to confirm that curve F in Figs. 5.8 and 5.9 indeed represents a diffusion- controlled interfacial polymerization, curve F in Fig. 5.9 (produced by Eq.

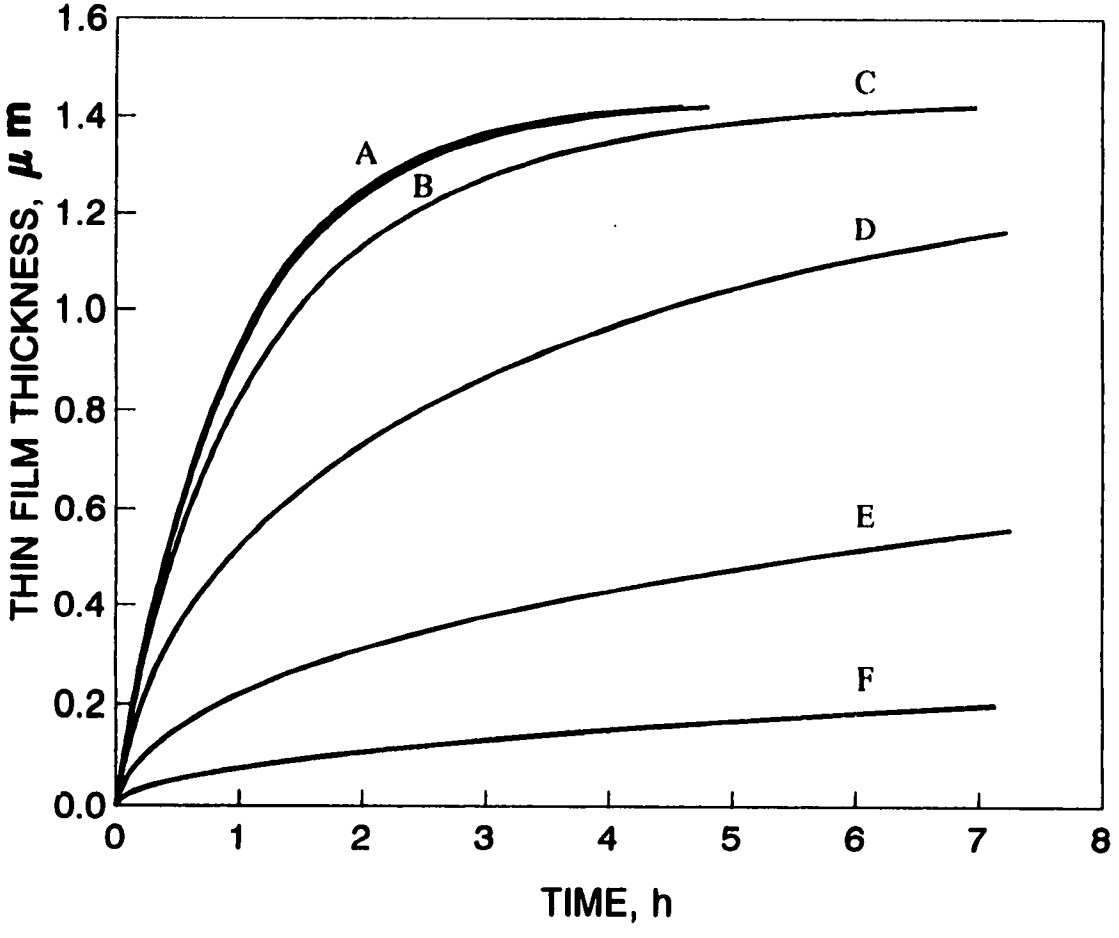

Fig. 5.9 Effect of diffusion coefficient and polymerization time on thin film thickness.

A: $D=5.27\times10^{-13}$, B: $D=5.27\times10^{-14}$, C: $D=5.27\times10^{-15}$,
D: $D=5.27\times10^{-16}$, E: $D=5.27\times10^{-17}$, F: $D=5.27\times10^{-18}\ m^2/s$.

The remaining parameters used to draw the curves are given in Table 5.1.

5.20) is replotted in Fig. 5.10 along with the square of the thin film thickness, X^2, versus t. X^2 linearly increases with polymerization time and has a correlation coefficient between X^2 and t of 0.999. This linear relationship is accurately described by Eq. 5.38. This result unambiguously demonstrates that the general model characterized by Eq. 5.20 can reduce to Eq. 5.38, under the diffusion- controlled condition specified in **Section 5.2.2.3.**

In comparing Fig. 5.8 with Fig. 5.3, and Fig. 5.9 with Fig. 5.4, the reaction rate constant and the diffusion coefficient have similar effects on the thickness and the reduced thickness of the thin film. This result can also be obtained by comparing Eq. 5.20 with Eqs. 5.28 and 5.32, respectively.

5.3.3 Effect of the concentration of monomer A on interfacial polymerization

Monomer concentration is another important parameter influencing interfacial polymerization and thin film formation.[130-136]

The relationships between thin-film thickness, initial concentration of monomer A, *C(0,0)*, and polymerization time are demonstrated in Fig. 5.11. The thin-film thickness increases with polymerization time and eventually approaches the maximum thickness. The higher the monomer concentration is, the faster the thin-film layer grows to give a thicker membrane. However, a higher concentration of monomer A results in

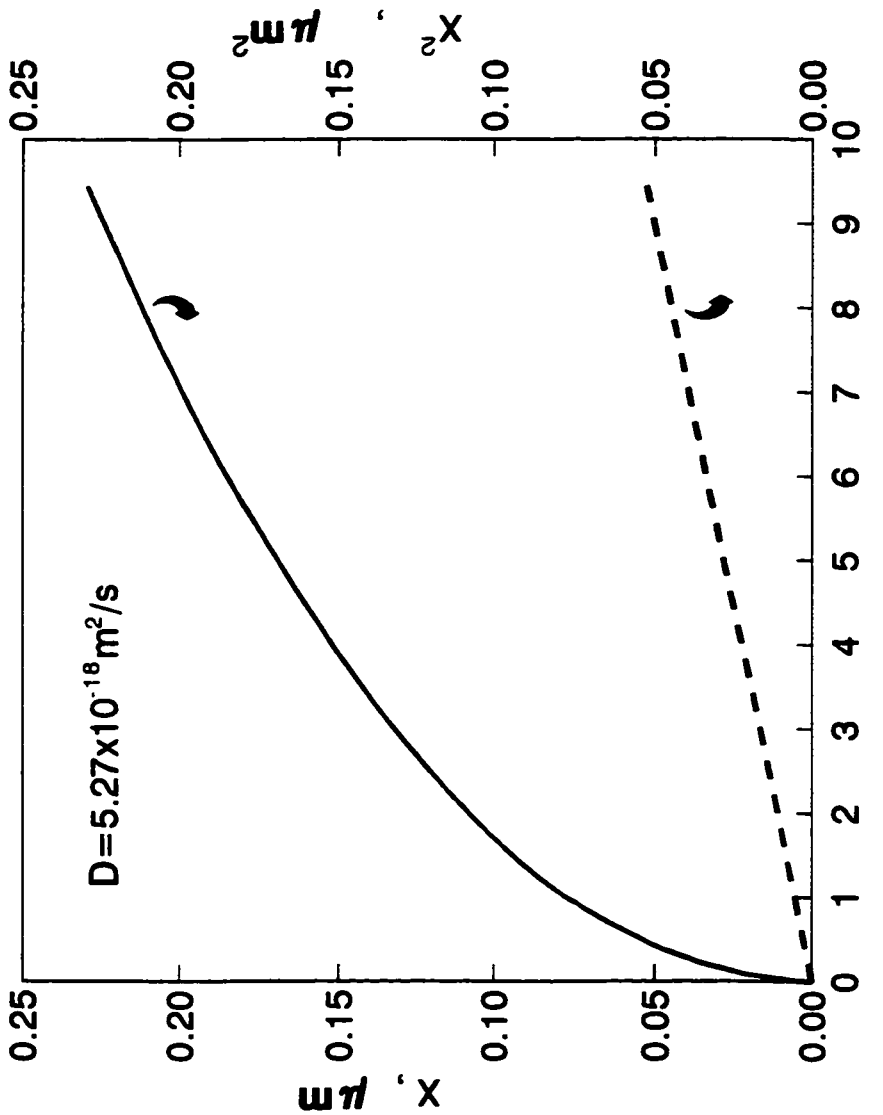

Fig. 5.10 The relationship between polymerization time and the thin film thickness X and X square.

The parameters used to generate the curves are given in Table 5.1.

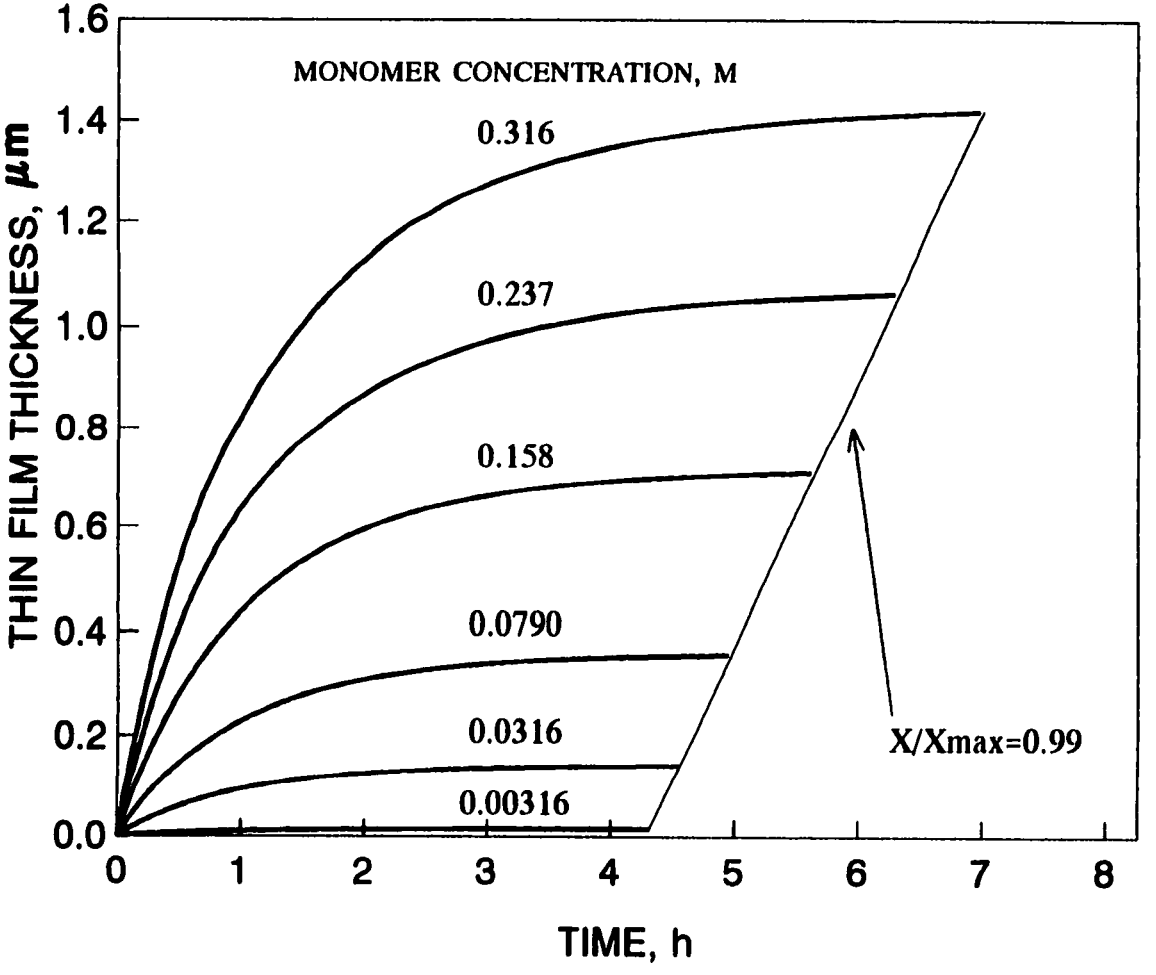

Fig. 5.11 Effect of the concentration of monomer A and polymerization time on thin film thickness.

The remaining parameters used to draw the curves are given in Table 5.1.

a longer polymerization time needed to reach the same reduced thickness, X/X_{max}, of 0.99 in Fig. 5.11. This dependence is also demonstrated by Fig. 5.12, particularly when $X/X_{max} > 0.8$.

The relationships between the reduced thickness of the thin film, the initial concentration, *C(0,0)*, and polymerization time are demonstrated in Fig. 5.12. For a given set of parameters (Table 5.1), and a low initial concentration, *C(0,0)*, the reduced thickness of the thin film approaches a maximum value of 1 more rapidly than at a higher initial concentration. Despite the two orders of magnitude difference in the initial concentration, *C(0,0)*, all of the curves in Fig. 5.12 are similar during the early stage of polymerization. This result is similar to the experimental work reported by Enkelmann and Wegner,[130,131] the reduced thicknesses of the thin films formed by liquid-liquid interfacial polymerization at varying diamine concentrations essentially fall on one curve.

The effect of the initial concentration, *C(0,0)*, on growth rate of the thin film is shown in Fig. 5.13. The growth rate of the thin film is given by Eq. 5.17. The higher the initial concentration of monomer **A** is, the larger the initial growth rate of the thin film is.

The growth rate decreases more rapidly at a higher initial concentration than at a lower initial concentration. All of these curves eventually approach zero with time, as expected. Consequently, the growth rate at a higher initial concentration of monomer **A** is always larger than that at a lower initial concentration.

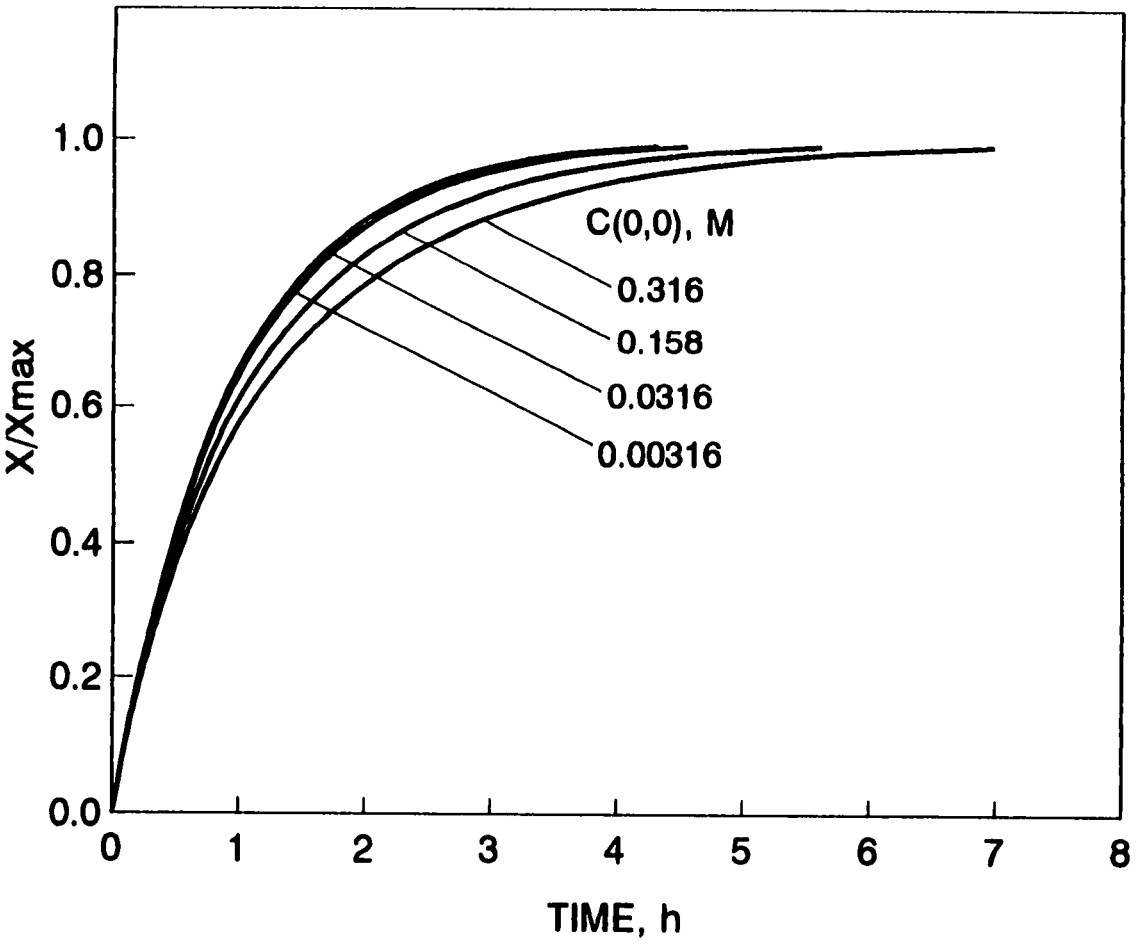

Fig. 5.12 Relationship between polymerization time, the initial concentration of monomer A and the reduced thickness of thin films.

The parameters used to generate the curves are given in Table 5.1.

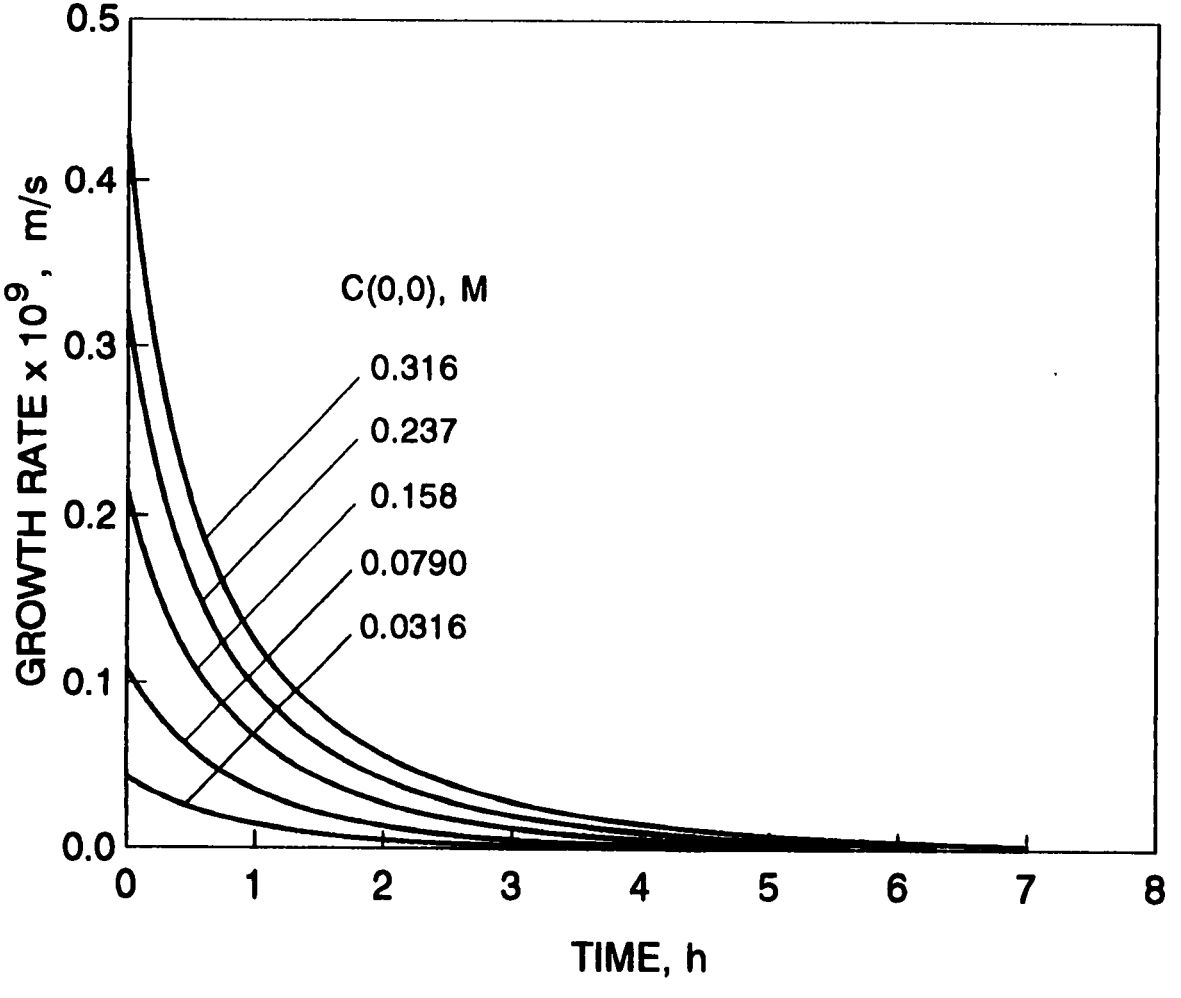

Fig. 5.13 Relationship between polymerization time, the initial concentration of monomer A and the growth rate of thin films.

The parameters used to generate the curves are given in Table 5.1.

These results indicate that the use of higher initial concentration of monomer **A** can significantly increase the growth rate of the thin film and shorten the polymerization time required for a certain film thickness, thereby increasing the efficiency of the membrane fabrication process.

5.3.4 Effect of the concentration of monomer B on interfacial polymerization

In this section, the effect of the concentration of monomer **B**, C_b, that reacts with monomer **A**, on interfacial polymerization is examined quantitatively. The concentration, C_b, is illustrated in Fig. 5.1, and stated mathematically in Eq. 5.1.

The effect of C_b on the growth rate of the thin film is shown in Fig. 5.14. In general, the curves in Fig. 5.14 look similar to those in Fig. 5.13. The higher the monomer concentration, C_b is, the larger the initial growth rate of the thin film is. The growth rate of the thin film decreases more rapidly with time at a higher concentration of monomer **B** than at a lower concentration, and eventually approaches to zero as polymerization time increases. In contrast to Fig. 5.13, the growth rate at a higher C_b is not always larger than that at a lower C_b, as shown in Fig. 5.14. This difference is due to rapid consumption of monomer **A**, that slows the growth rate of the thin film more rapidly at a higher C_b than at a lower C_b.

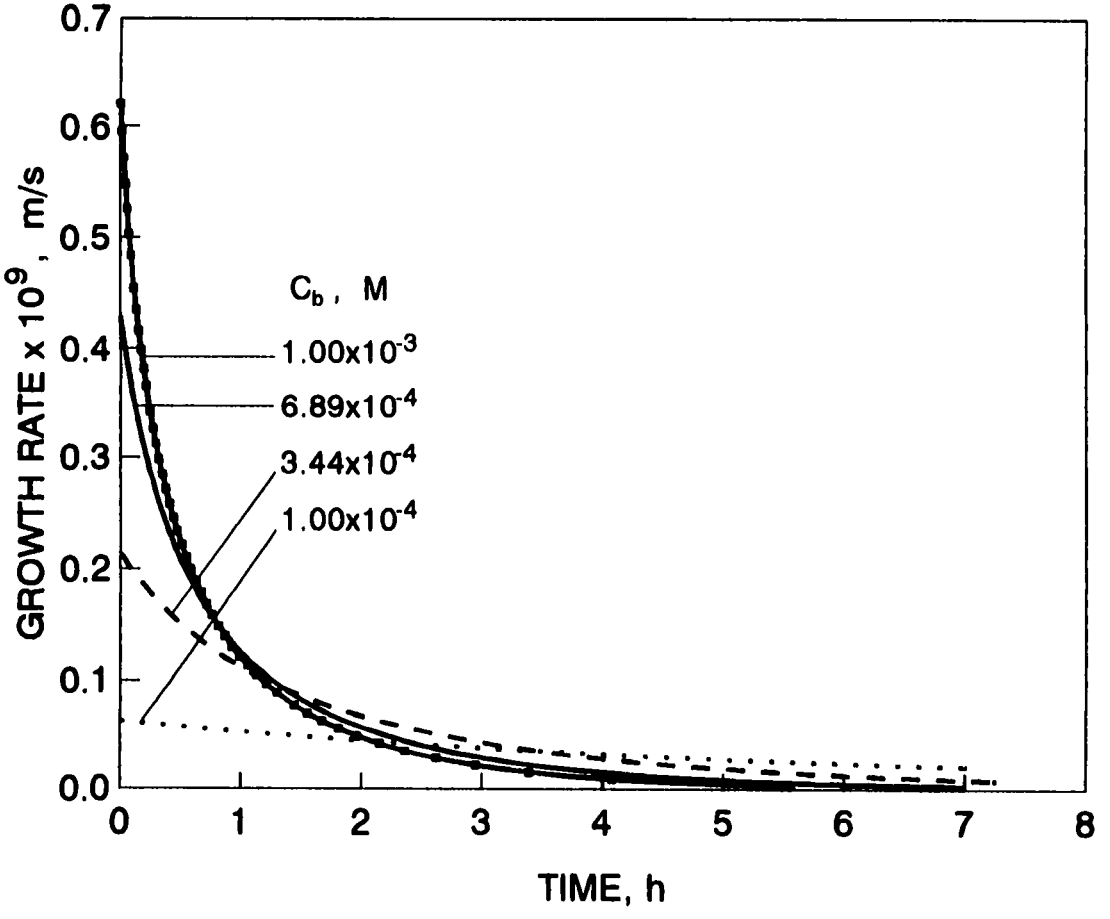

Fig. 5.14 Relationship between polymerization time, the concentration of monomer B and the growth rate of the thin films.

The remaining parameters used to draw the curves are given in Table 5.1.

The effect of C_b and polymerization time on thin-film thickness is displayed in Fig. 5.15. A wide concentration range from 6.89 x 10^{-1} to 6.89 x 10^{-5} M is examined. Curves in Fig. 5.15 can be classified into two groups, as described below.

The first group, represented by curves A to C, has a relatively high concentration of monomer **B**, C_b. The thickness of the thin film rapidly increases with polymerization time and reaches maximum thickness in less than 3 h. No significant increase in the thin film thickness is observed when increasing C_b by 200-fold, from 3.44×10^{-3} to 6.89×10^{-1} M, because these concentrations are large compared to the given concentration of monomer **A**.

The second group, represented by curves D to I, has a relatively lower concentration of monomer **B**. In this concentration range, between 6.89×10^{-5} and 1.0×10^{-3} M, the thickness of the thin film is very sensitive to C_b. A small change in C_b results in a significant change in the thin-film thickness, as shown in Fig. 5.15.

These results indicate that there is a practical upper limit to C_b for a given concentration of monomer **A**; beyond this limit any further increase in C_b does not significantly alter the thickness and growth rate of the thin film formed by interfacial polymerization. In contrast to Fig. 5.11, an increase in C_b does not result in an increase of the maximum thickness of the thin film. However, it significantly increases the growth rate of the thin film within a certain range of the C_b, between 6.89×10^{-5} and 3.44×10^{-3} kmol/m^3, as shown in Figs. 5.14 and 5.15, respectively.

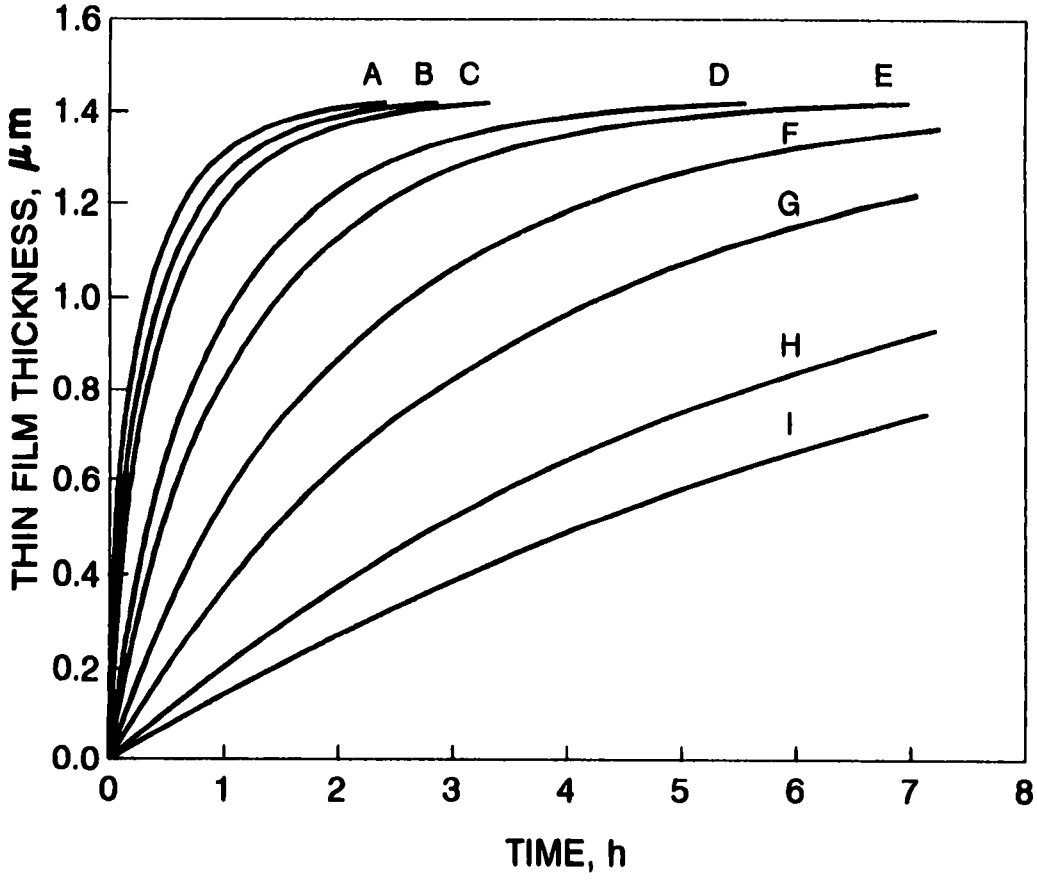

Fig. 5.15 Effect of the concentration of monomer B and polymerization time on thin film thickness.

A: 6.89×10^{-1}, B: 6.89×10^{-3}, C: 3.44×10^{-3},
D: 1.00×10^{-3}, E: 6.89×10^{-4}, F: 3.44×10^{-4},
G: 2.00×10^{-4}, H: 1.00×10^{-4}, I: 6.89×10^{-5} M.
The remaining parameters used to draw the curves are given in Table 5.1.

5.4 Summary

1. A general model for the formation of a thin film by both diffusion- and reaction-controlled interfacial polymerization under nonsteady-state boundary conditions has been developed. This model was then reduced to the following special models under given conditions:

   (1) Nonsteady-state boundary conditions,

   (a) reaction-controlled interfacial polymerization,

   (b) diffusion-controlled interfacial polymerization,

   (2) Constant monomer concentration in the support membrane phase,

   (a) both diffusion- and reaction-controlled interfacial polymerization,

   (b) reaction-controlled interfacial polymerization,

   (c) diffusion-controlled interfacial polymerization.

   Alternatively, these special models can be derived independently from the same set of assumptions. Both methods give identical analytical solutions.

2. The models developed are simple, have clear physical meaning, and predict results that would be expected for interfacial polymerization. The analytical solutions of

the models are easy to understand and use. This work has significantly extended the existing theories of thin film formation by interfacial polymerizations.

3. The effects of the reaction rate constant and the diffusion coefficient on thin film formation have been systematically studied. Both the reaction rate constant and the diffusion coefficient strongly affect the thin film formed by interfacial polymerization.

4. Three cases of interfacial polymerizations have been predicted by the model in terms of the rate controlling step: (1) diffusion-controlled, (2) reaction-controlled, and (3) both diffusion- and reaction-controlled.

5. Both monomer **A** and **B** concentrations have an important effect on the thin film formed. An increase in the concentration of monomer **A** not only increases the growth rate but also increases the maximum thickness of the thin film. However, increasing the concentration of monomer **B** (C_b) increases the growth rate of the thin film, but not the maximum thickness. The higher is the concentration of monomer **A**, the shorter is the polymerization time needed to obtain a certain thin film thickness. However, a higher concentration of monomer **A** requires longer reaction time to reach the same reduced thickness, X/X_{max}, of the thin film.

6. The thickness of the thin film formed by interfacial polymerization, controlled by both reaction rate and monomer diffusion, rapidly increases with time during the early stage of polymerization, then levels off with time as the polymerization proceeds. The growth rate of the thin-film layer decreases with polymerization

time. A relatively short polymerization time fixes the thin film thickness. Thus, lengthening the polymerization time in an attempt to increase the thin film thickness would be ineffective.

7. Although the models discussed above are developed for polymeric membrane-supported interfacial polymerization, they are mathematically suitable for any kind of interfacial polymerization, and for reactions of small molecules which satisfy the assumptions used to develop the models. The models developed provide an important guide for the effective control of the thin film thickness.

Chapter 6

Modelling the Formation of both Dense and Porous Thin Films

In order to correlate a relationship between the thickness of the newly formed thin-film layer and the kinetics of interfacial polymerization, a general model considering both monomer diffusion and reaction-controlled interfacial polymerization, under nonsteady-state conditions, was developed in the previous chapter. In general, the findings discussed in the previous chapter are important to effectively control membrane thickness.

The previous chapter dealt with a theoretical consideration of the formation of dense films, and no direct experimental evidence was given. This chapter extends the study to the formation of both dense and porous films, and the theoretical predictions are compared with experimental results.

6.1 Theory

A theoretical model for the formation of the surface barrier layer of a thin-film composite membrane by the interfacial polymerization is developed in this section.

6.1.1 Model Assumptions

The following simplifying assumptions are proposed to facilitate model development:

1. All of the assumptions in **Section 5.1.1** remain valid.
2. The thin film formed by the interfacial polymerization of monomers **A** and **B** consists of the fabricated polymer and voids.
3. Monomer **A**, with associated water molecules, diffuses from the support-membrane phase to the reaction zone. The diffusion coefficient of the monomer **A**, with associated water molecules, is assumed to be constant in the newly formed polymeric film.[138]

It was shown in Chapter 3 that there are microvoids in the newly formed polymer film. A similar microvoid structure was also observed for the capsules formed by interfacial polymerization of terephthaloyl dichloride and diethylenetriamine.[135,136] Janssen and te Nijenhuis[135] suggested that the formation of the microvoid structure in the capsule wall was due to the presence of water in the newly formed thin film. The water molecules and monomer **A** may diffuse at different rate in the newly formed film. However, Janssen and te Nijenhuis[138] assumed that diethylenetriamine and water diffuse together to simplify the model, and this assumption was supported by their experiment results. Therefore, this assumption was adopted and reflected by assumption 3 discussed above.

6.1.2 Model Development

In order to establish a model to describe the formation of both dense and porous thin films by interfacial polymerization, both interfacial reaction and monomer diffusion are considered. The formation of a thin film is due to interfacial reaction and monomer transport. The formation of microvoids in the newly formed film is treated as a result of water diffusion. If there is no water diffusion with monomer **A**, a dense film is formed.

The model development starts with the interfacial reaction to determine the thin-film growth rate due to the reaction, then deals with the diffusion of monomer **A** which also controls the thin-film growth rate. In order to solve these two rate equations, a mass balance is calculated to determine monomer **A** concentration at surface of the support membrane as a function of reaction time. The porosity of the thin film is obtained by calculating a ratio of water molecules to monomer **A** transported together.

A schematic representation of the model was given in Fig. 5.1, which is suitable for the formation of both dense and porous thin films. A list of all symbols used is given at the beginning of this thesis. Based on the above assumptions, the following equations have been formulated.

At time t, the growth rate of the thin film during the reaction is given by,

$$\frac{P\rho_p\phi_2}{M_P}\frac{dv_P}{dt}=k_r C(X,t) C_b \delta S \qquad 6.1$$

where ϕ_2 is the volume fraction of the polymer in the newly formed thin film. After rearrangement, the following equation is obtained,

$$\frac{dX}{dt} = \frac{k_f C(X,t) C_b}{\phi_2} \qquad 6.2$$

Based on assumption 9 in Chapter 5, the growth rate of the thin film must equal the rate of monomer transport. For monomer **A**, one has,

$$\frac{P\rho_p \phi_2}{M_P} \frac{dv_P}{dt} = -\frac{[C(X,t) - C(0,t)]S}{\frac{X\phi_1}{D_V} + \frac{X\phi_2}{D_P}} \qquad 6.3$$

where ϕ_1 is the volume fraction of the voids in the thin film formed by interfacial polymerization, D_P and D_V are the diffusion coefficient of monomer **A** in the polymer and in the voids, respectively.

Based on an assumption made by Janssen and te Nijenhuis,[138] assuming $D_V \gg D_P$ gives,

$$\frac{dX}{dt} = \frac{D_M[C(0,t) - C(X,t)]}{X\phi_2^2} \qquad 6.4$$

In contrast to Eq. 5.8, here,

$$D_M = D_P M_U / \rho_P \qquad 6.5$$

and D in Eq. 5.8 is equal to D_P in Eq. 6.5, i.e. $D = D_P$.

A material balance gives,

$$\frac{C(0,t)fLS}{K} + \int_0^x C(x,t)Sdx + \frac{2\phi_2 XS\rho_P P}{M_P} = \frac{C(0,0)fLS}{K} \qquad 6.6$$

Under nonsteady-state conditions, this equation is very important, it specifies the concentration of monomer A at the surface of support membrane as a function of time, i.e., $C(0,t)$. Eq. 6.6 represents the major difference of the current model from other models,[130,131,135,136,138] in which the reactant concentration at the surface of a thin film was assumed to be constant. For example, Janssen and te Nijenhuis[135,136,138] assumed that the diamine concentration at the surface of a capsule was constant during the reaction and obtained that the capsule wall thickness was proportional to a square root of reaction time. This result was supported by an experiment result for a short polymerization time. However, the model developed by Janssen and te Nijenhuis[135,136] predicts an unrealistic result under a limit condition, the capsule thickness approaches infinity when the reaction time approaches infinity.

As in the previous chapter, the following terms are defined to facilitate the solution of the above equations.

$$A_1 = \frac{2D_M k_f C_b C(0,0)fL}{\phi_2^3} \qquad 6.7$$

$$B_1 = \frac{4KD_M k_f C_b \rho_P}{M_U \phi_2^2} \qquad 6.8$$

$$C_1 = \frac{Kk_f C_b}{\phi_2} \qquad 6.9$$

$$D_1 = \frac{2k_f C_b fL}{\phi_2} + \frac{2KD_M}{\phi_2^2} \qquad 6.10$$

$$E_1 = \frac{2D_M fL}{\phi_2^2} \qquad 6.11$$

It is first necessary to determine the polymer volume fraction, ϕ_2, in the membrane. Janssen and co-workers[138] assumed that the flux of water through the capsule wall was proportional to the flux of an amine monomer. This assumption is adopted in this work and leads to,

$$J_{WATER} = \beta J_A \qquad 6.12$$

where J_{WATER} and J_A are the flux of water and monomer A across the newly formed thin film by diffusion, respectively. Therefore, the water transport rate is given by,

$$\frac{\rho_W \phi_1}{M_W} \frac{dv_P}{dt} = -\beta S \frac{C(X,t) - C(0,t)}{\frac{X\phi_1}{D_V} + \frac{X\phi_2}{D_P}} \qquad 6.13$$

where ß is the molar ratio of water to monomer A transported together by diffusion. Simplification of this equation gives,

$$\frac{dX}{dt}=\beta D_P M_W \frac{[C(0,t)-C(X,t)]}{X\phi_2\phi_1\rho_W} \qquad 6.14$$

Eq. 6.14 divided by Eq. 6.4 yields,

$$\phi_2=\frac{M_u\rho_W}{M_u\rho_W+\rho_P M_W\beta} \qquad 6.15$$

Assuming that the total volume of the newly formed thin film consists of polymer and voids, gives,

$$\phi_1=1-\phi_2=\frac{M_W\rho_P\beta}{M_u\rho_W+\rho_P M_W\beta} \qquad 6.16$$

Simultaneously solving Eqs. 6.2, 6.4 and 6.6 in the same way as in Chapter 5, gives a thin film growth rate as,

$$\frac{dX}{dt}=\frac{A_1-B_1X}{C_1X^2+D_1X+E_1} \qquad 6.17$$

Solving this equation yields the following relation between the required reaction time, t, and the thickness, X, of the thin film formed by the interfacial

polymerization,

$$t=-\left(\frac{E_1}{B_1}+\frac{A_1D_1}{B_1^2}+\frac{C_1A_1^2}{B_1^3}\right)Ln\left(1-\frac{X}{X_{max}}\right)-\frac{C_1}{2B_1}X^2-\left(\frac{D_1}{B_1}+\frac{C_1A_1}{B_1^2}\right)X \qquad 6.18$$

The concentrations of monomer **A** at $(0,t)$ and (X,t) are given by,

$$C(0,t)=\frac{1}{\frac{fL}{K}+\frac{X}{2}}\left[\frac{C(0,0)fL}{K}-\frac{2\phi_2 X\rho_P}{M_U}-\frac{C(X,t)}{2}X\right] \qquad 6.19$$

$$C(X,t)=\frac{\phi_2}{k_f C_b}\frac{A_1-B_1X}{C_1X^2+D_1X+E_1} \qquad 6.20$$

When t approaches infinity, monomer **A** is completely consumed by the reactions, hence $C(0,\infty)$ and $C(X,\infty)$ become zero, and X approaches X_{max}. As a result, f is obtained from Eq. 6.6 as,

$$f=\frac{2\phi_2 X_{max}\rho_P K}{M_U C(0,0)L} \qquad 6.21$$

In a similar manner, the maximum thickness of the thin film is obtained from Eq. 6.6 as,

$$X_{max}=\frac{fM_U C(0,0)L}{2\rho_P K\phi_2} \qquad 6.22$$

Alternatively, Eq. 6.7 divided by Eq. 6.8 yields,

$$X_{\max} = \frac{A_1}{B_1} \qquad 6.23$$

X_{max} can also be obtained experimentally. Eq. 6.23 correlates the maximum membrane thickness, X_{max}, with A_1 and B_1.

Mathematically, Eqs. 6.17-6.23 are quite similar to those obtained in Chapter 5. However, the results obtained in this chapter have significantly extended the model from only describing the formation of a dense membrane, to predicting the formation of both dense and porous membranes by interfacial polymerization.

6.2 Results and Discussion

The results obtained are discussed in the following sections.

6.2.1 Qualitative assessment of the model

The validity of the model can be qualitatively assessed in terms of the limiting conditions predicted by the model. Thus, the same conclusions as those drawn in the previous chapter follow. For example, the maximum growth rate, r_{max}, of the thin film is obtained at t=0 from Eq. 6.17 as,

$$r_{\max} = \frac{dX}{dt}\Big|_{t=0} = \frac{A_1}{E_1} = \frac{1}{\phi_2} k_f C(0,0) C_b \qquad 6.24$$

However, Eq. 6.24 differs from Eq. 5.24 by a factor of $1/\phi_2$ due to the formation of voids in the thin film.

The above general model is reduced to the following special models:

(1) under nonsteady-state conditions,

  (a) reaction-controlled interfacial polymerization,

  (b) diffusion-controlled interfacial polymerization,

(2) under the condition of constant concentration of monomer **A** in the support membrane,

  (a) reaction-controlled interfacial polymerization,

  (b) diffusion-controlled interfacial polymerization,

  (c) both diffusion and reaction-controlled interfacial polymerization.

The model development for these special cases is similar to those discussed in the previous chapter and is not discussed here.

6.2.2 Comparison of theoretical prediction with experimental results

In order to compare the theoretical prediction with experimental results, the general model discussed above should be correlated to real data.

In this thesis, the interfacial polymerization of **47** with **74**, shown in Scheme 3.1 is studied, where monomer **A** is 1,2-ethanediamine, **74**, monomer **B** is disulfonyl

chloride, **47**, and the small molecule **Z**, formed in each condensation reaction, is HCl. The general model can be correlated to the interfacial polymerization of **47** with **74** as shown in Scheme 3.1.

In order to avoid any ambiguity, it is important to emphasize the following points before fitting the model to the experimental data.

(1) The constant D_p defined in Eq. 6.3 is the diffusion coefficient of 1,2-ethanediamine in the newly formed thin film.

(2) The constant k defined in Eq. 5.4 is the apparent reaction rate constant, which is a combination of two constants: the real second order reaction rate constant k_r and the reaction zone thickness δ.

(3) The maximum film thickness, X_{max} given by Eq. 6.22 is constant and independent of reaction time.

These three parameters, D, k and X_{max} are very important and are estimated by fitting the model to experimental data.

It should be pointed out clearly that real second order reaction rate constant, k_r, can not be directly estimated from the current work. However, it can be indirectly estimated based on the apparent reaction rate constant k, defined in Eq. 5.4, and the reaction zone thickness δ.

In the following section, it is first to discuss the estimation of model parameters from the literature, then to fit the model to the experimental data. Finally,

the real second order reaction rate constant, k_r, is indirectly estimated from the apparent reaction rate constant k, and the reaction zone thickness δ. The estimated k_r and the diffusion coefficient of 1,2-ethanediamine, D, in the newly formed thin film is compared with the reported data in the literature to see whether they are in the same order of magnitude.

6.2.2.1 Estimation of model parameters from the literature

Morgan and co-workers[99-102] reported a systematic study on interfacial polymerization of diamines with diacid chlorides. They found that interfacial polymerization occurred in the organic phase close to the organic-aqueous interface. The swelling of a polymer depends on the solvents used. Poor solvents, such as xylene and carbon tetrachloride, caused the complete precipitation of a polyamide (Nylon 6-10) at all molecular weights.[101] In this work, a mixture of 20% (vol.) chloroform and 80% (vol.) carbon tetrachloride, a poor solvent for polysulfonamide, **75**, was used as the organic solvent for the interfacial polymerization. The use of such a poor solvent allows the assumption that the newly formed polymer does not dissolve in either the organic or aqueous phase. For a comparison of the theoretical prediction with experimental results, the general model discussed above is assumed to be applicable to the formation of the thin film by the interfacial polymerization of **47** with **74**, as shown in Scheme 3.1.

The diffusion coefficient of **74**, in the newly formed thin film, and the reaction rate constant of the interfacial polymerization of **47** with **74**, are needed in order to make a comparison of the model with experimental results. These diffusion coefficient and reaction rate constant can be estimated from data in the literature.

Diffusion coefficient

The diffusion coefficient of a solute in a polymer can range from 10^{-9} to 10^{-20} m^2/s, depending on the structures of both solute and polymer.[139] Zaikov et al.[139] found that an increase in either hydrophillicity or swelling of the polymers resulted in a great increase in the diffusion coefficient. The diffusion coefficient is usually small, if there is a strong interaction between a solute and a polymer.[139] For example, the diffusion coefficient of water in wool at 35 °C is 1.0×10^{-14} m^2/s,[140] while sulfuric acid in polypropylene is 7×10^{-17} m^2/s.[141] The diffusion coefficient of a disperse dye in polyethylene terephthalate at 70 °C can be as small as 9×10^{-20} m^2/s.[142] Sokolov and Nikonov[143] have reported that the diffusion coefficients of tetramethylenediamine in highly swollen polyamides are $1.8\text{-}3.6 \times 10^{-12}$ m^2/s. Enkelmann and Wegner reported that the diffusion coefficient of 1,2-hexanediamine in polyamide is 3.0×10^{-14} m^2/s.[144]

In next section, the estimated diffusion coefficient of 1,2-ethanediamine in the newly formed thin film by fitting the model to experimental data is compared with the reported diffusion coefficient discussed above.

Reaction rate constant

Reaction kinetics of sulfonyl halides with amines in homogeneous solutions have been well studied.[74-87] The reaction of benzene sulfonyl halides with amines in nonpolar solvents, and mixtures of polar and nonpolar solvents is complicated. Both second and third order reactions are present due to the catalytic effect of the amine reactants, any added tertiary amines, and the autocatalytic effect of the products.[145-155] However, in polar solvents, the reaction of sulfonyl halides with amines follows a second order reaction rate law.[75,76,87]

Kuritsyn and Kuritsyna[156] studied the kinetics of the reaction of aniline with 1,4-bezenedisulfonyl chloride in four different solvents: ethyl acetate, nitrobenzene, benzonitrile and acetonitrile. They found that the reaction was stepwise. The second order reaction rate constant of the first sulfonyl chloride group of 1,4-bezenedisulfonyl chloride with aniline (k_1) was twice as large as that of the second sulfonyl chloride group with aniline (k_2). The solvent used showed a strong effect on the reaction rate constant, e.g., in ethyl acetate at 25 °C, $k_1 = 6.87 \times 10^{-4}$ $m^3.kmol^{-1}s^{-1}$ and $k_2 = 3.42 \times 10^{-4}$ $m^3.kmol^{-1}s^{-1}$, respectively, and in acetonitrile at 25 °C, $k_1 = 1010 \times 10^{-4}$ 10^{-2} $m^3.kmol^{-1}s^{-1}$ and $k_2 = 338 \times 10^{-4}$ 10^{-2} $m^3.kmol^{-1}s^{-1}$, respectively.

Similarly, Mita et al.[87] studied intramolecular catalysis and cyclization in the reaction of diamines with 1,5-naphthalene disulfonyl chloride. The model which describes the reaction of 1,5-naphthalene disulfonyl chloride with primary amines having 6-18 carbon atoms, showed that the formation of 1,5-naphthalene

disulfonamides is stepwise. The reaction rate constant (k_1=4.4 x 10^{-1} $m^3.kmol^{-1}s^{-1}$) of the first sulfonyl chloride group of 1,5-naphthalene disulfonyl chloride with the alkyl amines is one order of magnitude larger than that (k_2=4.8 x 10^{-2} $m^3.kmol^{-1}s^{-1}$) of the second sulfonyl chloride group in chloroform at 40 °C.[87] The overall rate of polymerization is presumably controlled by the slow step. These reaction rate constants for diamines with 1,5-naphthalene disulfonyl chloride are comparable with those for the reaction of aniline with 1,4-bezenedisulfonyl chloride in a polar solvent discussed in the previous paragraph.

Okamoto et al.[107] studied the reaction kinetics of 1,5-naphthalene disulfonyl chloride with a primary amino-ended polyoxyethylene, and of primary amino-ended polyoxyethylene with chlorosulfonyl-ended polyoxyethylene in chloroform at 40 °C. They found that the second order reaction rates were independent of the degree of polymerization over the range of about 20 to 20000. These results suggest that Flory's basic concept[157] of the equal reactivity of a functional group in polymer chains holds for the polysulfonamide formed from primary amino-ended polyoxyethylene and chlorosulfonyl-ended polyoxyethylene, with the degree of polymerization up to 20000.[107]

Ciuffarin et al.[75] reported that the second order reaction rate constant of benzensulfonyl chloride with aniline was 4.25 x 10^{-2} $m^3.kmol^{-1}s^{-1}$ in acetonitrile-water (9:1) at 25 °C and 43.0 $m^3.kmol^{-1}s^{-1}$ for benzensulfonyl chloride with 1-butylamine in acetonitrile-water (1:1) at 25 °C.

The above results indicate that the second order reaction rate constants of aromatic sulfonyl chlorides with amines strongly depend on the solvent and vary in a large range between 3 x 10^{-4} and 43 $m^3.kmol^{-1}s^{-1}$.

In this work, a polysulfone support membrane impregnated with aqueous 1,2-ethanediamine solution was immersed into a solution of **47** in 20% (vol.) chloroform and 80% (vol.) carbon tetrachloride. The preceding discussion on the reaction kinetics of sulfonamide formation and the reaction condition employed in the current work allows to assume that the interfacial polymerization of **47** with **74** shown in Scheme 3.1 has a second order kinetics. Further, the reactivities of the sulfonyl chloride and amino groups in the forming polymer are independent of polymer chain length.[107,157,158]

In next section, the estimated reaction rate constant by fitting the model to experimental data is compared with the reported rate constant discussed above.

Reaction zone thickness

In order to estimate the apparent reaction rate constant defined in Eq. 5.4, the thickness of reaction zone, δ, is needed. MacRitchie[106,126] reported that the interfacial polymerization of sebacoyl chloride with hexanediamine occurred in a mixed monolayer of adsorbed monomers. MacRitchie's work allows to assume that the reaction zone thickness is constant and is estimated to be about 10 nm.

The degree of polymerization

The concept of the average degree of polymerization is important, this concept was also used by Mikos and Kiparissides[133] to describe a thin film formation by an interfacial radical polymerization. Fortunately, the exact value of the average degree of the polymerization is not needed when calculating the growth rate of the thin film on the basis of the repeating unit of the polymer.

6.2.2.2 Fitting the model to experimental data

In order to compare the model with experimental results, Eq. 6.18 was fitted to the experimental data presented in Figs. 3.4 and 6.1, and Table 6.2 using the UWHAUS program.[159]

The two parameters, the apparent reaction rate constant, k, defined in Eq. 5.4, and the maximum thin film thickness, X_{max}, given by Eq. 6.22, are estimated by comparison of the model with the experimental data. The other parameters used are listed in Table 6.1.

The initial concentration of 1,2-ethanediamine, $C(0,0)$, was measured by titration with 0.1 N hydrochloric acid aqueous solution.

The membrane thickness was measured by scanning electron microscopy, and the experimental details were described in Chapter 3. The original data of the thin film thickness are contained in Appendix A. The error bars, in Fig. 6.1, are plus and minus one standard deviation of the average thickness.

Table 6.1 Parameters used to fit the model to the experimental data

$C(0,0)=0.316$	kmol/m^3
$C_b=6.89 \times 10^{-4}$	kmol/m^3
$D=1.64 \times 10^{-15}$	m^2/s
$K=1.0$	dimensionless
$L=2.05 \times 10^{-4}$	m
$M_A=M_{74}=60.1$	kg/kmol
$M_B=M_{47}=705.6$	kg/kmol
$M_2=M_{HCl}=36.45$	kg/kmol
$\rho_P=1300$	kg/m^3
$\phi_2=0.65$	dimensionless

Table 6.2 The thin-film thickness as a function of polymerization time*

Polymerization time, h	0.25	0.5	1.0	2.0	3.0	5.0	10.0	15.0
Average thickness, μm	0.11	0.37	0.70	1.37	2.07	2.16	2.20	2.21
Standard deviation, μm	0.04	0.13	0.18	0.19	0.37	0.87	0.46	0.49

*$C(0,0)=0.316$ kmol/m^3

Based on the method reported by Janssen and te Nijenhuis,[135,136,138] the porosity, ϕ_1, was obtained by measuring the ratio of porous area to total area of the cross section of the thin film using a Sigma Scan System.[110] The experimental details were described in Chapter 3 of this thesis, with the original data given in Appendix C. The volume fraction, ϕ_2, of the polymer in the membrane was obtained from the following relation: $\phi_2 = 1-\phi_1$ (Eq. 6.16).

The results of data fitting are shown in Table 6.3 and Fig. 6.1.

Table 6.3 The results of data fitting with 95% confidence

Apparent reaction rate constant k	(2.48 ± 1.41) x 10^{-6} $m^4/(kmol.s)$
Maximum thin film thickness X_{max}	(2.40 ± 0.40) x 10^{-6} m
Correlation coefficient between k and X_{max}	-0.46
Number of degrees of freedom	7

In Fig. 6.1, the curve at the higher diamine concentration is produced by fitting Eq. 6.18 to the experimental data, and the curve at the lower diamine concentration is predicted by the model using Eq. 6.18 and the parameters obtained from the above data fitting. The results in Fig. 6.1 show that the model not only fits the experimental data well but also predicts a reasonable result at a different diamine concentration ($C(0,0)$= 0.174 $kmol/m^3$).

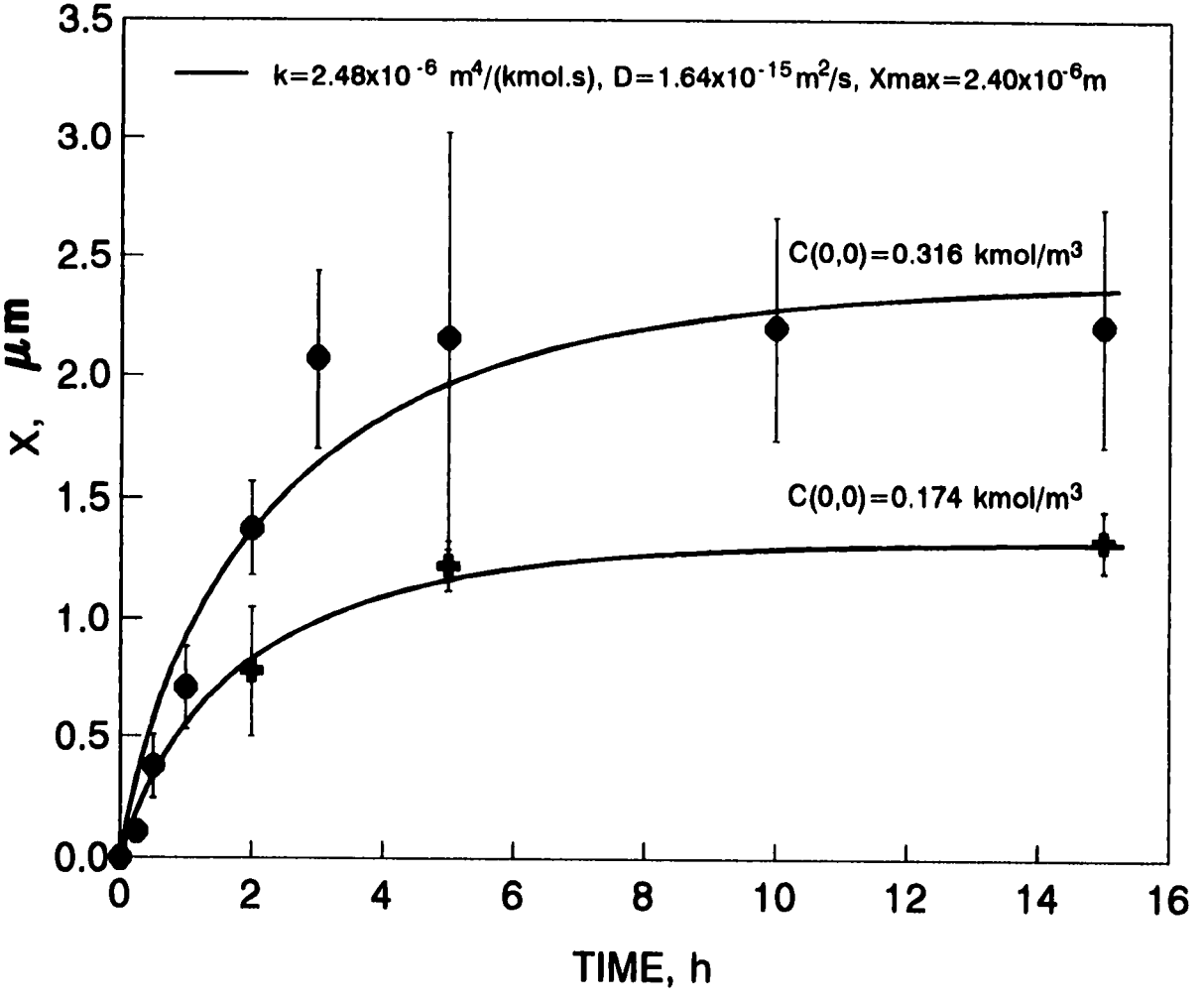

Fig. 6.1 Comparison of the theoretical model with experimental results. The curves are produced using Eq. 6.18 and parameters in Tables 6.1 and 6.3.

Initially, a diffusion coefficient of 1.64 x 10^{-15} m^2/s was selected to fit the data, which gave a convergent result, as shown in Fig. 6.1. A detail examination by systematically varying D from 1.64 x 10^{-15} to 1.64 x 10^{-9} m^2/s while keeping the other parameters fixed shows no significant change in curve shape as compared to the curve ($C(0,0)$= 0.316 kmol/m^3) in Fig. 6.1. This result suggests that curve fitting was not sensitive to the diffusion coefficient, D, because any value larger than 4.16 x 10^{-16} m^2/s gives a convergent data fitting. If the diffusion coefficient is smaller than 4.16 x 10^{-16} m^2/s, no convergent data fitting was obtained.

Based on the above results, it is possible to determine whether the above estimated parameters, k and D, are within the order of magnitude reported in the literature.

The diffusion coefficient of a solute in liquids has an order of magnitude of 1.0 x 10^{-9} m^2/s.[140,141] As discussed in **Section 6.2.2.1**, the diffusion coefficient of a solute in polymer can be in a range between 1.0 x 10^{-10} m^2/s and 1.0 x 10^{-20} m^2/s, depending on the physicochemical nature of solute and polymer. The diffusion coefficient of 1,2-ethanediamine in the newly formed thin film obtained from the above data fitting is indeed within the range reported in the literature.

Estimation of the real second order reaction rate constant, k_r, is very difficult, because it is buried in the apparent reaction rate constant, k (Eq. 5.4), and the exact reaction zone thickness, δ is not known. If assuming δ=10 nm, Eq. 5.4 gives k_r = 248 $m^3.kmol^{-1}s^{-1}$, which is about a half order of magnitude larger than the reaction rate

constant (43.0 $m^3.kmol^{-1}s^{-1}$) reported for the second order reaction of benzensulfonyl chloride with 1-butylamine in acetonitrile-water (1:1) at 25 °C,[75] and two and half orders of magnitude larger than the reaction rate constant (k_i =4.4 x 10^{-1} $m^3.kmol^{-1}s^{-1}$) reported for the reaction of 1,5-naphthalene disulfonyl chloride with the alkyl amines in chloroform at 40 °C.[87]

As discussed above, the second order reaction rate constant is very sensitive to the solvent used. The higher is the polarity of the solvent, the larger is the reaction rate constant. In this work, the interfacial polymerization of **47** with **74** shown in Scheme 3.1 took place at the interface between an aqueous diamine solution and an organic solution of chloroform and carbon tetrachloride containing **74**. In this reaction system, the reaction rate constant is expected to be large based on the above discussion. In addition, this high value (k_r = 248 $m^3.kmol^{-1}s^{-1}$) could be partially due to the unknown reaction zone thickness and other assumptions made in the model, because the maximum thickness of the thin film, X_{max}, obtained from data fitting has a relatively small error compared to the apparent reaction rate constant, k. This means that k includes most of the errors arisen from the factors discussed above. However, this value (k_r = 248 $m^3.kmol^{-1}s^{-1}$) is consistent with the fact that high molecular weight polysulfonamides have been readily synthesized by interfacial polymerization of aliphatic diamines with aromatic disulfonyl chlorides.[99, 100, 103, 160]

The above results and discussion suggest that the orders of magnitude of the estimated diffusion coefficient, D, and the reaction rate constant, k_r, are resonable.

6.2.3 Effect of water diffusion on the thickness of the thin film

The major difference between the current model and the model discussed in the previous chapter is that the current model considers water diffusion, which enables the model to describe the formation of a porous coating layer by interfacial polymerization.

A relation between the polymer volume fraction, ϕ_2, in the thin film formed by interfacial polymerization and the molar ratio (defined in Eq. 6.13) of water to the diamine monomer transported, has been established by the current model and is given by Eqs. 6.15 and 6.16, respectively. The relationship between the polymer volume fraction, ϕ_2, and the molar ratio, ß, is depicted in Table 6.4.

Table 6.4 The relationship between the polymer volume fraction, ϕ_2, in the membrane and the molar ratio, ß, of water to 1,2-ethanediamine monomer transported together

ß	ϕ_2
0	1.0
4	0.88
8	0.79
16	0.65
32	0.48
64	0.32

As can be seen in Table 6.4, the polymer volume fraction, ϕ_2, in the membrane decreases with an increase in ß. If no water molecules are transported with the diamine monomer, the polymer fraction in the membrane is equal to 1, and a dense membrane is formed. This case was discussed in the previous chapter. If any water is present, the interfacial polymerization of a diamine with a disulfonyl chloride produces a porous polysulfonamide thin film.

A typical effect of the polymer volume fraction on the thickness of the thin film is displayed in Fig. 6.2. At a given polymerization time, the thin-film thickness increases with deceasing the volume fraction of the polymer in the thin film. These computations indicate that the volume fraction of polymer in the membrane should be an important parameter in determining the porosity and thickness of the surface layer of thin-film composite membranes.

6.2.4 Kinetic behaviour of thin-film formation by interfacial polymerization

After establishing the model and a set of parameters, it is possible to study systematically the effects of different factors on the kinetics of the interfacial polymerization and on the formation of the thin film. In particular those parameters which are difficult to measure experimentally are of interest. The diamine diffusion coefficient and the apparent reaction rate constant obtained from the two parameter

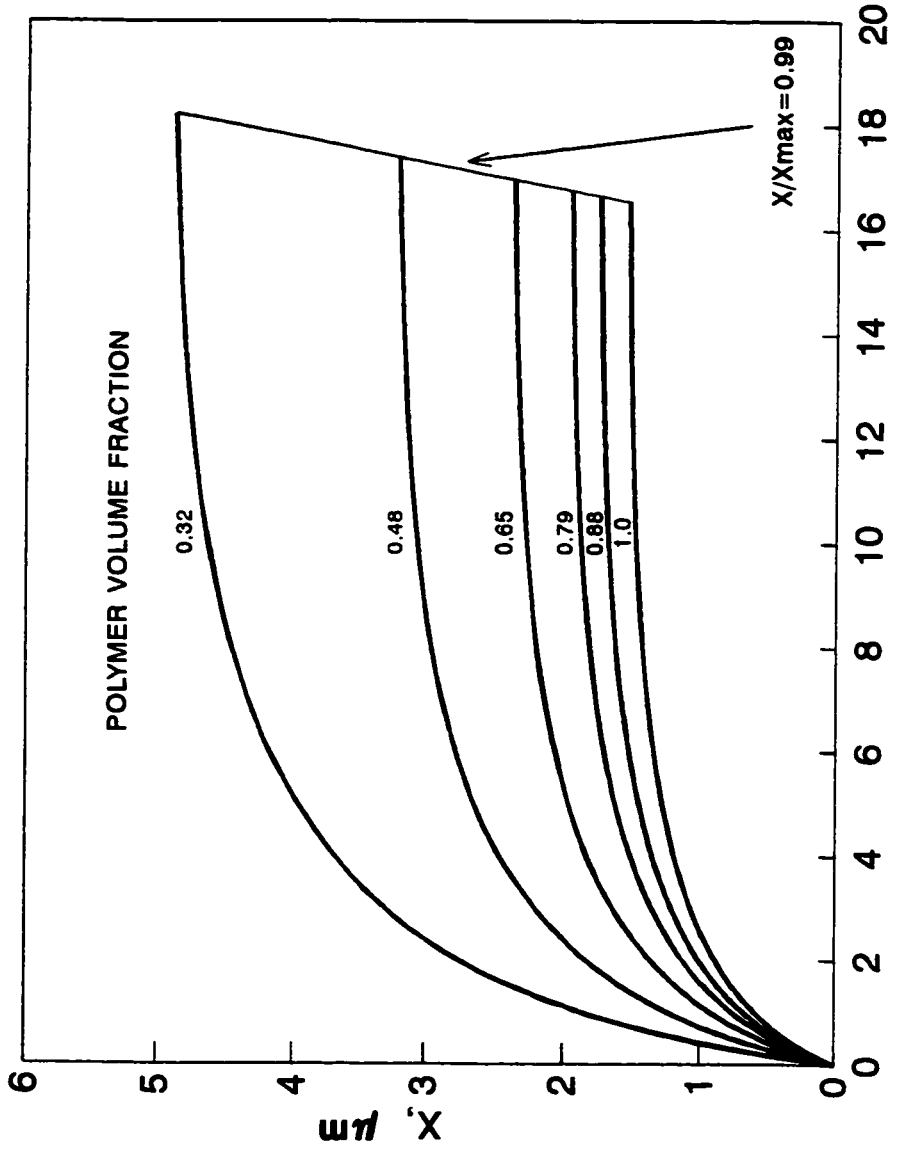

Fig. 6.2 The effect of the polymer volume fraction in the thin film on the thin-film thickness. The cures are produced using Eq. 6.18 and the parameters in Tables 6.1 and 6.3.

fitting of Eq. 6.18 to the experimental data using the UWHAUS program,[159] are used in the following sections.

The reduced thickness, X/X_{max}, is also a conversion on the basis of 1,2-ethanediamine monomer. The effect of polymerization time on thin-film growth rate and on the reduced thickness is illustrated in Fig. 6.3. The thin-film growth rate and the reduced thickness are calculated by Eqs. 6.17 and 6.18 using the parameters listed in Tables 6.1 and 6.3. The growth rate decreases rapidly with polymerization time for up to about 2 h, then levels off. The reduced thickness changes with time in the opposite direction, as expected. About 60% of the 1,2-ethanediamine monomer is consumed within the first two hours of polymerization under the given condition. The rest of the monomer is gradually consumed as the polymerization proceeds. These results indicate that under the given condition, a significant portion of the membrane formation occurs within the early time period of polymerization. It is thus inefficient to lengthen the polymerization time in an attempt to increase the thickness of the thin film.

Theoretical relationships between the diamine monomer concentration, the thin-film thickness, and polymerization time are depicted in Fig. 6.4. The monomer concentrations and the thin-film thickness are calculated using Eqs. 6.19, 6.20 and 6.18, and the parameters in Tables 6.1 and 6.3. According to the model, the concentrations of 1,2-ethanediamine in the support membrane, $C(0,t)$, and in the reaction zone, $C(X,t)$, (see Fig. 5.1) rapidly decrease during the polymerization for up

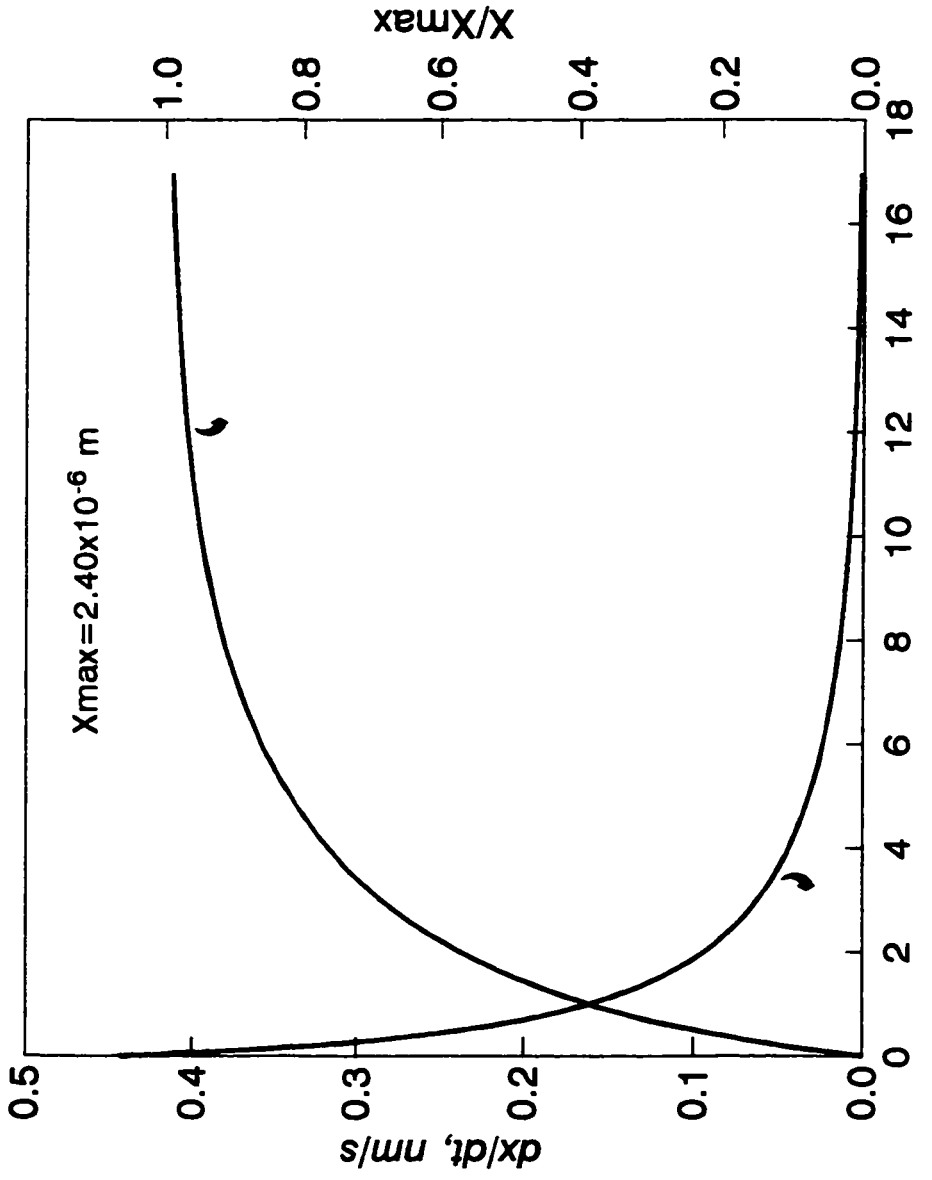

Fig. 6.3 The relationship between the polymerization time, the reduced thin-film thickness and the thin-film growth rate. The curves are produced using Eqs. 6.17 and 6.18 and the parameters in Tables 6.1 and 6.3.

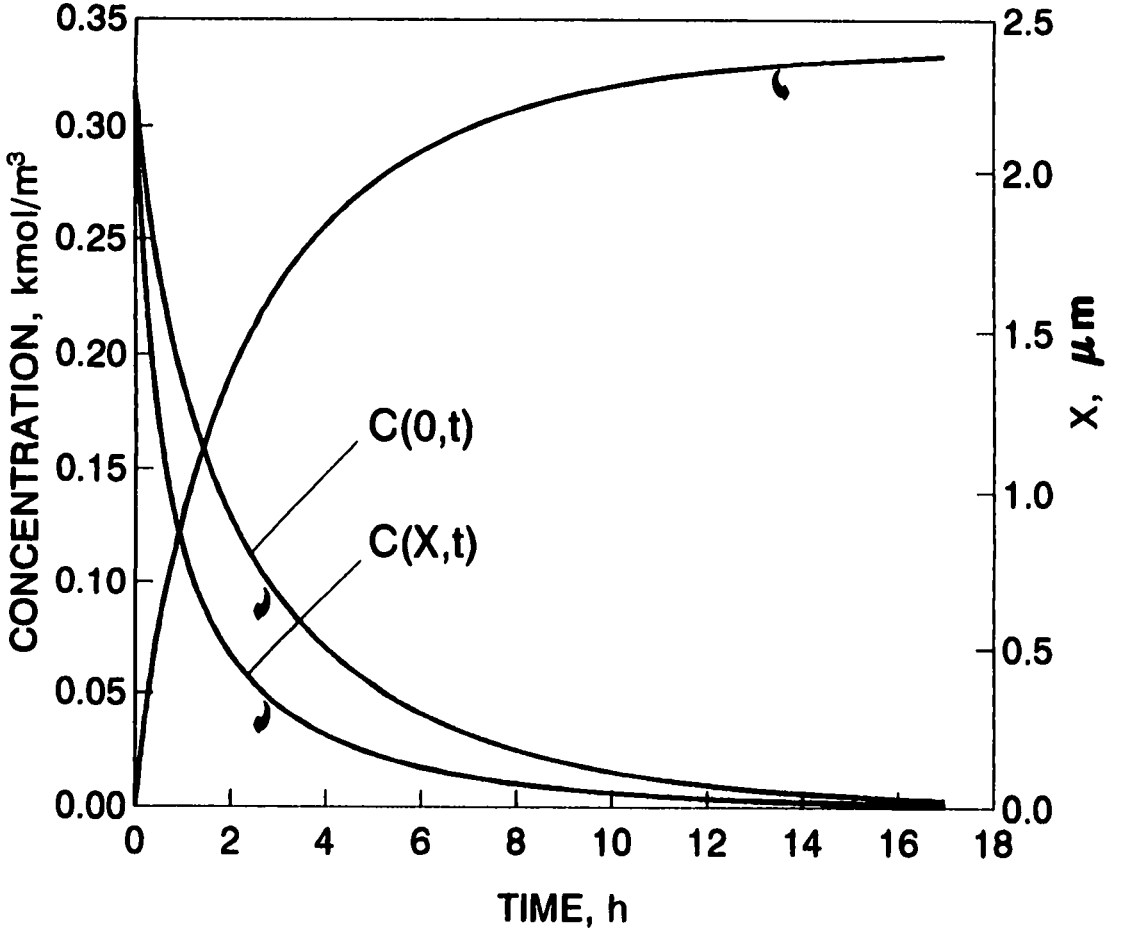

Fig. 6.4 The effect of polymerization time on thin-film thickness and the diamine concentration, at the surface of support membrane and in the reaction zone.

The curves are produced using Eqs. 6.18, 6.19 and 6.20 and parameters in Tables 6.1 and 6.3.

to 2 h, and then finally approach zero. This prediction is in accordance with the results shown in Fig. 6.3. The thin-film growth rate and the change in thickness are inversely proportional to each other due to the rapid consumption of the diamine monomer in the reaction system.

6.3 Summary

The following conclusions can be drawn from the above results and discussion.

1. A theoretical model describing both diffusion- and reaction-controlled interfacial polymerization under nonsteady-state conditions has been developed. The model describes the formation of both dense and porous thin films and is consistent with the experimental results.
2. The volume fraction of the polymer in the thin film decreases with an increase in the molar ratio of water to 1,2-ethanediamine transported together. The membrane thickness increases with a decrease in the polymer volume fraction in the membrane.
3. The growth rate of the thin film and the diamine monomer concentrations at the surface of the support membrane and in the reaction zone rapidly decrease with polymerization time. In contrast, the thin-film thickness rapidly increases with polymerization time in the early stage of polymerization, then levels off

with time. It is inefficient to lengthen the polymerization time in order to increase membrane thickness.

4. A higher initial diamine concentration gives a larger growth rate and thicker film than the lower initial diamine concentration at a given polymerization time. Increasing the diamine monomer concentration is a more effective method to increase thin-film thickness than increasing polymerization time.

5. The study has significantly extended understanding of the kinetics of interfacial polymerization and provides an important guide for effective control of the thickness of the surface barrier layer of a thin-film composite membrane prepared by interfacial polymerization.

Chapter 7

Conclusions and Future Work

A photoreactive monomer has been synthesized in high yield from commercially available starting materials in a two step reaction sequence. The problems associated with the low yields of monomer encountered in the previous synthesis developed in the McMaster membrane group have been successfully resolved by this work.

The photolysis of the model compound under mild conditions confirms that a variety of functional groups can be incorporated into the model compound. In each case, functionality is incorporated through an ester linkage in high yield. These model reactions provide a good foundation for the photochemical surface modification of thin-film composite diazoketone membranes.

Thin-film composite membranes having the photoreactive diazoketone groups as side chains to the backbone of the resulting polysulfonamide have been successfully fabricated by interfacial polymerization of disulfonyl chloride, **47**, with 1,2-ethanediamine, **74**. The compositions of the aqueous and organic phases employed during interfacial polymerization are important in determining membrane structure and performance. The addition of water-miscible solvents into either the organic or aqueous phases has been demonstrated to be effective in improving membrane performance.

The physical structures of the surface layer of the thin-film composite membranes have been shown to be dependent on the polymerization time, surfactant and co-solvent used. Shorter polymerization times produced thinner, smoother coating layers compared with longer polymerization times. Membrane thickness increased rapidly with polymerization times up to 3 hours. After this the thickness reached a limiting value. While the permeate fluxes of the membranes decreased with the length of the polymerization, the separations of the membranes were almost independent of polymerization time.

The method of photochemical surface modification of a diazoketone precursor membrane studied in this thesis proved effective in altering the chemical properties of the barrier layer and separation/flux performances of the thin-film composite membranes. However, it was also found that this photochemical method developed for altering surface functionality of a thin-film composite membrane can, with certain reagents, lead to an alteration in the physical structure of the thin film.

A method for preparation of specimens for surface characterization of a thin-film composite membrane by infrared spectroscopy has been developed. In addition, a model thin film was prepared by liquid-liquid interfacial polymerization of **47** with **74**. Characterization of this model thin film provides useful information for characterization of the surface layer of a thin-film composite membrane.

A general model for the formation of both dense and porous thin films by interfacial polymerization has been developed. Both diffusion and reaction-controlled

interfacial polymerization under nonsteady-state conditions is considered in this model. Either reaction controlled or diffusion-controlled interfacial polymerization has been successfully treated as special cases of the general model. The results predicted by the model are consistent with the experimental results. The general model developed in this thesis for thin film formation by interfacial polymerization is consistent with special models reported in the literature. The current model significantly extends existing theories.

The work conducted in this thesis extends the understanding of the formation of thin films by interfacial polymerization and provides an important guide for effective control of the thickness of the surface barrier layer of thin-film composite membranes prepared by interfacial polymerization. Both experimental results and modelling suggest that the slow polymerization reaction and water diffusion are responsible for the formation of porous surface layer of the polysulfonamide thin-film composite membranes.

Despite the positive results obtained by the approach of the photochemical surface modification, the current system has some drawbacks. Solubility of the photoreactive monomer **47** in common organic solvents is relatively low. The rate of reaction of **47** with 1,2-ethanediamine, **74**, is also low. As a result, open textured structures are formed in the surface barrier layer. This textured structure likely leads to the observed poor reproducibility in flux of the membranes.

Sulfonic acid groups formed from the hydrolysis of the sulfonyl chloride of the polymer end groups appeared to overwhelm the effect of photochemical surface

modification on membrane separation performance.

Water used in the polymerization step was found to be difficult to remove completely from the system and it appeared to interfere with the subsequent photoreactions.

In future work, the solubility of the photoreactive monomer should be improved by incorporation of the diazoketone moiety to smaller molecules with appropriate polarity.[72] The reactivity of the photoreactive monomer in polymerization reaction needs to be improved. This could be achieved, for example, by replacing 1,3,6-naphthalene trisulfonyl chloride with 1,3,5-benzene tricarbonyl chloride or by using 1,3,6-naphthalene trisulfonyl bromide in the synthesis of **47**, Scheme 2.1. The reaction of an aromatic disulfonyl bromide with a diamine is shown to be more rapid than that of the corresponding chloride.[75,76,146] The use of more reactive diamines should be considered.

The problems associated with slow polymerization could also be overcome by polymerization of preformed oligomers, although solubility considerations would be critical in this approach. Anionic end groups of the resulting polymers, that overwhelm the photochemical surface modification, should be avoided by end capping or other methods.[71] If the diazoketone is used as a photoreactive group in the surface layer, the use of water should be eliminated from the interfacial polymerization step to minimize the interference of water with the subsequent photoreactions. For example, this problem associated with the presence of water in the reaction system could be resolved using a "dry interfacial polymerization method" developed in the McMaster membrane group.[161]

Appendix A
Thickness of the thin film prepared by interfacial polymerization of 47 with 74

Membrane	I-DK-T-01	I-DK-T-02	I-DK-T-03	I-DK-T-04	I-DK-T-05	I-DK-T-06	I-DK-T-07	I-DK-T-08
Polymerization time, h	0.25	0.50	1.0	2.0	3.0	5.0	10	15
Thin film thickness x 10^6, m	0.07	0.49	0.68	1.46	1.80	1.95	2.49	1.76
	0.09	0.54	0.63	1.37	1.80	1.85	2.54	1.80
	0.09	0.49	0.73	1.32	1.76	1.90	2.63	1.90
	0.07	0.44	0.71	1.27	1.76	1.88	2.73	1.92
	0.09	0.59	0.68	1.37	1.85	1.88	2.82	1.90
	0.09	0.68	0.68	1.32	1.61	1.90	2.92	1.90
	0.09	0.68	0.73	1.34	1.90	1.88	2.73	1.89
	0.07	0.54	0.59	1.17	1.85	1.85	2.59	1.90
	0.07	0.49	0.76	1.17	1.56	2.95	2.39	2.00
	0.05	0.39	0.68	1.22	1.46	3.20	2.44	2.00
	0.09	0.39	0.63	1.17	1.61	3.17	2.34	1.85
	0.12	0.29	0.66	1.17	1.76	3.37	2.20	1.80
	0.07	0.29	0.63	1.17	1.80	3.32	2.15	1.85
	0.07	0.24	0.59	1.20	1.85	3.27	2.15	2.00
	0.07	0.24	0.63	1.22	1.66	3.41	1.90	2.05

0.10	0.24	0.54	1.22	1.70	3.44	1.76	2.07
0.12	0.34	0.73	1.27	1.95	3.17	1.71	2.09
0.07	0.37	0.78	1.27	2.24	3.12	1.46	2.17
0.12	0.20	0.68	1.44	2.15	3.17	1.41	1.71
0.12	0.29	0.44	1.46	2.44	3.12	1.46	1.76
0.12	0.19	0.78	1.36	2.44	3.17	1.71	1.80
0.12	0.24	0.78	1.32	2.54	3.42	1.91	1.46
0.12	0.32	0.68	1.34	2.68	3.51		1.41
0.12	0.24	0.63	1.39	2.68	3.17		1.56
0.07	0.24	0.58	1.37	2.73	3.37		1.56
0.05	0.29	0.49	1.56	2.05	3.41		1.61
0.10	0.46	0.59	1.71	2.29	3.41		1.71
0.15	0.31	0.73	1.76	2.39	3.37		1.76
0.24	0.32	0.76	1.80	2.49	3.42		1.71
0.19	0.20	0.73	1.80	2.51	1.02		1.27
0.22	0.20	0.39	1.71	2.54	1.02		1.71
	0.37	0.37	1.85	2.34	0.98		2.00
	0.46	0.68	1.46	2.15	0.88		2.02
	0.49	0.63	1.46	2.05	0.88		2.20
	0.39	0.63	1.51		0.92		2.19

	0.39	0.83	1.41		1.61		2.10
	0.49	1.09	1.27		1.80		1.56
	0.29	1.12	1.32		1.56		1.41
	0.41	1.22	1.17		1.51		2.93
		1.05	1.07		0.93		2.83
		0.93	1.17		0.93		2.73
			1.22		0.98		2.54
			1.41		1.02		2.68
			1.37		1.22		2.68
					1.27		2.68
					1.07		2.58
					1.17		2.54
					1.61		2.54
					0.93		2.24
					1.02		2.34
					1.22		2.39
					1.43		2.44
					0.93		2.68
					2.59		2.68
					2.44		2.68

					2.83		2.68
					2.93		2.92
					2.78		2.39
					2.87		210
					2.68		1.95
					2.44		2.15
					2.05		2.49
					2.63		2.49
					2.68		2.78
					2.29		2.98
					2.44		2.93
					2.44		2.93
					2.20		2.93
					2.44		3.12
					1.95		3.22
					1.76		3.22
					1.95		
					1.90		
					1.76		
					1.66		

Average thickness x 10^6, m	0.11	0.37	0.70	1.37	2.07	2.16	2.20	2.21
Standard deviation x 10^6, m	0.04	0.13	0.18	0.19	0.37	0.87	0.46	0.49

The conditions used to prepare the membranes listed in Appendix A are given in Table 3.1.

Appendix B
Thickness of the thin films prepared by interfacial polymerization of **47** with **74**

Polymerization time, h	2.0	5.0	15.0
Thin film thickness x 10^6, m	0.49	1.22	1.22
	0.34	1.07	1.32
	0.58	1.32	1.32
	0.68	1.12	1.22
	0.73	1.27	1.32
	0.68	1.07	1.22
	0.78	1.27	1.46
	1.02	1.37	1.37
	0.97	1.27	1.32
	0.63	1.37	1.46
	0.68	1.32	1.42
	0.78	1.17	1.32
	0.48	1.02	1.12
	0.48	1.32	1.22
	0.48	1.22	1.22
	0.53	1.12	1.37
	0.53	1.22	1.71
	0.51		1.41
	1.22		1.37
	1.37		
	1.17		
	1.07		
	0.78		

	0.73		
	0.63		
	1.37		
	1.37		
	1.27		
	1.07		
	0.88		
	0.78		
	1.02		
	0.63		
	0.61		
	0.63		
	0.58		
	0.39		
	0.68		
	0.54		
	0.59		
	0.87		
Average thickness x 10^6, m	0.77	1.22	1.33
Standard deviation x 10^6, m	0.27	0.10	0.13

The concentration of 74 in the aqueous phase is 0.33 M, other conditions used are the same as those used to prepare the membranes listed in Appendix A.

Appendix C
Porosity of the thin films prepared by interfacial polymerization of **47** with **74**

Membrane samples	Porous area μm^2	Total area μm^2	Porosity %
1	0.20	0.86	0.24
2	0.53	2.55	0.21
3	1.65	5.61	0.29
4	1.19	2.80	0.43
5	1.35	3.97	0.34
6	1.92	4.00	0.48
7	0.39	1.87	0.21
8	0.56	1.51	0.37
9	1.07	3.58	0.30
10	0.50	1.11	0.44
11	0.73	3.56	0.20
12	0.97	3.16	0.30
13	1.77	4.58	0.39
14	0.93	2.60	0.36
15	0.68	2.00	0.34
16	3.60	6.99	0.52
17	3.44	6.41	0.54
Average			0.35
Standard deviation			0.10

The membrane samples were randomly selected from the membranes listed in Appendix A and B. The porous area in the cross section of the surface layer of the thin-film composite membrane was measured using a Sigma Scan Scientific Measurement System.[110] The minimum pore size that can be measured is about 0.1 μm. The porosity of a thin film formed by interfacial polymerization of **47** with **74** is defined by a ratio of the area occupied by pores to the total area of the cross section of the surface layer of the TFC membrane.[135,136,138]

REFERENCES

1. K. Scott, Handbook of Industrial Membranes, 1st Ed., Elsevier Science Publishers Ltd., Oxford, 1995, p. 3.
2. S. Sourirajan and T. Matsuura, Reverse Osmosis/Ultrafiltration Process Principles, National Research Council Canada, Ottawa, 1985, p. 1.
3. H. K. Lonsdale, J. Memb. Sci., **10**, 81 (1982).
4. I. Cabasso, Membranes, in: Encyclopedia of Polymer Science and Engineering, J. I. Kroschwaitz (Ed.), John Wiley & Sons, New York, 1985, Vol. 9, p. 509.
5. R. J. Petersen, J. Memb. Sci., **83**, 81 (1993).
6. S. Kimura and S. Sourirajan, AIChE J. **13**, 497 (1967).
7. H. K. Lonsdale, U. Merten and R. L. Riley, J. Appl. Polym. Sci., **9**, 1341 (1965).
8. M. Soltanieh and W. N. Gill, Chem. Eng. Commun., **12**, 279 (1981).
9. W. Pusch, Desalination, **59**, 105 (1986).
10. J. M. Dickson, Fundamental Aspects of Reverse Osmosis, in: Reverse Osmosis Technology, Application for High-Purity-Water Production, B. S. Parekh (Ed.), Marcel Dekker, Inc., New York, 1988, p. 1.

11. H. Mehdizadeh and J. M. Dickson, J. Memb. Sci., **42**, 119 (1989).

12. E. A. Mason and H. K. Lonsdale, J. Memb. Sci., **51**, 1 (1990).

13. Anonymous, Chemical and Engineering News, April 11, 1960, p. 64.

14. S. Loeb and S. Sourirajan, U.S. Pat. 3,133,132, (May 12, 1964).

15. J. E. Cadotte, U.S. Patent 4,039,440, (Aug. 2, 1977).

16. L. T. Rozelle, J. E. Cadotte, K. E. Kobian, and C. V. Kopp Jr., Nonpolysaccharide membranes for reverse osmosis: NS-100 membranes, in: Reverse Osmosis and Synthetic Membranes, S. Sourirajan (Ed.), National Research Council Canada, Ottawa, 1977, p. 249.

17. R. J. Petersen and J. E. Cadotte, 5 Thin Film Composite Reverse Osmosis Membranes, in: Handbook of Industrial Membrane Technology, M. C. Porter (Ed.), Noyes Publications, Rark Ridge, New Jersey, 1990, p. 307.

18. M. Goto, T. Miyata, K. Uezu, T. Kajiyama, F. Nakashio, T. Haraguchi, K. Yamada, S. Ide, and C. Hatanaka, J. Memb. Sci., **96**, 299 (1994).

19. D. Mukherjee, A. Kulkarni, W. N. Gill, J. Memb. Sci., **97**, 231 (1994).

20. R. E. Kesting, Synthetic Polymeric Membranes, A Structural Perspective, 2ed Ed., John Wiley & Sons, Inc., New York, 1985, p. 106.

21. B. J. Trushinski, J. M. Dickson, R. F. Childs, B. E. McCarry, D. R. Gagnon, J. Appl. Polym. Sci., **54**, 1233 (1994).

22. D. R. Lloyd and T. B. Meluch, Selection and Evaluation of Membrane Materials for Liquid separation, in: Material Science of Synthetic Membranes, D. R. Lloyd

(Ed.), ACS Symposium Series 269, ACS, Washington, D.C., 1985, p. 47.

23. S. Sourirajan and T. Matsuura, Reverse Osmosis/Ultrafiltration Process Principles, National Research Council Canada, Ottawa, 1985, p. 359.

24. T. Matsuura and S. Sourirajan, J. Appl. Polym. Sci., **16**, 1663 (1972).

25. T. Matsuura and S. Sourirajan, J. Appl. Polym. Sci., **17**, 1043 (1973).

26. T. Matsuura, M. E. Benas, J. M. Dickson, and S. Sourirajan, J. Appl. Polym. Sci., **19**, 2473 (1975).

27. T. Matsuura, J. M. Dickson, and S. Sourirajan, I & EC Process Des. Dev., **15**, 149 (1976).

28. H. Sumitomo and K. Hashimoto, Adv. Polym. Sci., **64**, 63 (1985).

29. C. M. Hansen, I & EC Prod. Res. Dev., **8**, 2 (1969).

30. H. H. Hoehn, Aromatic polyamide membranes, in: Material Science of Synthetic Membranes, D. R. Lloyd (Ed.), ACS Symposium Series 269, ACS, Washington, D.C., 1985, p. 81.

31. H. Strathmann, K. Kock, P. Amar and R. W. Baker, Desalination, **16**, 179 (1975).

32. H. Strathmann and K. Kock, Desalination, **21**, 241 (1977).

33. D. M. Koenhen, M. H. V. Mulder and C. A. Smolders, J. Appl. Polym. Sci., **21**, 199 (1977).

34. M. H. V. Mulder, J. O. Hendrikman, J. G. Wijmans and C. A. Smolders, J. Appl. Polym. Sci., **30**, 2805 (1985).

35. H. Strathmann, Production of Microporous Media by Phase Inversion Processes, in: Material Science of Synthetic Membranes, D. R. Lloyd (Ed.), ACS Symposium Series 269, ACS, Washington, D.C., 1985, p. 165.

36. A. J. Reuvers, J. W. A. ven den Berg and C. A. Smolders, J. Memb. Sci., **34**, 45 (1987).

37. A. J. Reuvers and C. A. Smolders, J. Memb. Sci., **34**, 67 (1987).

38. C. W. Yao, R. P. Burford, A. G. Fane, C. J. D. Fell and R. M. McDonogh, J. Appl. Polym. Sci., **34**, 2399 (1987).

39. L. Zeman and G. Tkacik, J. Memb. Sci., **36**, 119 (1988).

40. H. Strathmann, Synthetic Membranes and Their Preparation, in: Handbook of Industrial Membrane Technology, M. C. Porter (Ed.), Noyes Publications, Rark Ridge, New Jersey, 1990, p. 1.

41. W. Pusch, Desalination, **77**, 35 (1990).

42. T. H. Young and L. W. Chen, J. Memb. Sci., **59**, 169 (1991).

43. P. Radovanovic, S. W. Thiel and S. T. Hwang, J. Memb. Sci., **65**, 213 (1992).

44. P. Radovanovic, S. W. Thiel and S. T. Hwang, J. Memb. Sci., **65**, 231 (1992).

45. J. A. van't Hof, A. J. Reuvers, R. M. Boom, H. H. M. Rolevink and C. A. Smolders, J. Memb. Sci., **70**, 17 (1992).

46. C. A. Smolders, A. J. Reuvers, R. M. Boom and I. M. Wienk, J. Memb. Sci.,

73, 259 (1992).

47. R. M. Boom, I. M. Wienk, Th. van den Boomgaard and C. A. Smolders, J. Memb. Sci., **73**, 277 (1992).

48. R. Nolte, K. Ledjeff, M. Bauer and R. Mülhaupt, J. Memb. Sci., **83**, 211 (1993).

49. M. D. Guiver, A. Y. Tremblay, and C. M. Tam, Reverse Osmosis Membranes from Novel Hydrophilic Polysulfones, in: Advances in Reverse Osmosis and Ultrafiltration, T. Matsuura and S. Sourirajan (Eds.), National research Council Canada, Ottawa, 1989, p. 53.

50. M. D. Guiver, A. Y. Tremblay, and C. M. Tam, U. S. Pat. 4,894,159, (Jan. 16, 1990).

51. Y. Himeshima and M. Kurihara, Jpn. Kokai Tokkyo Koho JP 63,04,803, Chem. Abstr. 108: 168808s.

52. Y. Himeshima and M. Kurihara, Jpn. Kokai Tokkyo Koho JP 63,101,425, Chem. Abstr. 109: 93886a.

53. X. R. Lu, C. J. Gao and X. Z. Sun, Desalination, **54**, 207 (1985).

54. S. S. Wang, L. A. Ling, L. L. Wu, Y. Y. Gao, S. X. Liu, Z. Z. Wang, L. M. Sheng, and D. K. Kang, Desalination, **62**, 221 (1987).

55. G. X. Liu and J. J. Wu, Desalination, **62**, 239 (1987).

56. W. H. Chan, S. Y. L. Lam-Leung and C. F. Ng, Polym. Commun., **32**, 501 (1991).

57. W. H. Chan, S. Y. L. Lam-Leung, C. F. Ng and S. S. Wang, Polymer, **34**, 4377 (1993).

58. J. M. Adduci and M. J. Amone, J. Polym. Sci., Part A: Polym. Chem., **27**, 1115 (1989).

59. J. M. Adduci and E. J. Kuckoff, J. Appl. Polym. Sci., **41**, 129 (1990).

60. J. M. Adduci and T. Rochanapruk, J. Polym. Sci., Part A: Polym. Chem., **29**, 453 (1991).

61. K. Kobayashi, S. Tsuneda, K. Saito, H. Yamagishi, S. Furusaki, and T. Sugo, J. Memb. Sci., **76**, 209 (1993).

62. S. Tsuneda, K. Saito, S. Furusaki, T. Sugo, and I. Ishigaki, J. Memb. Sci., **71**, 1 (1992).

63. S. Tsuneda, K. Saito, S. Furusaki, T. Sugo and J. Okamoto, J. Memb. Sci., **58**, 221 (1991).

64. K. Saito, T. Hori, S. Furusaki, T. Sugo, and J. Okamoto, Ind. Eng. Chem. Res., **26**, 1977 (1987).

65. K. Saito, K. Uezu, T. Hori, S. Furusaki, T. Sugo, and J. Okamoto, AIChE J., **34**, 411 (1988).

66. Y. Osada, K. Honda and M. Ohta, J. Memb. Sci., **27**, 327 (1986).

67. A. M. Mika, R. F. Childs, J. M. Dickson, B. E. McCarry, and Gagnon, J. Memb. Sci., **108**, 37 (1995).

68. M. Nyström and P. Järvinen, J. Memb. Sci., **60**, 275 (1991).

69. B. Ranby and J. F. Rabek, Photodegradation, Photo-Oxidation and Photostabilization of Polymers, Principles and Applications, John Wiley & Sons, London, 1975, p. 223.

70. S. K. Chadda, B. E. McCarry, R. F. Childs, C. V. Rogerson, I. O. Tse-Sheepy and J. M. Dickson, J. Appl. Polym. Sci. **34**, 2713 (1987).

71. J. M. Dickson and I. O. Tse-Sheepy, R. F. Childs, and B. E. McCarry, AIChE Symposium Series, 261, American Institute of Chemical Engineers, New York, 1988, p. 158.

72. B. J. Trushinski, J. M. Dickson, R. F. Childs, and B. E. McCarry, J. Appl. Polym. Sci., **48**, 187 (1993).

73. E. L. Cussler, R. Aris and A. Bhown, J. Memb. Sci., **43**, 149 (1989).

74. O. Rogne, J. Chem. Soc., (B), 1855 (1971).

75. E. Ciuffarin, L. Senatore and M. Isola, J. Chem. Soc., Perkin Trans. II, 468 (1972).

76. L. M. Litvinenko, N. T. Maleeva, V. A. Savelova and T. D. Kovach, J. Gen. Chem. USSR, **41**, 2648 (1971).

77. A. Arcoria, V. Librando, E. Maccarone, G. Musumarra, and G. A. Tomaselli, Tetrahedron, **33**, 105 (1977).

78. B. C. Lee, D. S. Sohn, J. H. Yoon, S. M. Yang, and I. Lee, Bull. Korean Chem. Soc., **14**, 621 (1993).

79. L. M. Litvinenko and V. A. Savelova, J. Gen. Chem. USSR, **38**, 712

(1968).

80. L. M. Litvinenko and V. A. Savelova, and V. A. Shatskaya, J. Gen. Chem. USSR, **38**, 747 (1968).

81. L. M. Litvinenko and V. A. Savelova, and V. A. Shatskaya, J. Gen. Chem. USSR, **38**, 987 (1968).

82. A. I. Bilobrova, Yu. A. Sharanin, A. F. Popov and L. M. Litvinenko, J. Org. Chem. USSR, **7**, 2250 (1974).

83. T. N. Solomoichenko, V. A. Savelova, and L. M. Litvinenko, J. Org. Chem. USSR, **10**, 539, (1974).

84. I. A. Belousova, V. A. Savelova, L. M. Litvinenko, and V. N. Matvienko, J. Org. Chem. USSR, **15**, 1759 (1979).

85. V. A. Savelova, I. A. Belousova, and L. M. Litvinenko, J. Org. Chem. USSR, **17**, 1333 (1981).

86. L. M. Litvinenko, V. A. Savelova, and I. A. Belousova, J. Org. Chem. USSR, **19**, 1326 (1983).

87. I. Mita, K. Toyoshima and A. Okamoto, Eur. Polym. J., **19**, 657 (1983).

88. R. W. Blevins, R. C. Daly, and S. R. Turner, Lithographic Resists, in: Encyclopedia of Polymer Science and Engineering, J. I. Kroschwitz (Ed.), John Wiley & Sons, New York, 1985, Vol. 9, p. 97.

89. A. Reiser, Photoreactive polymers: The Science and Technology of

Resists, John Wiley & Sons, New York, 1989.

90. E. Reichmanis and L. F. Thompson, Chem. Rev., **89**, 1273 (1989).

91. R. P. Ponomareva, A. M. Komagorov and N. A. Andronova, J. Org. Chem. USSR, **16**, 140 (1980).

92. J. J. M. Vleggaar, A. H. Huizer, P. A. Kraakman, W. P. M. Nijssen, R. J. Visser and C. A. G. O. Varma, J. Am. Chem. Soc., **116**, 11754 (1994).

93. A. Rosenfeld, R. Mitzner, B. Baumbach and J. Bending, J. Photochem. Photobiol., A: Chem., **55**, 259 (1990).

94. J. Andraos, Y. Chiang, C. G. Huang, A. J. Kresge, and J. C. Scaiano, J. Am. Chem. Soc., **115**, 10605 (1993).

95. M. Yagihara, Y. Kitahara and T. Asao, Chem. Lett., 1015 (1974).

96. W. Ando, Photochemistry of the Diazonium and Diazo Groups, in: The Chemistry of Diazonium and Diazo Groups, S. Patai (Ed.), John Wiley & Sons, New York, 1978, Part 1, p. 341.

97. K. Tanigaki, T. Honda and T. W. Ebbesen, J. Photopolym. Sci. Tech., **2**, 341 (1989).

98. P.D. Caesar, in: N. Rabjohn (Ed.), Organic Synthesis, Coll. Vol. 4, 693, 1963.

99. P. W. Morgan, Condensation Polymers: By Interfacial and Solution Methods, Interscience Publishers, A Division of John Wiley & Sons, New

York, 1965.

100. P. W. Morgan, Interfacial Polymerization, in: Encyclopedia of Polymer Science and Engineering, J. I. Kroschwaitz (Ed.),, John Wiley & Sons, New York, 1985, Vol. 8, p. 221.

101. P. W. Morgan and S. L. Kwolerk, J. Polym. Sci., **40**, 299, (1959).

102. (a) P. W. Morgan, J. Macromol. Sci. Chem. **A15** (5) 683, (1981). (b) P. W. Morgan, J. Polym. Sci., Polym. Symp. **72**, 27 (1985).

103. S. A. Sundet, W. A. Murphey and S. B. Speck, J. Polym. Sci., **40**, 389-397, (1959).

104. J. E. Cadotte, R. S. King, R. J. Majerle and R. J. Petersen, J. Macromol. Sci.-Chem., **A15**, 727 (1981).

105. J. H. Bradbury, 5. Kinetics and Mechanisms, in: Interfacial Synthesis, Vol. I, Fundamentals, F. Millich and C. E. Carraher,Jr. (Eds.), Marcel Dekker, Inc., New York and Basel, 1977, p. 77.

106. F. MacRitchie, Trans. Faraday Soc., **65**, 2503 (1969).

107. A. Okamoto, K. Toyoshima and I. Mita, Eur. Polym. J., **19**, 341 (1983).

108. R. C. Evers, J. Polym. Sci., Part A-1, **5**, 1797 (1967).

109. S. Siggia and J. G. Hanna, Quantitative Organic Annalysis via Functional Groups, 4th Ed., John Wiley and Sons, New York, 1979, p. 536.

110. D. R. Parker, J. Norby, and J. Bennington, Sigma Scan Scientific Measurement System, California, 1988.

111. J.-I. K. Almestead, B. Urwyler and J. Wirz, J. Am. Chem. Soc., **116**, 954 (1994).

112. J. Andraos, A. J. Kresge and V. V. Popik, J. Am. Chem. Soc., **116**, 961 (1994).

113. F. G. Donnan, Zeits. Elektrochem. Ang. Phys. Chem., **17**, 572 (1911). J. Memb. Sci., **100**, 45 (1995), A Complete Translation.

114. E. H. Cwirko and B. G. Carbonell, J. Memb. Sci., **48**, 155 (1990).

115. A. Kulkarni, and W. N. Gill, The Effect of Solvent Post-Treatment on the Surface and Transport Characteristics of Thin-Film Composite Membranes, Poster Session: No. 19, 8th Annual Meeting of the North American Membrane Society, Citadel Inn, Ottawa, May 18-22, 1996.

116. K. Kono, F. Tabata and T. Takagishi, J. Memb. Sci., **76**, 233 (1993).

117. R. C. Weast, CRC Handbook of Chemistry and Physics, 70th Ed., CRC Press, Inc. Boca Raton, Florida, 1969-1970, D-163.

118. (a) L. F. Fieser and M. Fieser, Advanced Organic Chemistry, Reinhold Book Corporation, New York, 1961, p. 607. (b) R. C. Weast, CRC Handbook of Chemistry and Physics, 70th Ed., CRC Press, Inc. Boca Raton, Florida, 1969-1970, D-163.

119. M. W. Urban, Vibrational Spectroscopy of Molecules and Micromolecules on Surfaces, John Wiley and Sons, Inc., New York, 1993.

120. L. J. Ballemy, The Infrared Spectra of Complex Molecules, Chapman and

Hall, London, 1975, p. 183.

121. K. W. Evanson and M. W. Urban, J. Appl. Polym. Sci., **42**, 2287 (1991).

122.. A. M. Lichkus, P. C. Painter and M. M. Coleman, Macromolecules, **21**, 2636 (1988).

123. R. T. Conley, Infrared Spectroscopy, Allyn and Bacon, Inc., Boston, 1972, p. 176.

124. W. J. MacKnight, L. W. McKenna, B. E. Bead, and R. S. Stein, J. Phys. Chem., **72**, 1122 (1968).

125. T. R. Earnest, Jr., and W. J. MacKnight, Macromolecules, **13**, 844 (1980).

126. F. MacRitchie, 6. Interface effects on chemical reaction rate, in: Interfacial Synthesis, Vol. I, Fundamentals, F. Millich and C. E. Carraher,Jr. (Eds.), Marcel Dekker, Inc., New York and Basel, 1977, p. 103.

127. H. B. Tsai and Y. D. Lee, J. Polym. Sci., Part A: Polym. Chem., **25**, 1505 (1987).

128. H. B. Tsai and Y. D. Lee, J. Polym. Sci., Part A: Polym. Chem., **25**, 2195 (1987).

129. P. G. Kosky and E. P. Boden, J. Polym. Sci., Part A: Polym. Chem., **28**, 1507 (1990).

130. V. Enkelmann and G. Wegner, Die Makromolekulare Chemie, **157**, 303

(1972).

131. V. Enkelmann and G Wegner, Appl. Polym. Symp., **26**, 365 (1975).

132. R. G. Pearson and E. L. Williams, J. Polym. Sci., Polym. Chem., **23**, 9 (1985).

133. A. G. Mikos and C. Kiparissides, J. Memb. Sci., **59**, 205 (1991).

134. P. J. Flory, Principles of Polymer Chemistry, Cornell University Press, Ithaca, NY, 1953.

135. L. J. J. M. Janssen and K. te Nijenhuis, J. Memb. Sci., **65**, 59 (1992).

136. L. J. J. M. Janssen and K. te Nijenhuis, J. Memb. Sci., **65**, 69 (1992).

137. U. R. Evans, Trans. Amer. Electrochem. Soc., **46**, 247 (1925).

138. L. J. J. M. Janssen, A. Boersma and K.te Nijenhuis, J. Memb. Sci., **79**, 11 (1993).

139. G. E. Zaikov, A.P. Lordanskii, and V. S. Markin, Diffusion of Electrolytes in Polymers, VSP, Utrecht, The Netherlands, 1988, Chapter 5, p. 127.

140. J. A. Barrie, Chapter 8: Water in polymers, in: J. Crank and G. S. Park, Diffusion in Polymers, Academic Press, London and New York, 1968, p. 259.

141. G. E. Zaikov, A.P. Lordanskii, and V. S. Markin, Diffusion of Electrolytes in Polymers, VSP, Utrecht, The Netherlands, 1988, Chapter 6, p. 161.

142 R. H. Peters, Chapter 9: Kinetics of dyeing, in: J. Crank and G. S. Park, Diffusion in Polymers, Academic Press, London and New York, 1968, p. 315.

143. L. B. Sokolov and V. Z. Nikonov, 8. Copolycondensation and microscopic

kinetics, in: F. Millich and C. E. Carraher,Jr. (Ed.), Interfacial Synthesis, Vol. I, Fundamentals, Marcel Dekker, Inc., New York and Basel, 1977, p. 167.

144. V. Enkelmann and G. Wegner, J. Appl. Polym. Sci., **21**, 997 (1977).

145. L. M. Litvinenko, and A. F. Popov, J. Gen. Chem. USSR, **36**, 1523 (1966).

146. L. M. Litvinenko and V. A. Savelova, J. Gen. Chem. USSR, **36**, 1530 (1966).

147. L. M. Litvinenko, A. F. Popov, and T. V. Slyusarskaya, J. Gen. Chem. USSR, **37**, 972 (1967).

148. L. M. Litvinenko and V. A. Savelova, J. Gen. Chem. USSR, **38**, 721 (1968).

149. L. M. Litvinenko, and A. F. Popov, J. Gen. Chem. USSR, **38**, 1912 (1968).

150. V. A. Savelova, T. N. Solomoichenko, and L. M. Litvinenko, J. Org. Chem. USSR, **9**, 109 (1973).

151. L. M. Litvinenko, A. F. Popov, and L. I. Deraza, J. Org. Chem. USSR, **9**, 773 (1973).

152. L. M. Litvinenko, M. T. Maleeva, V. A. Savelova, and O. I. Butko, J. Org. Chem. USSR, **9**, 2139 (1973).

153. V. A. Savelova, V. A. Shat-skaya, L. M. Litvinenko, and N. I. Nikishina, J. Gen. Chem. USSR, **44**, 1081 (1974).

154. V. G. Zaslavskii, V. A. Savelova, L. M. Litvinenko, and T. N. Solomoichenko, J. Org. Chem. USSR, **16**, 1078 (1980).

155. V. A. Shatskaya, V. A. Savelova, and L. M. Litvinenko, J. Org. Chem. USSR, **21**, 796 (1985).

156. L. V. Kuritsyn and V. M. Kuritsyna, J. Org. Chem. USSR, **8**, 103 (1972)

157. P. J. Flory, Principle of Polymer Chemistry, Cornell U. P., Ithaca, NY, 1953, p. 75.

158. A. Okamoto, T. Aoki and I. Mita, Eur. Polym. J., **19**, 661 (1983).

159. D. A. Meeter, Non-linear Least Squares (UWHAUS), University of Wisconsin Computing Center, 1965.

160. R. C. Evers and G. F. L. Ehlers, J. Polym. Sci., Part A-1, **5**, 1797, (1967).

161. K. Rilling, J. M. Dickson, R. F. Childs, D. R. Gagnon, Canadian Docket, 49656CAN9A, USSN: 08/084, 891, 1995.

IMAGE EVALUATION
TEST TARGET (QA-3)

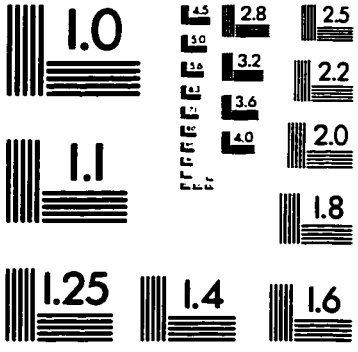

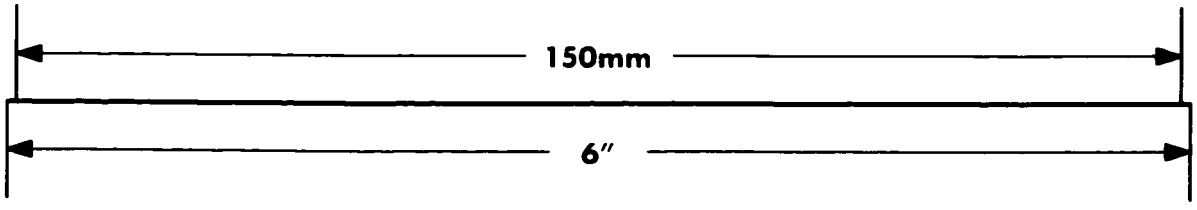

APPLIED IMAGE, Inc
1653 East Main Street
Rochester, NY 14609 USA
Phone: 716/482-0300
Fax: 716/288-5989